論文 / 著書情報
Article / Book Information

題目(和文)	ロタキサンを活用した高機能超分子メカノフォアの創製
Title(English)	Development of Highly Functional Supramolecular Mechanophores Based on Rotaxane
著者(和文)	村松達也
Author(English)	Tatsuya Muramatsu
出典(和文)	学位:博士(工学), 学位授与機関:東京工業大学, 報告番号:甲第12546号, 授与年月日:2023年9月22日, 学位の種別:課程博士, 審査員:相良 剛光,早川 晃鏡,道信 剛志,VACHA MARTIN,難波江 裕太
Citation(English)	Degree:Doctor (Engineering), Conferring organization: Tokyo Institute of Technology, Report number:甲第12546号, Conferred date:2023/9/22, Degree Type:Course doctor, Examiner:,,,,
学位種別(和文)	博士論文
Type(English)	Doctoral Thesis

Development of Highly Functional Supramolecular Mechanophores Based on Rotaxane

（ロタキサンを活用した高機能超分子メカノフォアの創製）

Tatsuya Muramatsu

2023

Table of Contents

Chapter 1. General Introduction ----- 1

1.1. Force Sensors for Piconewton Range ----- 2

1.2. Mechanochromic Molecular Assemblies in Polymeric Materials ----- 3

1.3. Mechanochromic Mechanophores

1.3.1. Mechanophores ----- 5

1.3.2. “Covalent” Mechanochromic Mechanophores ----- 7

1.3.3. “Non-Sacrificial” Mechanochromic Mechanophores ----- 19

1.4. Mechanophores Utilizing Rotaxanes ----- 29

1.5. Processes Related to Photoexcitation

1.5.1. Energy Levels and Transitions in Molecules ----- 34

1.5.2. Photo-Induced Electron Transfer ----- 36

1.5.3. Förster (Fluorescence) Resonance Energy Transfer (FRET) ----- 37

1.5.4. Dexter Energy Transfer ----- 38

1.5.5. Charge Transfer Interaction ----- 39

1.5.6. Excimer and Exciplex ----- 40

1.6. Objective ----- 41

1.7. Outline of the Thesis ----- 43

1.8. References ----- 44

Chapter 2. Mechanoresponsive Behavior of a Polymer-Embedded Red-light Emitting Rotaxane Mechanophore ----- 55

2.1. Introduction ----- 57

2.2. Results and Discussion

2.2.1. Molecular Designs ----- 59

2.2.2. Fundamental photophysical Properties of **1** and **2** in Solutions ----- 61

2.2.3. Introduction of **2** into Polyurethane ----- 62

2.2.4. Mechanoresponsive Luminescence Behavior of **2-PU** ----- 66

2.2.5. Changes in the Photophysical Properties of **2-PU** Films upon Swelling ----- 70

2.2.6. Fluorescence Lifetime Measurements of **2-PU** Films Before and After Swelling ----- 75

2.3. Conclusion ----- 77

2.4. Experimental Section

2.4.1. General Methods ----- 78

2.4.2. Synthesis Schemes ----- 80

2.4.3. Polymer Synthesis and Preparation of Polyurethane Films ----- 84

2.4.4. Methods of Sonomechanochemical Experiment ----- 86

2.5. References ----- 88

Chapter 3. Rotaxane-Based Dual Function Mechanophores Exhibiting Reversible and Irreversible Responses ----- 92

3.1. Introduction ----- 94

3.2. Results and Discussion

3.2.1. Molecular Designs ----- 97

3.2.2. Fundamental Photophysical Properties of **Rot1–3** in Solutions ----- 100

3.2.3. Introduction of **Rot1–3** into Polyurethanes ----- 105

3.2.4. Mechanoresponsive Luminescence Behavior of **Rot1–3PU** ----- 113

3.2.5. Sonomechanochemical Experiments of **Rot1–3PU** ----- 118

3.2.6. Verification of Force-Induced Dethreading ----- 121

3.3. Conclusion ----- 131

3.4. Experimental Section

3.4.1. General Methods ----- 132

3.4.2. Synthesis of Rotaxanes ----- 135

3.4.3. Polymer Synthesis and Preparation of Polyurethane Films ----- 163

3.4.4. Thermal Treatment for **Rot1** or **Rot2** Solutions ----- 164

3.4.5. Mass Spectroscopic Studies for **Rot1PU** or **Rot4PU** Films After Stretching ----- 164

3.5. References ----- 165

Chapter 4. Force-induced Shuttling of Rotaxanes Controls Fluorescence Resonance Energy Transfer in Polymer Hydrogels ----- 171

4.1. Introduction ----- 173

4.2. Results and Discussion

4.2.1. Molecular Designs ----- 176

4.2.2. Fundamental Photophysical Properties of **An**, **BP**, **AnBP**, and **RotAnBP** in Solutions ----- 178

4.2.3. Incorporation of **RotAnBP** into Polyurethane-urea ----- 182

4.2.4. Investigation of Mechanoresponsive Behavior of **RotAnBP-PUU Hydrogels** and Dry **RotAnBP-PUU** films ----- 188

4.3. Conclusion ----- 196

4.4. Experimental Section

4.4.1. General Methods ----- 197

4.4.2. Synthesis Procedure ----- 199

4.4.3. Polymer Synthesis and Preparation of Dry **RotAnBP-PUU** Films and **RotAnBP-PUU** Hydrogels ----- 205

4.4.4. Calculation of Spectral Overlap Integral and Förster Distance ----- 206

4.4.5. Examination of the Penetration of the Red Fluorescence Emitted by **RotAnBP-PUU** Hydrogels ----- 207

4.5. References ----- 209

Chapter 5 Conclusions and Perspectives ----- 214

List of Publications ----- 219

Acknowledgments ----- 221

Chapter 1

General Introduction

1.1. Force Sensors for Piconewton Range

Forces surround us everywhere and contribute significantly to the deformation and movement of every substance. The magnitude of forces varies from large, as exerted by heavy machinery, to small, as generated by cell migration. Although methods for evaluating large forces have been established, the development of force sensors that can evaluate small forces in piconewton range is still a challenging task. Such small forces include forces applied to a single polymer chain constituting polymeric materials and forces that are received by extracellular matrices when cells move. Recently, as methods for detecting weak forces in living systems, double stranded DNA-based force sensors using Förster (fluorescence) resonance energy transfer (FRET) are developed.[1,2] These DNA-based force sensors are composed of duplex hairpin with a fluorophore and quencher pair. When a force is applied to the sensor, the double stranded DNA changes to a single stranded DNA and the FRET efficiency from the fluorophore to the quencher changes as the distance between the fluorophore and the quencher alters. The magnitude of force applied to the sensors can be quantitatively evaluated by complex equations based on FRET efficiency. Walther's group recently reported that the DNA-based sensors can be also introduced into hydrogels to evaluate forces inside polymeric materials.[3] In general, however, introduction of DNA sensors into polymeric materials is still challenging and the sensors are unstable under ambient conditions. Besides, as force sensors that image membrane tension in living systems, flippers consisting of an electron-rich dithieno[3,2-*b*:2',3'-*d*]thiophene (DTT) donor connected to an electron-poor DTT acceptor have been reported.[4] In the force-free state, the flippers are twisted due to the methyl groups next to the single bond connecting the two DTTs. When planarization of the flippers occurs by physical compression, the fluorescence color and lifetime are changed.

In polymer chemistry, two methods have been mainly reported to evaluate the forces applied to materials. One approach is to physically dope molecular microcrystals, which

display mechanochromic behavior by controlling the molecular assembled structures, into polymeric materials. The other approach is covalently incorporating molecular units, so-called "*mechanochromic mechanophores*", that exhibit changes in their photophysical properties at a single molecule level when subjected to forces, into polymeric materials.

1.2. Mechanochromic Molecular Assemblies in Polymeric Materials

Molecular assemblies of organic or organometallic molecules have been developed as candidates for force sensors.[5] This is because that the photoluminescence properties of these materials are influenced by their molecular arrangements, and rearrangement of molecular packing by mechanical stimulation leads to alteration of the photophysical properties. By physically dispersing such dyes in the polymeric materials, the polymers will exhibit changes in fluorescence properties upon deformation. For the first example, Weder et al. demonstrated that when a linear low-density polyethylene film in which a cyano-functionalized oligo(*p*-phenylene vinylene) microcrystals exhibiting excimer emission are dispersed is stretched, the microcrystals are cracked and the molecules are separated. As a result, the amount of dye displaying monomer fluorescence increases,

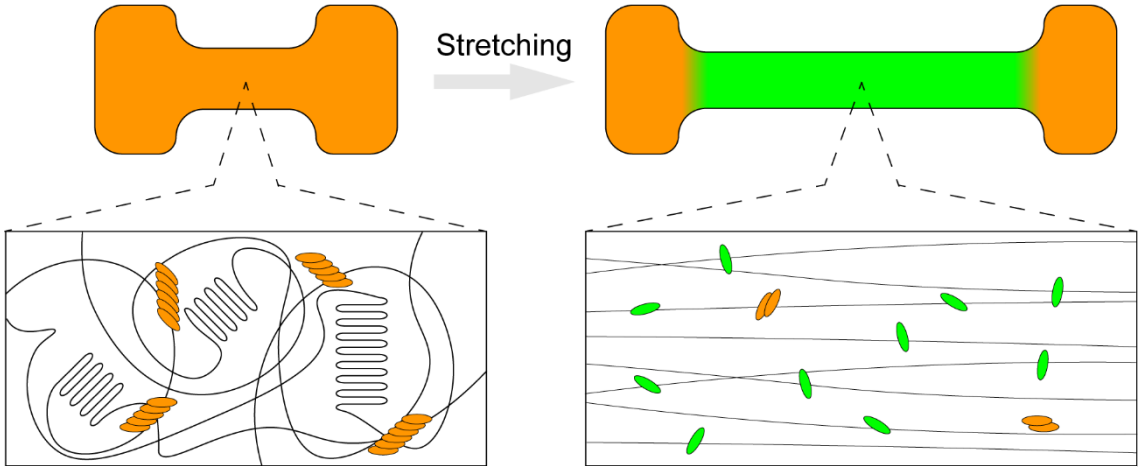

Figure 1-1. Schematic illustration of operating mechanism of mechanochomic polymers in which microcrystalline dyes are dispersed. The pristine polymer film shows orange emission due to the excimer emission of aggregated dyes, while the green fluorescence is observed in the stretched film, resulting from molecularly separated dyes.

altering the fluorescent color of the polymeric material (Figure 1-1).[6,7] Following the work, applications of this mechanochromic mechanism to other polymers[8–11] and other dyes[12–14] have also been reported. This strategy requires rupturing the weak intermolecular interactions such as π-π interaction, hydrogen bonds, and charge-transfer interaction between molecules that form molecular assembled structures to induce changes in the luminescence properties. The force required to break one weak intermolecular interaction is essentially several to several tens of piconewton.[15–18] However, these mechanochromic crystals are not suitable for detecting forces ranging from pico- to nanonewton order because the mechanochromic crystals consist of numerous molecules, which results in a significantly higher force threshold. Besides, as the size of crystals is inhomogeneous, the threshold of force required to cause changes in photophysical properties varies depending on the crystal. Thus, in order to develop mechanochromic crystals that can quantitatively evaluate forces at piconewton order, the molecular assemblies must consist of a specific number of molecules and the number of molecules must be reduced to a minimum.[19]

1.3 Mechanochromic Mechanophores

1.3.1 Mechanophores

Before 2000, polymer mechanochemistry had been intensively studied on the degradation behavior of polymers based on ultrasound-induced scission of molecular chains. In contrast, in the 2000s, attention has begun to focus on converting destructive mechanical energy into productive forms that allow for mechanoresponsive functions.[20–22] This inspiration is mainly triggered by three researches: the reversible mechanochemistry of palladium-coordinated polymers,[23] the evaluation of the relationship between mechanical properties and equilibrium dissociation of polymer networks cross-linked by coordination bonds,[24] and the specific cleavage of azo-functionalized polyethylene glycols by ultrasonication.[25] Through these studies, molecular units that exhibit various responses when subjected to force were defined as "*mechanophores*".[20] The term "*mechanophore*" was first used in 2006 for the ring-opening reaction of 1,2-disubstituted benzocyclobutene with mechanical stimuli by Moore et al.[26] *Trans* and *cis* isomers of a 1,2-disubstituted benzocyclobutene undergo mechanically induced ring-opening reaction in a conrotarory and disrotary process, respectively, that yield identical products. This result differs from photochemically or thermally induced ring-opening reactions, which yield different products depending on the isomer, indicating that the application of a mechanical stimulus can allow forbidden or slow processes to proceed. So far, many mechanophores have been reported to exhibit various responses, including the release of small molecules (Figure 1-2a),[27–31] induction of catalytic function (Figure 1-2b),[32–36] and gated degradation (Figure 1-2c).[37–39] In particular, mechanochromic mechanophores showing changes in photophysical properties (Figure 1-2d) are fascinating tools to visualize the failure of polymeric materials.[40,41] Mechanochromic mechanophores can be classified into two types. One is "covalent" mechanophores which are activated by the scission of one or more covalent bonds. The other is "non-sacrificial" mechanophores which are activated by the control of intermolecular interactions or molecular conformational changes.

Compared to mechanochromic dyes, mechanochromic mechanophores have a specific force threshold for activation, enabling the quantitative evaluation of forces.

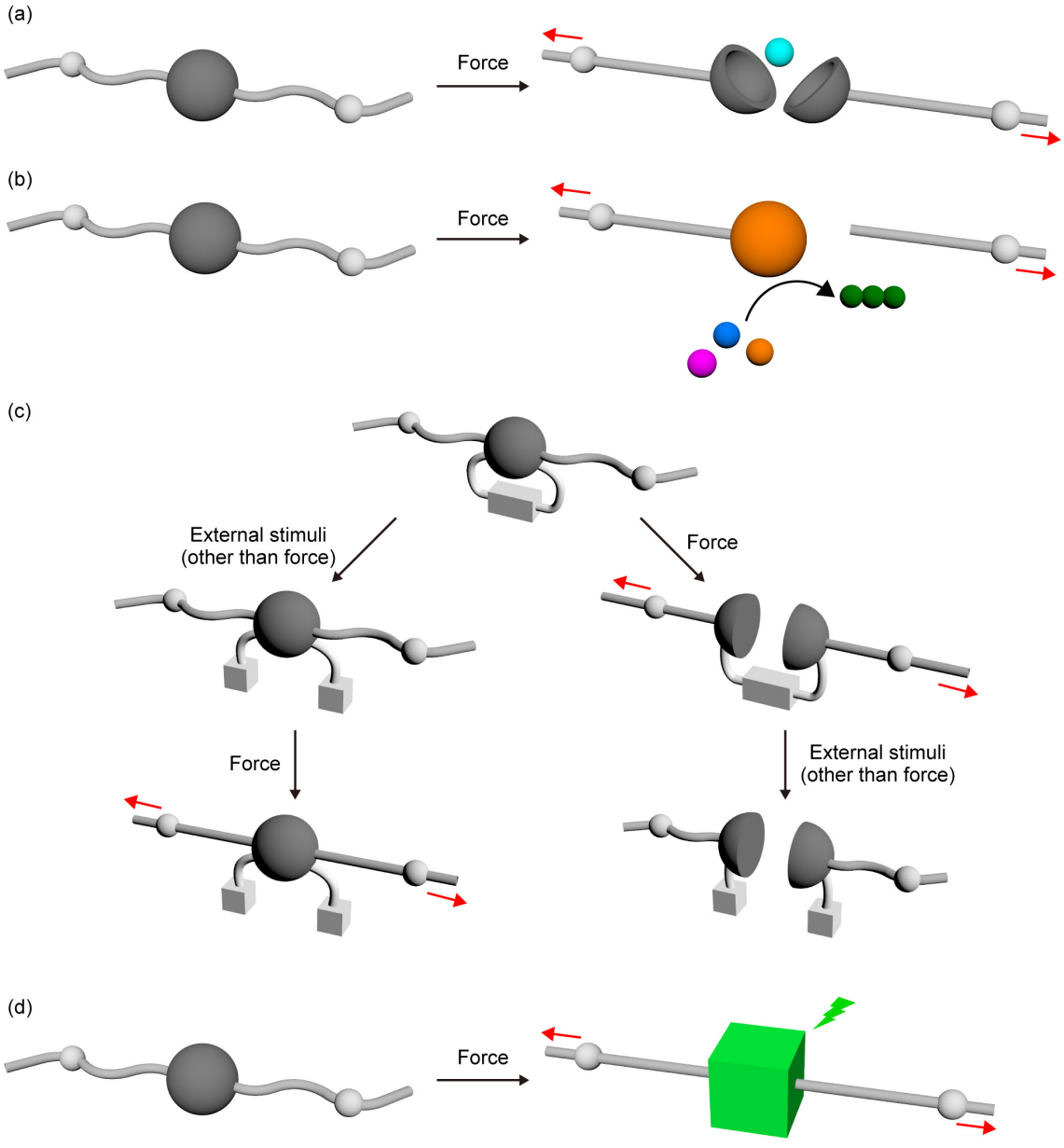

Figure 1-2. Schematic illustration of mechanophores displaying (a) release of small molecules, (b) induction of catalytic function, (c) gated degradation, and (d) changes in photophysical properties.

1.3.2. "Covalent" Mechanochromic Mechanophores

Spiropyran and Naphthopyran mechanophores

In 2009, Moore, Sottos, and co-workers first demonstrated a mechanochromic mechanophore based on a spiropyran which is well-known as a photochromic molecule (Figure 1-3a, **SP1**).[42] When poly(methyl acrylate) (PMA) chains are covalently incorporated into the spiropyran so that a force is transduced to the central C-O bond, the bond is cleaved upon the deformation of the polymer. Consequently, the colorless spiropyran changes to the merocyanine structure showing red color (Figure 1-3a, right). The generated merocyanine returns to the initial spiropyran upon exposure to visible light. The magnitude of the forces required for activation was calculated to be 4.3 nN by using the constrained geometries simulate external force (CoGEF) method[43] on density functional theory (DFT) calculation. This value is tuned by changing the position of the polymer attachment. If two polymer chains are attached to the 8-position of the benzopyran and 1'-position of the indoline part (Figure 1-3b, **SP2**), the force of 2.6 nN causes the mechanochemical activation of spiropyran.[44] Also, Craig and co-workers quantified the threshold forces for activation by using single molecule force spectroscopy (SMFS) carried by atomic force microscopy (AFM).[45] The ring-opening reactions of **SP1** and **SP2** require forces of 260 ± 15 pN and 240 ± 15 pN, respectively. In contrast, both **SP1** and **SP2** show color-changing behavior at similar strains and stress in polydimethylsiloxane (PDMS).[46] This result indicates that such small differences in

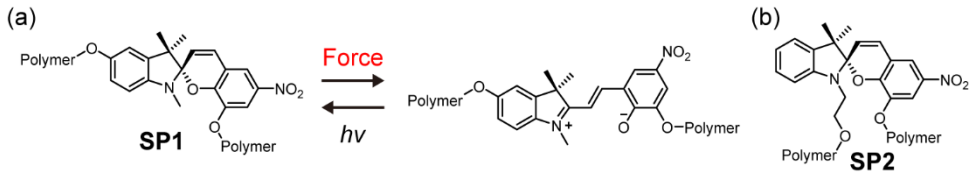

Figure 1-3. (a) Molecular structure and operating mechanism of spiropyran mechanophore **SP1**. (b) Molecular structure of **SP2**.

threshold forces for activation hardly affect the mechanical activation of mechanophores in bulk polymeric materials due to the complex nature of the macroscopic system.

Following the report on the spiropyran mechanophore, several types of pyran derivatives such as spirothiopyran (Figure 1-4a)[47] and naphthopyran (Figure 1-4b)[48-50] have been investigated as mechanochromic mechanophores. Weng and co-workers reported that a yellow spirothiopyran changes to green thiomerocyanine upon mechanical activation.[47] The formed thiolate could be used for further thiol-ene reaction with alkenes incorporated into polymer backbones, which is useful for developing stress-responsive materials and fundamental examination of polymer dynamics. Moore and co-workers reported that colors of PDMS films in which the naphthopyran mechanophore is covalently incorporated change from colorless to yellow color upon stretching (Figure 1-4b).[48] The mechanochemical reactivity of naphthopyran depends on the regiochemistry, similar to spiropyran derivatives. When the polymer chain is attached to the 5-position of naphthopyran, the C-O bond was selectively cleaved with an estimated required force of 4.1 nN. However, naphthopyrans featuring a polymer at the 8- or 9-position (Figure 1-4c) undergo homolytic cleavage at the polymer attachement with a bigger force of 6.3 nN

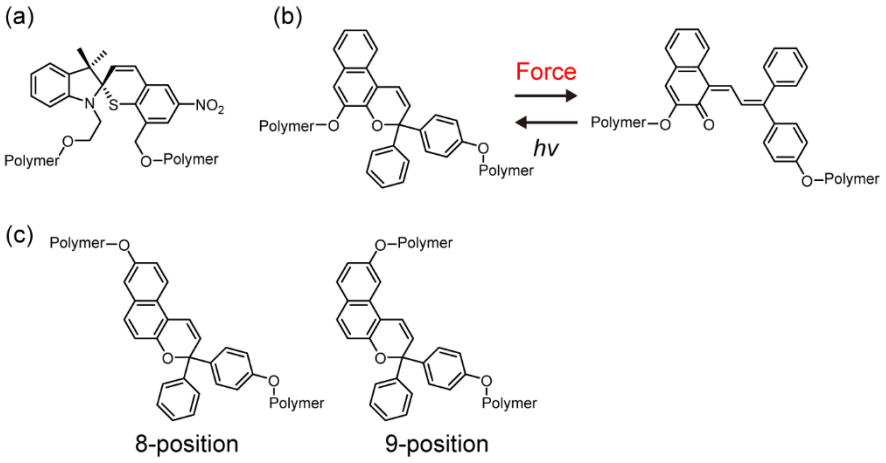

Figure 1-4. (a) Molecular structure of a spirothiopyran mechanophore. (b) Molecular structure and operating mechanism of a naphthopyran mechanophore substituted at 5-position. (c) Molecular structures of naphthopyrans substituted at 8- and 9- positions.

because the force is not well transduced to the central C-O bond. Thus, the proper position of polymer attachment is significant for successful mechanochemical activation.

Radical-generating mechanophores

Mechanochromic mechanophores generating radicals via homolytic cleavage have been reported. One example is a diarylbibenzofuranone (DABBF) unit reported by Otsuka group (Figure 1-5a).[51] They investigated the mechanoresponsive behavior of DABBF by incorporating it into polyurethane elastomer. When the polymer film is stretched, the central C-C bond of DABBF is selectively cleaved, leading to the generation of stable radicals that exhibit a blue color. After the stretched polyurethane is left at room temperature for several hours, the blue color gradually fades as the radicals recombine with each other. The advantage of mechanophores generating stable radicals is that the amount of generated radicals can be quantitatively evaluated using electron paramagnetic resonance (EPR) spectroscopy. Determination of the activated amount of DABBF in the polymer would lead to a more precise understanding of the failure and fatigue mechanisms in polymeric materials. Other examples of radical-generating mechanophores include tetraarylsuccinonitrile (TASN, Figure 1-5b),[52–55]

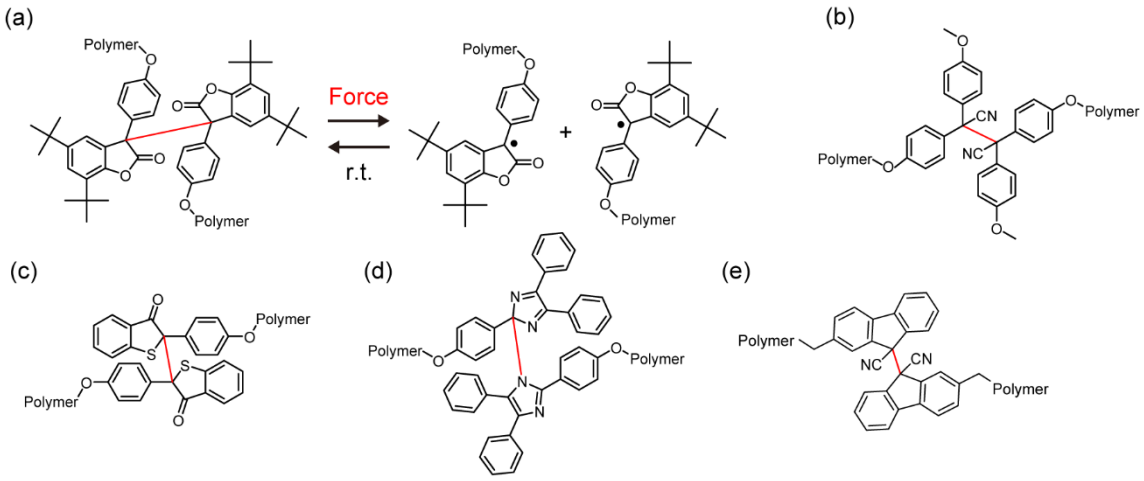

Figure 1-5. (a) Molecular structure and operating mechanism of DABBF. (b-e) Molecular structures of (b) TASN, (c) DABBT, (d) HABI, and (e) DFSN. Covalent bonds to be cleaved are highlighted in red color.

diarylbibenzothiophenonyl (DABBT, Figure 1-5c),[56] hexaarylbiimidazole (HABI, Figure 1-5d),[57] and difluorenylsuccinonitrile (DFSN, Figure 1-5e).[58–60] The force required for activation of TASN has been quantitatively evaluated using SMFS on AFM and calculated to be between 130–180 pN, which is weaker than that of spiropyrans.[61]

1,2-Dioxetane mechanophores

1,2-Dioxetane derivatives are well-known as chemiluminescent molecules and thermally decompose into one ground-state ketone species and one excited-state ketone species exhibiting luminescence when the excited ketone returns to the ground state. Chen, Sijbesma, and co-workers reported that a bis(adamantyl)-1,2-dioxetane derivative functions as a mechanophore (Figure 1-6a).[62,63] When a polymer containing the dioxetane is stretched, the dioxetane derivative undergoes scission of the covalent bond and exhibits blue chemiluminescence. By physically doping various fluorophores into the polymer, the respective fluorescence color can be obtained due to energy transfer from the excited ketone to acceptor fluorophores. The authors achieved blue, green, yellow, and red fluorescence colors by mixing the polymer containing the dioxetane mechanophore with 9,10-diphenylanthracene, perylene, 4,7-di(thiophen-2-yl)-benzo[*c*][1,2,5]thiadiazole,

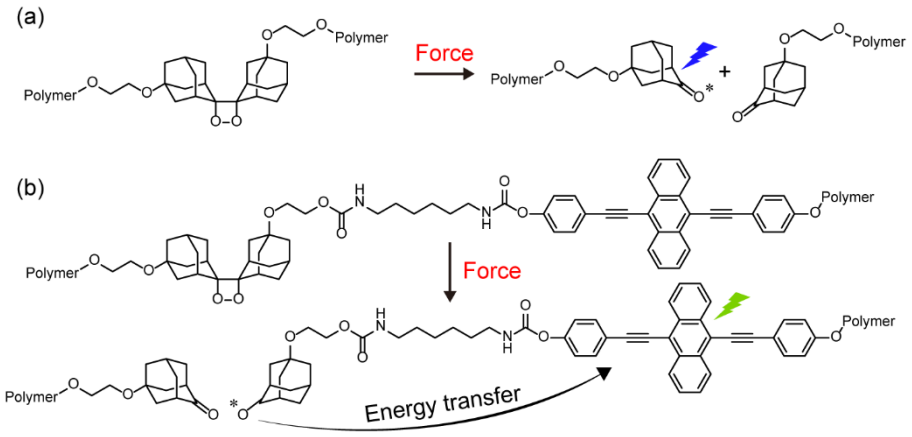

Figure 1-6. (a) Molecular structure and operating mechanism of a 1,2-dioxetane mechanophore. (b) One example of force-induced energy transfer from an activated 1,2-dioxetane mechanophore to an acceptor fluorophore which is introduced in the vicinity of the 1,2-dioxetane.

and *N*,*N*'-bis(2,5-di-*tert*-butylphenyl)-3,4,9,10-perylene dicarboximide, respectively. Furthermore, Chen et al. reported that the efficiency of the energy transfer can be improved by introducing the fluorophore in the vicinity of the dioxetane derivative, rather than simply mixing fluorophores into polymers (Figure 1-6b).[64–66] While the dioxetane mechanophore can achieve various fluorescence colors by utilizing energy transfer with other fluorophores and does not require excitation light, the luminescence can only be observed immediately after the polymer is stretched due to their short lifetimes of luminescence, which is a disadvantage.

Cycloadduct mechanophores

Cycloadducts such as Diels-Alder adducts, [4+4] cycloadducts, and [2+2] cycloadducts can function as mechanophores. For example, a dimer of anthracene changes its structure into two anthracene moieties and exhibits purple fluorescence when a force is applied, as two C-C bonds bridging the two anthracenes are cleaved (Figure 1-7a).[67] In the case of a Diels-Alder adduct consisting of an anthracene unit and a maleimide unit, a *retro* Diels-Alder reaction is induced by applying force via polymers which are attached to the anthracene and maleimide units, and the fluorescence of anthracene is observed (Figure 1-7b).[68] By using an π-extended anthracene moiety, the susceptibility to oxygen quenching would decrease and fluorescence quantum yield increases, which leads to an improvement in the detectability of mechanical failure (Figure 1-7c).[69] Boulatov and co-workers reported that mechanophores based on cinnamic acid dimer undergo retro [2+2] cyclization upon applying force (Figure 1-7d).[70,71] Interestingly, forces required for activation depend on stereoisomers, that is, syn- and anti-dimers were dissociated when subjected to a force 1 and 2 nN, respectively. [2+2] Coumarin cycloadducts also function as mechanophores which show turn-on of blue fluorescence (Figure 1-7e).[72]

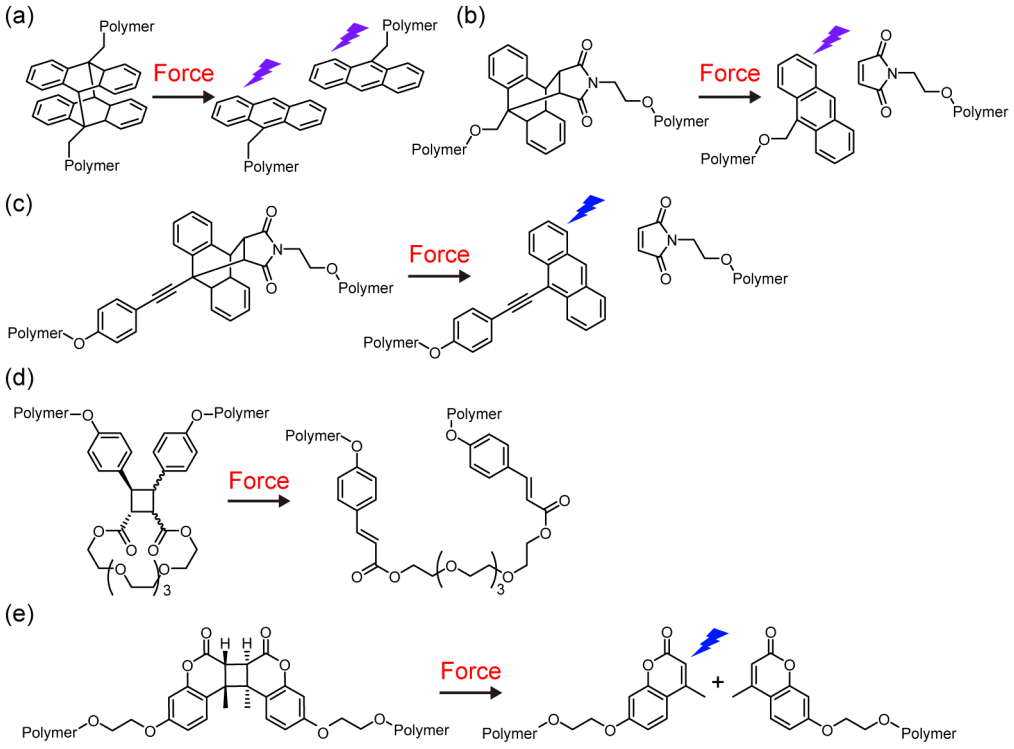

Figure 1-7. Molecular structures and operating mechanism of (a) a [4+4] cycloadduct of anthracene, (b) an anthracene-maleimide Diels-Alder adduct, (c) a 9-π-extended anthracene-maleimide Diels-Alder adduct, (d) a [2+2] cycloadduct of cinnamic acid, and (e) a [2+2] cycloadduct of coumarin.

Rhodamine-based mechanophores

Rhodamines are well-known fluorophores that exhibit high molar extinction coefficient and fluorescence quantum yield, and can function as mechanophores. The first reported rhodamine-based mechanophore was based on a rhodol fluorophore, which is colorless and exhibits very weak blue fluorescence (Figure 1-8a). The rhodol mechanophore which is subjected to the force via polymer chains upon compression of the polymer undergoes ring-opening and generates a zwitterion, resulting in a red color and red fluorescence.[73] The original state recovers after a long time at room temperature. However, the rhodol mechanophore is less activated when the polymer is stretched, resulting in negligible changes in absorption and luminescence properties. To overcome the problem, a rhodamine mechanophore having two tertiary amines and three polymer attachments was

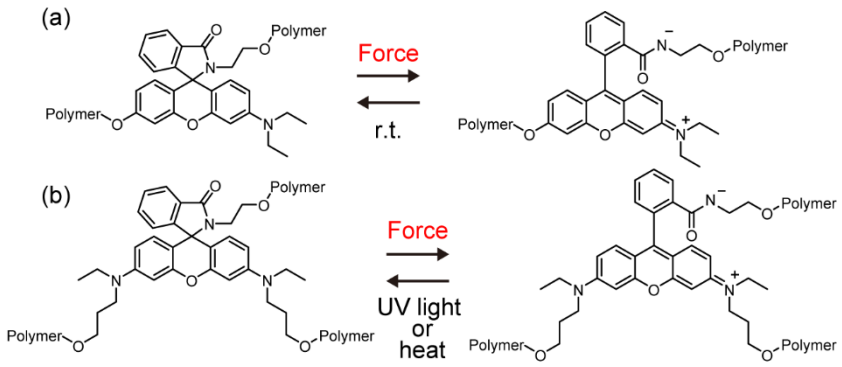

Figure 1-8. Molecular structures and operating mechanism of (a) two-functionalized rhodol and (b) three-functionalized rhodamine mechanophores.

reported by Bai et al (Figure 1-8b).[74] The introduction of two tertiary amines into the phenyl group increases the fluorescence quantum yield in the zwitterionic state. Besides, the three polymers introduced to the mechanophore enable sufficient forces to be transduced to the rhodamine by using rhodamine as crosslinkers, increasing the amount of mechanophores that are activated. Furthermore, it exhibits a unique three-color mechanochromism, showing blue fluorescence in the initial state, pink fluorescence when the polymer is stretched, and yellow fluorescence after the force is removed. The difference in fluorescence colors of the polymer upon stretching and relaxation is due to the dihedral angle between the phenyl group with an amidate ion and the xanthene having two amino groups. Upon applying forces to the ring-opened form, the conformation of the zwitterion is planarized and the π-electrons in the phenyl ring are delocalized to that of the xanthene, leading to red-shifted fluorescence. In contrast, the zwitterion returns to its bent geometry when the force is removed, resulting in blue-shifted fluorescence.

Recently, Chen's group developed rhodamine-like mechanophores composed of two spirolactam rings and an aminobenzopyranoxanthene, and regio- and stereo-specific isomers are obtained by changing the positional relationship of the two spirolactam rings (Figure 1-9a).[75] In these mechanophores, the ring-opening reaction of the two spiro rings is cooperative, and their mechanoresponsiveness is dependent on the molecular geometry

and the polarity of the solvent. The magnitude of force required for their ring opening is weaker than that of regular rhodamine mechanophores according to CoGEF calculations and is calculated to be between 200 and 600 pN from SMFS tests on AFM.

Besides, they developed a novel near-infrared (NIR) emissive mechanophore comprised of semirhodamine and coumarin units (Rh-Co, Figure 1-9b).[76] The ring-closed form shows a yellow color and no fluorescence, while green color and NIR emission are observed upon mechanically induced ring-opening. When the mechanically open form is left at room temperature for several hours, a color change and disappearance of NIR luminescence are observed as the spiro-ring closes.

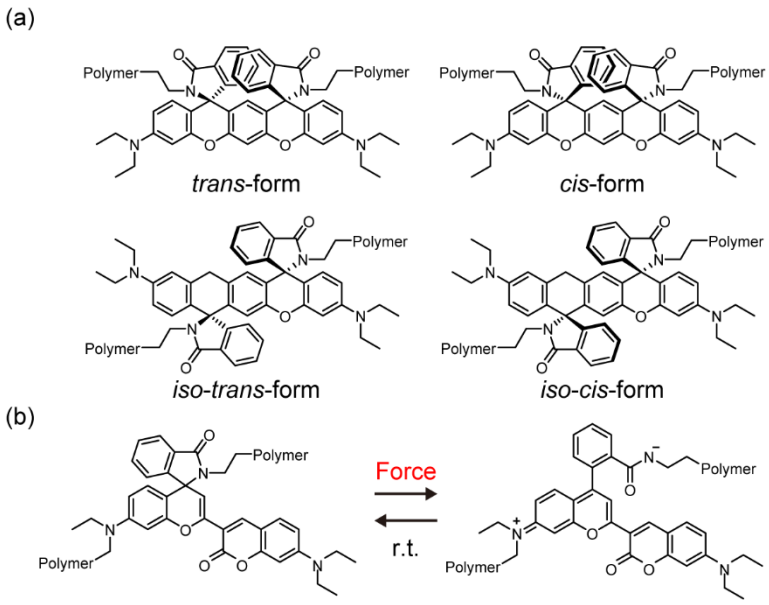

Figure 1-9. (a) Molecular structures of regio- and stereo-specific bis-rhodamine-like mechanophores. (b) Molecular structure and operating mechanism of Rh-Co.

Ladderane mechanophores

In 2017, Xia group reported on a mechanically responsive non-conjugated polymer that is converted to a conjugated polymer when subjected to force. The non-conjugated polymer is obtained by ring-opening metathesis polymerization (ROMP) of [5]-ladderanes (Figure 1-10a).[77] Once a force is applied to the colorless polyladderane, the

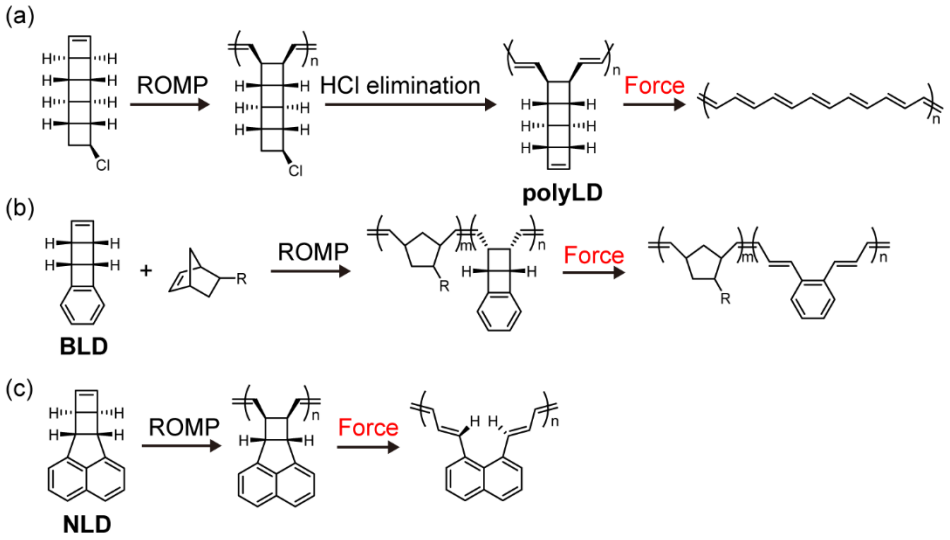

Figure 1-10. Molecular structures of (a) LD, (b) BLD, and (c) NLD monomers and the mechanoresponsive behavior of polymers obtained from the corresponding monomer through ROMP.

cyclobutene rings sequentially open and partially convert to black conjugated polyacetylene. A problem of this mechanophore is difficulties in the synthesis of ladderane (LD) monomer and its derivatives, leading to the limitation of mass production and functionalization of the resulting polymer. Besides, an HCl/HBr elimination step is required to generate terminal olefins after ring-opening metathesis synthesis (ROMP). This results in polymer degradation and broadened the molecular weight distribution. To overcome these issues, they developed a benzoladderane (BLD) monomer and prepared a triblock copolymer of norbornene and BLD monomers (Figure 1-10b).[78] When a force is applied to this polymer solution by sonication, the color of the solution changes from colorless to yellow resulting from the generation of poly(*o*-phenylene-hexatrienylene). The BLD monomer was scalable in synthesis, however, the synthesis cost is expensive and the monomer could not be functionalized with electron-withdrawing groups. Seeking further improvement, they designed bicyclo[2.2.0]hex-5-ene-2,3-*peri*-naphthalene (NLD) monomer which can be synthesized from readily available starting materials with multi-gram scale and functionalized with both electron-rich and electron-poor substituents (Figure 1-10c).[79] This mechanophore achieves not only color change but also

fluorescence color change from blue to yellow. The force required for activating ladderane mechanophores has been quantitatively evaluated by SMFS.[80] LD and NLD have similar threshold forces of 1910 pN and 1920 pN, respectively, while BLD has a smaller threshold force of 1800 pN. The differences in the threshold forces presumably depend on the stereochemistry and electronic properties of the cyclobutene which is first opened.

Others

Dithiomaleimide (DTM) has been used for labeling proteins and self-reporting fluorescent agents. Weder et al. demonstrated that a DTM derivative is a candidate for a mechanophore (Figure 1-11a) based on the fact that the fluorescent properties of DTM depend on the substituent and that the binding energy of thioesters is lower than that of C-C bonds.[81] PMA and poly(ε-caprolactone) (PCL) featuring one DTM mechanophore in the center of each polymer chain show green fluorescence. Upon sonication of the polymer solutions, one C-S bond is cleaved and the fluorescence intensities of the two polymers decrease.

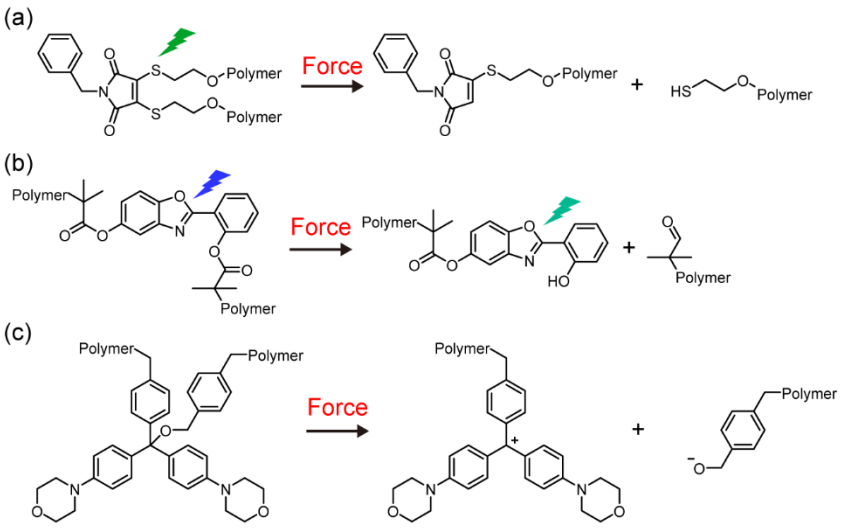

Figure 1-11. Molecular structures and operating mechanism of (a) DTM, (b) 2-(2'-hydroxyohenyl)benzoxazole, and (c) triarylmethane mechanophores.

Weder's group also reported an approach to design mechanochromic mechanophores via cleavage of a weak ester bond coupled to a fluorophore.[82] Specifically, they prepared 2-(2'-hydroxyphenyl)benzoxazole in which two hydroxy groups at 2'-position of phenyl ring and 5-position of benzoxazol were functionalized with initiator groups for atom transfer radical polymerization and then synthesized PMA using the initiator (Figure 1-11b). When a solution of PMA with 2-(2'-hydroxyphenyl)benzoxazole was sonicated, the ester bond at phenyl ring is cleaved, and 2-(2'-hydroxyphenyl)benzoxazole exhibited excited-state intramolecular proton transfer (ESIPT), resulting in a red-shift of the fluorescence wavelength.

Besides, they recently reported that a triarylmethane unit, which is known as a protecting group for hydroxy groups, functions as a mechanochromic mechanophore (Figure 1-11c).[83] Although a triarylmethanol structure doesn't show any color, the C-O bond is heterolytically cleaved when a force is applied to the mechanophore and the resulting triarylmethane cation shows green color.

The "covalent" mechanophores described above display low reversibility because a large energy is required to recombine cleaved covalent bonds. Even for radical-generating mechanophores whose radicals can recombine easily in solutions, the distance between generated radicals is far and molecular motion is restricted in polymeric matrices, leading to low reversibility. To address this problem, Moore and co-workers developed an oxazine mechanophore (Figure 1-12a) that can quickly recover its initial state despite "covalent" mechanophore.[84] In the case of spiropyrans and naphthopyrans, isomerization from cis to trans forms occurs after the cleavage of their C-O bonds, which complicates the reverse reaction. In contrast, the oxazine mechanophore doesn't need such an isomerization and exhibits reversible and instant color changes. Using this motif, a mechanophore exhibiting near-infrared fluorescence has also been developed (Figure 1-12b).[85]

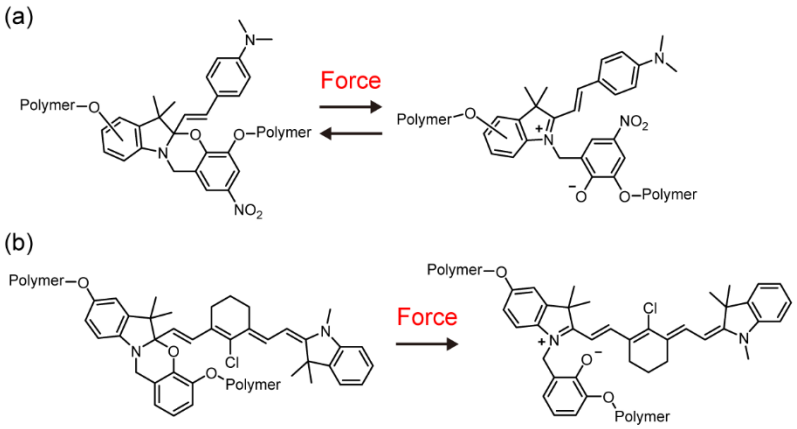

Figure 1-12. Molecular structures and operating mechanism of (a) an oxazine mechanophore and (b) an oxazine-based mechanophore showing near infrared emission.

1.3.3. “Non-Sacrificial” Mechanochromic Mechanophores

Due to its operating mechanism, “covalent” mechanophores have several challenges in addition to low reversibility. For example, the activation of such mechanophores requires large forces (~1 nN, at least 160 pN) to cleave covalent bonds, which is not suitable for the detection of forces of several to 100 pN that is generated by cells or is received by a single polymer chain before scission of covalent bonds. Besides, some mechanophores would be activated by external stimuli other than force, such as heat, light, and pH changes. To overcome these inherent issues, "non-sacrificial" mechanophores, which exhibit changes in photophysical properties through (i) conformational changes in molecules or (ii) control of intra- or intermolecular interaction, have recently attracted attention.[40] In particular, “non-sacrificial” mechanophore based on controlling intra- or intermolecular interactions are called supramolecular mechanophores.

Universal joint mechanophores

To the best of my knowledge, a universal joint mechanophore is the first example of a “non-sacrificial” mechanochromic mechanophore.[86] This mechanophore is composed of two 5,5’-diphenyl-2,2’-bithiophene energy donors which three-dimensionally connect to a porphyrin energy acceptor to form universal joint-like architecture (Figure 1-13). In

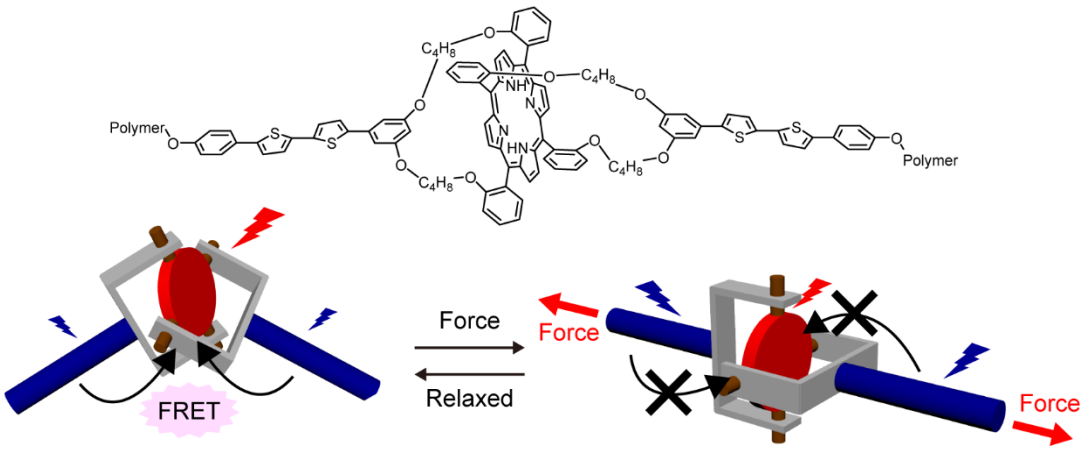

Figure 1-13. Molecular structure and schematic illustration of operating mechanism of a universal joint-shaped mechanophore.

solutions and a PDMS film before stretching, red fluorescence is mainly observed because directions of transition dipole moments of the bithiophene donors and the porphyrin acceptor are random, leading to efficient FRET from the energy donor to the energy acceptor. When a force is applied to the PDMS film in which the mechanophore is introduced, the FRET efficiency significantly decreases because the transition dipole moments of donor and acceptor become mutually perpendicular, and thus blue fluorescence of the donor is observed. This ratiometric mechanochromic luminescence by controlling the FRET efficiency is reversible, however, the reverse process takes some long time, presumably due to slow conformational relaxation in the viscoelastic material.

FLAP mechanophore

Saito and co-workers developed a flapping molecular force probe (FLAP) composed of two rigid anthraceneimide fused with a flexible cyclooctatetraene (COT) (Figure 1-14a).[87] In the ground state of FLAP, the COT ring is most stable in its bent form. When excited, FLAP has two energy minima in the singlet excited state with bent and planar structures which show blue and green fluorescence, respectively. In viscous matrices such

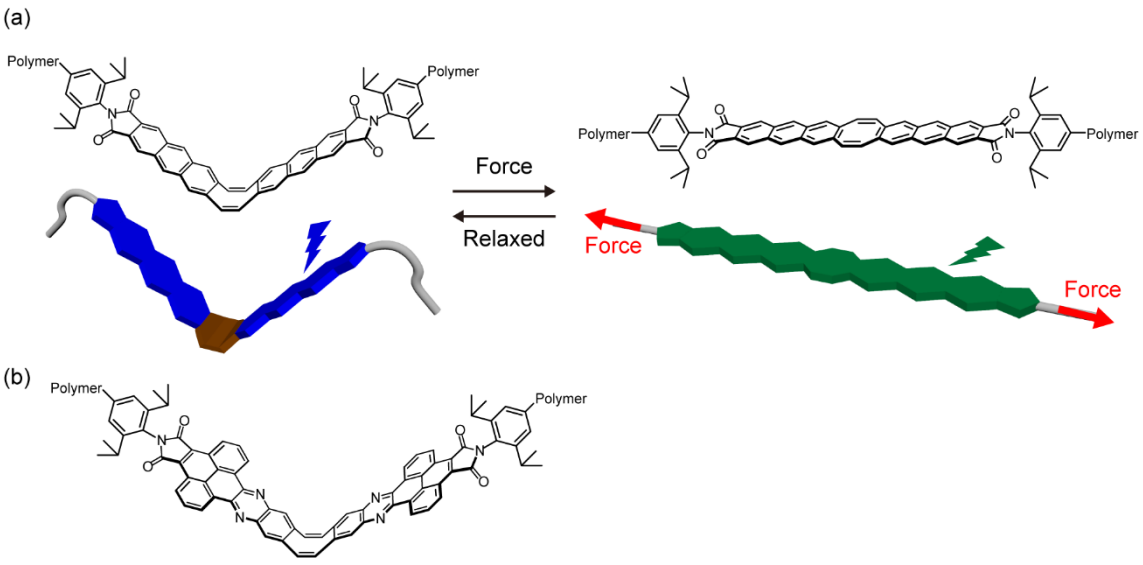

Figure 1-14. (a) Molecular structure and operating mechanism of a FLAP mechanophore based on anthraceneimides. (b) Molecular structure of a FLAP mechanophore featuring pyreneimide-fused pyrazaacene.

as polymers, the conformational change is hampered and blue fluorescence is preferentially observed. Upon applying forces to the FLAP mechanophore via polymer chains, FLAP becomes planar and the planar FLAP exhibits green fluorescence due to the extended π-conjugation. The bend form rapidly recovers after removing forces, indicating high reversibility. Based on DFT calculation, the planarization of FLAP requires ~100 pN, which is much smaller than the forces required for the activation of "covalent" mechanophores. However, for this molecule, the energy barrier for activation from the bent form to the planar form in the excited state is low. Therefore, a small amount of green fluorescence derived from the planar form is observed even when no force is applied, resulting in a low mechanoresponsiveness. To increase the activation barrier, they also reported a new FLAP mechanophore using pyreneimide-fused pyrazaacene as rigid wings (Figure 1-14b).[88] The excited-state planarization of the new FLAP mechanophore is surpressed in the force-free state, leading to the improvement of the mechanoresponsive luminescence behavior.

Cu complex mechanophores

Cu(I) complexes coordinated by four nitrogen atoms (Figure 1-15) don't display phosphorescence as nonradiative relaxation is dominant due to quick ligand exchange in solutions. In contrast, the ligand exchange is slow in the solid state, leading to the observation of strong red phosphorescence. Filonenko et al. reported that the Cu complexes function as mechanophores.[89,90] When the complex is incorporated into the

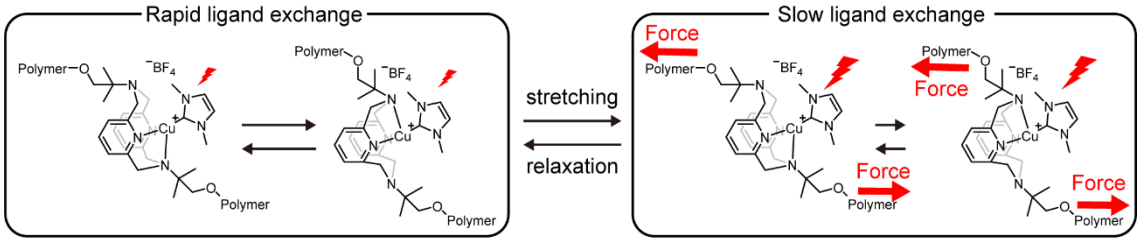

Figure 1-15. Molecular structures and operating mechanism of a Cu-comlex mechanophore.

polyurethane, the ligand exchange occurs, although not as rapid as in solutions, and weak phosphorescence is observed in the force-free state. Applying forces to the Cu complex prevents the ligand exchange, resulting in strong phosphorescence.

Torsion spring mechanophores

Sommer and co-workers reported mechanochromic torsional spring mechanophores. The firstly reported torsion spring mechanophore consists of diketopyrrolopyrrole (DPP) as an electron acceptor and two phenyl groups substituted at the ortho-position of DPP as electron donors (Figure 1-16a).[91] In the force-free state, the dihedral angle between DPP and two phenyl groups is large due to the steric hindrance between them, and thus charge transfer interaction between phenyl groups and DPP is negligible. When a force is applied to the mechanophore via polymer chains attached to two phenyl groups, the dihedral angle becomes small and the contribution of charge transfer interactions increases, which leads to red-shifted absorption and fluorescence spectera. The mechanoresponsive behavior is instant and reversible, however, the changes in the photophysical properties are small. To improve the mechanochromic response, they developed an *ansa*-DAD spring in which two donors are mechanically coupled via a linker (Figure 1-16b).[92] Besides, the donor

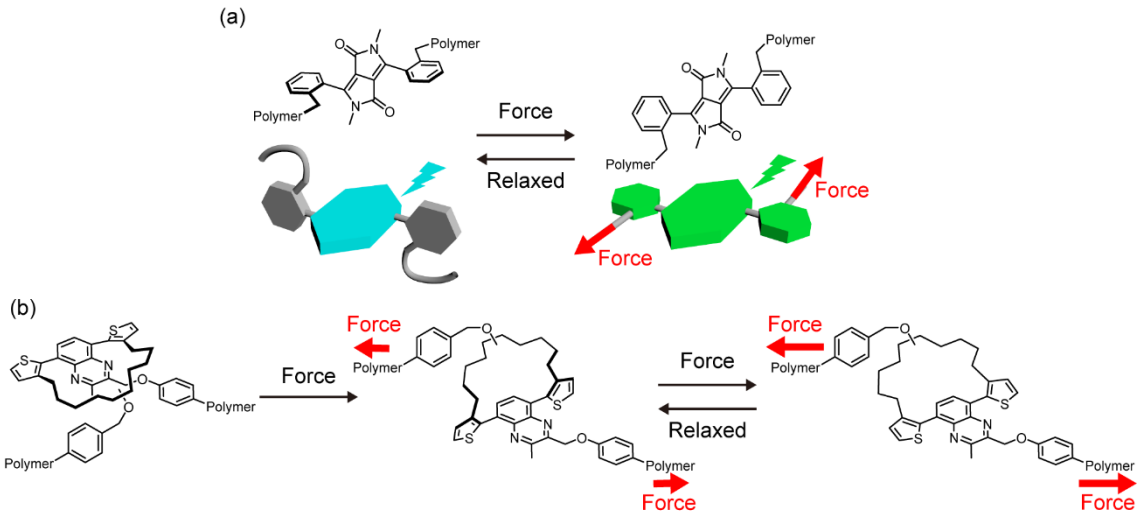

Figure 1-16. Molecular structures and operating mechanism of (a) prototype of DAD spring and (b) *ansa*-DAD spring mechanophores.

and acceptor are replaced with thiophene and quinoxaline derivatives, respectively. The mechanophore undergoes conformational redistribution in the form of a thiophene ring flip followed by planarization. The thiophene ring flip is induced by small forces compared to the planarization of the torsion spring and causes significant changes in the fluorescence wavelength. In torsion spring mechanophores, the planarization is fully reversible, however, the ring flip is irreversible.

ESIPT-based mechanophore

Sijbesma and Ma's group reported mechanophores based on the reversible control of ESIPT by mechanically conformational changes.[93] They introduced (2-hydroxyphenyl)benzimidazole having four hydroxy groups into a polyurethane (Figure 1-17), and the resulting polyurethane film showed blue-green fluorescence of keto form due to ESIPT besides blue fluorescence of enol form. When a force is applied to the mechanophore via the polymer chains, the dihedral angle between the phenyl group and benzimidazole unit becomes larger, which prevents the formation of hydrogel bonds between the hydroxy group and nitrogen atom. Consequently, the ESIPT luminescence is suppressed, and the intensity of blue fluorescence increases. This process is reversible, similar to other "non-sacrificial" mechanophores.

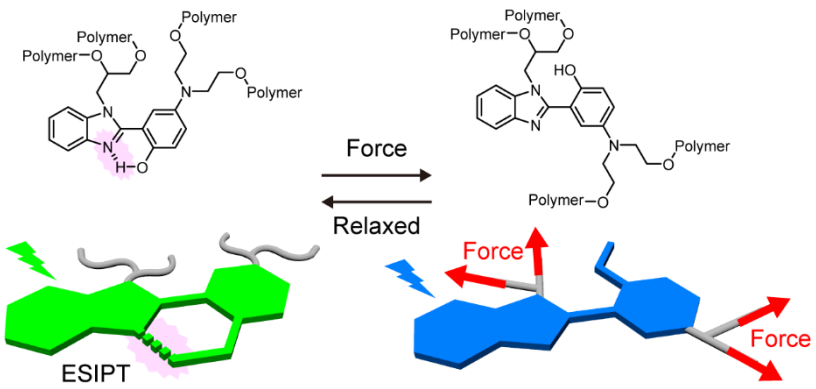

Figure 1-17. Molecular structure and operating mechanism of a ESIPT-based mechanophore.

Mechanophores based on vase-kite conformational changes

A tetraquinoxaline cavitand (QxCav)-based mechanophore is reported by Dalcanale and co-workers (Figure 1-18).[94] QxCav shows two conformations of an expanded kite and a contracted vase, and the vase form is more stable. When the rigid polyurethane in which QxCav is incorporated is stretched, the absorption and fluorescence wavelength are slightly red-shifted with conformational changes from the vase to the kite. While the mechanical activation of QxCav was observed when QxCav was introduced into a rigid PU film, a PDMS film in which QxCav was incorporated doesn't show any color changes upon deformation. This might result from the higher magnitude of force required for activation of QxCav than that of spiropyran mechanophores which are successfully activated in the PDMS.[43]

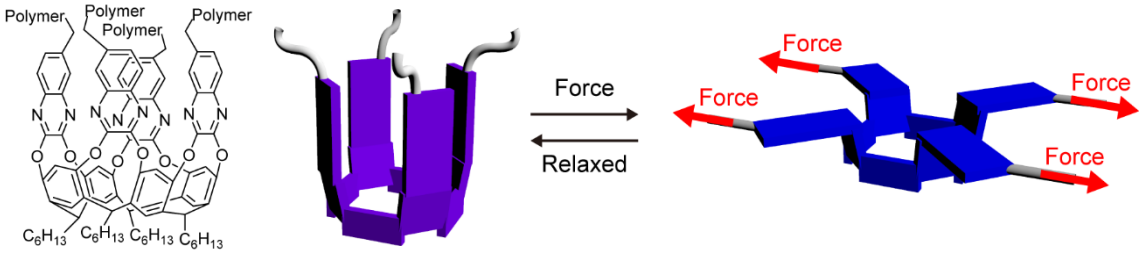

Figure 1-18. Molecular structure and operating mechanism of a mechanophore based on vase-kite isomerization.

Loop mechanophores

Weder et al. reported a loop-shaped mechanophore in which two perylene diimide units are covalently connected via a flexible chain (Figure 1-19a).[95] In the force-free state, this mechanophore folds into a loop and displays red luminescence due to the excimer formation. The loop structure is changed to linear form when the PMA containing loop mechanophore is subjected to mechanical stimuli and the intensity of monomer fluorescence increases. The fluorescence color change is reversibly and ratiometrically altered in proportion to the strain of the polymer.

Imato and co-workers also demonstrate that a linear molecule in which one pyrene and two naphthalene diimide derivatives are connected works as a "non-sacrificial" mechanophore (Figure 1-19b).[96] The pyrene and naphthalene diimide are stacked to form a CT complex and pyrene fluorescence is quenched in the force-free state. When forces are applied to poly(ε-caprolactone) in which the mechanophore is incorporated, the CT complex is broken and the polymer films display blue fluorescence of pyrene. Although the operating mechanism of this mechanophore is similar to Weder's loop mechanophore, the films don't show reversible mechanoresponsive behavior. This is because the strain-induced crystallization of poly(ε-caprolactone) restricts the molecular mobility of the mechanophore and prevents restoration of the CT complex.

Li et al. recently introduced dipyrene-terminated oligosilanes whose working mechanism is similar to the two loop-like mechanophores (Figure 1-19c).[97] In the case of two pyrenes linked with three silicon atoms, the pyrenes easily fold and show excimer emission. This excimer formation is dissociated by applying force, leading to an increase

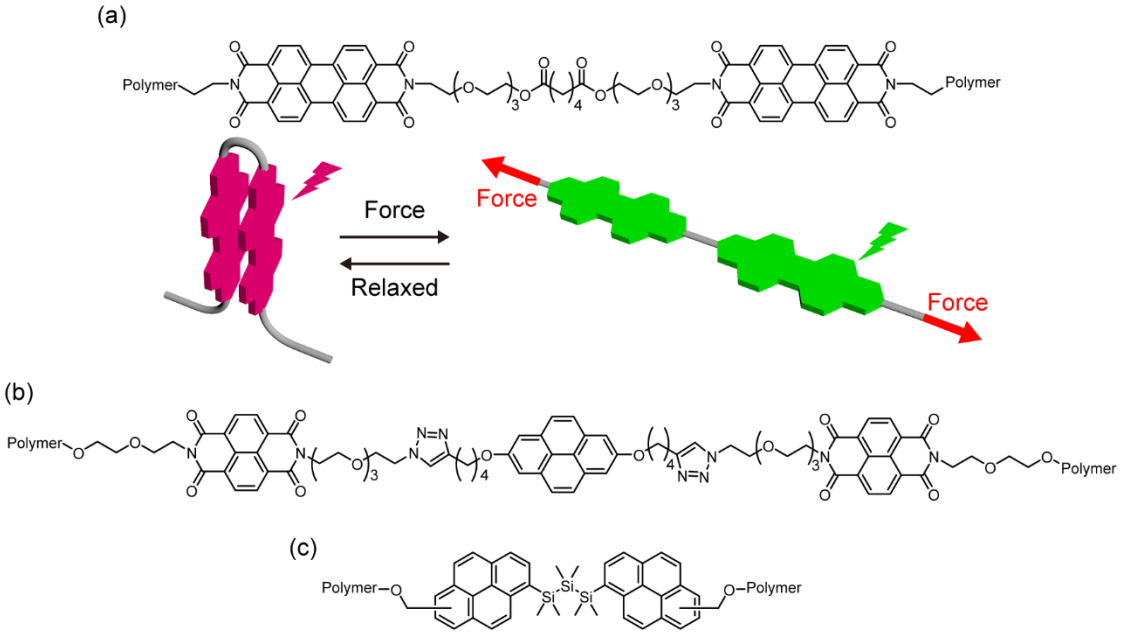

Figure 1-19. (a) Molecular structure and operating mechanism of a loop mechanophore based on two perylene diimide. (b,c) Molecular structures of loop-like mechanophores based on (b) one pyrene and two naphthalene diimide derivatives and (c) dipyrene-terminated oligosilanes.

in monomer emission intensity. The decrease in the amount of silicon atoms causes the limitation of conformational change, leading to difficulty in excimer formation and less mechanoresponsiveness.

Cyclophane mechanophores

Sagara group has developed a cyclophane-based mechanophore in which two 1,6-bis(phenylethynyl)pyrenes are linked via flexible ethylene glycol chains (Figure 1-20a).[98] In the force-free state, two pyrene derivatives form excimer and exhibit green fluorescence. When a force is applied to the cyclophane, the distance between the pyrene derivatives increases and the excimer formation is suppressed. Thus, the blue monomer

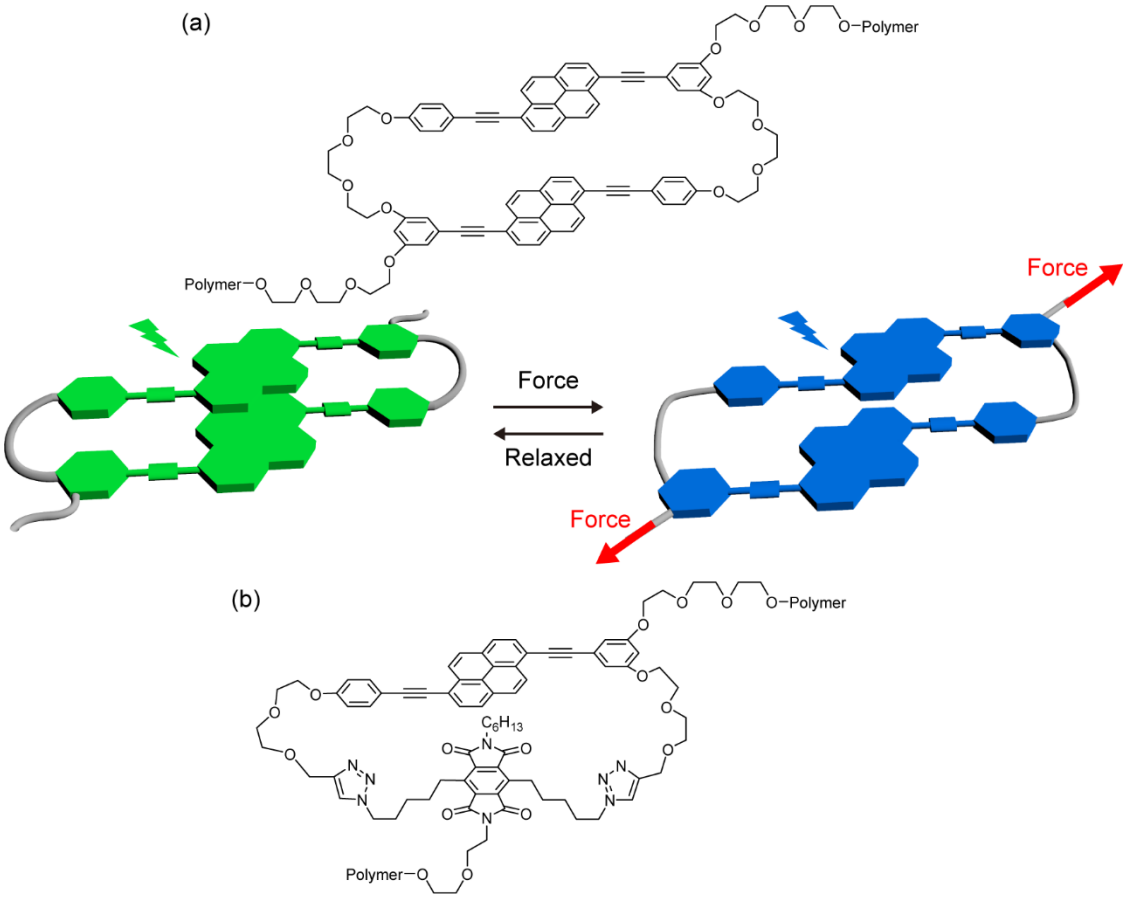

Figure 1-20. (a) Molecular structure and operating mechanism of a cyclophane-based mechanophore featuring two pyrene derivatives. (b) Molecular structure of a cyclophane-based mechanophore composed of a π-extended pyrene and PMDI.

emission is observed. This mechanophore shows a correlation between the strain of the polymer and the ratio of monomer to excimer emission intensity, similar to the loop mechanophore that Weder's group reported.[95] However, the fraction of excimer formation is limited in the polymer, the change in the fluorescent color is small and evaluation by the naked eye is difficult. Sagara group also reported another cyclophane mechanophore in which a blue-light emitting 1,6-bis(phenylethynyl)pyrene and a pyromellitic diimide (PDMI) form a CT complex with reddish-orange emission in the force-free state (Figure 1-20b).[99] When a force is applied to PU film containing the cyclophane, the intensity of CT emission decreases, while blue fluorescence intensity increases due to spatial separation between the pyrene derivative and PDMI. As a result, the ratiometrically reversible change in the emission color was detectable by the naked eye compared to the first cyclophane mechanophore.

Mechanophore using host-guest chemistry

Dalcanale and co-workers reported that a host-guest complex mechanophore composed of an N-methyl pyridinium salt linked to a pyrene unit and tetraphosphonate cavitand as guest and host, respectively (Figure 1-21).[100] The tetraphosphonate cavitand interacts with pyridinium salt to form a stable complex in non-polar solvents and PDMS which is

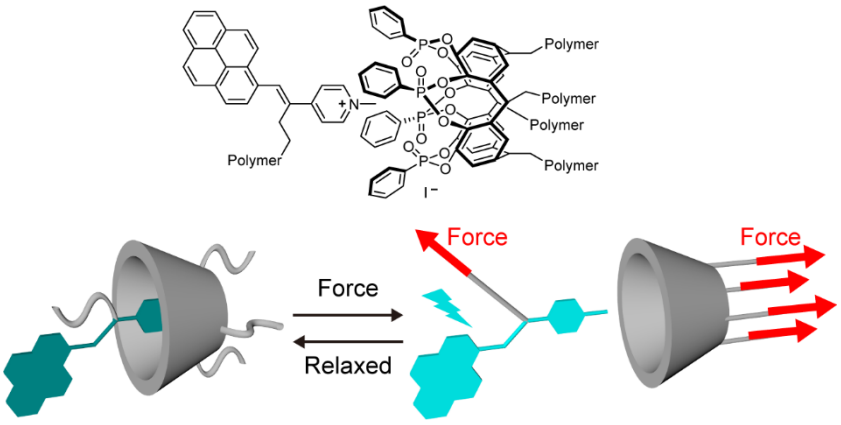

Figure 1-21. (a) Molecular structure and operating mechanism of a mechanophore featuring based on host-guest chemistry.

a hydrophobic matrix, resulting in quenching the pyrene fluorescence. When the complex is subjected to forces, the host and guest are spatially separated and thus the fluorescence of pyrene is observed.

1.4. Mechanophores Utilizing Rotaxanes

Mechanically interlocked molecules (MIMs) are molecules with mechanical bonds in which two or more molecules are not spatially separated from each other even though the molecules are not linked via any covalent bonds.[101–104] Two typical examples of MIMs are catenanes composed of two or more topologically linked macrocyclic molecules (Figure 1-22a) and rotaxanes which consist of at least one cyclic molecule (ring) threaded onto at least one linear molecule (axle) with two bulky end groups (stoppers) preventing the dethreading of the ring (Figure 1-22b). These MIMs show unique molecular motions such as circumrotation and elongation of catenane (Figure 1-22a) besides molecular shuttling of rotaxane (Figure 1-22b). Using such molecular motions, MIMs can be exploited to achieve various functional materials such as molecular switches,[105–108] molecular muscles,[109–111] and molecular pumps.[112–116] The architectures are also fascinating platforms to design supramolecular mechanophores because the interlocked structure and the molecular motions allow us to easily achieve chromic properties and

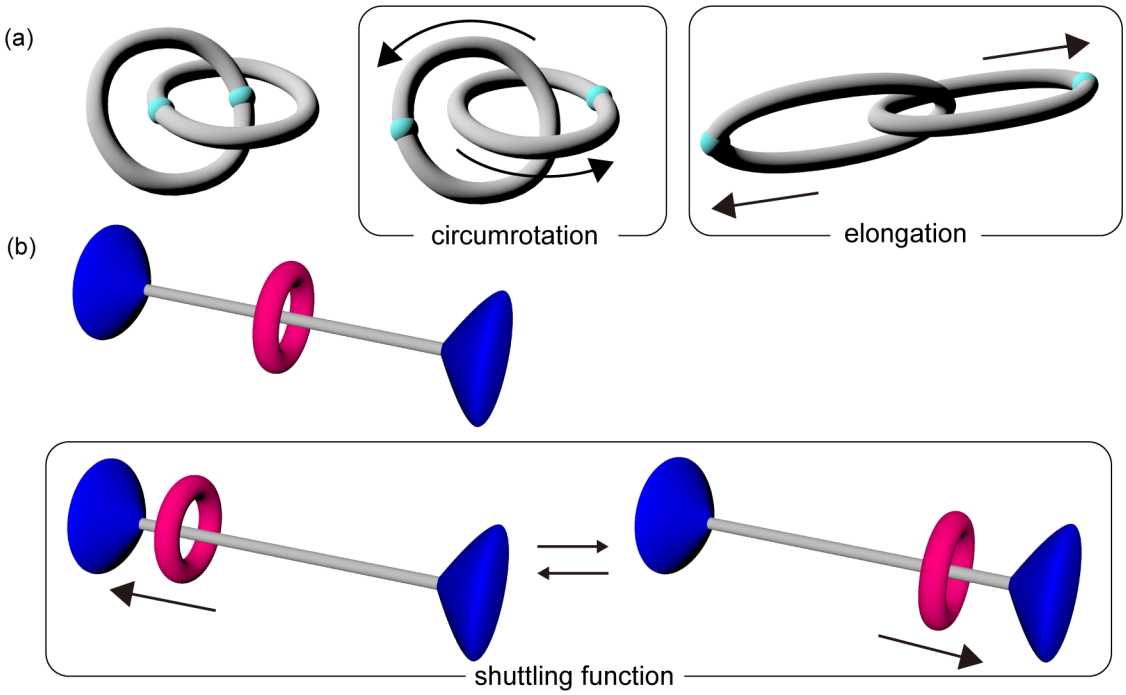

Figure 1-22. Schematic illustration of structures and molecular motions of (a) catenane and (b) rotaxane.

reversible nature after introducing proper π-conjugated groups to ring or axle moieties. In this context, several mechanophores have been reported exploiting rotaxane.[117–125]

Stoddart and co-workers first demonstrated that a rotaxane works as a mechanophore in 2011.[117] The rotaxane in which a cyclobis(paraquat-*p*-phenylene) (CBPQT) cycle is threaded onto an axle equipped with dioxynaphthalene (DNP) in its center has an absorption band in the visible region due to CT complex between CBPQT and DNP (Figure 1-23). When THF solutions of the rotaxane are sonicated, the intensity of CT absorption decreases presumably due to the collapse of the interlocked structure.

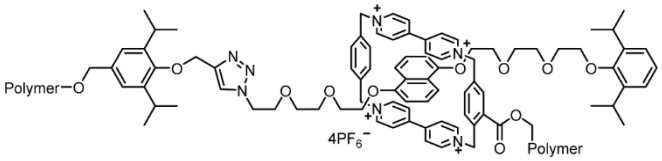

Figure 1-23. Molecular structure of the first reported rotaxane-based mechanophore.

Following the report, Sagara group has recently developed rotaxane-based supramolecular mechanophores composed of a cycle containing a fluorophore and an axle molecule equipped with an electronically matched quencher at its center and two stoppers in the peripheral positions.[118–122] In the first report, a benzothiadiazole derivative and a naphthalene diimide are chosen as the fluorophore and quencher, respectively (Figure 1-24).[118] In the force-free state, the cycle is preferably located around the quencher due to

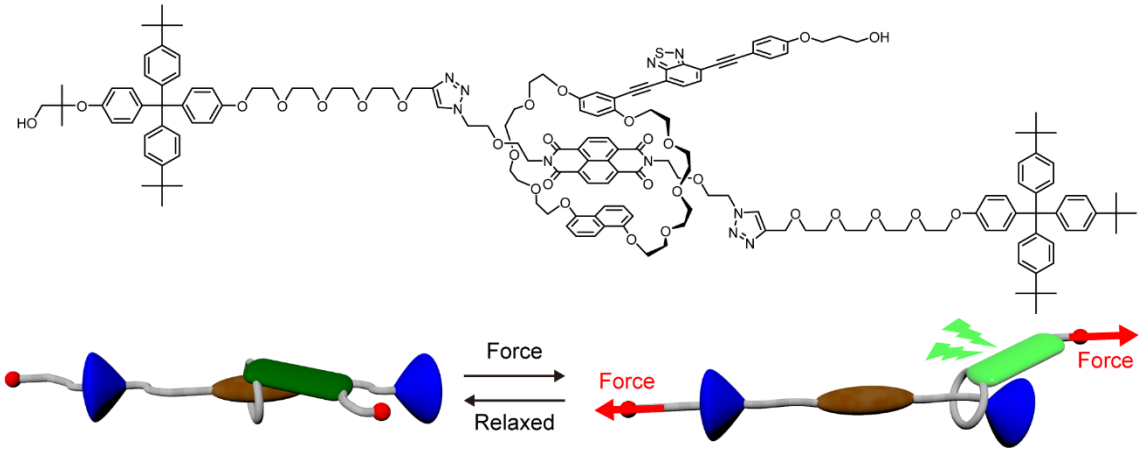

Figure 1-24. Molecular structure and schematic illustration of operating mechanism of our rotaxane-based mechanophore.

CT interaction, and the CT interaction between the cycle and quencher or photo-induced electron transfer (PeT) causes the quenching of fluorescence. Upon applying forces to the rotaxane, the cycle is pulled away from the quencher, leading to strong green fluorescence. The mechanoresponsive luminescence behavior of the rotaxane mechanophore is instant and reversible.

One advantage of this rotaxane-based supramolecular mechanophore is readily alteration of the fluorescence color by changing the fluorophore to other ones.[119] The rotaxane containing blue-emissive pyrene, green-emissive anthracene, or orange-emissive 4-(dicyanomethylene)-2-methyl-6-(4-dimethylaminostyryl)-4*H*-pyran derivatives, respectively, shows on/off switching of the corresponding fluorescence color (Figure 1-25). Besides, a polyurethane elastomer displaying on/off switching of white

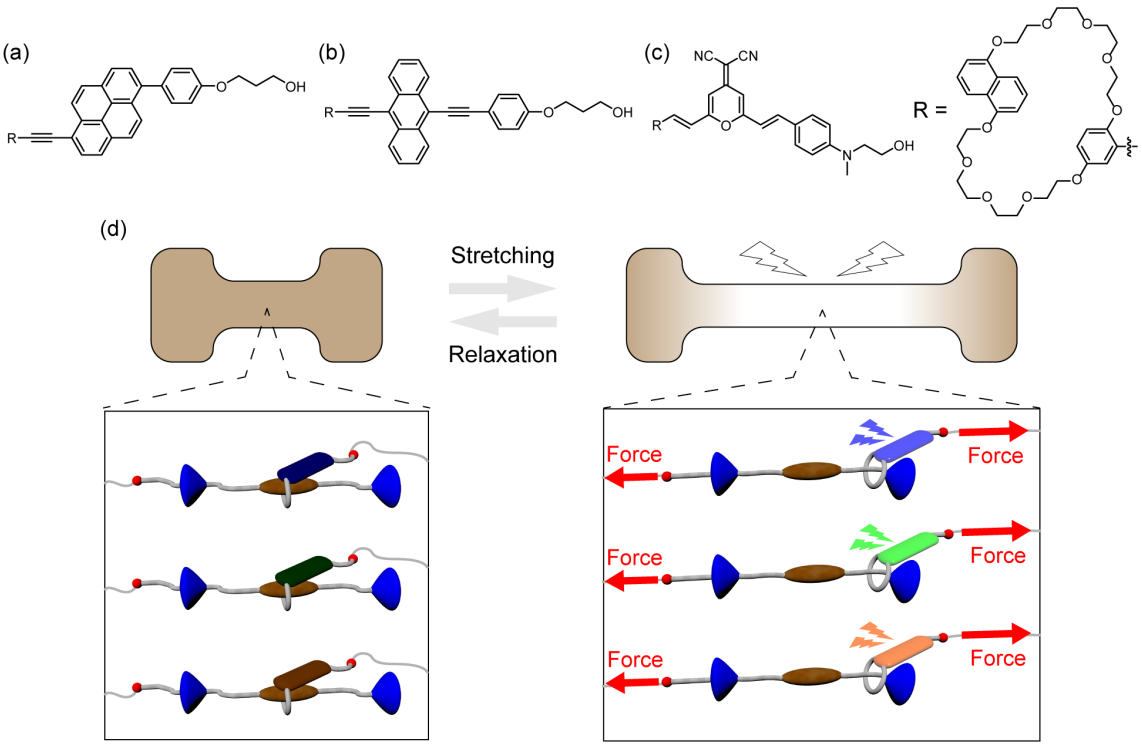

Figure 1-25. (a-c) Molecular structures of (a) blue-, (b) green, and (c) orange-emitting cyclic compounds. (d) Schematic illustration of white-light-emitting mechanoresponsive polyurethane elastomer blending three polymers with different rotaxane-based mechanophores

luminescence upon deformation can be prepared by blending the appropriate amount of each rotaxane-incorporated polymer.

Recently, De Bo group also published several reports on mechanophores using rotaxane structure.[123–125] In 2018, they prepared a rotaxane having a mechano-active furan-maleimide cycloadduct as one side of a stopper and examined the impact of rotaxane structure on the activation of the "covalent" mechanophore (Figure 1-26a).[123] Unlike when the polymers are introduced directly into the cycloadduct, the force begins to be applied to the cycloadduct after the cyclic molecule moves to the stopper in the rotaxane. Besides, tensile stress is distributed not only in the DA adduct but also where the cyclic and axle molecules are in contact. Due to these effects, the cycloadduct on the axle molecule of rotaxane has a slower mechano-activation rate than when a polymer chain is simply introduced to the cycloadduct. In contrast, if the stopper is changed to a

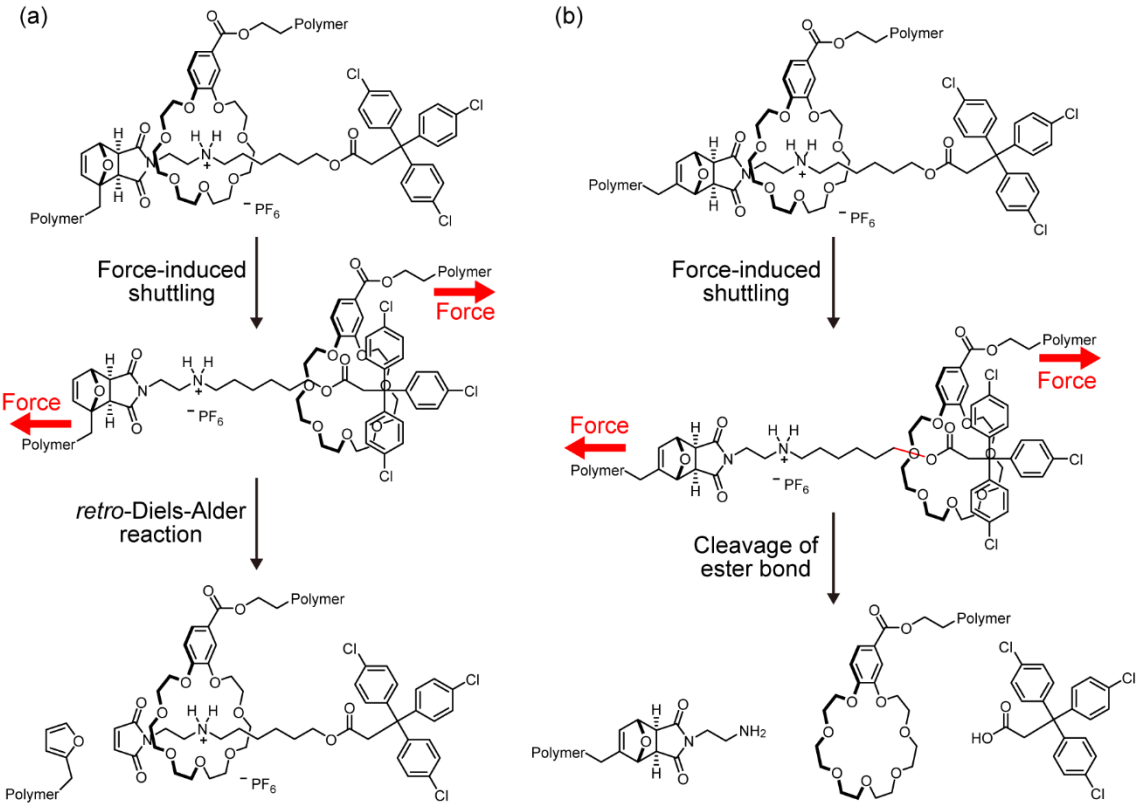

Figure 1-26. Operating mechanism of (a) retro-Diels-Alder reaction on rotaxane structure and (b) collapse of the interlocked molecule due to the cleavage of ester bond on the axle.

mechano-inactive cycloadduct, the mechano-behavior of this rotaxane changes drastically.[124] When force is applied and the cyclic molecule moves into the stopper, a covalent bond breakage occurs at the ester bond site on the axle since tensile stress is especially applied (Figure 1-26b). In 2021, they reported a mechanochromic rotaxane-based supramolecular mechanophore that uses different mechanisms from ours.[125] The rotaxane has aminochloromaleimide (ACM) moiety on the axle and ACM is included by the cycle featuring both a hydrogen bond donor unit (pyridyl-2,6-dicarboxyamide) and a hydrogen bond acceptor crown ether-like region (Figure 1-27). The ACM unit shows very weak fluorescence in water, while the ACM included by cycle displays strong green fluorescence due to the presence of two electron-rich aromatic groups and the hydrogen bond network. Thus, the polyacrylamide gels containing this rotaxane show strong green fluorescence before stretching and the fluorescence intensity decreases upon deformation because the cycle is pulled away from the ACM unit. This mechanochromic behavior is theoretically reversible, however, the initial fluorescence did not recover in the polyacrylamide gels. This indicates that the cycle cannot return to near the ACM unit probably due to the formation of strong hydrogen bonds between polar groups in the gel and rotaxane components after stretching and/or the mechanical dissociation of the interlocked structure.

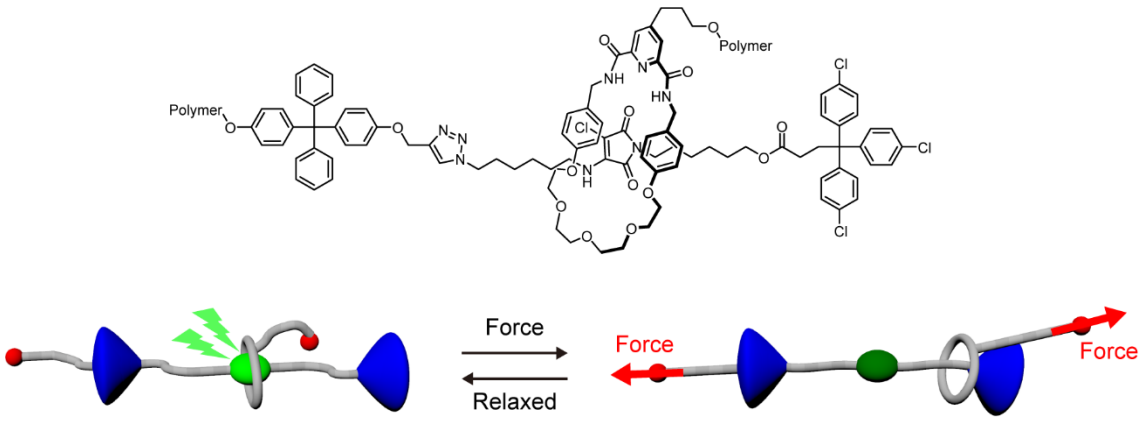

Figure 1-27. Molecular structure and schematic illustration of operating mechanism of a rotaxane-based mechanophore reported by De Bo group.

1.5. Processes Related to Photoexcitation[126,127]

1.5.1 Energy Levels and Transitions in Molecules

In general, molecules exist in a stable ground state with the lowest electronic energy, however, when they are excited by light, they transition to an excited state with high electronic energy. The electronic state transition of a photoexcited molecule is shown as a Jablonski diagram (Figure 1-28). The left axis shows the energy of the molecule. One electron in the electronic ground state (S_0) is excited to a higher energy state (S_1, S_2, and so on) by light excitation. After the transition to the highly excited state, the electrons undergo transition to the lowest excited singlet state (S_1) via vibrational relaxation and internal conversion. Then, the electrons return to the ground state with fluorescence and/or non-radiative deactivation. Fluorescence appears in a longer wavelength range compared to the absorbed light because absorption is the transition from the lowest vibrational level of the S_0 state to various vibrational levels of the excited state, whereas fluorescence is the transition from the lowest vibrational level of the S_1 state to the various vibrational levels of the S_0 state. In this situation, fluorescence and/or non-radiative deactivation rarely occur from excited states at energy levels higher than the S_1 state, which is called Kasha's rule. In addition to fluorescence and/or non-radiative deactivation,

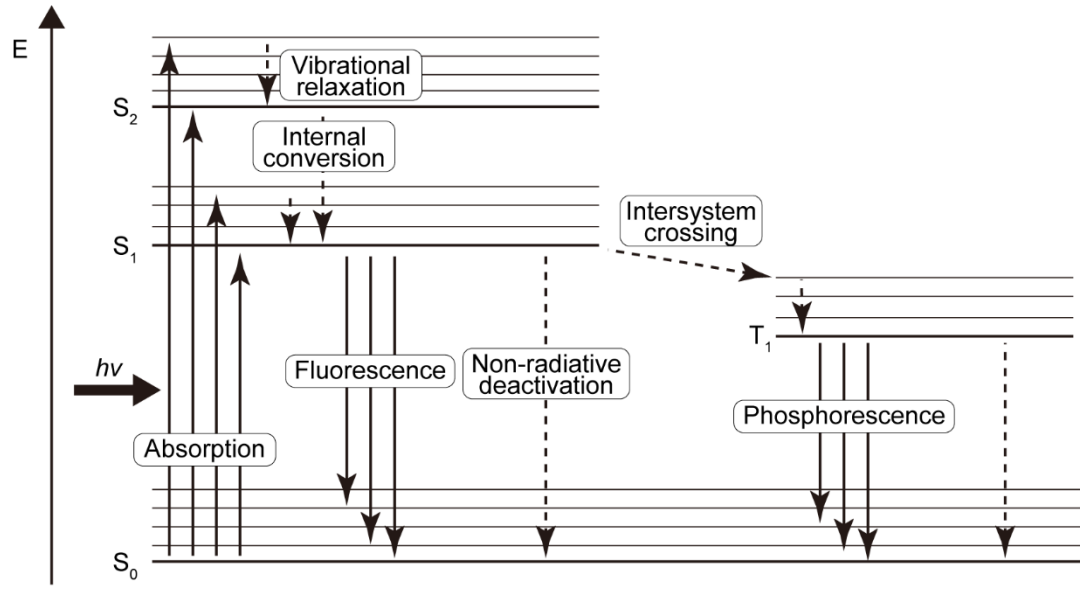

Figure 1-28. Jablonski diagram.

transition from the S_1 to the lowest excited triplet state (T_1) can occur, which is called intersystem crossing. This transition is forbidden in principle because of the difference in spin multiplicity, however, spin-orbit interactions make the transition permissible. The probability of intersystem crossing increases mainly in the presence of atoms with large atomic numbers or metals with unpaired electrons. The process of returning from the T_1 state to the ground state can also emit light, which is called phosphorescence. Since the T_1 state is a lower energy state than S1, phosphorescence is observed at longer wavelengths than fluorescence and has a significantly longer lifetime.

The ratio of the number of photons absorbed by a molecule to the number of photons of fluorescence is called the fluorescence quantum yield. When a molecule in the excited singlet state returns to the ground state via fluorescence, non-radiative deactivation, and intersystem crossing, the quantum yield of fluorescence φ is given as the following equation.

$$\varphi = \frac{K_f}{K_f + K_n + K_{ISC}} \quad (1)$$

where K_f, K_n, and K_{ISC} are the rate constants for the respective reactions. Besides, the concentration of an excited molecule decays with a first-order exponential function in a decay process unless other transitions, such as twisted intramolecular charge transfer, are involved. The value at which the concentration becomes 1/e of its initial value is called the lifetime τ and is given by

$$\tau = \frac{1}{K_f + K_n + K_{ISC}} \quad (2)$$

These transitions occur within a single molecule, and when two or more molecules exist in close proximity, the intermolecular interactions that act between them can cause various phenomena such as intermolecular electron transfers, energy transfers, and charge transfers. These lead to photophysical properties different from those of the original molecule.

1.5.2. Photo-Induced Electron Transfer (PeT)

Photo-induced electron transfer (PeT) is an electron transfer process that occurs from a photo-excited electron donor to a ground-state electron acceptor (d-PeT), or from an excited electron acceptor to a ground-state electron donor (a-PeT). The lowest unoccupied molecular orbital (LUMO) of the acceptor needs to be lower than that of donor in d-PeT, and the highest occupied molecular orbital (HOMO) of acceptor needs to be lower than that of donor in a-PeT. (Figure 1-29). In the former process, an electron of the donor, which have transitioned to the LUMO upon excitation, is transferred to the LUMO of the acceptor molecule. As a result, no fluorescence of the donor is observed if the donor is a fluorophore. In contrast, in the latter process, an electron in the HOMO of the donor is transferred to a hole in the HOMO of the acceptor molecule generated by the excitation. Consequently, an excited electron of the acceptor molecule is unable to return to the original ground state, resulting in no fluorescence if the acceptor is a fluorophore. In our rotaxane-based supramolecular mechanophore, the d-PeT occurs in the force-free state, which partially plays a role in causing quenching of fluorescence.

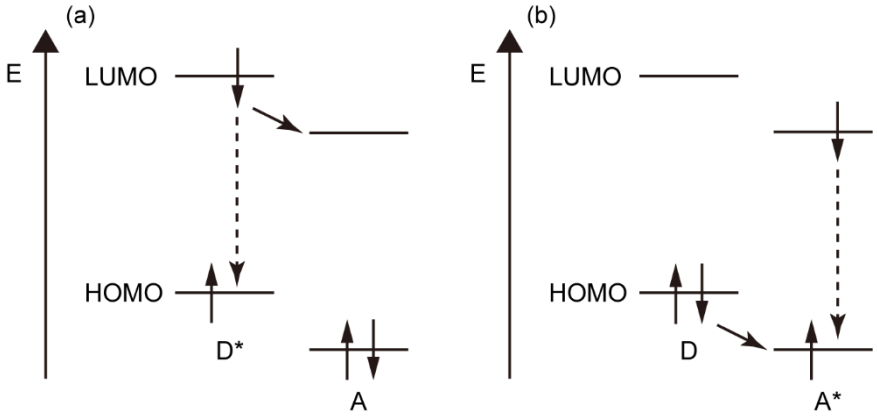

Figure 1-29. Mechanism of (a) d-PeT and (b) a-PeT.

1.5.3. Förster (Fluorescence) Resonance Energy Transfer (FRET)

When a ground-state acceptor molecule is placed in the vicinity of an excited fluorescent donor molecule, the resonance of the wave functions of each molecule causes an energy transfer, resulting in a ground-state donor and an excited acceptor (Figure 1-30). This energy transfer, which does not require overlapping electronic orbitals between molecules, is called Förster (fluorescent) resonance energy transfer. The efficiency of FRET is described by the following equations.

$$E=\frac{R_0^6}{R_0^6+r^6} \quad (3)$$

$$R_0^6=\frac{9}{4(2\pi)^5} * \frac{2303}{N} * \kappa^2 \varphi_D n^{-4} J(\lambda) \quad (4)$$

$$J(\lambda) = \int f(\lambda)\varepsilon(\lambda)\lambda^4 d\lambda \quad (5)$$

$$\kappa^2 = (cos^2\theta_r - 3\cos\theta_A\cos\theta_D)^2 \quad (6)$$

where, $f(\lambda)$ is the normalized fluorescence intensity of the donor, $\varepsilon(\lambda)$ is the extinction coefficient of the acceptor, N is Avogadro's number,φ_D is the fluorescence quantum yield of the donor, n is the refractive index, θ_r is the angle between the transition dipole moments of donor and acceptor (Figure 1-31), θ_A and θ_D are the angles between the transition dipole moment of the acceptor or donor and the line connecting the two fluorophores, respectively, and the constants preceding κ have an aggregate value of 8.79 $\times 10^{-11}$ M cm nm^2. From these equations, FRET efficiency largely depends on the overlap of the fluorescence spectrum of the donor molecule and the absorption spectrum of the

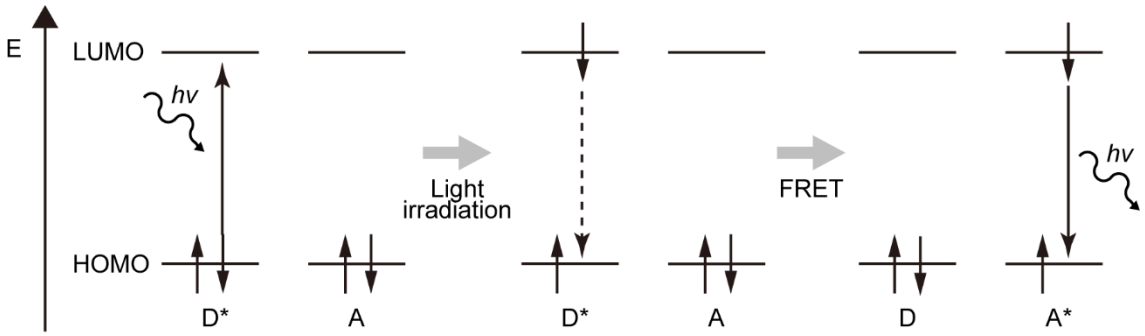

Figure 1-30. Mechanism of FRET.

acceptor molecule, the distance between the donor and acceptor, and the orientation of the transition dipole moment of the two molecules. Although the FRET efficiency is inversely proportional to the one-sixth power of the distance between the donor-acceptor, energy transfer could take place even at a relatively long distance (100 Å).

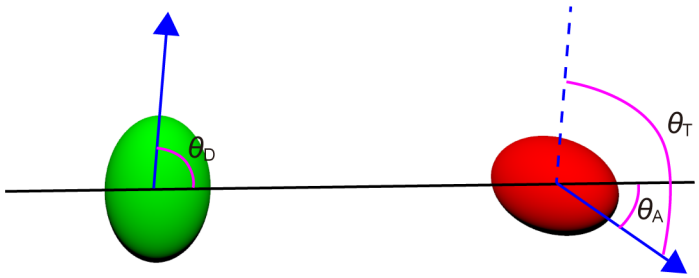

Figure 1-31. Relative arrangement of transition dipole moments (blue arrows) for a donor and an acceptor. The black line is the line connecting the donor and acceptor.

1.5.4. Dexter Energy Transfer

The energy transfer that occurs when electrons are exchanged between an excited donor molecule and a ground-state acceptor molecule is called Dexter energy transfer (Figure 1-32). In the Dexter mechanism, unlike FRET, the overlap of the electronic orbitals of the donor-acceptor molecule is important. The energy transfer rate constant is given by the following equation.

$$k_{\mathrm{ET}} = \left(\frac{4\pi^2}{h}\right)K^2 \exp\left(-\frac{2r}{L}\right) \qquad (6)$$

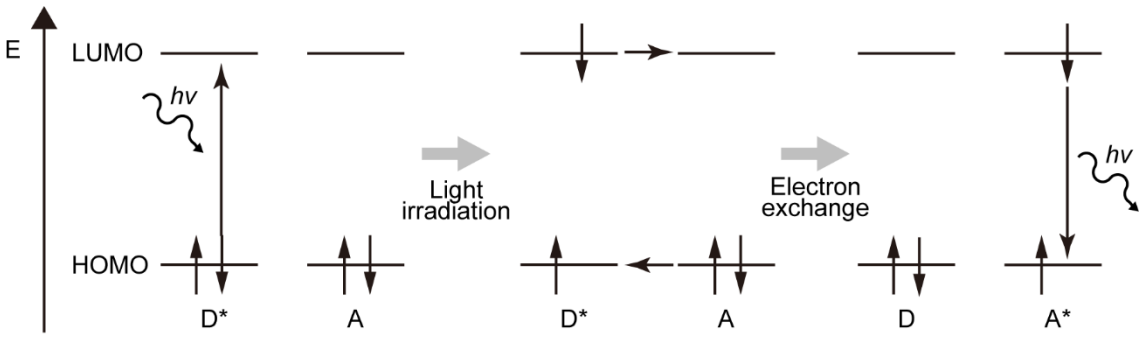

Figure 1-32. Mechanism of Dexter energy transfer.

where *K* is a constant and *L* is the sum of the van der Waals radii of the donor and acceptor molecules. Since the magnitude of the electronic wavefunction decays exponentially with distance from the nucleus, the energy transfer rate constant decreases exponentially as the distance between the donor-acceptor increases.

1.5.5 Charge Transfer Interaction

CT complexes are complexes formed by electron-donating molecules with low ionization potentials and electron-withdrawing molecules with high electron affinity in the ground state (Figure 1-33). The CT complex exhibits a broad absorption band with no vibrational structure in the longer wavelength region, which is not observed in each of the constituent molecules. The broadening is attributed to the small binding energy of CT complexes, which can undergo equilibrium mixtures of many different geometries. Furthermore, the absorption wavelength of the CT complex varies greatly with the polarity of the solvent. This is because CT complexes are stabilized by solvation and the maximum of the absorption band shifts to the longer wavelength region in polar solvents.

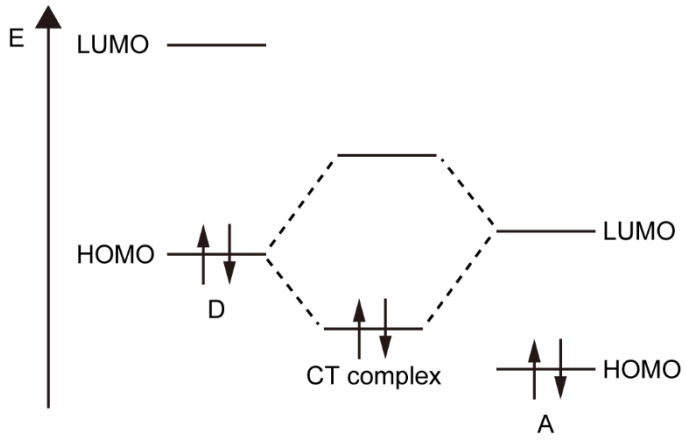

Figure 1-33. Mechanism of CT interaction.

1.5.6. Excimer and Exciplex

While CT complexes are formed by partial charge transfer between a donor and an acceptor in the ground state, the collision of an excited molecule with another molecule in the ground state form a stable exciter state dimer. This dimer is termed “excimer” when the dimer is composed of the same two molecules, or “exciplex” when two different molecules are involved. Excited complexes are readily formed under conditions of high concentration or in compounds in which two fluorophores are linked consecutively, and they exhibit emission at longer wavelength regions than the respective single molecule.

1.6. Objective

In this thesis, I demonstrate further functionalization of rotaxane-based supramolecular mechanophores. Forces at several to several tens of piconewton generated by cells have important effects on biological system such as cell adhesion and cell migration. Thus, detailed evaluation and visualization of the forces is important to understand their roles. Besides, piconewton forces on each polymer chain that constitute one polymer material are involved in the mechanical properties of the material and visualization of such forces could lead to improved functionalities of the materials. However, few methods have been developed to easily evaluate and visualize piconewton forces so far. In this context, mechanophores based on supramolecular chemistry, in which intra- or intermolecular interactions are controlled by mechanical forces, are useful tools to detect forces at the several tens of piconewtons. Therefore, a library of supramolecular mechanophores would be of value not only for polymer mechanochemistry but also for mechanobiology. Particularly, the rotaxane architecture is a fascinating platform to design supramolecular mechanophores, since the interlocked ring and axle moieties allow to elicit desirable photophysical properties that can be altered through the mechanically-induced molecular-shuttling function. However, reports on supramolecular mechanophores using rotaxane are limited.

Accordingly, I present three strategies to functionalize rotaxane-based supramolecular mechanophores: First is the development of a rotaxane-based supramolecular mechanophore with a red fluorophore. Previously developed rotaxane-based supramolecular mechanophores that exhibit ON/OFF switching of blue, green, and orange fluorescence are not suitable for biological applications. This is because inside cells, some intracellular structures emit luminescence in visible wavelength region (autofluorescence), reducing detection sensitivity, and because excitation light in short wavelength region is harmful to cell. In contrast, red and near-infrared fluorescence are less affected by the autofluorescence and are less harmful to cells. Therefore, red and

near-infrared fluorescence are often used in the field of bioimaging. In this respect, the development of a red light-emitting rotaxane is necessary for the application of supramolecular mechanophores as imaging tools for cell migration in the future.

The second is the development of rotaxane-based supramolecular mechanophores displaying both reversible and irreversible responses depending on the magnitude of the applied force. As in conventional rotaxane-based mechanophores, the reversible response is due to the molecular shuttling mechanism, while the irreversible response is ascribed to the force-induced dethreading of the cycle from the stopper moiety. This approach is based on knowledge developed in the context of other responsive supramolecular materials, notably rotaxanes that was designed to allow the ring to selectively pass through moderately bulky portions of the axle in response to external stimuli.[128–133] It was also shown that rotaxanes can be dethreaded by mechanical force.[134–136] However, to the best of my knowledge, this mechanism has not been strategically utilized to develop mechanophores.

The third is the control of FRET by force using rotaxane-based supramolecular mechanophores. In conventional rotaxane-based supramolecular mechanophores, on/off switching of fluorescence has been achieved by controlling the assembly and dissociation of fluorophore and quencher by force-induced molecular shuttling function. These studies motivated me to develop rotaxane-based supramolecular mechanophores that control not only fluorescence but also various other photofunctions. Then, I focused on FRET and incorporated the FRET mechanism into rotaxane-based supramolecular mechanophores to reveal that mechanochromic responses are attainable in rotaxanes featuring other photofunctional groups.

1.7. Outline of the Thesis

In Chapter 1, an introduction to mechanophores and an overview of processes related to photoexcitation are given. The objective of the thesis is also stated.

In Chapter 2, a rotaxane-based supramolecular mechanophore displaying changes in the red fluorescence intensities was developed. The fundamental photophysical properties and mechanoresponsive luminescence behavior were examined in the solution and polymer films. Unlike conventional rotaxane-based mechanophores, the polymer film exhibits fluorescence even in its initial state. However, swelling the film with organic solvents suppresses the strong initial fluorescence, which improves the ratio of fluorescence intensity change.

In Chapter 3, a development of rotaxane-based supramolecular mechanophores showing both reversible and irreversible changes in the fluorescence properties is given. The rotaxane-incorporated polyurethane film exhibits a reversible response on the first stretching cycle, but when stretching cycles are repeated, the film shows fluorescence even in relaxed states. The irreversible behavior is proven to be caused by force-induced dethreading.

In Chapter 4, the mechanical control of FRET was achieved using a rotaxane-based supramolecular mechanophore. The mechanoresponsive luminescence behavior of the synthesized rotaxane was examined using polyurethane-urea hydrogels. Besides, rotaxane mechanophores have proven to be useful for applications in color materials, as they allow for tuning the emission color by simply modifying existing motifs with FRET acceptors.

In Chapter 5, conclusions and future perspectives of the study are summarized.

1.8. References

(1) Hu, Y.; Duan, Y.; Salaita, K. DNA Nanotechnology for Investigating Mechanical Signaling in the Immune System. *Angew. Chem. Int. Ed.* **2023**, e202302967.

(2) Liu, Y.; Galior, K.; Ma, V. P.; Salaita, K. Molecular Tension Probes for Imaging Forces at the Cell Surface. *Acc. Chem. Res.* **2017**, *50*, 2915–2924.

(3) Creusen, G.; Schmidt, R. S.; Walther, A. One-Component DNA Mechanophores for Facile Mechanosensing in Photopolymerized Hydrogels and Elastomers. *ACS Macro Lett.* **2021**. *10*, 671–678.

(4) Chen, X. X.; Bayard, F.; Gonzalez-Sanchis, N.; Pamungkas, K. K. P.; Sakai, N.; Matile, S. Fluorescent Flippers: Small-Molecule Probes to Image Membrane Tension in Living Systems. *Angew. Chem. Int. Ed.* **2023**, *62*, e202217868.

(5) Sagara, Y.; Yamane, S.; Mitani, M.; Weder, C.; Kato, T. Mechanoresponsive Luminescent Molecular Assemblies: An Emerging Class of Materials. *Adv. Mater.* **2016**, *28*, 1073–1095.

(6) Löwe, C; Weder, C. Oligo(*p*-phenylene vinylene) Excimers as Molecular Probes: Deformation-Induced Color Changes in Photoluminescent Polymer Blends. *Adv. Mater.* **2002**, *14*, 5.

(7) Crenshaw, B. R.; Weder, C. Deformation-Induced Color Changes in Melt-Processed Photoluminescent Polymer Blends. *Chem. Mater.* **2003**, *15*, 4717–4724.

(8) Crenshaw, B. R.; Weder, C. Self-Assessing Photoluminescent Polyurethanes. *Macromolecules* **2006**, *39*, 9581–9589.

(9) Crenshaw, B. R.; Burnworth, M.; Khariwala, D.; Hiltner, A.; Mather, P. T.; Simha, R.; Weder, C. Deformation-Induced Color Changes in Mechanochromic Polyethylene Blends. *Macromolecules* **2007**, *40*, 2400–2408.

(10) Lott, J.; Weder, C. Luminescent Mechanochromic Sensors Based on Poly(vinylidene fluoride) and Excimer-Forming *p*-Phenylene Vinylene Dyes. *Macromol. Chem. Phys.* **2010***, 211,* 28–34.

(11) Kinami, M.; Crenshaw, B. R.; Weder, C. Polyesters with Built-in Threshold Temperature and Deformation Sensors. *Chem. Mater.* **2006**, *18*, 946–955.

(12) Donati, F.; Pucci, A.; Cappelli, C.; Mennucci, B.; Ruggeri, G. Modulation of the Optical Response of Polyethylene Films Containing Luminescent Perylene Chromophores. *J. Phys. Chem. B* **2008**, *112*, 3668–3679.

(13) Pucci, A.; Di Cuia, F.; Signori, F.; Ruggeri, G. Bis(benzoxazolyl)stilbene Excimers as Temperature and Deformation Sensors for Biodegradable Poly(1,4-butylene succinate) Films. *J. Mater. Chem.* **2007**, *17*, 783-790.

(14) Pucci, A.; Bertoldo, M.; Bronco, S. Luminescent Bis(benzoxazolyl)stilbene as a Molecular Probe for Poly(propylene) Film Deformation. *Macromol. Rapid Commun.* **2005***, 26,* 1043–1048.
(15) Sluysmans, D.; Zhang, L.; Li, X.; Garci, A.; Stoddart, J. F.; Duwez, A. S. Viologen Tweezers to Probe the Force of Individual Donor-Acceptor π-Interactions. *J. Am. Chem. Soc.* **2020**, *142*, 21153-21159.
(16) Lussis, P.; Svaldo-Lanero, T.; Bertocco, A.; Fustin, C. A.; Leigh, D. A.; Duwez, A. S. A Single Synthetic Small Molecule That Generates Force Against a Load. *Nat. Nanotechnol.* **2011**, *6*, 553-557.
(17) Van Quaethem, A.; Lussis, P.; Leigh, D. A.; Duwez, A.-S.; Fustin, C.-A. Probing the Mobility of Catenane Rings in Single Molecules. *Chem. Sci.* **2014**, *5*. 1449–1452.
(18) Sluysmans, D.; Hubert, S.; Bruns, C. J.; Zhu, Z.; Stoddart, J. F.; Duwez, A. S. Synthetic Oligorotaxanes Exert High Forces When Folding under Mechanical Load. *Nat. Nanotechnol.* **2018**, *13*, 209–213.
(19) Sagara, Y.; Komatsu, T.; Ueno, T.; Hanaoka, K.; Kato, T.; Nagano, T. Covalent Attachment of Mechanoresponsive Luminescent Micelles to Glasses and Polymers in Aqueous Conditions. *J. Am. Chem. Soc.* **2014**, *136*, 4273–4280.
(20) Li, J.; Nagamani, C.; Moore, J. S. Polymer Mechanochemistry: from Destructive to Productive. *Acc. Chem. Res.* **2015**, *48*, 2181–2190.
(21) De Bo, G. Polymer Mechanochemistry and the Emergence of the Mechanophore Concept. *Macromolecules* **2020**, *53*, 7615–7617.
(22) Caruso, M. M.; Davis, D. A.; Shen, Q.; Odom, S. A.; Sottos, N. R.; White, S. R.; Moore, J. S. Mechanically-Induced Chemical Changes in Polymeric Materials. *Chem. Rev.* **2009**, *109*, 5755–5798.
(23) Paulusse, J. M.; Sijbesma, R. P. Reversible Mechanochemistry of a Pd(II) Coordination Polymer. *Angew. Chem. Int. Ed.* **2004**, *43*, 4460–4462.
(24) Yount, W. C.; Loveless, D. M.; Craig, S. L. Small-Molecule Dynamics and Mechanisms Underlying the Macroscopic Mechanical Properties of Coordinatively Cross-Linked Polymer Networks. *J. Am. Chem. Soc.* **2005**, *127*, 14488–14496.
(25) Berkowski, K. L.; Potisek, S. L.; Hickenboth, C. R.; Moore, J. S. Ultrasound-Induced Site-Specific Cleavage of Azo-Functionalized Poly(ethylene glycol). *Macromolecules* **2005**, *38*, 8975–8978.
(26) Hickenboth, C. R.; Moore, J. S.; White, S. R.; Sottos, N. R.; Baudry, J.; Wilson, S. R. Biasing Reaction Pathways with Mechanical Force. *Nature* **2007**, *446*, 423–427.

(27) Diesendruck, C. E.; Steinberg, B. D.; Sugai, N.; Silberstein, M. N.; Sottos, N. R.; White, S. R.; Braun, P. V.; Moore, J. S. Proton-Coupled Mechanochemical Transduction: a Mechanogenerated Acid. *J. Am. Chem. Soc.* **2012**, *134*, 12446–12449.
(28) Larsen, M. B.; Boydston, A. J. "Flex-Activated" Mechanophores: Using Polymer Mechanochemistry to Direct Bond Bending Activation. *J. Am. Chem. Soc.* **2013**, *135*, 8189–8192.
(29) Diesendruck, C. E.; Peterson, G. I.; Kulik, H. J.; Kaitz, J. A.; Mar, B. D.; May, P. A.; White, S. R.; Martinez, T. J.; Boydston, A. J.; Moore, J. S. Mechanically Triggered Heterolytic Unzipping of a Low-Ceiling-Temperature Polymer. *Nat. Chem.* **2014**, *6*, 623–628.
(30) Hu, X.; Zeng, T.; Husic, C. C.; Robb, M. J. Mechanically Triggered Small Molecule Release from a Masked Furfuryl Carbonate. *J. Am. Chem. Soc.* **2019**, *141*, 15018–15023.
(31) Sun, Y.; Neary, W. J.; Burke, Z. P.; Qian, H.; Zhu, L.; Moore, J. S. Mechanically Triggered Carbon Monoxide Release with Turn-On Aggregation-Induced Emission. *J. Am. Chem. Soc.* **2022**, *144*, 1125–1129.
(32) Piermattei, A.; Karthikeyan, S.; Sijbesma, R. P. Activating Catalysts with Mechanical Force. *Nat. Chem.* **2009**, *1*, 133–137.
(33) Michael, P.; Binder, W. H. A Mechanochemically Triggered "Click" Catalyst. *Angew. Chem. Int. Ed.* **2015**, *54*, 13918–13922.
(34) Wei, K.; Gao, Z.; Liu, H.; Wu, X.; Wang, F.; Xu, H. Mechanical Activation of Platinum-Acetylide Complex for Olefin Hydrosilylation. *ACS Macro Lett.* **2017**, *6* , 1146–1150.
(35) Michael, P.; Sheidaee Mehr, S. K.; Binder, W. H. Synthesis and Characterization of Polymer Linked Copper(I) Bis(N-heterocyclic carbene) Mechanocatalysts. *J. Polym. Sci., Part A: Polym. Chem.* **2017***, 55,* 3893–3907.
(36) Lu, Y.; Sugita, H.; Mikami, K.; Aoki, D.; Otsuka, H. Mechanochemical Reactions of Bis(9-methylphenyl-9-fluorenyl) Peroxides and Their Applications in Cross-Linked Polymers. *J. Am. Chem. Soc.* **2021**, *143*, 17744–17750.
(37) Lin, Y.; Kouznetsova, T. B.; Chang, C. C.; Craig, S. L. Enhanced Polymer Mechanical Degradation Through Mechanochemically Unveiled Lactonization. *Nat. Commun.* **2020**, *11*, 4987.
(38) Lin, Y.; Kouznetsova, T. B.; Craig, S. L. Mechanically Gated Degradable Polymers. *J. Am. Chem. Soc.* **2020**, *142*, 2105–2109.
(39) Hsu, T. G.; Zhou, J.; Su, H. W.; Schrage, B. R.; Ziegler, C. J.; Wang, J. A Polymer with "Locked" Degradability: Superior Backbone Stability and Accessible Degradability Enabled by Mechanophore Installation. *J. Am. Chem. Soc.* **2020**, *142*, 2100–2104.

(40) Traeger, H.; Kiebala, D. J.; Weder, C.; Schrettl, S. From Molecules to Polymers-Harnessing Inter- and Intramolecular Interactions to Create Mechanochromic Materials. *Macromol. Rapid Commun.* **2021**, *42*, e2000573.
(41) He, S.; Stratigaki, M.; Centeno, S. P.; Dreuw, A.; Gostl, R. Tailoring the Properties of Optical Force Probes for Polymer Mechanochemistry. *Chemistry* **2021**, *27*, 15889–15897.
(42) Davis, D. A.; Hamilton, A.; Yang, J.; Cremar, L. D.; Van Gough, D.; Potisek, S. L.; Ong, M. T.; Braun, P. V.; Martinez, T. J.; White, S. R.; Moore, J. S.; Sottos, N. R. Force-Induced Activation of Covalent Bonds in Mechanoresponsive Polymeric Materials. *Nature* **2009**, *459*, 68–72.
(43) Beyer, M. K. The Mechanical Strength of a Covalent Bond Calculated by Density Functional Theory. *J. Chem. Phys.* **2000**, *112*, 7307–7312.
(44) Kim, T. A.; Robb, M. J.; Moore, J. S.; White, S. R.; Sottos, N. R. Mechanical Reactivity of Two Different Spiropyran Mechanophores in Polydimethylsiloxane. *Macromolecules* **2018**, *51*, 9177–9183.
(45) Gossweiler, G. R.; Kouznetsova, T. B.; Craig, S. L. Force-Rate Characterization of Two Spiropyran-Based Molecular Force Probes. *J. Am. Chem. Soc.* **2015**, *137*, 6148–6151.
(46) Lin, Y.; Barbee, M. H.; Chang, C. C.; Craig, S. L. Regiochemical Effects on Mechanophore Activation in Bulk Materials. *J. Am. Chem. Soc.* **2018**, *140*, 15969–15975.
(47) Zhang, H.; Gao, F.; Cao, X.; Li, Y.; Xu, Y.; Weng, W.; Boulatov, R. Mechanochromism and Mechanical-Force-Triggered Cross-Linking from a Single Reactive Moiety Incorporated into Polymer Chains. *Angew. Chem. Int. Ed.* **2016**, *55*, 3040–3044.
(48) Robb, M. J.; Kim, T. A.; Halmes, A. J.; White, S. R.; Sottos, N. R.; Moore, J. S. Regioisomer-Specific Mechanochromism of Naphthopyran in Polymeric Materials. *J. Am. Chem. Soc.* **2016**, *138*, 12328–12331.
(49) McFadden, M. E.; Robb, M. J. Force-Dependent Multicolor Mechanochromism from a Single Mechanophore. *J. Am. Chem. Soc.* **2019**, *141*, 11388–11392.
(50) Versaw, B. A.; McFadden, M. E.; Husic, C. C.; Robb, M. J. Designing naphthopyran mechanophores with tunable mechanochromic behavior. *Chem. Sci.* **2020**, *11*, 4525–4530.
(51) Imato, K.; Kanehara, T.; Ohishi, T.; Nishihara, M.; Yajima, H.; Ito, M.; Takahara, A.; Otsuka, H. Mechanochromic Dynamic Covalent Elastomers: Quantitative Stress Evaluation and Autonomous Recovery. *ACS Macro Lett.* **2015**, *4*, 1307–1311.

(52) Sumi, T.; Goseki, R.; Otsuka, H. Tetraarylsuccinonitriles as Mechanochromophores to Generate Highly Stable Luminescent Carbon-Centered Radicals. *Chem. Commun.* **2017**, *53*, 11885–11888.
(53) Ishizuki, K.; Aoki, D.; Goseki, R.; Otsuka, H. Multicolor Mechanochromic Polymer Blends That Can Discriminate between Stretching and Grinding. *ACS Macro Lett.* **2018**, *7*, 556–560.
(54) Kato, S.; Ishizuki, K.; Aoki, D.; Goseki, R.; Otsuka, H. Freezing-Induced Mechanoluminescence of Polymer Gels. *ACS Macro Lett.* **2018**, *7*, 1087–1091.
(55) Kato, S.; Furukawa, S.; Aoki, D.; Goseki, R.; Oikawa, K.; Tsuchiya, K.; Shimada, N.; Maruyama, A.; Numata, K.; Otsuka, H. Crystallization-induced Mechanofluorescence for Visualization of Polymer Crystallization. *Nat. Commun.* **2021**, *12*, 126.
(56) Ishizuki, K.; Oka, H.; Aoki, D.; Goseki, R.; Otsuka, H. Mechanochromic Polymers That Turn Green Upon the Dissociation of Diarylbibenzothiophenonyl: The Missing Piece toward Rainbow Mechanochromism. *Chemistry* **2018**, *24*, 3170–3173.
(57) Verstraeten, F.; Gostl, R.; Sijbesma, R. P. Stress-Induced Colouration and Crosslinking of Polymeric Materials by Mechanochemical Formation of Triphenylimidazolyl Radicals. *Chem. Commun.* **2016**, *52*, 8608–8611.
(58) Sakai, H.; Sumi, T.; Aoki, D.; Goseki, R.; Otsuka, H. Thermally Stable Radical-Type Mechanochromic Polymers Based on Difluorenylsuccinonitrile. *ACS Macro Lett.* **2018**, *7*, 1359–1363.
(59) Watabe, T.; Otsuka, H. Swelling-induced Mechanochromism in Multinetwork Polymers. *Angew. Chem. Int. Ed.* **2023**, *62*, e202216469.
(60) Sakai, H.; Aoki, D.; Seshimo, K.; Mayumi, K.; Nishitsuji, S.; Kurose, T.; Ito, H.; Otsuka, H. Visualization and Quantitative Evaluation of Toughening Polymer Networks by a Sacrificial Dynamic Cross-Linker with Mechanochromic Properties. *ACS Macro Lett.* **2020**, *9*, 1108–1113.
(61) van Galen, M.; Kaniraj, J. P.; Albada, B.; Sprakel, J. Single-Molecule Force Spectroscopy of a Tetraaryl Succinonitrile Mechanophore. *J. Phys. Chem. C Nanomater. Interfaces* **2022**, *126*, 1215–1221.
(62) Chen, Y.; Spiering, A. J.; Karthikeyan, S.; Peters, G. W.; Meijer, E. W.; Sijbesma, R. P. Mechanically Induced Chemiluminescence from Polymers Incorporating a 1,2-Dioxetane Unit in the Main Chain. *Nat. Chem.* **2012**, *4*, 559–562.
(63) Ducrot, E.; Chen, Y.; Bulters, M.; Sijbesma, R. P.; Creton, C. Toughening Elastomers with Sacrificial Bonds and Watching Them Break. *Science* **2014**, *344*, 186–189.

(64) Yuan, W.; Yuan, Y.; Yang, F.; Wu, M. J.; Chen, Y. L. Improving Mechanoluminescent Sensitivity of 1,2-Dioxetane-Containing Thermoplastic Polyurethanes by Controlling Energy Transfer across Polymer Chains. *Macromolecules* **2018**, *51*, 9019–9025.
(65) Yang, F.; Yuan, Y.; Sijbesma, R. P.; Chen, Y. L. Sensitized Mechanoluminescence Design toward Mechanically Induced Intense Red Emission from Transparent Polymer Films. *Macromolecules* **2020**, *53*, 905–912.
(66) Cao, B. H.; Chen, W.; Wei, W. Y.; Chen, Y. L.; Yuan, Y. Carbon Dots Intensified Mechanochemiluminescence from Waterborne Polyurethanes as Tunable Force Sensing Materials. *Chinese J. Polym. Sci.* **2021**, *39*, 1403–1411.
(67) Song, Y.-K.; Lee, K.-H.; Hong, W.-S.; Cho, S.-Y.; Yu, H.-C.; Chung, C.-M. Fluorescence Sensing of Microcracks Based on Cycloreversion of a Dimeric Anthracene Moiety. *J. Mater. Chem.* **2012**, *22*, 1380–1386.
(68) Church, D. C.; Peterson, G. I.; Boydston, A. J. Comparison of Mechanochemical Chain Scission Rates for Linear versus Three-Arm Star Polymers in Strong Acoustic Fields. *ACS Macro Lett.***2014**, *3*, 648–651.
(69) Gostl, R.; Sijbesma, R. P. π-extended Anthracenes as Sensitive Probes for Mechanical Stress. *Chem. Sci.* **2016**, *7*, 370–375.
(70) Li, M.; Zhang, H.; Gao, F.; Tang, Z.; Zeng, D.; Pan, Y.; Su, P.; Ruan, Y.; Xu, Y.; Weng, W. A Cyclic Cinnamate Dimer Mechanophore for Multimodal Stress Responsive and Mechanically Adaptable Polymeric Materials. *Polym. Chem.* **2019**, *10*, 905–910.
(71) Zhang, H.; Li, X.; Lin, Y.; Gao, F.; Tang, Z.; Su, P.; Zhang, W.; Xu, Y.; Weng, W.; Boulatov, R. Multi-Modal Mechanophores Based on Cinnamate Dimers. *Nat. Commun.* **2017**, *8*.
(72) Kean, Z. S.; Gossweiler, G. R.; Kouznetsova, T. B.; Hewage, G. B.; Craig, S. L. A Coumarin Dimer Probe of Mechanochemical Scission Efficiency in the Sonochemical Activation of Chain-Centered Mechanophore Polymers. *Chem. Commun.* **2015**, *51*, 9157–9160.
(73) Wang, Z.; Ma, Z.; Wang, Y.; Xu, Z.; Luo, Y.; Wei, Y.; Jia, X. A Novel Mechanochromic and Photochromic Polymer Film: When Rhodamine Joins Polyurethane. *Adv. Mater.* **2015**, *27*, 6469–6474.
(74) Wang, T.; Zhang, N.; Dai, J.; Li, Z.; Bai, W.; Bai, R. Novel Reversible Mechanochromic Elastomer with High Sensitivity: Bond Scission and Bending-Induced Multicolor Switching. *ACS Appl. Mater. Interfaces* **2017**, *9*, 11874–11881.
(75) Wu, M.; Li, Y.; Yuan, W.; De Bo, G.; Cao, Y.; Chen, Y. Cooperative and Geometry-Dependent Mechanochromic Reactivity through Aromatic Fusion of Two Rhodamines in Polymers. *J. Am. Chem. Soc.* **2022**, *144*, 17120–17128.

(76) Yang, F.; Li, X.; Chen, Y. A Chromic and Near‐Infrared Emissive Mechanophore Serving as a Versatile Force Meter in Micelle‐Hydrogel Composites. *Adv. Optical Mater.* **2022,** *10*, 2102552.
(77) Chen, Z.; Mercer, J. A. M.; Zhu, X.; Romaniuk, J. A. H.; Pfattner, R.; Cegelski, L.; Martinez, T. J.; Burns, N. Z.; Xia, Y. Mechanochemical Unzipping of Insulating Polyladderene to Semiconducting Polyacetylene. *Science* **2017**, *357*, 475–479.
(78) Yang, J.; Horst, M.; Romaniuk, J. A. H.; Jin, Z.; Cegelski, L.; Xia, Y. Benzoladderene Mechanophores: Synthesis, Polymerization, and Mechanochemical Transformation. *J. Am. Chem. Soc.* **2019**, *141*, 6479–6483.
(79) Yang, J.; Horst, M.; Werby, S. H.; Cegelski, L.; Burns, N. Z.; Xia, Y. Bicyclohexene-peri-naphthalenes: Scalable Synthesis, Diverse Functionalization, Efficient Polymerization, and Facile Mechanoactivation of Their Polymers. *J. Am. Chem. Soc.* **2020**, *142*, 14619–14626.
(80) Horst, M.; Yang, J.; Meisner, J.; Kouznetsova, T. B.; Martinez, T. J.; Craig, S. L.; Xia, Y. Understanding the Mechanochemistry of Ladder-Type Cyclobutane Mechanophores by Single Molecule Force Spectroscopy. *J. Am. Chem. Soc.* **2021**, *143*, 12328–12334.
(81) Karman, M.; Verde-Sesto, E.; Weder, C.; Simon, Y. C. Mechanochemical Fluorescence Switching in Polymers Containing Dithiomaleimide Moieties. *ACS Macro Lett.* **2018**, *7*, 1099–1104.
(82) Karman, M.; Verde-Sesto, E.; Weder, C. Mechanochemical Activation of Polymer-Embedded Photoluminescent Benzoxazole Moieties. *Acs Macro Lett.* **2018**, *7*, 1028–1033.
(83) Hemmer, J. R.; Rader, C.; Wilts, B. D.; Weder, C.; Berrocal, J. A. Heterolytic Bond Cleavage in a Scissile Triarylmethane Mechanophore. *J. Am. Chem. Soc.* **2021**, *143*, 18859–18863.
(84) Qian, H.; Purwanto, N. S.; Ivanoff, D. G.; Halmes, A. J.; Sottos, N. R.; Moore, J. S. Fast, Reversible Mechanochromism of Regioisomeric Oxazine Mechanophores: Developing in situ Responsive Force Probes for Polymeric Materials. *Chem* **2021**, *7*, 1080–1091.
(85) Qi, Q.; Sekhon, G.; Chandradat, R.; Ofodum, N. M.; Shen, T.; Scrimgeour, J.; Joy, M.; Wriedt, M.; Jayathirtha, M.; Darie, C. C.; Shipp, D. A.; Liu, X.; Lu, X. Force-Induced Near-Infrared Chromism of Mechanophore-Linked Polymers. *J. Am Chem. Soc.* **2021**, *143*, 17337–17343.
(86) Ogi, S.; Sugiyasu, K.; Takeuchi, M. Synthesis of a Doubly Strapped Light-Harvesting Porphyrin Bearing Energy Donor Molecules Hanging on to the Straps: An Attempt toward Macroscopic Control over Molecular Conformation that Affects the

Efficiency of Fluorescence Resonance Energy Transfer. *Bull. Chem. Soc. Jpn.* **2011**, *84*, 40–48.
(87) Kotani, R.; Yokoyama, S.; Nobusue, S.; Yamaguchi, S.; Osuka, A.; Yabu, H.; Saito, S. Bridging Pico-to-Nanonewtons with a Ratiometric Force Probe for Monitoring Nanoscale Polymer Physics before Damage. *Nat. Commun.* **2022**, *13*, 303.
(88) Yamakado, T.; Saito, S. Ratiometric Flapping Force Probe That Works in Polymer Gels. *J. Am. Chem. Soc.* **2022**, *144*, 2804–2815.
(89) Filonenko, G. A.; Khusnutdinova, J. R. Dynamic Phosphorescent Probe for Facile and Reversible Stress Sensing. *Adv. Mater.* **2017**, *29*, 1700563.
(90) Filonenko, G. A.; Lugger, J. A. M.; Liu, C.; van Heeswijk, E. P. A.; Hendrix, M.; Weber, M.; Muller, C.; Hensen, E. J. M.; Sijbesma, R. P.; Pidko, E. A. Tracking Local Mechanical Impact in Heterogeneous Polymers with Direct Optical Imaging. *Angew. Chem. Int. Ed.* **2018**, *57*, 16385–16390.
(91) Raisch, M.; Maftuhin, W.; Walter, M.; Sommer, M. A Mechanochromic Donor-Acceptor Torsional Spring. *Nat. Commun.* **2021**, *12*, 4243.
(92) Hertel, R.; Maftuhin, W.; Walter, M.; Sommer, M. Conformer Ring Flip Enhances Mechanochromic Performance of ansa-Donor-Acceptor-Donor Mechanochromic Torsional Springs. *J. Am. Chem. Soc.* **2022**, *144*, 21897–21907.
(93) Hu, H.; Cheng, X.; Ma, Z.; Sijbesma, R. P.; Ma, Z. Polymer Mechanochromism from Force-Tuned Excited-State Intramolecular Proton Transfer. *J. Am. Chem. Soc.* **2022**, *144*, 9971–9979.
(94) Torelli, M.; Terenziani, F.; Pedrini, A.; Guagnini, F.; Domenichelli, I.; Massera, C.; Dalcanale, E. Mechanically-Driven Vase-Kite Conformational Switch in Cavitand Cross-Linked Polyurethanes. *ChemistryOpen* **2020**, *9*, 261–268.
(95) Traeger, H.; Sagara, Y.; Kiebala, D. J.; Schrettl, S.; Weder, C. Folded Perylene Diimide Loops as Mechanoresponsive Motifs. *Angew. Chem. Int. Ed.* **2021**, *60*, 16191–16199.
(96) Imato, K.; Yamanaka, R.; Nakajima, H.; Takeda, N. Fluorescent Supramolecular Mechanophores Based on Charge-Transfer Interactions. *Chem. Commun.* **2020**, *56*, 7937–7940.
(97) Zhu, G.; Yu, T.; Chen, J.; Hu, R.; Yang, G.; Zeng, Y.; Li, Y. Dipyrene-Terminated Oligosilanes Enable Ratiometric Fluorescence Response in Polymers toward Mechano- and Thermo-Stimuli. *ACS Appl. Mater. Interfaces* **2023**, *15*, 11033–11041.
(98) Sagara, Y.; Traeger, H.; Li, J.; Okado, Y.; Schrettl, S.; Tamaoki, N.; Weder, C. Mechanically Responsive Luminescent Polymers Based on Supramolecular Cyclophane Mechanophores. *J. Am. Chem. Soc.* **2021**, *143*, 5519–5525.

(99) Thazhathethil, S.; Muramatsu, T.; Tamaoki, N.; Weder, C.; Sagara, Y. Excited State Charge-Transfer Complexes Enable Fluorescence Color Changes in a Supramolecular Cyclophane Mechanophore. *Angew. Chem. Int. Ed.* **2022**, e202209225.
(100) Früh, A. E.; Artoni, F.; Brighenti, R.; Dalcanale, E. Strain Field Self-Diagnostic Poly(dimethylsiloxane) Elastomers. *Chem. Mater.* **2017**, *29*, 7450-7457.
(101) Balzani, V.; Gómez-López, M.; Stoddart, J. F. Molecular Machines. *Acc. Chem. Res.* **1998***, 31,* 405–414.
(102) Stoddart, J. F. The Chemistry of the Mechanical Bond. *Chem. Soc. Rev.* **2009**, *38*, 1802–1820.
(103) Stoddart, J. F. Putting Mechanically Interlocked Molecules (MIMs) to Work in Tomorrow's World. *Angew. Chem. Int. Ed.* **2014**, *53*, 11102–11104.
(104) Erbas-Cakmak, S.; Leigh, D. A.; McTernan, C. T.; Nussbaumer, A. L. Artificial Molecular Machines. *Chem. Rev.* **2015**, *115*, 10081–10206.
(105) Bissell, R. A.; Cordova, E.; Kaifer, A. E.; Stoddartt, J. F. A Chemically and Electrochemically Switchable Molecular Shuttle. *Nature* **1994**, *369*, 133–137.
(106) Iijima, T.; Vignon, S. A.; Tseng, H. R.; Jarrosson, T.; Sanders, J. K.; Marchioni, F.; Venturi, M.; Apostoli, E.; Balzani, V.; Stoddart, J. F. Controllable Donor-Acceptor Neutral [2]Rotaxanes. *Chemistry* **2004**, *10*, 6375–6392.
(107) Saha, S.; Stoddart, J. F. Photo-Driven Molecular Devices. *Chem. Soc. Rev.* **2007**, *36*, 77–92.
(108) Fioravanti, G.; Haraszkiewicz, N.; Kay, E. R.; Mendoza, S. M.; Bru-no, C.; Marcaccio, M.; Wiering, P. G.; Paolucci, F.; Rudolf, P.; Brouwer, A. M.; Leigh, D. A. Three State Redox-Active Molecular Shuttle That Switches on Solution and on a Surface. *J. Am. Chem. Soc.* **2008**, *130*, 2593–2601.
(109) Bruns, C. J.; Stoddart, J. F. Rotaxane-Based Molecular Muscles. *Acc. Chem. Res.* **2014**, *47*, 2186–2199.
(110) Huang, T. J.; Brough, B.; Ho, C.-M.; Liu, Y.; Flood, A. H.; Bonvallet, P. A.; Tseng, H.-R.; Stoddart, J. F.; Baller, M.; Magonov, S. A Nanomechanical Device Based on Linear Molecular Motors. *Appl. Phys. Lett.* **2004**, *85*, 5391–5393.
(111) Liu, Y.; Flood, A. H.; Bonvallet, P. A.; Vignon, S. A.; Northrop, B. H.; Tseng, H.-R.; Jeppesen, J. O.; Huang, T. J.; Brough, B.; Baller, M.; Magonov, S.; Solares, S. D.; Goddart, W. A.; Ho, C.-M.; Stoddart, J. F. Linear Artificial Molecular Muscles. *J. Am. Chem. Soc.* **2005**, *127*, 9745–9759.
(112) Cheng, C.; McGonigal, P. R.; Schneebeli, S. T.; Li, H.; Vermeulen, N. A.; Ke, C.; Stoddart, J. F. An Artificial Molecular Pump. *Nat. Nanotechnol.* **2015**, *10*, 547–553.

(113) Guo, Q. H.; Qiu, Y.; Kuang, X.; Liang, J.; Feng, Y.; Zhang, L.; Jiao, Y.; Shen, D.; Astumian, R. D.; Stoddart, J. F. Artificial Molecular Pump Operating in Response to Electricity and Light. *J. Am. Chem. Soc.* **2020**, *142*, 14443–14449.
(114) Li, X.; David, A. H. G.; Zhang, L.; Song, B.; Jiao, Y.; Sluysmans, D.; Qiu, Y.; Wu, Y.; Zhao, X.; Feng, Y.; Mosca, L.; Stoddart, J. F. Fluorescence Quenching by Redox Molecular Pumping. *J. Am. Chem. Soc.* **2022**, *144*, 3572–3579.
(115) Canton, M.; Groppi, J.; Casimiro, L.; Corra, S.; Baroncini, M.; Silvi, S.; Credi, A. Second-Generation Light-Fueled Supramolecular Pump. *J. Am. Chem. Soc.* **2021**, *143*, 10890–10894.
(116) Corra, S.; Bakic, M. T.; Groppi, J.; Baroncini, M.; Silvi, S.; Penocchio, E.; Esposito, M.; Credi, A. Kinetic and Energetic Insights into the Dissipative Non-Equilibrium Operation of an Autonomous Light-Powered Supramolecular Pump. *Nat. Nanotechnol.* **2022**, *17*, 746–751.
(117) Stoll, R. S.; Friedman, D. C.; Stoddart, J. F. Mechanically Interlocked Mechanophores by Living-Radical Polymerization from Rotaxane Initiators. *Org. Lett.* **2011**, *13*, 2706–2709.
(118) Sagara, Y.; Karman, M.; Verde-Sesto, E.; Matsuo, K.; Kim, Y.; Tamaoki, N.; Weder, C. Rotaxanes as Mechanochromic Fluorescent Force Transducers in Polymers. *J. Am. Chem. Soc.* **2018**, *140*, 1584–1587.
(119) Sagara, Y.; Karman, M.; Seki, A.; Pannipara, M.; Tamaoki, N.; Weder, C. Rotaxane-Based Mechanophores Enable Polymers with Mechanically Switchable White Photoluminescence. *ACS Cent. Sci.* **2019**, *5*, 874–881.
(120) Muramatsu, T.; Sagara, Y.; Traeger, H.; Tamaoki, N.; Weder, C. Mechanoresponsive Behavior of a Polymer-Embedded Red-Light Emitting Rotaxane Mechanophore. *ACS Appl. Mater. Interfaces* **2019**, *11*, 24571–24576.
(121) Muramatsu, T.; Okado, Y.; Traeger, H.; Schrettl, S.; Tamaoki, N.; Weder, C.; Sagara, Y. Rotaxane-Based Dual Function Mechanophores Exhibiting Reversible and Irreversible Responses. *J. Am. Chem. Soc.* **2021**, *143* , 9884–9892.
(122) Muramatsu, T.; Shimizu, S.; Clough, J. M.; Weder, C.; Sagara, Y. Force-Induced Shuttling of Rotaxanes Controls Fluorescence Resonance Energy Transfer in Polymer Hydrogels. *ACS Appl. Mater. Interfaces* **2023**, *15*, 8502–8509.
(123) Zhang, M.; De Bo, G. Impact of a Mechanical Bond on the Activation of a Mechanophore. *J. Am. Chem. Soc.* **2018**, *140*, 12724–12727.
(124) Zhang, M.; De Bo, G. Mechanical Susceptibility of a Rotaxane. *J. Am. Chem. Soc.* **2019**, *141*, 15879–15883.

(125) Sandoval-Torrientes, R.; Carr, T.; De Bo, G. A Mechanochromic Hydrogen-Bonded Rotaxane. *Macromol. Rapid Commun.* **2021**, *42*, e2000447.
(126) 井上晴夫、伊藤攻、分子光化学の原理、丸善出版、2014、p.327–364.
(127) 長村利彦、川井秀記、光化学—基礎から応用まで、講談社、2017、p.50–85.
(128) Chatterjee, M. N.; Kay, E. R.; Leigh, D. A. Beyond Switches: Ratcheting a Particle Energetically Uphill with a Compartmentalized Molecular Machine. *J. Am. Chem. Soc.* **2006**, *128*, 4058–4073.
(129) Baroncini, M.; Silvi, S.; Venturi, M.; Credi, A. Photoactivated Directionally Controlled Transit of a Non-Symmetric Molecular Axle Through a Macrocycle. *Angew. Chem. Int. Ed.* **2012**, *51*, 4223–4226.
(130) Cheng, C.; McGonigal, P. R.; Schneebeli, S. T.; Li, H.; Vermeulen, N. A.; Ke, C.; Stoddart, J. F. An Artificial Molecular Pump. *Nat. Nanotech.* **2015**, *10*, 547–553.
(131) Martinez-Cuezva, A.; Rodrigues, L. V.; Navarro, C.; Carro-Guillen, F.; Buriol, L.; Frizzo, C. P.; Martins, M. A. P.; Alajarin, M.; Berna, J. Dethreading of Tetraalkylsuccinamide-Based [2] Rotaxanes for Preparing Benzylic Amide Macrocycles. *J. Org. Chem.* **2015**, *80*, 10049–10059.
(132) Pezzato, C.; Cheng, C.; Stoddart, J. F.; Astumian, R. D. Mastering the Non-Equilibrium Assembly and Operation of Molecular Machines. *Chem. Soc. Rev.* **2017**, *46*, 5491–5507.
(133) Pezzato, C.; Nguyen, M. T.; Kim, D. J.; Anamimoghadam, O.; Mosca, L.; Stoddart, J. F. Controlling Dual Molecular Pumps Electrochemically. *Angew. Chem. Int. Ed.* **2018**, *57*, 9325–9329.
(134) Brough, B.; Northrop, B. H.; Schmidt, J. J.; Tseng, H.-R.; Houk, K. N.; Stoddart, J. F.; Ho, C.-M. Evaluation of Synthetic Linear Motor-Molecule Actuation Energetics. *Proc. Natl. Acad. Sci. U. S. A.* **2006**, *103*, 8583–8588.
(135) Dunlop, A.; Wattoom, J.; Hasan, E. A.; Cosgrove, T.; Round, A. N. Mapping the Positions of Beads on a String: Dethreading Rotaxanes by Molecular Force Spectroscopy. *Nanotechnology* **2008**, *19*, 345706.
(136) De Bo, G. Mechanochemistry of the Mechanical Bond. *Chem. Sci.* **2018**, *9*, 15–21.

Chapter 2

Mechanoresponsive Behavior of a Polymer-Embedded Red-Light Emitting Rotaxane Mechanophore

This chapter is reprinted with permission from ACS Appl. Mater. Interfaces **2019**, *11*, 24571–24576.

Abstract

A red light-emitting photoluminescent supramolecular mechanophore based on an interlocked molecular motif is presented. The rotaxane-based mechanophore contains a cyclic compound featuring a π-extended 4,4-difluoro-4-bora-3a,4a-diaza-s-indacene (BODIPY) dye as a red emitter that was threaded onto a dumbbell-shaped molecule containing an electron-poor 1,4,5,8-naphthalenetetracarboxylic diimide quencher at its center. Through two aliphatic hydroxyl groups attached to the dumbbell and the cycle, the mechanophore was covalently embedded into the backbone of a thermoplastic polyurethane elastomer. The mechanophore is only weakly photoluminescent in solution, indicating that the BODIPY's emission is efficiently quenched. Solution-cast films of the rotaxane-containing polymer, by contrast, show an appreciable photoluminescence, which suggests that during film formation, some of the emitting cycles are trapped in positions away from the quencher. Interestingly, the emission intensity could be significantly reduced by swelling the films with an organic solvent and the emission increased again upon drying, suggesting that such solvent plasticization causes a reversible rearrangement. In both dry and solvent-swollen films, uniaxial deformation caused a significant, reversible increase of the emission intensity, on account of mechanically induced shuttling of the emitters away from and back to the quenchers. It is shown that the properties of the polymer can be tuned by the solvent, and that such plasticizing extends the small palette of approaches that allow modification of the activation stress of a given material system.

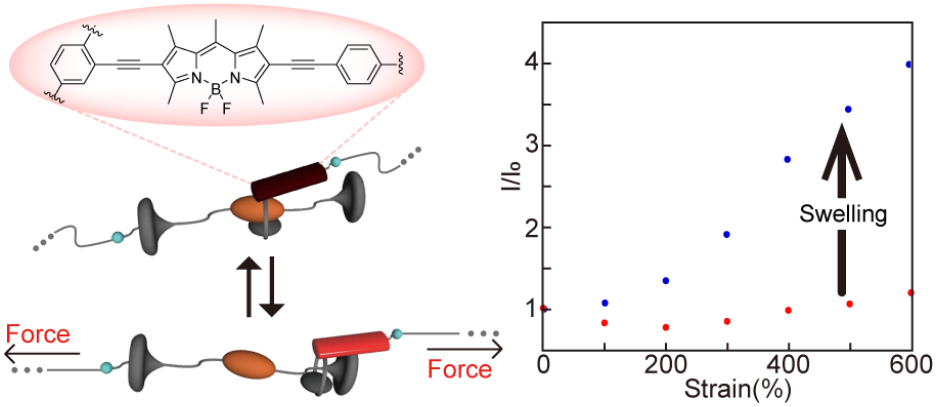

2.1. Introduction

The visualization and quantification of mechanical stresses in polymers represent a technologically important but a challenging task.[1–3] As demonstrated first a decade ago, mechanochromic mechanophores—motifs that display mechanically activated photophysical changes and can be integrated into polymers—represent an attractive approach to solve this problem.[4] In the meantime, many color-changing mechanophores and corresponding motifs which change their photoluminescence properties have been investigated.[4–21] While the latter require auxiliary means for detection, a change of the emission color and/or intensity can often be detected more easily than an absorption color change.[22]

Most of the fluorescent mechanophores reported so far, emit in the blue and green wavelength region. For instance, non-emissive anthracene−maleimide Diels−Alder adducts exhibit blue emission after activation[5–8] and a bathochromic shift of the emission band can be achieved by the extension of π-conjugation of the anthracene moiety.[9] 1,2-Dioxetane, which is a chemiluminescent mechanophore, exhibits blue emission upon activation.[10–12] A mechanophore based on an aliphatic ester of 2-(2′-hydroxyphenyl)benzoxazole was shown to switch from blue to green emission after cleavage of the ester bond, which enabled an excited-state intramolecular proton transfer mechanism.[13] Finally, the green fluorescent dithiomaleimide motif was used as a mechanically responsive turn-off motif.[14] While the number of papers dealing with blue- or green-emissive mechanophores is steadily increasing, reports on orange or red light-emitting systems are still limited. However, such systems are useful, in particular, in applications that require the simultaneous use of several mechanophores, for example, in bioimaging, where several fluorescent dyes are utilized to visualize living cells and their functions,[22] or to create white light.[21] So far, rhodamine derivatives,[15] an Eu^{3+} complex,[16] several copper complexes,[17,18] and a rotaxane having π-extended 4-(dicyanomethylene)-2-methyl-6-(4-dimethylaminostyryl)-4*H*-pyran group as the emitter[21] were used as

orange or red light-emitting mechanophores that can visualize mechanical stress when embedded in a polymer. In these motifs, the scission of a covalent bond, the dissociation between Eu^{3+} ions and a coordinating ligand, a change of the ligand exchange rate, and the shuttling function of rotaxanes were exploited to the change red-emissive character of the respective motif. Red emission was also observed from a merocyanine that was accessed by mechanically induced ring-opening of a spiropyran,[4,20] although the quantum yield was low.[9,23]

Sagara group recently reported supramolecular rotaxane-based mechanoluminophores composed of a cycle with an appended luminophore and a dumbbell-shaped molecule containing an electronically matched quencher and two stopper groups.[19,21] Linear polyurethane (PU) elastomers containing these motifs exhibit instantly reversible on/off switching of their photoluminescence and the emission color could be turned from blue to green to orange via the choice of the emitter. The activation does not involve any bond cleavage, but relies instead on the temporary separation of the luminophores and the quencher. As a result, the activation energy is low, the process is completely and instantly reversible, and the activation is fast and specific to mechanical force. Here, I demonstrate that this approach can be utilized to create a red light-emitting mechanophore. Interestingly, an elastic PU containing the mechanophore shows non-negligible red emission in the absence of any stress, which contrasts the behavior of previously investigated PUs with other rotaxane-containing mechanoluminophores.[19,21] I also show that the properties of the red-emissive PU can be tuned by incorporation of a plasticizing solvent, and thereby extend the small palette of approaches that allow modification of the threshold stress required for the activation of a given mechanophore in a given polymer system.[24]

2.2. Results and Discussion

2.2.1. Molecular Designs

A π-extended 4,4-difluoro-4-bora-3a,4a-diaza-*s*-indacene (BODIPY) dye was used as the red emitter in this study. BODIPYs represent a well-known family of fluorophores that exhibit usually high quantum efficiency and allow facile molecular structure variations, which has led researchers to investigate a large number of derivatives that cover a broad range of emission colors.[25] I first synthesized the red light-emitting π-extended BODIPY derivative **1**, in which the dye forms part of a cyclic structure composed of a naphthalene group and two tetraethylene glycol chains (Figure 2-1).[26] Phenylethynyl groups were introduced at the 2- and 6- positions of the BODIPY to extend its π-conjugation.[27–29] The rotaxane-based supramolecular mechanophore **2** was then synthesized through a 1,3-dipolar cycloaddition-type click reaction.[30] The product was characterized to satisfaction by ^{1}H and ^{13}C NMR spectroscopy and high-resolution electrospray ionization-mass spectrometry (see Figure 2-2 and the Experimental Section for details). The dumbbell-shaped molecule, which constitutes the second part of the rotaxane, contains an electron-poor 1,4,5,8-naphthalenetetracarboxylic diimide (NpI)[31–34] as a matching quencher and

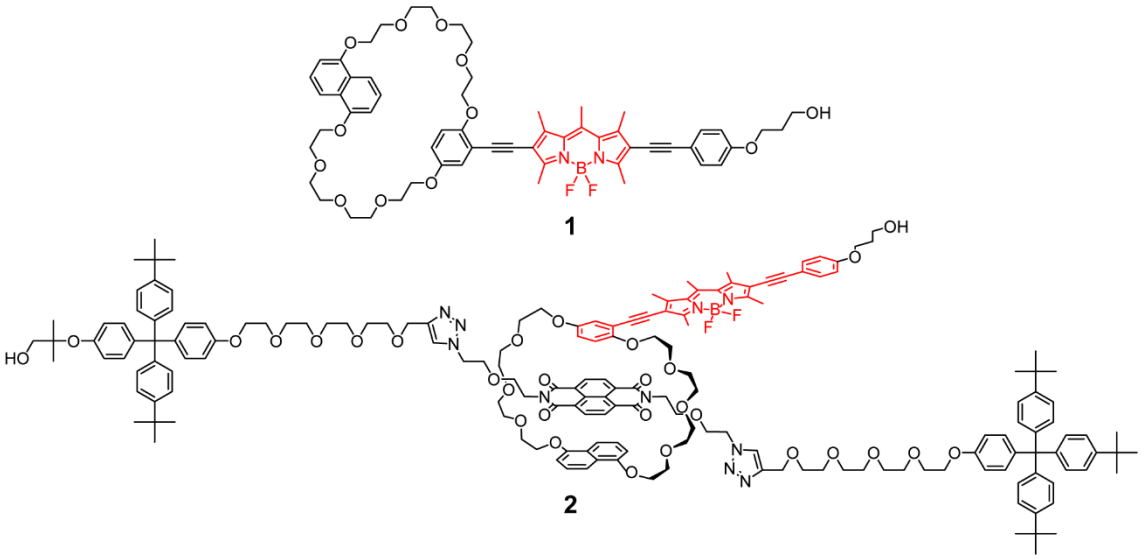

Figure 2-1. Molecular structures of the BODIPY-based cyclic compound **1** and rotaxane-based supramolecular mechanophore **2**.

two tetraphenyl methane units featuring three *tert*-butyl groups as stoppers.[35–37] The emitter and one of stopper groups were equipped with hydroxyl groups in order to covalently incorporate the mechanophore into polymers.[19,21] As illustrated in Figure 2-3, weak emitter−quencher interactions should place the emitter preferentially near the quencher in the absence of mechanical force, so that the red luminescence is quenched by the NpI group. The application of mechanical stress transduced to the mechanophore through polymer chains was expected to cause sliding of the cyclic emitter along the axle, thereby turning on the red luminescence.[19,21]

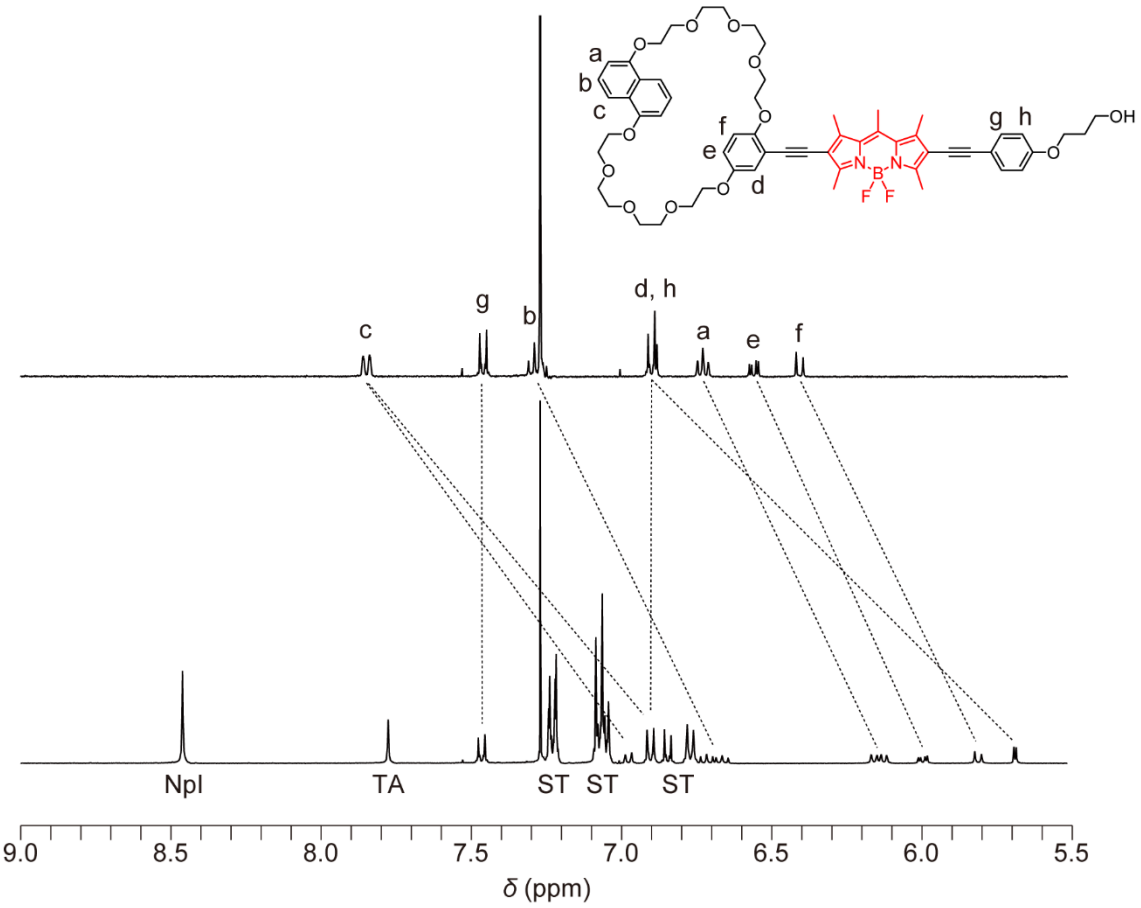

Figure 2-2. Partial ^{1}H NMR spectra of the BODIPY-based, cyclic luminophore **1** (top) and the corresponding rotaxane **2** (bottom). The abbreviations "ST", "TA", and "NpI" indicate signals ascribed to the stoppers, triazole, and quencher moieties, respectively. Both spectra were measured in $CDCl_3$ at 293 K.

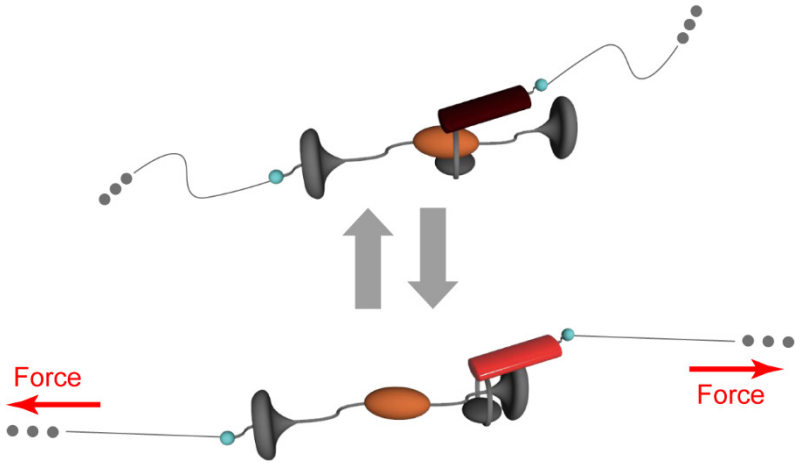

Figure 2-3. Schematic illustration of the working mechanism of the red light emitting, rotaxane-based mechanophore **2**.

2.2.2. Fundamental Photophysical Properties of 1 and 2 in Solutions

Absorption and photoluminescence measurements were performed before the mechanophore was introduced into a polymer. A solution of cyclic compound **1** in chloroform (c = 1.0 × 10^{-5} M) displays an absorption band with a maximum at 575 nm (Figure 2-4a, red line). A slight red shift of the absorption band was observed after rotaxane formation. The increased absorbance between 350 and 400 nm after rotaxane formation is ascribed to the NpI group in the rod molecule. The chloroform solution of **1** exhibits bright red photoluminescence and the emission peak features a maximum at 620 nm (Figure 2-4b). The quantum yield of **1** is 0.32 and this value is similar to those of reported red-emissive BODIPY derivatives.[25,28,29] As expected, little photoluminescence was observed from a solution of rotaxane **2**, which confirms that the photoluminescence of the red emitter was efficiently quenched by the NpI group. Indeed, the quantum yield decreased from 0.32 to below 0.01.

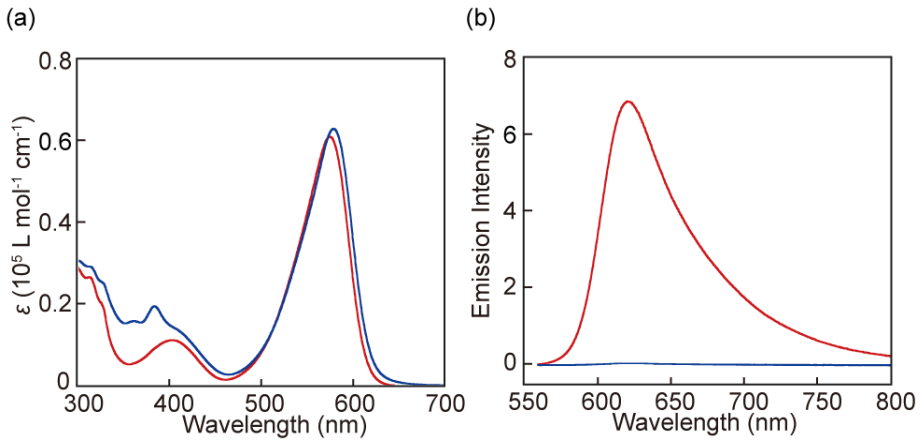

Figure 2-4. (a) Optical absorption and (b) photoluminescence spectra of cyclic compound **1** (red) and rotaxane **2** (blue) in chloroform (recorded at $c = 1.0 \times 10^{-5}$ M). The photoluminescence spectra were recorded with excitation light of 550 nm.

2.2.3. Introduction of 2 into Polyurethane

The mechanophore **2** was covalently introduced into a thermoplastic PU elastomer by a polyaddition reaction with poly(tetrahydrofuran), 4,4-methylenebis(phenylisocyanate), and 1,4-butanediol. This matrix was chosen, as its mechanical behavior proved to be useful to investigate the reversible mechanoactivation of other mechanophores.[19,21] The concentration of the mechanophore in the monomer feed was ca. 0.2 wt %. On account of its low concentration, the incorporation of the mechanophore in the polymer could not be identified by ^{1}H NMR spectroscopy (Figure 2-5). However, optical absorption and emission spectra of PU **2-PU** reveal the presence of the mechanophore and reveal that embedding **2** into the macromolecules has almost no effect on the photophysical properties of the rotaxane in solution (Figure 2-6).

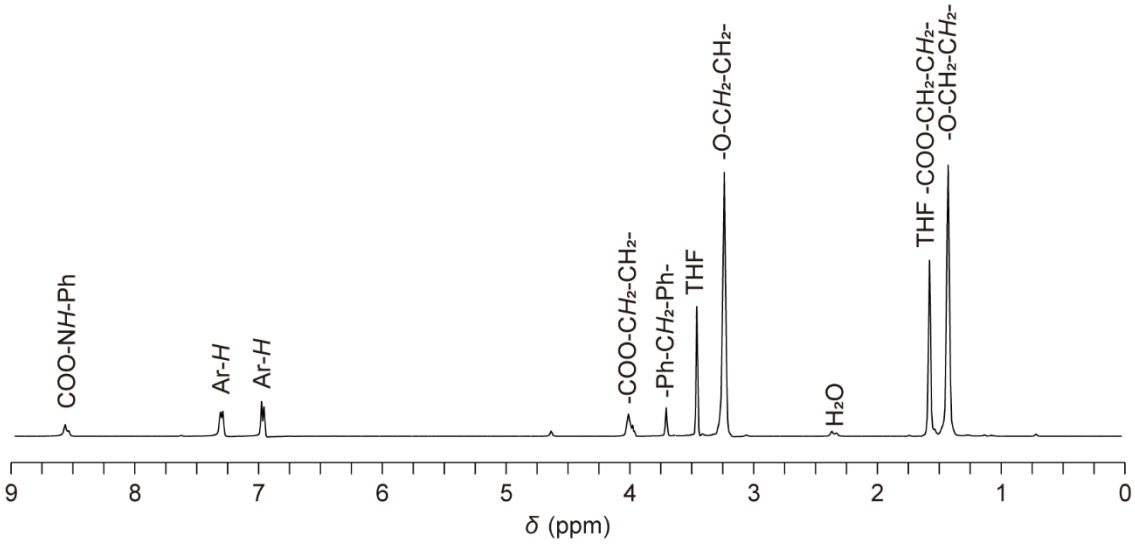

Figure 2-5. ^{1}H NMR spectrum of **2-PU** in THF-d_8. Signals are characterized as protons of the polyurethane chains. No signals ascribed to the rotaxane mechanophore are observed due to its low concentration. The spectrum was measured at 293 K.

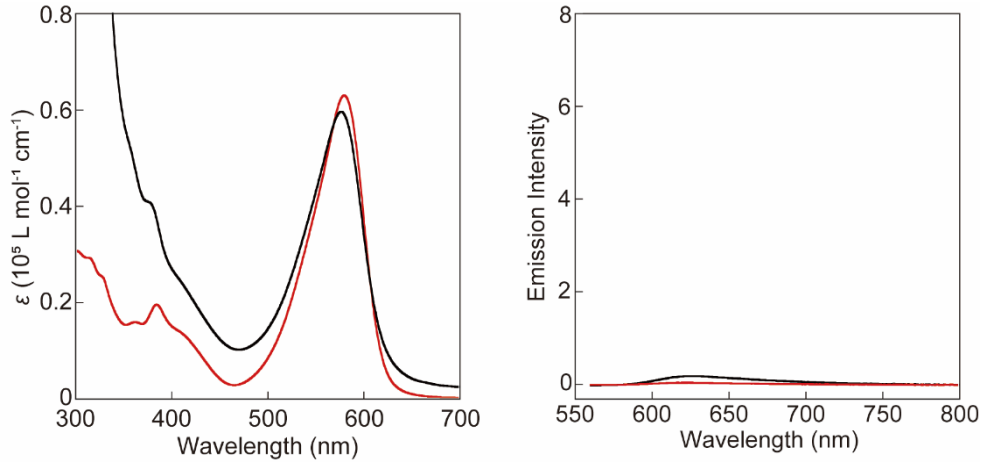

Figure 2-6. (a) Absorption and (b) photoluminescence spectra of **2** in chloroform (red) and **2-PU** in tetrahydrofuran (black). The concentration of **2** was 1.0×10^{-5} M. The concentration of **2-PU** (21 mg/mL) was tuned so that the absorbance caused by the mechanophore was comparable to that of **2**. The emission spectra were recorded with excitation light of 550 nm.

Thermogravimetric analysis (TGA) (Figure 2-7a) and differential scanning calorimetric (DSC) measurements (Figure 2-7b) revealed that **2-PU** has similar thermal properties as related to PUs that Sagara group previously reported,[19,21,38,39] that is, the DSC shows a broad peak corresponding to melting or disordering of the hard segments around 180 °C, while the TGA scan shows that decomposition gradually occurs above 300 °C. After 80−100 μm thin films of **2-PU** were prepared by solution casting, the specimens were subjected to dynamic mechanical analysis (DMA) (Figure 2-7c). The DMA traces show a glassy regime below −60 °C and a rubbery plateau that reaches from

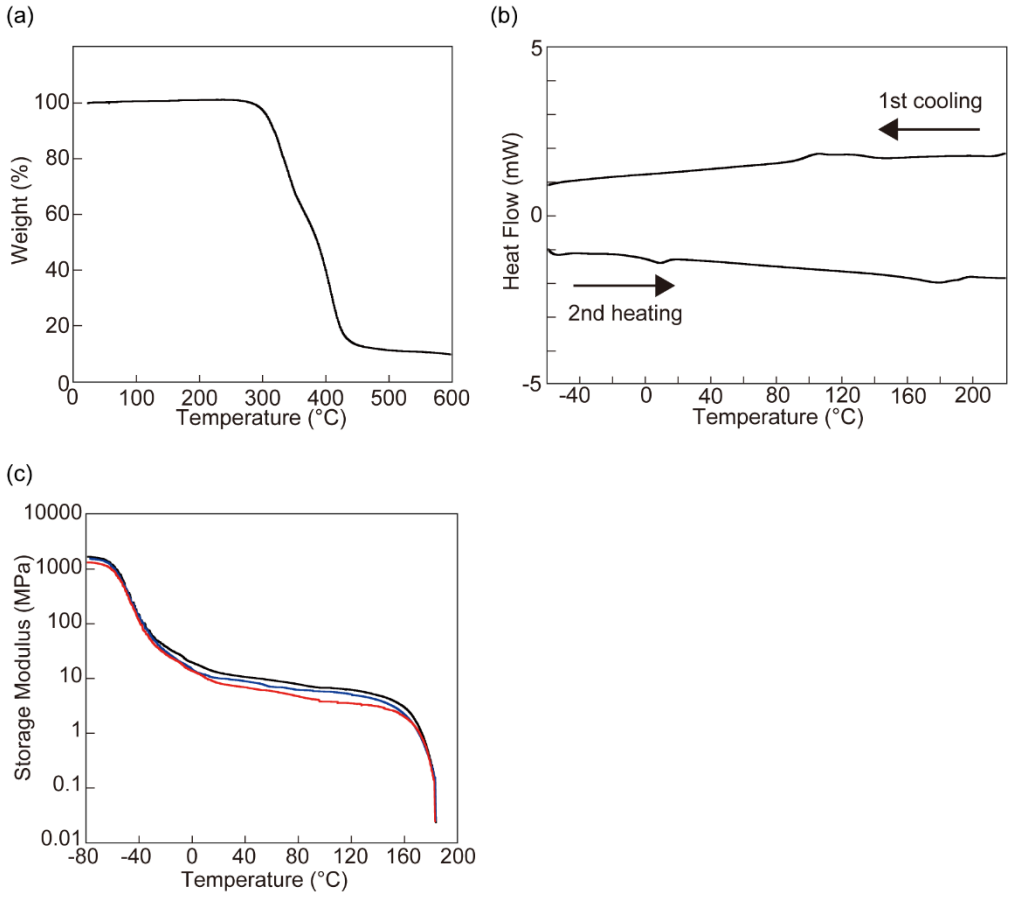

Figure 2-7. (a) Thermogravimetric analyses (TGA) trace of **2-PU**. The TGA experiment was conducted under air at a heating rate of 10 °C/min. (b) Differential scanning calorimetry (DSC) traces of **2-PU**. The heating and cooling rates were 10 °C/min. (c) Dynamic mechanical analysis (DMA) traces of **2-PU**. The graph shows data from three different samples. The tests were conducted under N_2 at a heating rate of 3 °C/min, a frequency of 1 Hz, and an amplitude of 15 μm.

above T_g to the failure temperature of ca. 180 °C. Uniaxial tensile tests (Figure 2-8, Table 1) reveal a Young's modulus of 13 ± 3 MPa and show that the introduction of the (small amount of) rotaxane has not changed the mechanical properties of the polymer.[19,21]

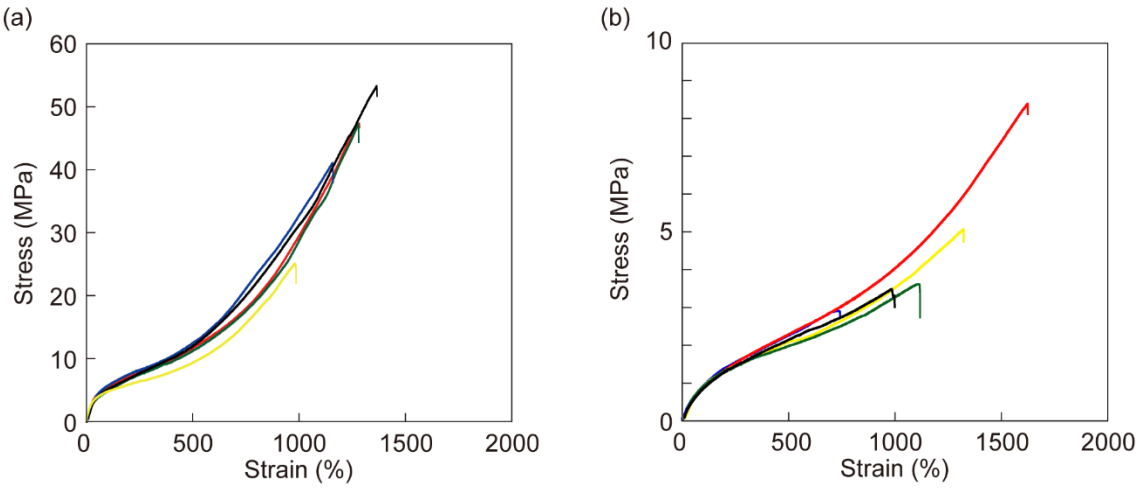

Figure 2-8. Stress-strain curves of (a) solution-cast **2-PU** films and (b) phenylacetonitrile swollen **2-PU** films. The graph shows data obtained from five different specimen. The experiments were conducted with a strain rate of 300 mm/min at room temperature.

Table 1. Mechanical data of the polyurethanes extracted from tensile tests.[a)]

	Elongation at break (%)	Stress at break (MPa)	Young's modulus[b)] (MPa)
2-PU	1230 ± 180	43 ± 18	13 ± 3
Swollen 2-PU	1160 ± 460	4.6 ± 4	5.8 ± 2

[a)]All data were extracted from the stress-strain curves shown in Figure 2-8 and represent averages of 5 measurements ± standard deviation. [b)]The Young's moduli were derived from the slopes of the stress-strain curves in the strain regime of 0.5–1.0%.

2.2.4. Mechanoresponsive Luminescence Behavior of 2-PU

Contrary to my initial expectations, as-prepared, solution-cast **2-PU** films exhibit weak red photoluminescence under ambient conditions (Φ = 0.04), although the tetrahydrofuran (THF) solution of this polymer is hardly emissive (Figure 2-6b). This behavior mirrors one of the solution-cast polymer containing a rotaxane-based mechanophore with 4,7-bis-(phenylethynyl)-2,1,3-benzothiadiazole as the green emitter, which also shows faint photoluminescence.[19] To explore the origin of this behavior, I prepared physical blends of mechanophore **2** and a similar reference PU made without a covalently incorporated mechanophore (**2inPU**). Solution-cast **2inPU** films also show red emission (Figure 2-9), which confirms that this effect is not related to any mechanical force that is transduced via the polymer. The behavior of both the **2inPU** reference blend as well as the mechano-active polymer **2-PU**, is consistent with kinetic trapping of arrangements in which the emitters are placed away from the quenchers upon drying. Such trapping is possible because of the weak interaction between the luminophore and the quencher, and the limited mobility in the dried state. The fact that the shape of the emission spectra of the luminophore solution (Figure 2-4b), the reference PU films

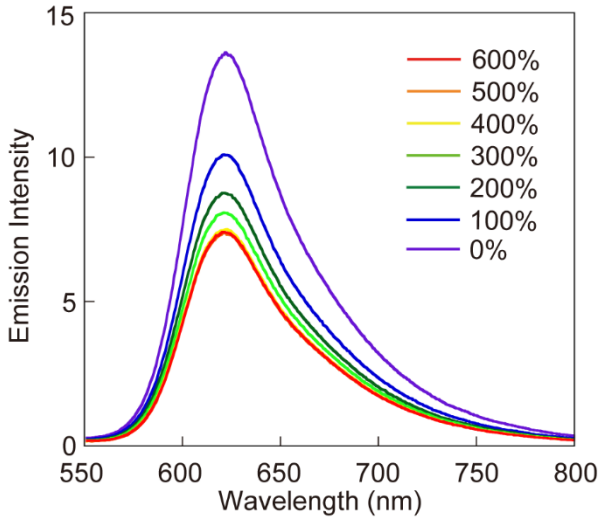

Figure 2-9. Photoluminescence spectra of a pristine **2inPU** film recorded upon uniaxial deformation to the strains indicated. The emission spectra were recorded with excitation light of 385 nm

(**1inPU** and **2inPU**, Figures 2-9 and 2-10), and **2-PU** films are very similar suggests that the PU matrix does not influence the photophysical properties of the BODIPY-based fluorophore. When **2-PU** films were uniaxially stretched, the emission intensity initially decreased but then gradually increased when the strain $\lambda = (L - L_0)/L_0$ exceeded 200% (Figure 2-11a). The fact that reference films based on a physical blend of the reference PU and compounds **1** (**1inPU**) or **2** (**2inPU**) show only a decrease of the emission intensity when stretched (Figures 2-9 and 2-10) suggests that the intensity decrease observed for **2-PU** at low strains can be attributed to a decrease of the film thickness, before additional mechanophores are activated at higher strains and the emission intensity increases. The reference experiments further highlight that the covalent incorporation of the mechanophore into the polymer chains is a requirement for its mechanical activation.

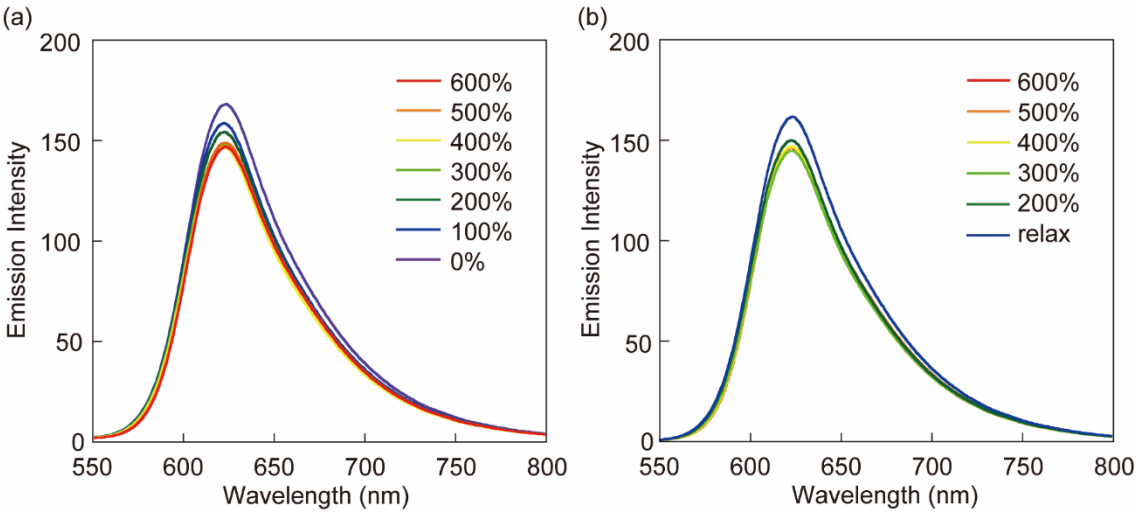

Figure 2-10. Photoluminescence spectra of a pristine **1inPU** film recorded upon (a) uniaxial deformation to the strains indicated and (b) releasing the stress so that the sample can relax from a strain of 600% to the strains indicated. The emission spectra were recorded with excitation light of 385 nm.

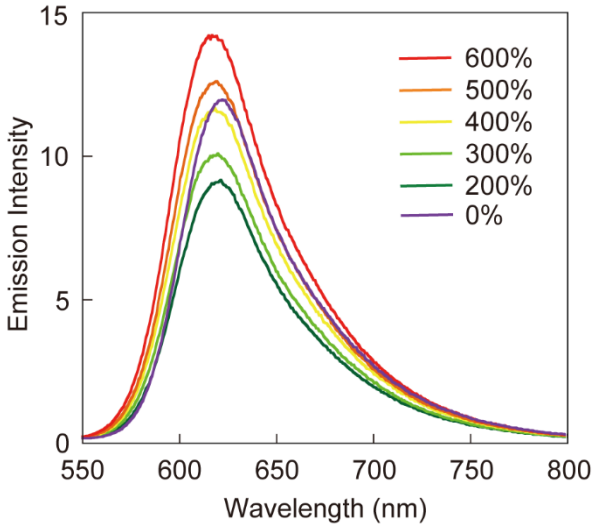

Figure 2-11. Emission spectra of a solution-cast **2-PU** film recorded upon uniaxial tensile deformation to the strain indicated. The emission spectra were recorded with excitation at 385 nm.

The mechanoresponsive behavior of **2-PU** was also investigated by sonomechanochemical experiments, which are routinely used to probe the mechanically induced scission of covalent bonds (Figure 2-12). Thus, when THF solutions of **2-PU** were sonicated over the course of 60 min, a gradual decrease of the molecular weight and a concomitant increase of the photoluminescence intensity were observed. These results indicate the scission of covalent bonds in the mechanophore or dethreading of the cycle upon sonication.

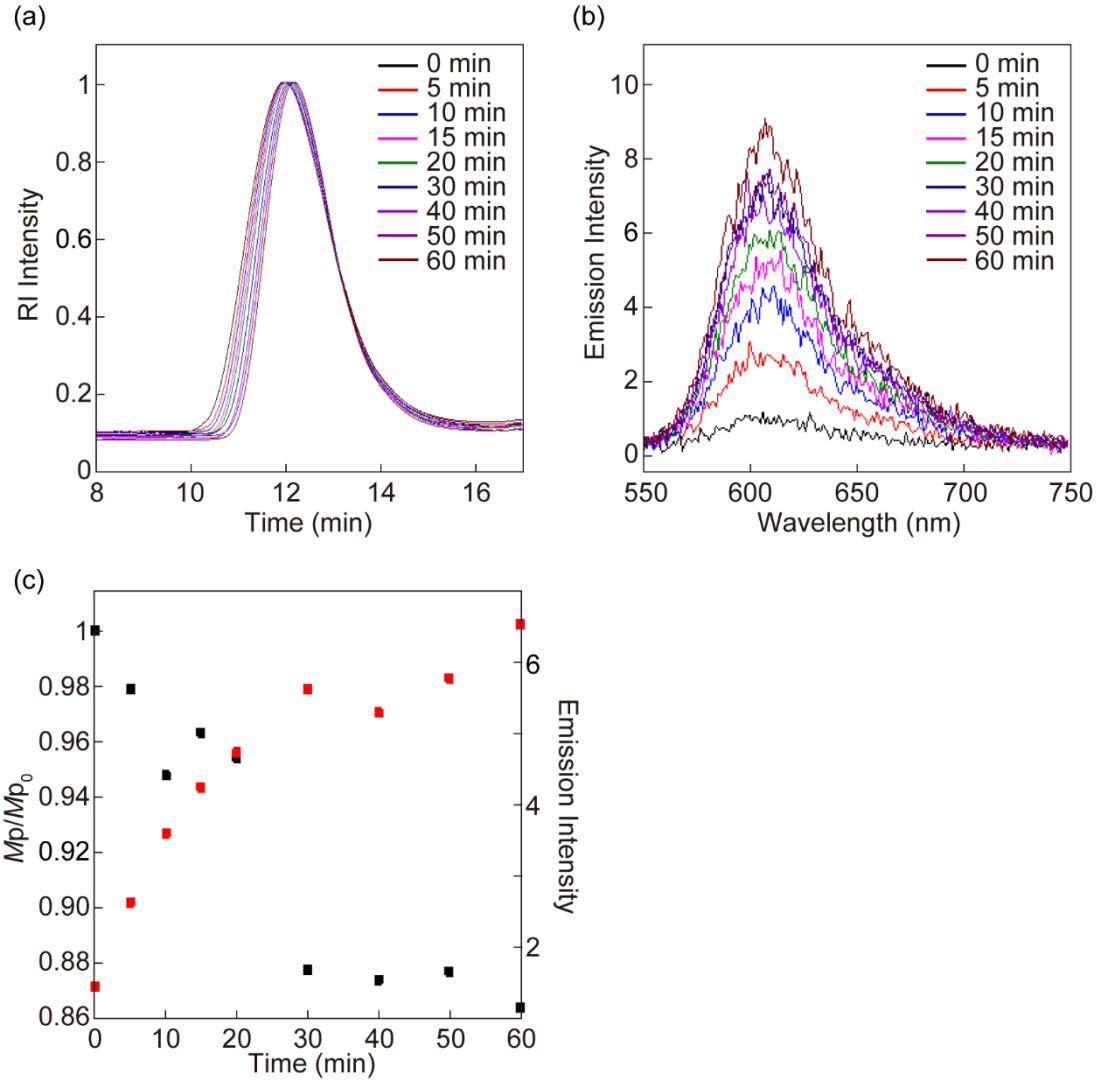

Figure 2-12. (a) Size exclusion chromatography (SEC) traces of **2-PU** upon sonication for 1 h. The traces were normalized to the peak maximum of the chromatograms. (b) Changes of the photoluminescence spectra of the solutions upon sonication. (c) Mp/Mp_0 (black) and emission intensity (red) as a function of sonication time. Mp/Mp_0 is the ratio between the polymer's molar mass of the SEC trace after sonication for time t and the molar mass at t = 0 min. The emission intensity is based on the integration of the fluorescence spectra to reduce the impact of the limited signal to noise ratio. All sonication experiments were made with solutions of **2-PU** in THF.

2.2.5. Changes in the Photophysical Properties of 2-PU Films upon Swelling

Interestingly, swelling the **2-PU** films with organic solvents leads to a decrease of the initial emission intensity (Table 2). This effect was observed when the films were immersed in ethyl acetate, chloroform, acetone, and phenylacetonitrile, whereas MeOH, EtOH, hexane, and water did not swell the polymer sufficiently to change the emission intensity significantly. The swelling-induced photoluminescence reduction was fully reversible, that is, when the solvent was evaporated under ambient conditions, the emission intensity gradually increased (Figure 2-13), suggesting that the effect is related to the increased mobility upon plasticization: in the presence of the solvent, the shuttling of the cycle along the axle is restored, the average distance between quencher and emitter is decreased, and the fluorescence is reduced. In order to conduct quantitative experiments with solvent-swollen films under ambient conditions, I swelled **2-PU** with phenylacetonitrile, as the high boiling point (233 °C) renders the evaporation of this solvent slow. Upon swelling with phenylacetonitrile, the quantum yield of **2-PU** decreased from 0.04 to below 0.01.

Table 2. Results of swelling tests for **2-PU** films in various solvents

Swollen with strong quenching effect	Acetonitrile, Acetone, Chlorobenzene, Chloroform, Dichloromethane, Ethyl Acetate, Phenylacetonitrile
Swollen with weak quenching effect	Tetrachloromethane, Toluene
Not swelled	Hexane, Methanol, Ethanol, Water

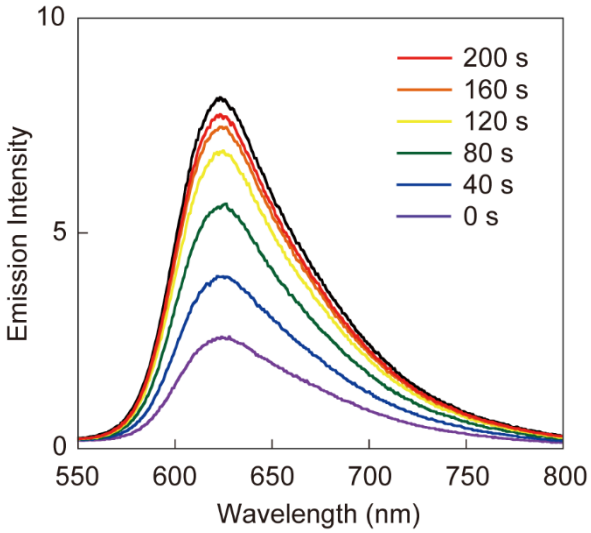

Figure 2-13. Emission spectra of a **2-PU** film swollen with rapidly evaporating ethyl acetate. The data collection was started just after removing the film from the solvent (t = 0 s) and spectra were acquired after maintaining the sample for the times indicated under ambient conditions. The black line represents the emission spectrum of a solution-cast **2-PU** film recorded under the same conditions. The emission spectra were recorded with excitation at 385 nm.

As shown in Figure 2-14a, straining the phenylacetonitrile-swollen **2-PU** film to a strain of 600% leads to an increase of the emission intensity of ca. 400% (λ_{em} = 617 nm). Plots of the relative emission intensities, that is, the ratio of the emission intensities of the stretched (I) and unstretched sample (I_0) recorded at 620 nm, of the solvent-cast **2-PU** film and the phenylacetonitrile-swollen film as a function of strain, show that the solvent-containing film exhibits a much larger contrast (Figure 2-14b). Stress−strain curves reveal that the **2-PU** films become much softer and weaker upon swelling and the stress required to achieve deformation and trigger the mechanoresponse is significantly reduced (Figure 2-14c). In the case of the dry material, a stress of 16 MPa is required to achieve a strain of 600%, while this value is reduced to 1.9 MPa upon swelling. Such plasticization (which could likely be achieved with nonvolatile plasticizers) allows one to modify the mechanoresponse of a given polymer and one can tailor the properties easily in this way.

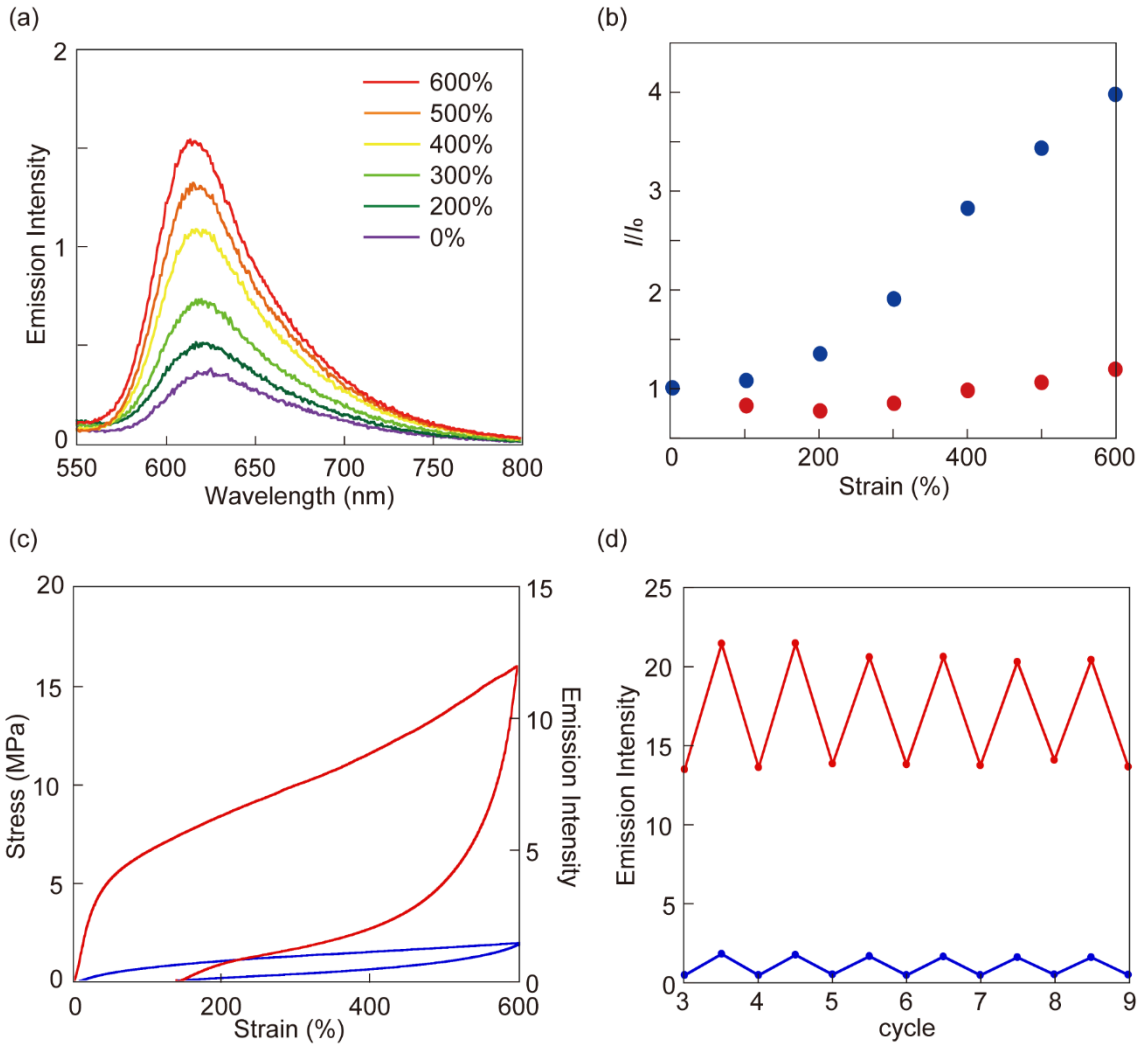

Figure 2-14. (a) Emission spectra of a phenylacetonitrile swollen **2-PU** film recorded upon uniaxial tensile deformation to the strain indicated. (b) Plots of the relative emission intensity I/I_0 of a solution-cast (red) and a phenylacetonitrile swollen (blue) **2-PU** film as a function of strain. (c) Stress−strain curves of a solution-cast (red) and a phenylacetonitrile swollen (blue) **2-PU** film. (d) Emission intensities recorded upon deformation for a solution cast (red) and a phenylacetonitrile swollen (blue) **2-PU** film over 9 cycles. The emission spectra were recorded with excitation at 385 nm and emission intensities in (b, d) were recorded at 620 nm.

The hysteresis observed in the strain–stress curves upon uniaxial elongation and stress release (Figure 2-14c) are also reflected in the corresponding emission intensities (Figure 2-15). Samples which had been swelled with phenylacetonitrile and were subsequently dried in vacuo for 1 day show a similarly small change of the relative emission intensity upon stretching (Figure 2-16) as the dry films after casting (Figure 2-11), although the original mechanical properties were not completely restored (Figure 2-17), perhaps because of residual solvent. The emission intensities recorded during several loading–unloading cycles with a strain of 600% (Figure 2-14d) reveal reversible and rapid switching between constant states of low and high emission intensity for both, solution-cast and phenylacetonitrile swollen **2-PU** films. The absolute emission intensities of the solvent-containing films are lower than those of the dry sample because the applied mechanical stress and the quantum yield of the mechanophore are both lower. As mentioned before, the quantum yield of **1** in chloroform is 0.32, while the value decreases to 0.19 in acetonitrile.

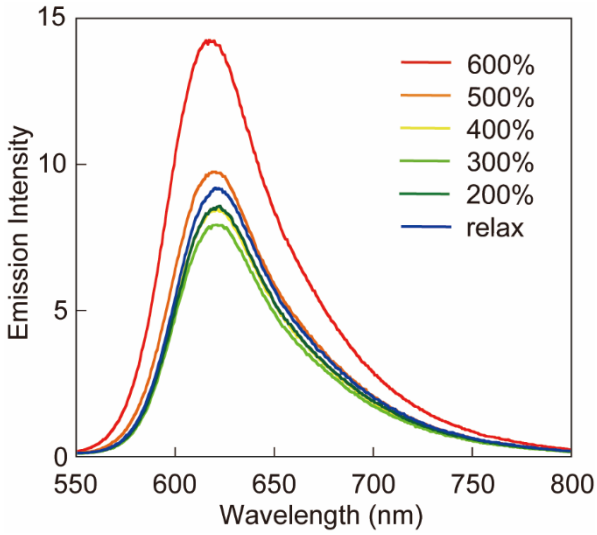

Figure 2-15. Photoluminescence spectra of **2-PU** acquired upon releasing the mechanical stress after stretching the film to a strain of 600%. The emission spectra were recorded with excitation light of 385 nm.

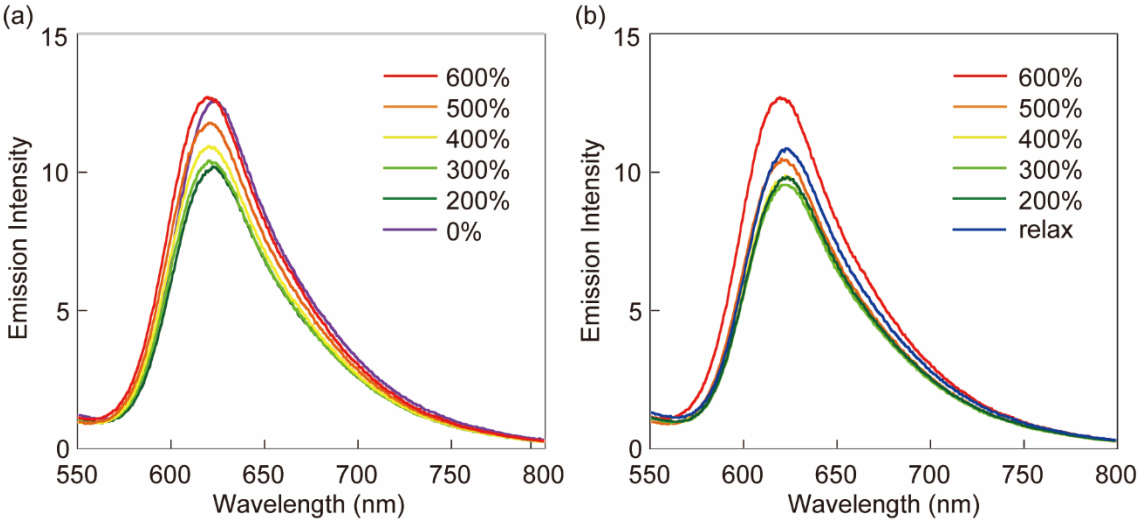

Figure 2-16. Photoluminescence spectra of a dried **2-PU** film (a) upon applying mechanical stress and (b) releasing mechanical stress. The film had been swelled in phenylacetonitrile for 1 day, then dried in vacuo for 1 day. The emission spectra were recorded with excitation light of 385 nm.

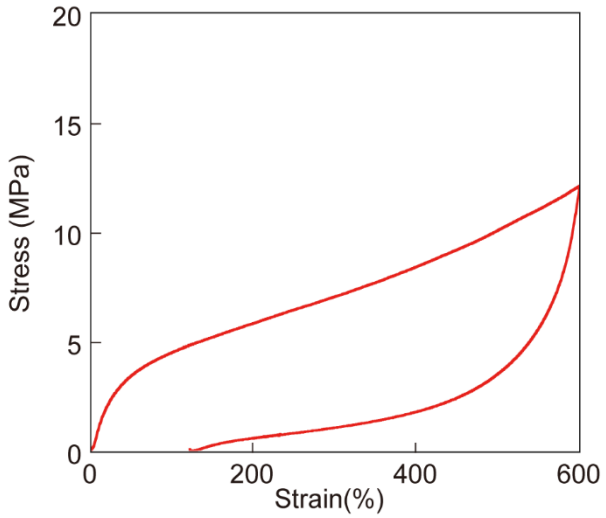

Figure 2-17. Stress-strain curve of the dried **2-PU** after swelling with phenylacetonitrile for a day.

2.2.6. Fluorescence Lifetime Measurements of 2-PU Films Before and After Swelling

To further probe the proposed working mechanism at play in **2-PU** films, as depicted in Figure 2-3, emission lifetime measurements were performed (Figure 2-18). The reference **1inPU** gave a decay profile that can be fitted with a biexponential decay function with calculated emission lifetimes of 2.6 and 3.6 ns. This suggests that the naphthalene group of compound **1** affects the BODIPY luminophores, resulting in two emission species. Similar multi-lifetime emission decays were also observed for other luminescent cyclophanes featuring 1,5-disubstituted naphthalene moieties.[40,41] Emissive states with shorter lifetimes were observed for solution-cast **2- PU** films. This change in emission decay is related to quenching by the NpI group, and reflects that in the solution-cast **2-PU** films, the latter resides, on average, in the vicinity of the cycle. Upon deformation to a strain of 600%, the emission lifetime becomes longer, indicative of an increase of the population of red luminophores that are located away from the NpI groups. Together with the emission intensities, these results support the working mechanism depicted in Figure

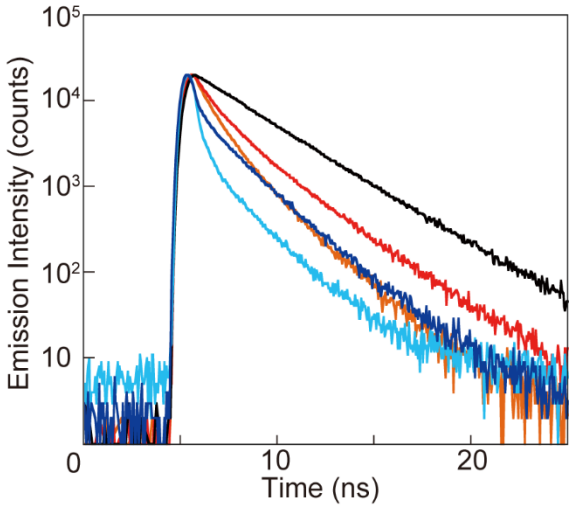

Figure 2-16. Emission decay profiles of a solution-cast **2-PU** film recorded before and after uniaxial deformation to a strain of 600% (orange and red) and of a phenylacetonitrile swollen **2-PU** film recorded before and after uniaxial deformation to a strain of 600% (light and dark blue). The emission decay profile of **1** in chloroform (black line) is also shown. All decay profiles were monitored at 620 nm, with excitation at 590 nm

2-3. The solvent-swollen **2-PU** film also shows a strain-induced increase of the emission lifetime, although both lifetimes are shorter than solvent-free samples, on account of solvent effects. Thus, molecular shuttling effects play a pivotal role in the swelling-induced changes of the mechano-responsive luminescence exhibited by **2-PU**. Upon solvent casting, some of the red light emitters are trapped in thermodynamically unfavorable locations toward the ends of the dumbbell's axle, as a result of the weak quencher−cycle interactions. After solvent swelling, the molecular mobility is increased and a portion of the kinetically trapped emitters can slide toward the NpI moiety where it is localized on account of (weak) interactions. Consequently, the emission intensity is reduced upon swelling and the emission contrast between unstretched and stretched samples becomes much larger than in the solvent-free material.

2.3. Conclusion

In summary, a new type of red light-emitting mechanophore was accessed through a supramolecular approach. The BODIPY-containing rotaxane is only weakly photoluminescent in solution, indicating that the emitter is efficiently quenched by the diimide present in the rotaxane's axle. By contrast, solution-cast films of the rotaxane-containing PU prepared, show an appreciable red luminescence, which suggests that during film formation a portion of the emitting cycles are trapped away from the quencher. However, the fluorescence intensity of the solid material, as well as its mechanical strength and stiffness, can be significantly reduced by swelling the polymer films with an organic solvent. In all cases, uniaxial deformation increased the emission intensity, on account of the mechanically induced shuttling of the rotaxane. Compared to the red-emissive, mechano-responsive Eu complexes investigated previously,[16] the present mechanophore shows instantly reversible changes when covalently introduced into PU chains and the activation of rotaxane-based mechanophore requires weaker forces, as no scission of the coordination bond is needed. Because red light-emitting mechanophores are very useful when it comes to biological application to visualize small mechanical forces, other approaches to develop red-emissive supramolecular mechanophores as well as efforts to integrate and investigate rotaxane mechanophores in other polymer matrices are undergoing in Sagara group.

2.4. Experimental Section

2.4.1. General Methods

All reagents and solvents were purchased from Tokyo Kasei, FUJIFILM Wako Pure Chemical Corporation, Kanto Chemical, or Merck. Unless otherwise noted, all reactions were carried out under nitrogen atmosphere. Flash silica gel column chromatography was performed with a Biotage Isolera Flash system using Biotage Flash Cartridges or SHOKO-scientific Purif-Pack-EX cartridges. Recycling preparative gel permeation chromatography (GPC) was conducted with a Japan Analytical Industry LaboACE. Inhibitor-free anhydrous tetrahydrofuran was used as solvent for the synthesis of polymers. Poly(tetrahydrofuran) (M_n = 2,000 g/mol) was dried *in vacuo* at 100 °C for 4 h before use. 4,4'-Methylenebis(phenylisocyanate) and 1,4-butanediol were distilled under vacuum and stored over molecular sieves at 4 °C and room temperature, respectively. ^{1}H NMR spectra were measured with a JEOL JNM-ECX 400 spectrometer and all chemical shifts are reported on the δ-scale in ppm relative to the signal of tetramethylsilane (TMS, at 0.00) even in in some cases referencing was based on residual solvent protons (THF at 1.72) as an internal standard. Proton-decoupled ^{13}C NMR spectra were performed with a JEOL JNM-ECX 400 spectrometer and all chemical shifts (δ) are quoted in ppm using residual solvent as the internal standard ($CDCl_3$ at 77.16). Coupling constants (J) are quoted in Hz and relative intensities are also shown. High resolution electrospray ionization (ESI) mass spectra were measured with a Thermo Scientific Exactive.

Absorption spectra were recorded on a JASCO V-550. Steady-state fluorescence spectra of solutions were measured with a JASCO FP-6500 and the spectra were corrected for the detector nonlinearity. Steady-state fluorescence spectra of films during deformation experiments were monitored with an Ocean Optics QEPro-FL equipped with an LLS-385 LED light source and a Reflection/Backscattering Probe R400-7-UV-VIS; these spectra were not corrected. Time-resolved fluorescence measurements were carried

out with a Hamamatsu Photonics Quantaurus-Tau. Quantum efficiencies were measured with a Hamamatsu Photonics Quantaurus-QY.

Size-exclusion chromatography (SEC) experiments were carried out on an Agilent 1200 series HPLC system equipped with an Agilent PLgel mixed guard column (particle size = 5 μm) and two Agilent PLgel mixed-D columns (ID = 7.5 mm, L = 300 mm, particle size = 5 μm). Signals were monitored on a UV detector (Agilent 1200 series), an Optilab REX interferometric refractometer, and a miniDawn TREOS light scattering detector (Wyatt Technology Corp.). Samples were injected using THF as the eluent at 30 °C and a flow rate of 1.0 mL/min. Data analyses were conducted on Astra software (Wyatt Technology Corp.) and molecular weights were calculated based on narrow-molecular-weight polystyrene calibration (from 580 to 364,000 g/mol).

Differential scanning calorimetry (DSC) measurements were performed under N_2 on a Hitachi DSC7020 at heating and cooling rates of 10 °C/min. Thermogravimetric analyses (TGA) were conducted under air with a Mettler-Toledo Star^e system at a rate of 10 °C/min. Stress–strain measurements were carried out under ambient conditions with a SHIMADZU AGS-100NX equipped with a 100 N load cell at a strain rate of 300 mm/min. Dynamic mechanical analyses (DMA) were conducted under N_2 with a TA Instruments DMA Q800 at a heating rate of 3 °C/min, a frequency of 1 Hz, and an amplitude of 15 μm.

2.4.2. Synthesis Schemes

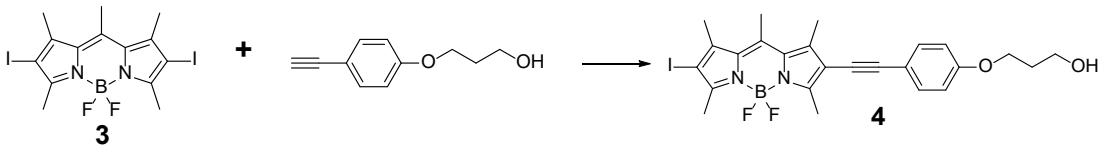

Conditions: $Pd(PPh_3)_4$, CuI, *i*-Pr_2NH, THF, r.t., 24 h.

Compound 4. A mixture of 2,6-diiodo-functionalized pentamethyl BODIPY **3**[42] (555 mg, 1.08 mmol), 3-(4-ethynylphenoxy)-1-propanol[43] (190 mg, 1.08 mmol), $Pd(PPh_3)_4$ (124 mg, 0.108 mmol), CuI (21 mg, 0.108 mmol) and *i*-Pr_2NH (5 mL) in THF (40 mL) was stirred under nitrogen atmosphere for 24 h at r.t. The reaction mixture was then poured into ethyl acetate (150 mL), the organic layer was separated off, washed with 5% aq. HCl (100 mL), saturated aq. $NaHCO_3$ (100 mL), and saturated aq. NaCl (100 mL), dried over $MgSO_4$ and filtered, and the solvent was evaporated. The crude product thus isolated was purified by flash column chromatography on silica gel (eluent: dichloromethane to dichloromethane/acetone = 9:1) to afford compound **4** (90.0 mg, 0.16 mmol, 15%) as a red solid.

^1H NMR (400 MHz, $CDCl_3$): δ = 1.65 (t, J = 5.2 Hz, 1H), 2.07 (quin, J = 6 Hz, 2H), 2.48 (s, 3H), 2.56 (s, 3H), 2.62 (s, 3H), 2.66 (s, 3H), 2.67 (s, 3H), 3.89 (q, J = 6 Hz, 2H), 4.16 (t, J = 6 Hz, 2H), 6.89 (d, J = 8.8 Hz, 2H), 7.45 (d, J = 8.8 Hz, 2H).

MS(MALDI-TOF): m/z: 562.20 (calcd. $[M]^+$ = 562.11).

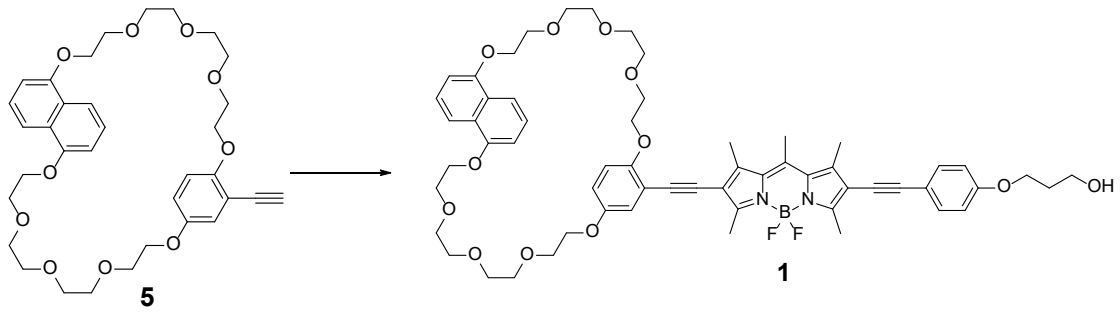

Conditions: compound **4**, $Pd(PPh_3)_4$, CuI, *i*-Pr_2NH, THF, r.t., 24 h.

Compound 1. A mixture of compound **4** (90.3 mg, 0.160 mmol), compound **5**[19] (97.7 mg, 0.160 mmol), $Pd(PPh_3)_4$ (9.20 mg, 7.96×10^{-3} mmol), CuI (1.52 mg, 7.96×10^{-3} mmol) and *i*-Pr_2NH (5 mL) in THF (40 mL) was stirred under nitrogen atmosphere for 24 h at r.t. The reaction mixture was then poured into ethyl acetate (150 mL), the organic layer was separated off, washed with 5% aq. HCl (100 mL), saturated aq. $NaHCO_3$ (100 mL), and saturated aq. NaCl (100 mL), dried over $MgSO_4$ and filtered, and the solvent was evaporated. The crude product thus isolated was purified by flash column chromatography on silica gel (eluent: dichloromethane/acetone = 9:1 to dichloromethane/acetone = 4:1) and recycling GPC (eluent: chloroform) to afford compound **1** (30.0 mg, 0.0287 mmol, 18%) as a dark red solid.

^{1}H NMR (400 MHz, $CDCl_3$): δ = 1.68 (t, J = 5.2 Hz, 1H), 2.07 (quin, J = 6 Hz, 2H), 2.54 (s, 3H), 2.57 (s, 3H), 2.66 (s, 3H), 2.68 (s, 6H), 3.59–3.90 (m, 26H), 3.95–4.02 (m, 4H), 4.15 (t, J = 6 Hz, 2H), 4.18–4.23 (m, 4H), 6.40 (d, J = 8.8 Hz, 1H), 6.55 (dd, J = 3.2, 8.8 Hz, 1H), 6.72 (t, J = 7.2 Hz, 2H), 6.84–6.91 (m, 3H), 7.24–7.30 (m, 2H), 7.45 (d, J = 8.8 Hz, 2H), 7.84 (d, J = 8.4 Hz, 2H).

^{13}C NMR (100 MHz, $CDCl_3$): δ = 13.59, 13.66, 16.01, 16.03, 16.88, 32.01, 60.02, 65.53, 68.00, 68.02, 68.04, 68.56, 69.70, 69.80, 69.82, 70.74, 70.82, 70.93, 70.95, 70.99, 71.03,

80.41, 85.98, 93.08, 96.32, 105.62, 113.21, 113.53, 114.54, 114.66, 115.63, 115.82, 116.23, 116.47, 118.11, 125.20, 125.23, 126.71, 131.94, 131.98, 132.81, 141.50, 141.60, 142.24, 152.42, 153.44, 154.34, 154.37, 156.28, 156.63, 158.81.

HRMS (ESI): m/z: 1067.4657 (cacld. [M]+ = 1067.4653).

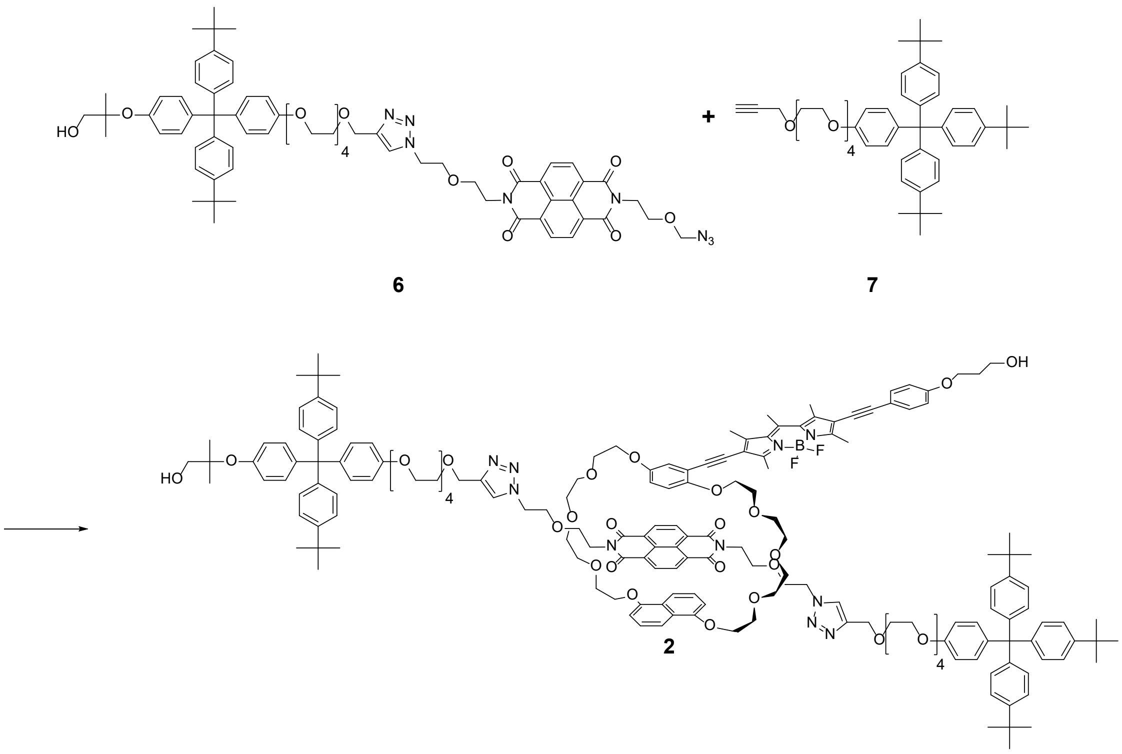

Conditions: Compound **1**, $CuSO_4$, sodium ascorbate, $CHCl_3$, H_2O, r.t., 24 h.

Compound 2. A mixture of sodium ascorbate (51.2 mg, 0.258 mmol), and copper(II) sulfate (20.6 mg, 0.129 mmol) in water (1 mL) was added to a solution of compound **1** (104 mg, 0.0861 mmol), **6**[19] (90.0 mg, 0.0861 mmol), and **7**[19] (64.6 mg, 0.0861 mmol) in chloroform (0.5 mL) and the mixture was vigorously stirred for 24 h at r.t. The suspension was poured into a mixture of water (100 mL) and chloroform (100 mL), before the organic layer was separated off, washed with saturated aq. NaCl solution (2 × 100 mL), dried over $MgSO_4$ and filtered, and the solvent was evaporated. The crude product thus obtained was

purified by flash column chromatography on silica gel (eluent: dichloromethane/acetone = 4:1 to dichloromethane/acetone = 1:1) and recycling GPC (eluent: chloroform) to afford compound **2** (53.0 mg, 0.0176 mmol, 19%), as a dark purple solid.

^{1}H NMR (400 MHz, $CDCl_3$): δ = 1.28 (s, 6H), 1.29 (s, 45H), 1.73 (s, 1H), 2.07 (quin, *J* = 6.0 Hz, 2H), 2.23 (t, *J* = 6.4 Hz, 1H), 2.45 (s, 3H), 2.57 (s, 3H), 2.60 (s, 3H), 2.70 (s, 3H), 2.71 (s, 3H), 3.57–4.18 (m, 82H), 4.54 (t, *J* = 5.2 Hz, 4H), 4.68 (s, 4H), 5.68 (d, *J* = 3.2 Hz, 1H), 5.80 (d, *J* = 9.2 Hz, 1H), 5.98 (dd, *J* = 3.2, 8.2 Hz, 1H), 6.10–6.16 (m, 2H), 6.66 (t, *J* = 8.0 Hz, 1H), 6.73 (t, *J* = 8.4 Hz, 1H), 6.76 (d, *J* = 8.8 Hz, 4H), 6.84 (d, *J* = 8.8 Hz, 2H), 6.90 (d, *J* = 8.8 Hz, 3H), 6.97 (d, *J* = 8.4 Hz, 1H), 7.03–7.08 (m, 16H), 7.20–7.24 (m, 10H), 7.46 (d, *J* = 8.8 Hz, 2H), 7.77 (s, 2H), 8.46 (s, 4H).

^{13}C NMR (100 MHz, $CDCl_3$): δ = 13.46, 13.79, 15.88, 16.29, 17.17, 23.27, 31.79, 32.05, 34.39, 34.40, 38.50, 50.48, 60.20, 60.51, 63.04, 63.13, 64.65, 65.68, 67.15, 67.26, 67.29, 67.39, 67.52, 67.98, 68.76, 69.46, 69.77, 69.85, 70.02, 70.10, 70.45, 70.59, 70.66, 70.68, 70.70, 70.85, 70.94, 71.01, 71.12, 71.16, 71.23, 71.33, 71.37, 71.46, 80.28, 80.52, 85.48, 92.19, 96.60, 103.61, 103.66, 109.68, 111.44, 113.13, 113.21, 113.33, 114.25, 114.36, 114.67, 115.64, 116.04, 116.29, 116.68, 122.29, 123.77, 123.80, 123.92, 124.13, 124.22, 124.88, 124.95, 124.98, 125.20, 130.75, 130.81, 131.23, 131.84, 131.97, 132.13, 132.23, 132.30, 132.97, 139.66, 139.81, 141.66, 141.92, 142.39, 142.75, 144.10, 144.22, 145.09, 148.37, 148.54, 150.95, 151.74, 152.44, 153.20, 153.23, 156.47, 156.63, 156.72, 156.98, 158.97, 163.25.

HRMS (ESI): m/z: 1503.7761 (cacld. $[M+2H]^{2+}$ = 1503.7755).

2.4.3. Polymer Synthesis and Preparation of Polyurethane Films

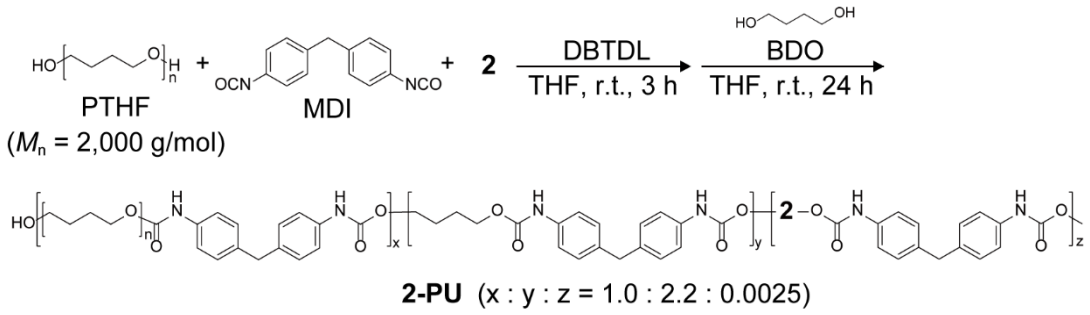

*Synthesis of polyurethane **2-PU**.*

Dibutyltin dilaurate (4 drops) was added to a stirred mixture of **2** (10 mg, 3.33×10^{-3} mmol), poly(tetrahydrofuran) (M_n = 2,000 g/mol, 3.00 g, 1.50 mmol), and 4,4′-methylenebis(phenylisocyanate) (1.26 g, 5.04 mmol) in THF (30 mL) and the mixture was stirred at r.t. for 3 h. A solution of 1,4-butanediol (297 mg, 3.30 mmol) in THF (10 mL) was then added and the reaction mixture was stirred at room temperature for an additional 24 h. EtOH (2 mL) was added to the reaction mixture and after stirring for another 30 min the reaction mixture was poured into EtOH (400 mL). The purple precipitate was collected by filtration, dissolved in THF (300 mL), the solution was filtrated through a cotton filter while approximately half of solvent evaporated, and the polymer was precipitated into hexane (300 mL). The precipitate was filtered off and dried *in vacuo* for 24 h at room temperature to afford **2-PU** as a purple rubbery solid (3.84 g, 84%, M_n = 59 kDa).

*Preparation of **2-PU** films.*

2-PU (300 mg) was dissolved in THF (10 mL) and the solution was divided between three round poly(tetrafluoroethylene) molds (32 × 3.5 mm). The molds were placed in a

well-ventilated hood under an inverted funnel so that the evaporation rate was controlled. The solvent was evaporated overnight under ambient conditions and the resulting films were further dried *in vacuo* at room temperature overnight. The films thus obtained were smooth and transparent. The thickness of the films was 80–100 μm, as measured by a digital caliper.

*Preparation of **1inPU** and **2inPU** films.*

A solution of compound **1** or **2** in THF (2 mL) was added to a THF solution (8 mL) of a reference polyurethane without any mechanophore, but of otherwise similar composition, which had been prepared in our previous study,[19] (ca. 0.3 g, M_n = 115 kDa) so that the concentration of compound **1** or **2** was same as that of the rotaxane units in **2-PU**. The mixture was divided between three round poly(tetrafluoroethylene) molds (32 × 3.5 mm) and the films were dried as described above. The films thus obtained are smooth and transparent. The thickness of the films was 80–100 μm, as measured by a digital caliper.

*Preparation of swollen **2-PU** films.*

The prepared **2-PU** film was swelled in solvents for 1 day at room temperature in glass vials. Then, the films were picked up and wicked with a paper tissue, then cut for experiments.

2.4.4. Methods of Sonomechanochemical Experiment

Sonication Experiment

Sonication experiments were performed with a Branson Model 450 digital ultrasonic horn sonifier with a 13 mm tip. A PMX07R-20 refrigerated circulating cooling/heating bath from VWR containing 1/1 (v/v) water and ethylene glycol was used to maintain the sample temperature at 20 °C during sonication experiments. A solution containing the polymer in THF (Macron fine chemicals, ChromAR HPLC) with a concentration of 0.97 mg/mL was prepared and 20 mL were filled into a Suslick cell equipped with a gas outlet and a septum. The solution was degassed by purging with nitrogen for 15 min, cooled to 20 °C by immersion in the cooling bath, and submitted to sonication pulses of 0.5 s with an amplitude of 15% and a power density of 10.4 Wcm^{-2} delayed by intermittent pauses of 1 s. Samples (350 μL) were taken after 0, 5, 10, 15, 20, 30, 40, 50, and 60 min with a syringe.

Fluorescence spectroscopy

Fluorescence spectroscopy was carried out with a Horiba Fluorolog 3 spectrometer with right angle illumination equipped with a 450 W Xenon light source for excitation and a FL-1030-UP photomultiplier as the detector. Spectra were recorded with a beam slit of 1.5 nm and an excitation wavelength of 550 nm. Fluorescence spectra were integrated between 560 and 750 nm to lower the impact of the low signal to noise ratio.

Size exclusion chromatography

Prior to SEC analysis, all samples were filtered with a 0.22 μm nylon syringe filter. Molecular weights were determined relative to polystyrene standards from 2,340 to 364,000 g/mol (Agilent Technologies) and were normalized between 0 and 17 min of elution time. The determined number-average molecular weight (M_n) at sonication time t were divided by the M_n at $t = 0$ min and plotted against sonication time.

2.5. References

(1) Caruso, M. M.; Davis, D. A.; Shen, Q.; Odom, S. A.; Sottos, N. R.; White, S. R.; Moore, J. S. Mechanically-Induced Chemical Changes in Polymeric Materials. *Chem. Rev.* **2009**, *109*, 5755−5798.

(2) Li, J.; Nagamani, C.; Moore, J. S. Polymer Mechanochemistry: From Destructive to Productive. *Acc. Chem. Res.* **2015**, *48*, 2181− 2190.

(3) Calvino, C.; Neumann, L.; Weder, C.; Schrettl, S. Approaches to Polymeric Mechanochromic Materials. J. *Polym. Sci., Part A: Polym. Chem.* **2017**, *55*, 640−652.

(4) Davis, D. A.; Hamilton, A.; Yang, J.; Cremar, L. D.; Van Gough, D.; Potisek, S. L.; Ong, M. T.; Braun, P. V.; Martínez, T. J.; White, S. R.; Moore, J. S.; Sottos, N. R. Force-Induced Activation of Covalent Bonds in Mechanoresponsive Polymeric Materials. *Nature* **2009**, *459*, 68−72.

(5) Sulkanen, A. R.; Sung, J.; Robb, M. J.; Moore, J. S.; Sottos, N. R.; Liu, G.-y. Spatially Selective and Density-Controlled Activation of Interfacial Mechanophores. *J. Am. Chem. Soc.* **2019**, *141*, 4080−4085.

(6) Sung, J.; Robb, M. J.; White, S. R.; Moore, J. S.; Sottos, N. R. Interfacial Mechanophore Activation Using Laser-Induced Stress Waves. *J. Am. Chem. Soc.* **2018**, *140*, 5000−5003.

(7) Li, H.; Göstl, R.; Delgove, M.; Sweeck, J.; Zhang, Q.; Sijbesma, R. P.; Heuts, J. P. A. Promoting Mechanochemistry of Covalent Bonds by Noncovalent Micellar Aggregation. *ACS Macro Lett.* **2016**, *5*, 995−998.

(8) Gossweiler, G. R.; Hewage, G. B.; Soriano, G.; Wang, Q.; Welshofer, G. W.; Zhao, X.; Craig, S. L. Mechanochemical Activation of Covalent Bonds in Polymers with Full and Repeatable Macroscopic Shape Recovery. *ACS Macro Lett.* **2014**, *3*, 216−219.

(9) Göstl, R.; Sijbesma, R. P. π-Extended Anthracenes as Sensitive Probes for Mechanical Stress. *Chem. Sci.* **2016**, *7*, 370−375.

(10) Clough, J. M.; van der Gucht, J.; Sijbesma, R. P. Mechanoluminescent Imaging of Osmotic Stress-Induced Damage in a Glassy Polymer Network. *Macromolecules* **2017**, *50*, 2043−2053.

(11) Ducrot, E.; Chen, Y.; Bulters, M.; Sijbesma, R. P.; Creton, C. Toughening Elastomers with Sacrificial Bonds and Watching Them Break. *Science* **2014**, *344*, 186−189.

(12) Chen, Y.; Spiering, A. J. H.; Karthikeyan, S.; Peters, G. W. M.; Meijer, E. W.; Sijbesma, R. P. Mechanically Induced Chemiluminescence From Polymers Incorporating a 1,2-Dioxetane Unit in the Main Chain. *Nat. Chem.* **2012**, *4*, 559−562.

(13) Karman, M.; Verde-Sesto, E.; Weder, C. Mechanochemical Activation of Polymer-Embedded Photoluminescent Benzoxazole Moieties. *ACS Macro Lett.* **2018**, *7*, 1028−1033.
(14) Karman, M.; Verde-Sesto, E.; Weder, C.; Simon, Y. C. Mechanochemical Fluorescence Switching in Polymers Containing Dithiomaleimide Moieties. *ACS Macro Lett.* **2018**, *7*, 1099−1104.
(15) Wang, T.; Zhang, N.; Dai, J.; Li, Z.; Bai, W.; Bai, R. Novel Reversible Mechanochromic Elastomer with High Sensitivity: Bond Scission and Bending-Induced Multicolor Switching. *ACS Appl. Mater. Interfaces* **2017**, *9*, 11874−11881.
(16) Balkenende, D. W. R.; Coulibaly, S.; Balog, S.; Simon, Y. C.; Fiore, G. L.; Weder, C. Mechanochemistry with Metallosupramolecular Polymers. *J. Am. Chem. Soc.* **2014**, *136*, 10493−10498.
(17) Filonenko, G. A.; Khusnutdinova, J. R. Dynamic Phosphorescent Probe for Facile and Reversible Stress Sensing. *Adv. Mater.* **2017**, *29*, 1700563.
(18) Filonenko, G. A.; Lugger, J. A. M.; Liu, C.; van Heeswijk, E. P. A.; Hendrix, M. M. R. M.; Weber, M.; Müller, C.; Hensen, E. J. M.; Sijbesma, R. P.; Pidko, E. A. Tracking Local Mechanical Impact in Heterogeneous Polymers with Direct Optical Imaging. *Angew. Chem. Int. Ed.* **2018**, *57*, 16385−16390.
(19) Sagara, Y.; Karman, M.; Verde-Sesto, E.; Matsuo, K.; Kim, Y.; Tamaoki, N.; Weder, C. Rotaxanes as Mechanochromic Fluorescent Force Transducers in Polymers. *J. Am. Chem. Soc.* **2018**, *140*, 1584− 1587.
(20) Kim, T. A.; Robb, M. J.; Moore, J. S.; White, S. R.; Sottos, N. R. Mechanical Reactivity of Two Different Spiropyran Mechanophores in Polydimethylsiloxane. *Macromolecules* **2018**, *51*, 9177−9183.
(21) Sagara, Y.; Karman, M.; Seki, A.; Pannipara, M.; Tamaoki, N.; Weder, C. Rotaxane-Based Mechanophores Enable Polymers with Mechanically Switchable White Photoluminescence. *ACS Cent. Sci.* **2019**, *5*, 874−881.
(22) Ueno, T.; Nagano, T. Fluorescent Probes for Sensing and Imaging. *Nat. Methods* **2011**, *8*, 642−645.
(23) Chibisov, A. K.; Görner, H. Photoprocesses in SpiropyranDerived Merocyanines. *J. Phys. Chem. A* **1997**, *101*, 4305−4312.
(24) Kida, J.; Imato, K.; Goseki, R.; Aoki, D.; Morimoto, M.; Otsuka, H. The Photoregulation of a Mechanochemical Polymer Scission. *Nat. Commun.* **2018**, *9*, 3504.
(25) Loudet, A.; Burgess, K. BODIPY Dyes and Their Derivatives: Syntheses and Spectroscopic Properties. *Chem. Rev.* **2007**, *107*, 4891− 4932.

(26) Bruns, C. J.; Basu, S.; Stoddart, J. F. Improved Synthesis of 1,5-Dinaphtho[38]crown-10. *Tetrahedron Lett.* **2010**, *51*, 983−986.
(27) Rödle, A.; Ritschel, B.; Mück-Lichtenfeld, C.; Stepanenko, V.; Fernandez, G. Influence of Ester versus Amide Linkers on the Supramolecular Polymerization Mechanisms of Planar BODIPY Dyes. *Chem.—Eur J.* **2016**, *22*, 15772−15777.
(28) Liras, M.; Iglesias, M.; Sanchez, F. Conjugated Microporous Polymers Incorporating BODIPY Moieties as Light-Emitting Materials and Recyclable Visible-Light Photocatalysts. *Macromolecules* **2016**, *49*, 1666−1673.
(29) Bonardi, L.; Ulrich, G.; Ziessel, R. Tailoring the Properties of Boron−Dipyrromethene Dyes with Acetylenic Functions at the 2,6,8 and 4-B Substitution Positions. *Org. Lett.* **2008**, *10*, 2183−2186.
(30) Rostovtsev, V. V.; Green, L. G.; Fokin, V. V.; Sharpless, K. B. A Stepwise Huisgen Cycloaddition Process: Copper(I)-Catalyzed Regioselective "Ligation" of Azides and Terminal Alkynes. *Angew. Chem. Int. Ed.* **2002**, *41*, 2596−2599.
(31) Jacquot de Rouville, H.-P.; Iehl, J.; Bruns, C. J.; McGrier, P. L.; Frasconi, M.; Sarjeant, A. A.; Stoddart, J. F. A Neutral Naphthalene Diimide [2]Rotaxane. *Org. Lett.* **2012**, *14*, 5188−5191.
(32) Choudhary, U.; Northrop, B. H. Rotaxanes and Biofunctionalized Pseudorotaxanes via Thiol-Maleimide Click Chemistry. *Org. Lett.* **2012**, *14*, 2082−2085.
(33) Cougnon, F. B. L.; Jenkins, N. A.; Pantos, G. D.; Sanders, J. K., M. Templated Dynamic Synthesis of a [3]Catenane. *Angew. Chem. Int. Ed.* **2012**, *51*, 1443−1447.
(34) Hamilton, D. G.; Davies, J. E.; Prodi, L.; Sanders, J. K. M. Synthesis, Structure and Photophysics of Neutral π-Associated [2]Catenanes. *Chem.—Eur J.* **1998**, *4*, 608−620.
(35) Gibson, H. W.; Lee, S. H.; Engen, P. T.; Lecavalier, P.; Sze, J.; Shen, Y. X.; Bheda, M. New Triarylmethyl Derivatives: "Blocking Groups" for Rotaxanes and Polyrotaxanes. *J. Org. Chem.* **1993**, *58*, 3748−3756.
(36) Dichtel, W. R.; Miljanic, O. Š.; Spruell, J. M.; Heath, J. R.; Stoddart, J. F. Efficient Templated Synthesis of Donor−Acceptor Rotaxanes Using Click Chemistry. *J. Am. Chem. Soc.* **2006**, *128*, 10388−10390.
(37) Gong, C.; Gibson, H. W. Synthesis and Characterization of a Polyester/Crown Ether Rotaxane Derived from a Difunctional Blocking Group. *Macromolecules* **1996**, *29*, 7029−7033.
(38) Ayer, M. A.; Simon, Y. C.; Weder, C. Azo-Containing Polymers with Degradation On-Demand Feature. *Macromolecules* **2016**, *49*, 2917−2927.
(39) Crenshaw, B. R.; Weder, C. Self-Assessing Photoluminescent Polyurethanes. *Macromolecules* **2006**, *39*, 9581−9589.

(40) Sagara, Y.; Seki, A.; Kim, Y.; Tamaoki, N. Linearly Polarized Photoluminescence From an Asymmetric Cyclophane Showing Thermo- and Mechanoresponsive Luminescence. J. Mater. Chem. C 2018, 6, 8453−8459.
(41) Sagara, Y.; Weder, C.; Tamaoki, N. Asymmetric Cyclophanes Permit Access to Supercooled Nematic Liquid Crystals with StimulusResponsive Luminescence. *Chem. Mater.* **2017**, *29*, 6145−6152.
(42) Bonnier, C.; Machin, D. D.; Abdi, O.; Koivisto, B. D. Manipulating Non-Innocent π-spacers: The Challenges of Using 2,6-Disubstituted BODIPY Cores within Donor–Acceptor Light-Harvesting Motifs. *Org. Biomol. Chem.* **2013**, *11*, 3756–3760.
(43) Ma, Z.; Li, Y.-B.; Deng, K.; Lei, S.-B.; Wang, Y.-Y.; Wang, P.; Yang, Y.-L.; Wang, C.; Huang, W. Supramolecular Assemblies of Tetrahydroxyloligo(phenyleneethynylene) with Cross-Shaped Side Chains and Its Coadsorption with Diacids on Graphite. *J. Phys. Chem. C* **2010**, *114*, 11460–11465.

Chapter 3

Rotaxane-Based Dual Function Mechanophores Exhibiting Reversible and Irreversible Responses

Abstract

Mechanochromic mechanophores permit the design of polymers that indicate mechanical events through optical signals. Here I report rotaxane-based supramolecular mechanophores that display both reversible and irreversible fluorescence changes. These responses are triggered by different forces and are achieved by exploiting the molecular shuttling function and force-induced dethreading of rotaxanes. The new rotaxane mechanophores are composed of a ring featuring a luminophore, which is threaded onto an axle with a matching quencher and two stoppers. In the stress-free state, the luminophore is preferentially located in the proximity of the quencher, and the emission is quenched. The luminophore slides away from the quencher when a force is applied and the fluorescence is switched on. This effect is reversible, unless the force is so high that the luminophore-carrying ring slips past the stopper and dethreading occurs. I show that the combination of judiciously selected ring and stopper moieties is crucial to attain interlocked structures that display such a dual response. PU elastomers that contain such doubly responsive rotaxanes exhibit reversible fluorescence changes over multiple loading−unloading cycles due to the shuttling function, whereas permanent changes are observed upon repeated deformations to high strains due to breakage of the mechanical bond upon dethreading of the ring from the axle. This response allows one, at least conceptually, to monitor the actual deformation of polymer materials and examine mechanical damage that was inflicted in the past on the basis of an optical signal.

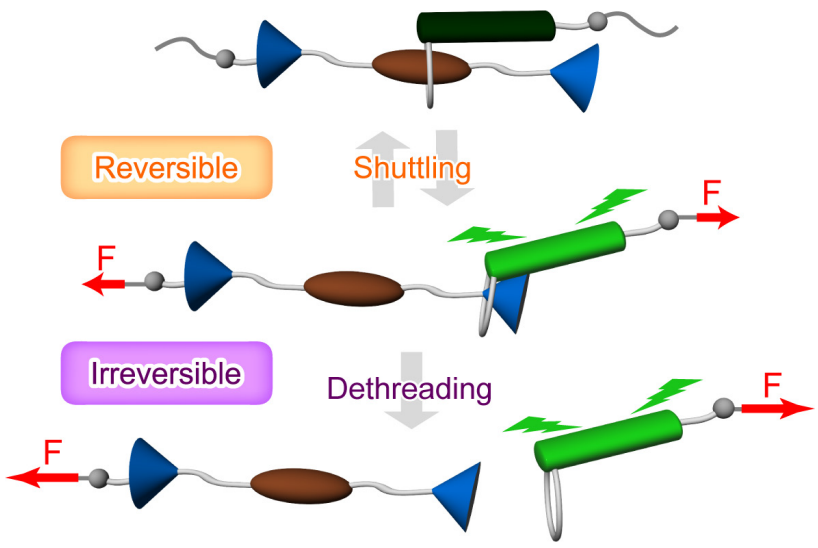

3.1. Introduction

Mechanochromic mechanophores are molecular motifs whose optical absorption or emission characteristics change when they experience a certain mechanical force.[1–4] Polymers comprising such moieties can display force-induced optical changes, which in turn are useful to signal these mechanical events. The operating mechanism of many mechanophores involves covalent bond scission, for example in spiropyran[5–8] and naphthopyran detivatives,[9–11] 1,2-dioxetanes,[12,13] Diels−Alder adducts,[14,15] radical-generating motifs,[16–18] benzoxazoles,[19] and others.[20–25] Breaking covalent bonds typically requires activation forces in excess of 200 pN,[26–30] and with few exceptions,[25] the re-formation of the severed bonds is kinetically or thermodynamically stifled, limiting the reversibility of the responsive behavior. A different possibility to achieve mechanochromic effects is to mechanically alter structures formed by weak inter- or intramolecular interactions.[4,31–42] Examples of such "noncovalent" mechanophores include motifs in which mechanically induced changes of host−guest[35] or charge-transfer interactions[40] alter the photophysical properties. Such transformations are generally thought to require lower activation forces than covalent mechanophores and are a priori reversible.[4,37–45] In this context, Sagara group recently reported rotaxane-based supramolecular mechanophores composed of luminophore-containing cycles that were threaded onto axles equipped with electronically matched quenchers.[37–39] These motifs are activated when the luminophores are pulled away from the quenchers. This operating principle makes the response fully reversible. Thus, the fluorescence intensity of elastomers containing such rotaxane mechanophores increases upon deformation, and this effect is instantly reversible over many deformation−relaxation cycles. Zhang and De Bo reported that it is also possible to create rotaxane mechanophores that display irreversible mechanoresponses.[46] This was possible by incorporating a mechanically weak bond into the axle, which was selectively and irreversibly cleaved when solutions of a polymer containing this mechanophore were sonicated. I here report a new type of mechanophore

that displays both reversible and irreversible responses (Figure 3-1), depending on the magnitude of the applied force. As in Sagara group's previous studies,[37–39] the design is based on the molecular shuttling function of rotaxanes containing a quencher–emitter pair. In the force-free state, attractive interactions cause the luminophore-containing cycle to be preferentially located in the proximity of a quencher that is fixed in the rotaxane's axle so that the emission is quenched. When a weak force is applied, the luminophore is moved away from the quencher, and its fluorescence is turned on. This effect is reversible, unless the force is sufficiently high to cause dethreading. The approach builds on the knowledge developed in the context of other responsive supramolecules,[47–55] notably rotaxanes that were designed so that the rings can selectively pass moderately bulky parts of the axle in response to redox reactions[51,53,55] or light exposure.[47,50,52,53] It was also shown that rings can be dethreaded by mechanical force.[48,49,54] For example, Ho, Stoddart, Houk, and co-

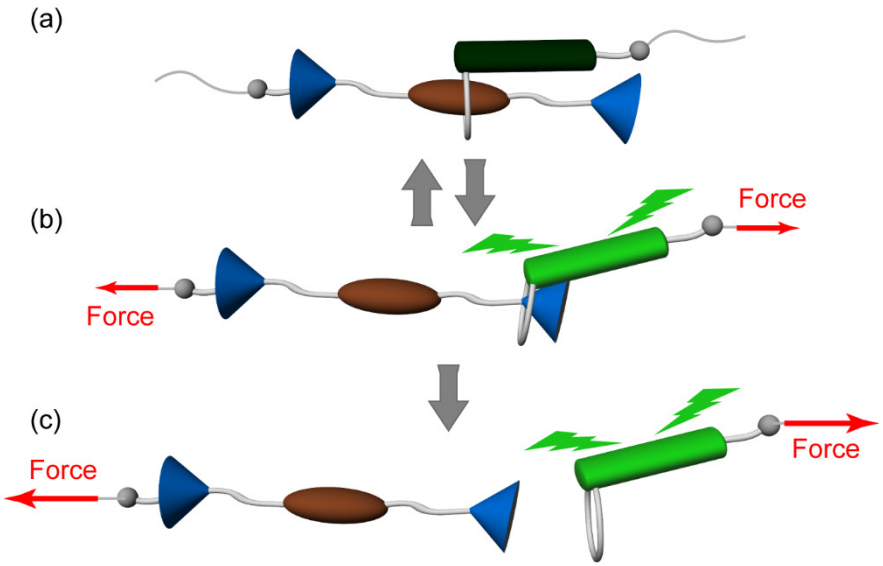

Figure 3-1. Schematic illustration of the operating principle of rotaxanebased mechanophores that display reversible or irreversible responses. (a) In the initial force-free state the cycle carrying the luminophore (dark green) is preferentially located in the proximity of a quencher (brown), and the emission is quenched. (b) The application of force displaces the luminophore (green), and the fluorescence is switched on. This effect is reversible unless the force is so high. (c) The ring slips past the stopper (blue), and dethreading occurs when large forces are applied. The motif is equipped with two reactive groups (gray) that permit the integration into polymer chains.

workers used single molecule force spectroscopy to show that a cyclobis(paraquat-*p*-phenylene) ring slips from an axle equipped with a 2,6-diisopropylphenyl stopper when a sufficiently large force is applied.[48] In this process, the rotaxane's mechanical bond is broken, while covalent bond scission is absent. Sagara group previously demonstrated that ultrasonication of solutions of polymers containing rotaxane mechanophores can irreversibly break the mechanical bond;[37,39] however, no irreversible effects were observed in the solid state. Thus, while the force-induced dethreading of rotaxanes is well-known, this mechanism has not been strategically utilized to develop mechanophores displaying two responses that are triggered at different force levels.

3.2. Results and Discussion

3.2.1. Molecular Designs

To achieve the targeted two-step response, the new rotaxane-based supramolecular mechanophore **Rot1** was conceived (Figure 3-2). *p*-Di-*tert*-butylbenzene, which is much smaller than the tris(*p*-*tert*-butylphenyl)phenylmethane groups used in Sagara group's previous studies,[37–39] was selected as a stopper that was expected to enable force-induced dethreading. As the matching ring, 1,5-dinaphtho[32]crown-8 cycle was modified, which is also smaller than the cycle Sagara group previously employed.[37–39] Pyromellitic diimide (PMDI)[56] was chosen as a suitable electron-deficient quencher based on the assumption that this motif should also allow shuttling of the rather small ring along the axle. 9,10-Bis(phenylethynyl)anthracene, which is known for its highly emissive character and electron-donating properties,[38,57–60] was used as luminophore. The latter and one of the stoppers were equipped with hydroxyl groups that permit the covalent integration of the mechanophore into polymers. To explore the role of the stopper size and axle length, I also prepared the rotaxanes **Rot2** and **Rot3** (Figure 3-2). **Rot2** features bulky tris(*p*-*tert*-butylphenyl)phenylmethane groups as stoppers, which impeded dethreading in previous rotaxane mechanophores,[37–39] and no mechanically induced dethreading was expected for this motif. **Rot2** also features a longer axle, which served to increase the solubility of the precursors and offers an extended quencher−emitter distance in the force-activated state. In **Rot3**, I combined the smaller stoppers with the longer axle. Rotaxanes **Rot1**, **Rot2**, and **Rot3** were synthesized through 1,3-dipolar cycloaddition-type click reactions[61] between alkyne and azide groups in the corresponding axle precursors in the presence of the **An** ring (see the Experimental Section for details). The three rotaxanes were characterized by ^{1}H and ^{13}C NMR spectroscopy as well as by high-resolution electrospray ionization mass spectrometry. The rotaxane formation was confirmed by shifts of the peaks corresponding to the aromatic protons (Figure 3-3) and the quenched fluorescence (see below).

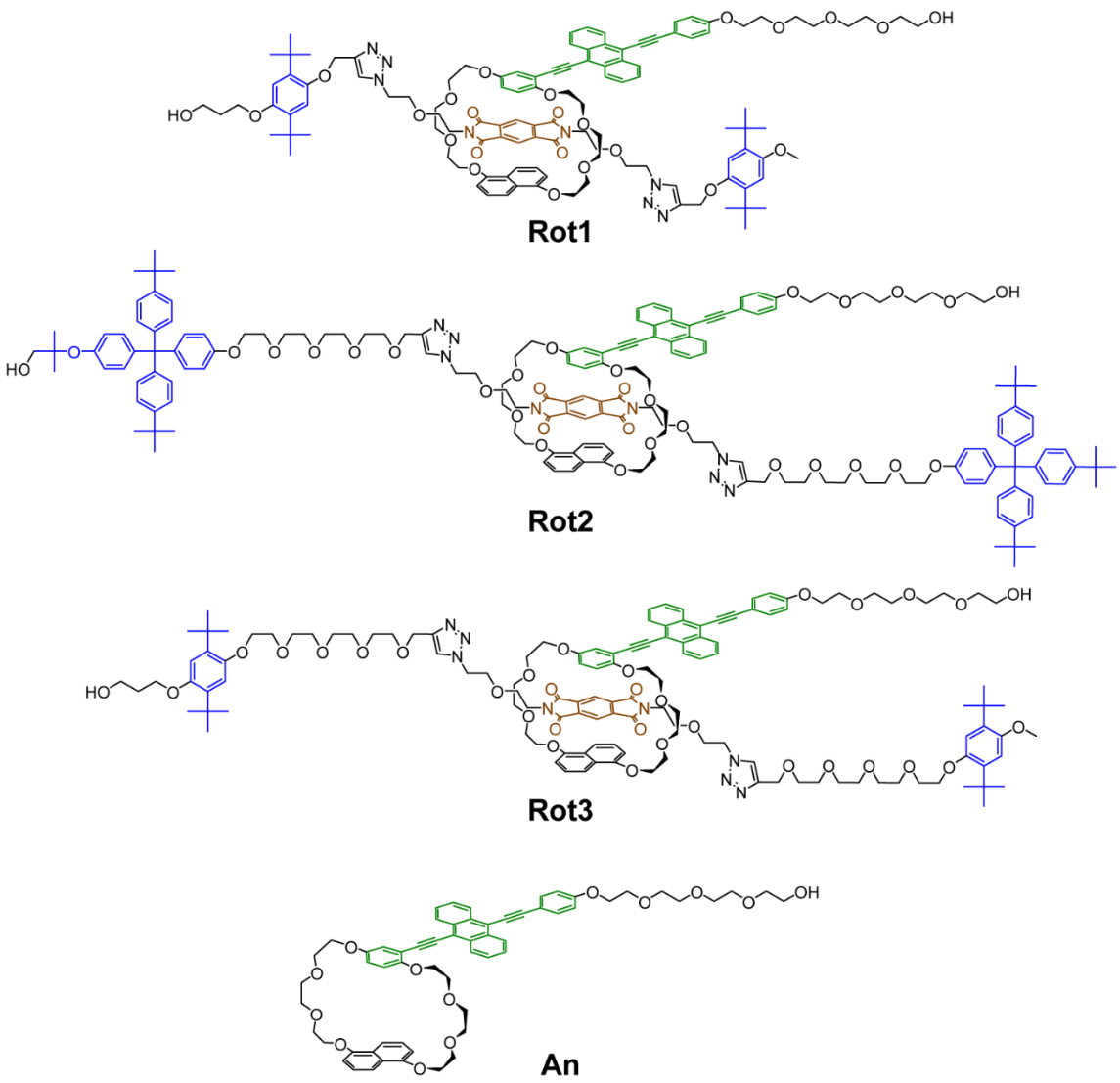

Figure 3-2. Molecular structures of the rotaxane-based supramolecular mechanophores **Rot1**, **Rot2**, **Rot3**, and the ring-luminophore motif **An**.

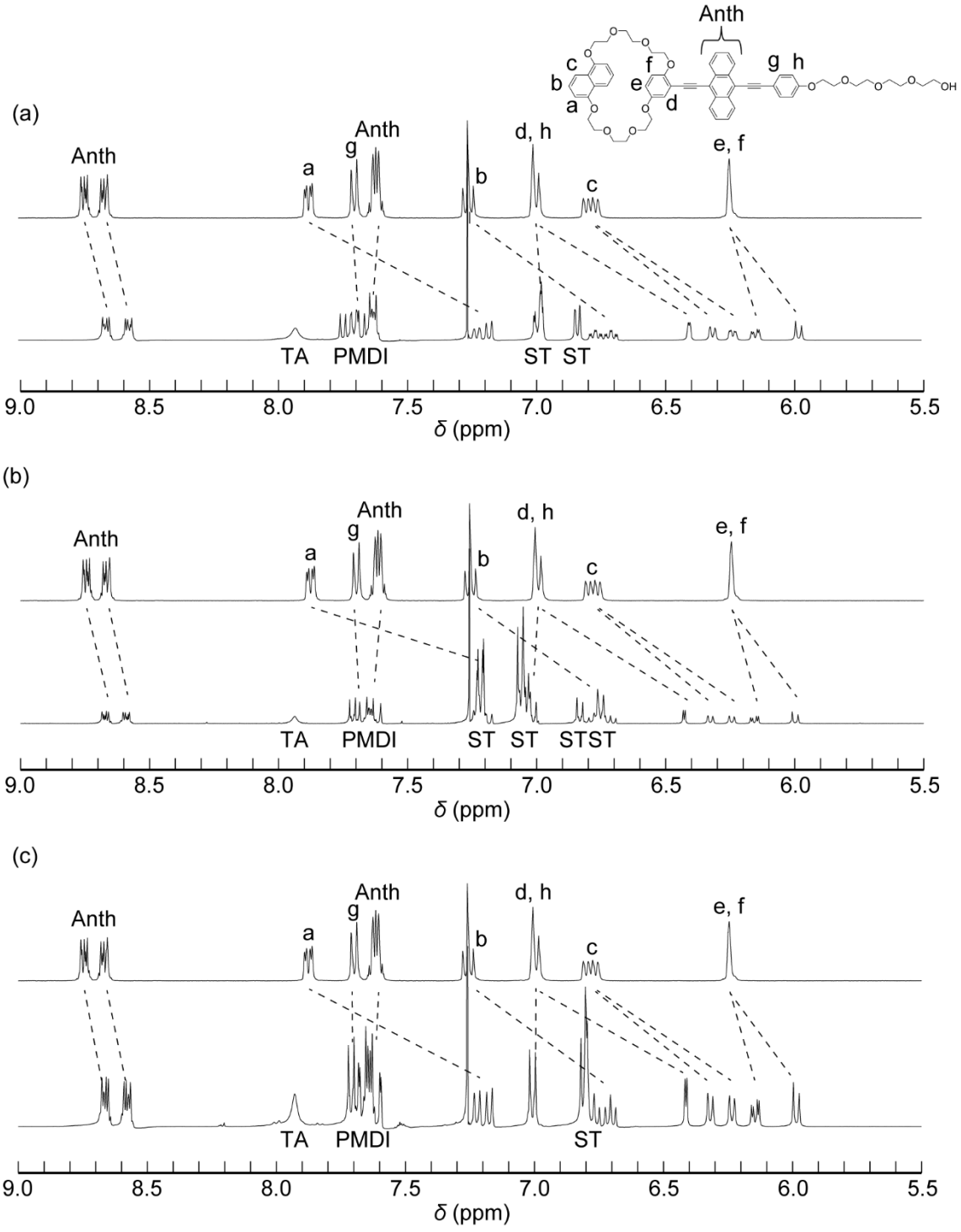

Figure 3-3. Comparison of the aromatic region of the ^{1}H NMR spectra of **An** (top) and the rotaxanes (bottom) (a) **Rot1**, (b) **Rot2**, and (c) **Rot3**. The abbreviations "ST", "TA", and "PMDI" indicate signals ascribed to the stoppers, triazole, and quencher moieties, respectively. All spectra were recorded in $CDCl_3$ at r.t. with 400 MHz.

3.2.2. Fundamental Photophysical Properties of Rot1–3 in Solutions

Absorption and fluorescence spectra of **Rot1**, **Rot2**, **Rot3**, and the free **An** were measured in dilute chloroform solutions to elucidate the photophysical properties of these motifs. The absorption spectrum of **An** (c = 1.0 × 10^{-5} M) shows a band between 400 and 500 nm with maxima at 452 and 478 nm (Figure 3-4, black dashed lines). The absorption bands of **Rot1**, **Rot2**, and **Rot3** show similar features (Figure 3-4, black solid lines); however, the peaks are slightly red-shifted, and the band shows a tail toward lower energy due to charge-transfer interactions between the luminophore and the PMDI. The slightly higher absorbance of the rotaxanes around 350 nm is attributed to the PMDI groups. The fluorescence spectrum of **An** displays green emission with maxima at 497 and 525 nm (Figure 3-4, red, green, and blue dashed lines), while solutions of **Rot1**, **Rot2**, and **Rot3** hardly fluoresce (Figure 3-4, red, green, and blue solid lines). These results show that the PMDI effectively quenches the emission of the luminophore in the force-free state. To ascertain that the ring can dethread by slippage across a *p*-di-*tert*-butylbenzene stopper, toluene solutions of **Rot1** and **Rot2** were kept under reflux over the course of 3 h (see Figures 3-5−8 and the Experimental Section for details). As expected, the fluorescence intensity of the **Rot1** solution increased significantly due to dethreading, while no changes were observed for the **Rot2** solution.

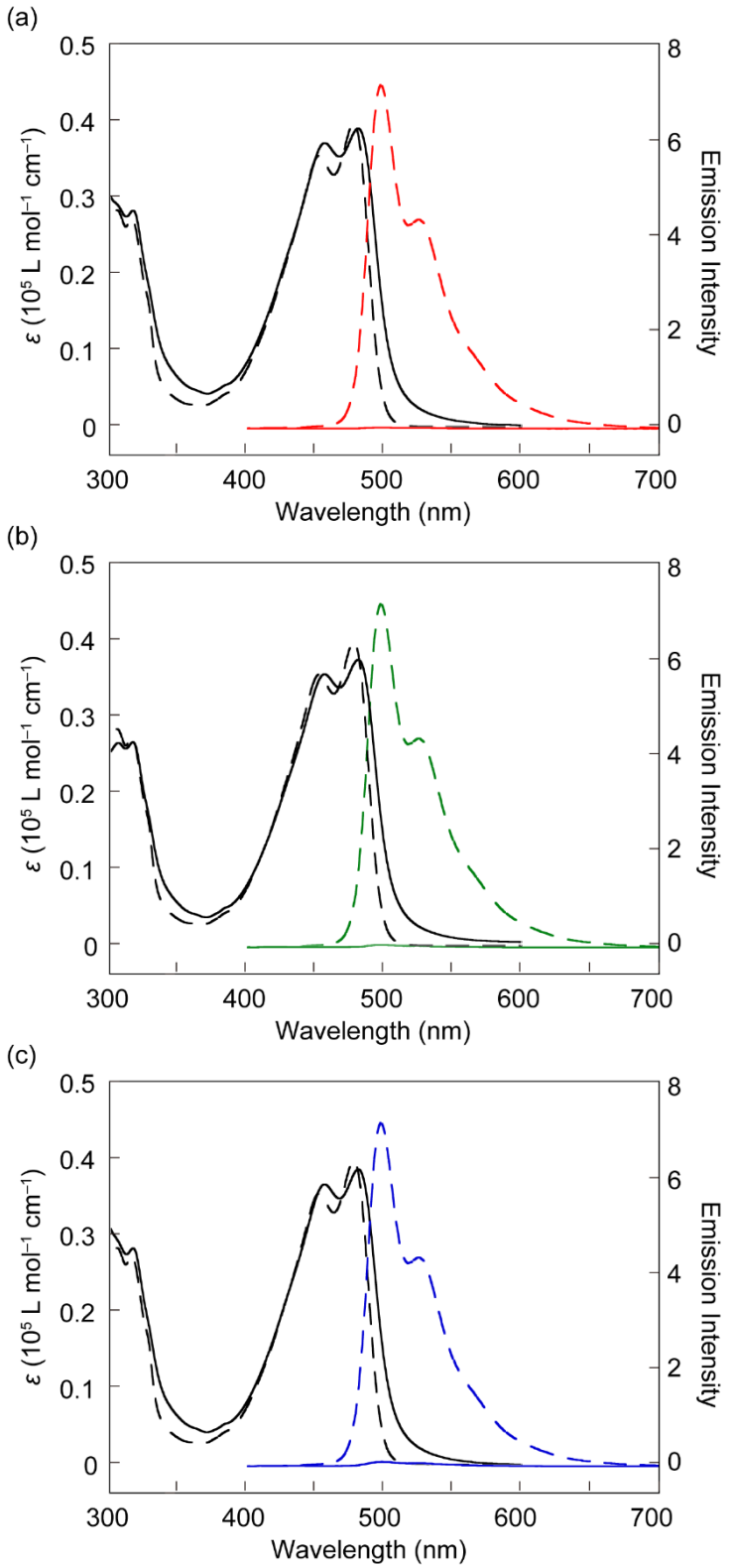

Figure 3-4. UV−vis absorption (black) and fluorescence spectra (red, green, and blue) of **An** (dashed lines), **Rot1** (a, solid line), **Rot2** (b, solid line), and **Rot3** (c, solid line) in chloroform (c = 1.0 × 10^{-5} M, λ_{ex} = 365 nm) measured at r.t.

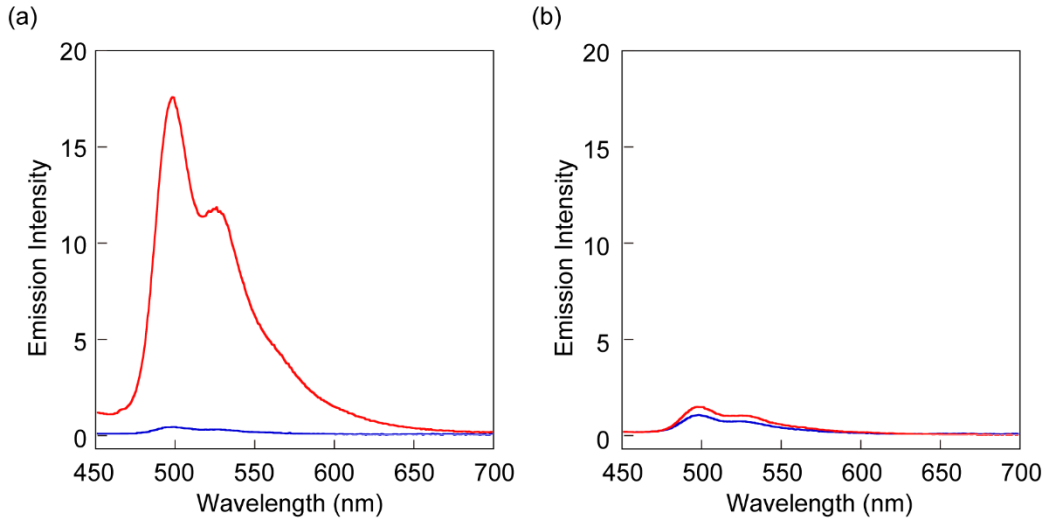

Figure 3-5. Fluorescence spectra of chloroform solutions of (a) **Rot1** and (b) **Rot2** before (blue line) and after (red line) kept under reflux for 3 h in toluene. The concentration of solutions remained constant before and after thermal treatment. All fluorescence spectra were recorded with excitation at 365 nm at r.t.

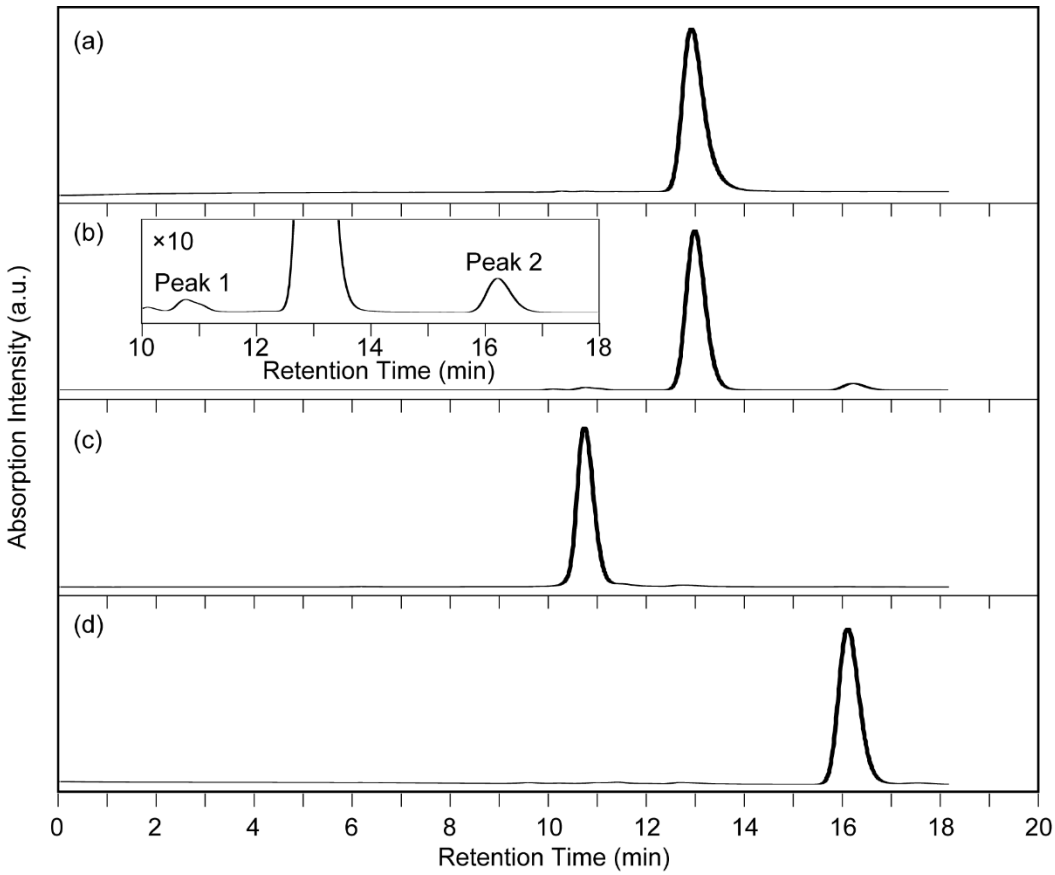

Figure 3-6. HPLC traces of (a) **Rot1**, (b) **Rot1** after kept under reflux for 3 h in toluene, (c) axle **26**, and (d) ring **An**. Eluent: methanol/isopropanol = 70/30. Flow rate: 0.3 mL/min. Detection wavelength: 254 nm.

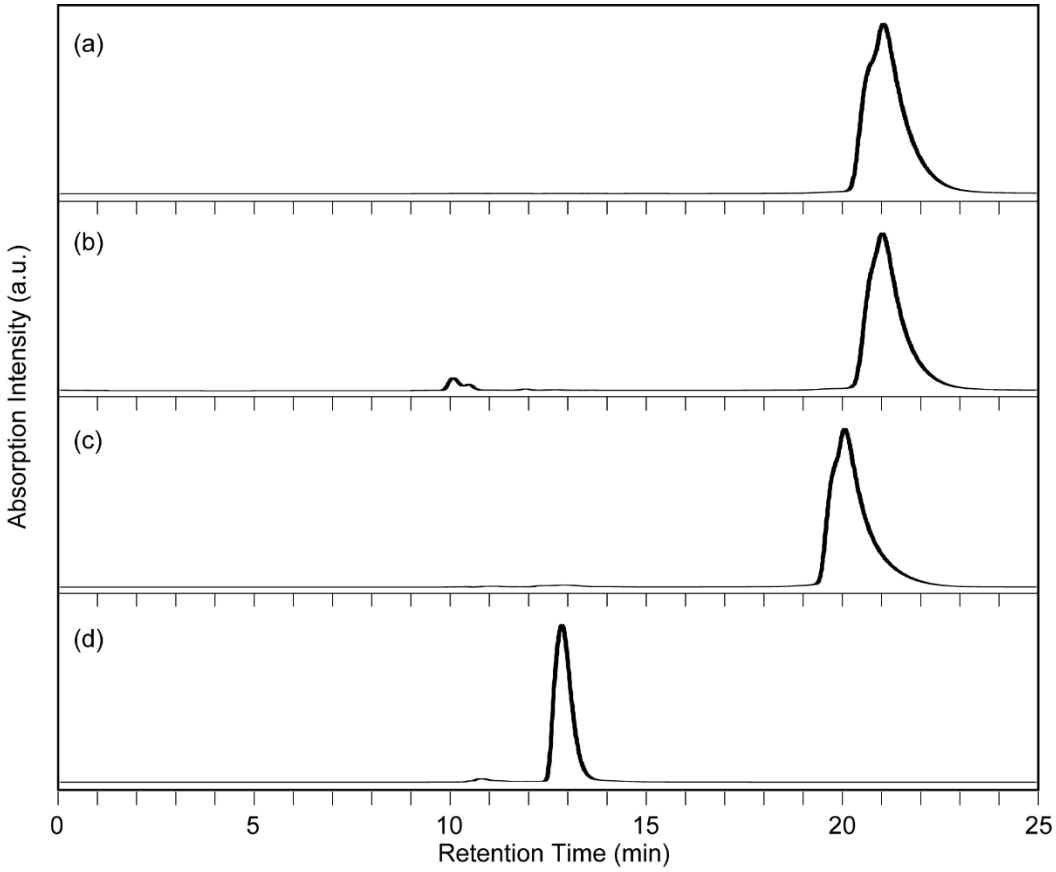

Figure 3-7. HPLC traces of (a) **Rot2**, (b) **Rot2** after kept under reflux for 3 h in toluene, (c) axle **28**, and (d) ring **An**. Eluent: : acetonitrile/isopropanol = 70/30. Flow rate: 0.3 mL/min. Detection wavelength: 254 nm.

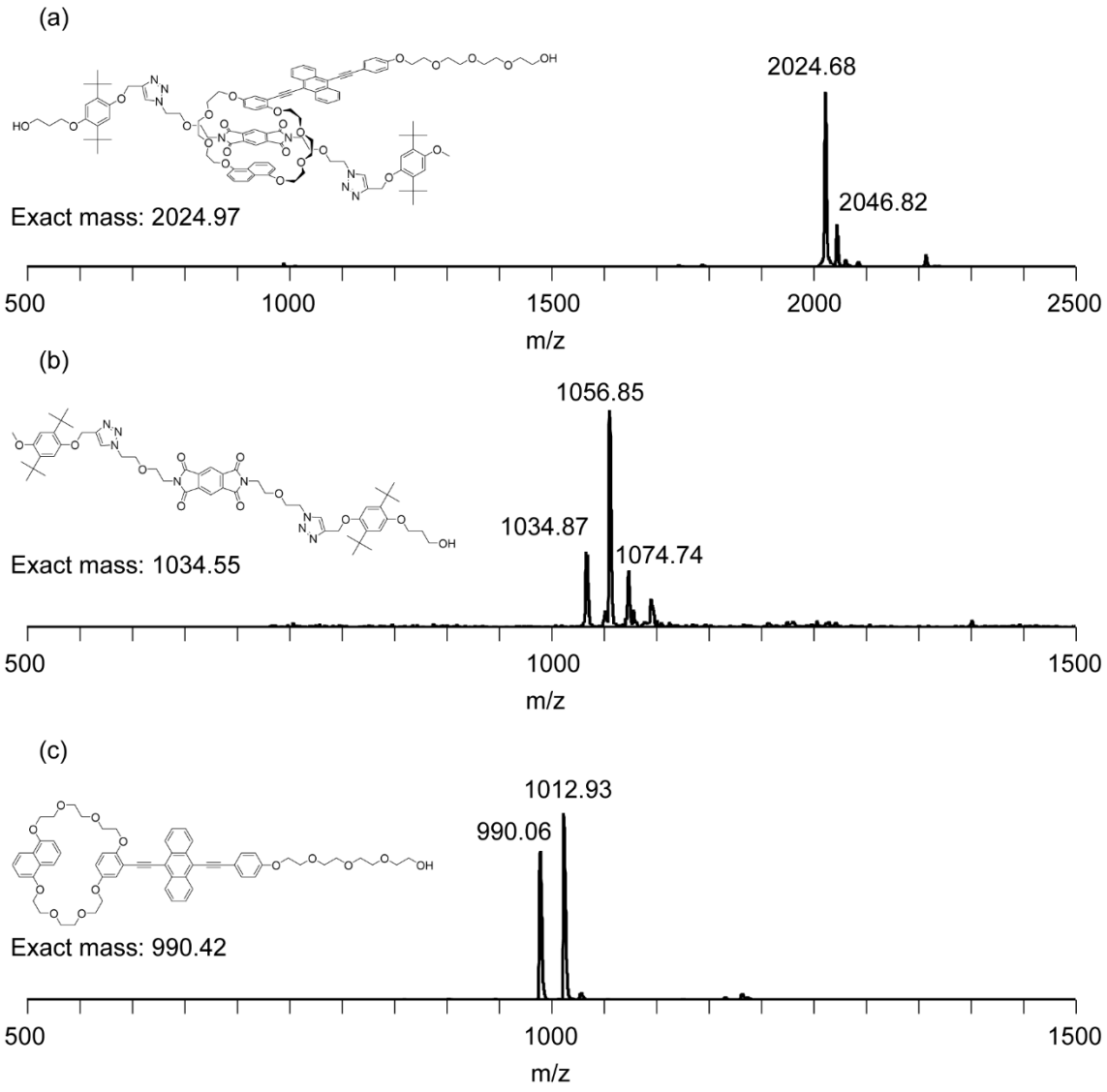

Figure 3-8. MALDI-TOF-MS spectra of (a) **Rot1**, (b) the sample collected from the Peak 1, and (c) the sample collected from the Peak 2. The Peak 1 and Peak 2 are shown in Figure 3-6.

3.2.3. Introduction of Rot1–3 into Polyurethanes

The mechanophores **Rot1**, **Rot2**, and **Rot3** were individually integrated into the backbone of linear, segmented polyurethane (PU) elastomers (**Rot1PU**, **Rot2PU**, and **Rot3PU**). The synthesis of these PUs mirrored the approach that Sagara group previously employed to explore the functionality of mechanophores[37–39,42] and involved the polyaddition reaction of telechelic poly(tetrahydrofuran)diol (number-average molecular weight, $M_n \approx$ 2000 g/mol), 4,4-methylenebis(phenyl isocyanate), and 1,4-butanediol in the presence of 0.05 mol % of the respective rotaxane mechanophore. Because of their low concentration, the rotaxanes are not discernible in the ^{1}H NMR spectra of the polymers (Figure 3-9). However, the presence of their characteristic absorption bands in tetrahydrofuran (THF) solutions of **Rot1PU**, **Rot2PU**, and **Rot3PU** corroborates the successful integration of the mechanophores (Figure 3-10). The fluorescence spectra show that the emission remains quenched after polymerization (Figure 3-10). Overall, the spectra of the PUs mirror those of the corresponding rotaxanes, indicating that the incorporation of **Rot1**, **Rot2**, and **Rot3** into the polymer backbone hardly affects their photophysical properties in solution.

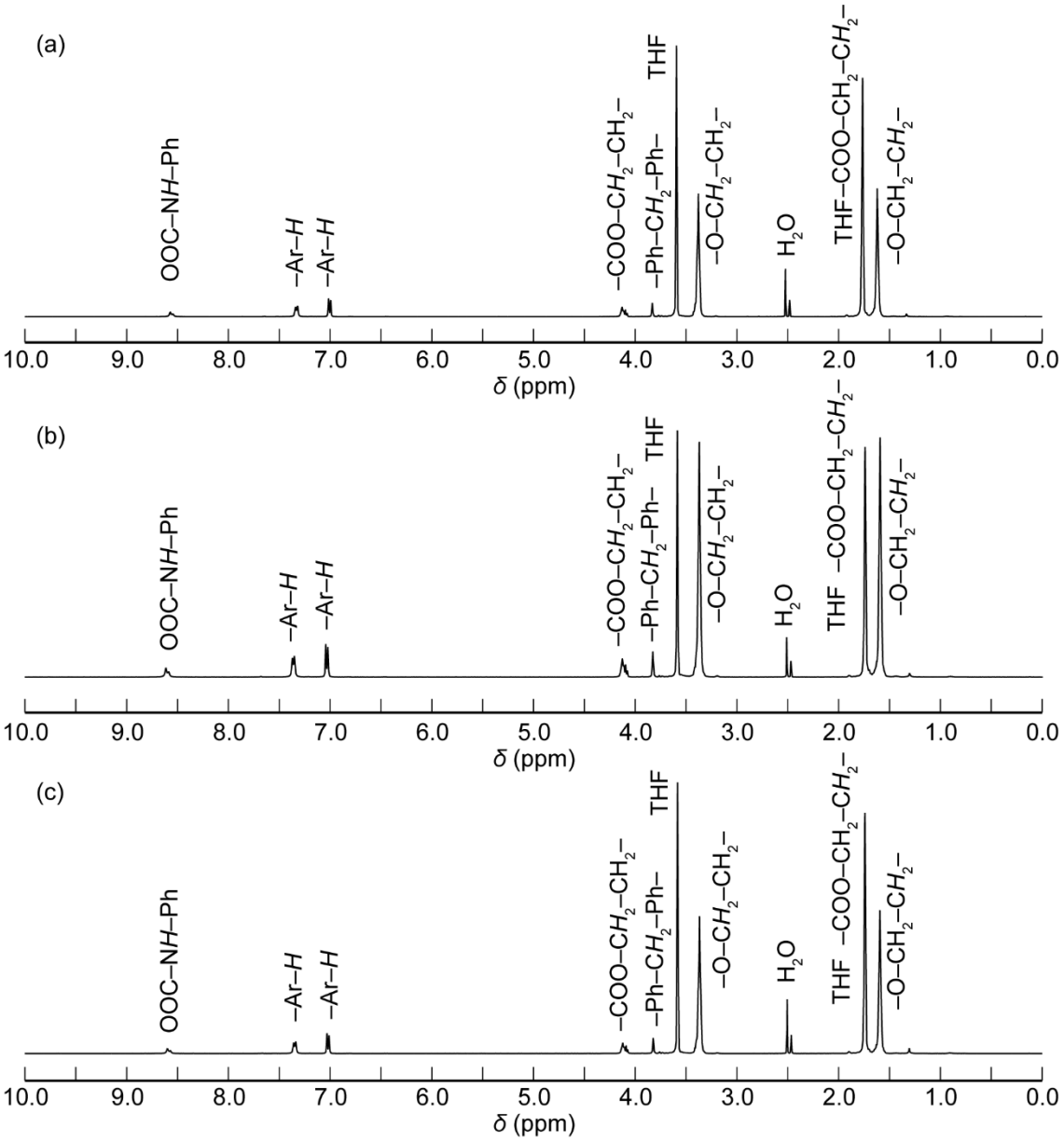

Figure 3-9. Comparison of the ^{1}H NMR (400 MHz, THF-d_8) spectra of (a) **Rot1PU**, (b) **Rot2PU**, and (c) **Rot3PU**. The different signals were assigned to the protons of the polyurethane chain and no signals ascribed to the rotaxane mechanophores were observed due to its low concentration in the polymer chain. All spectra were recorded at r.t.

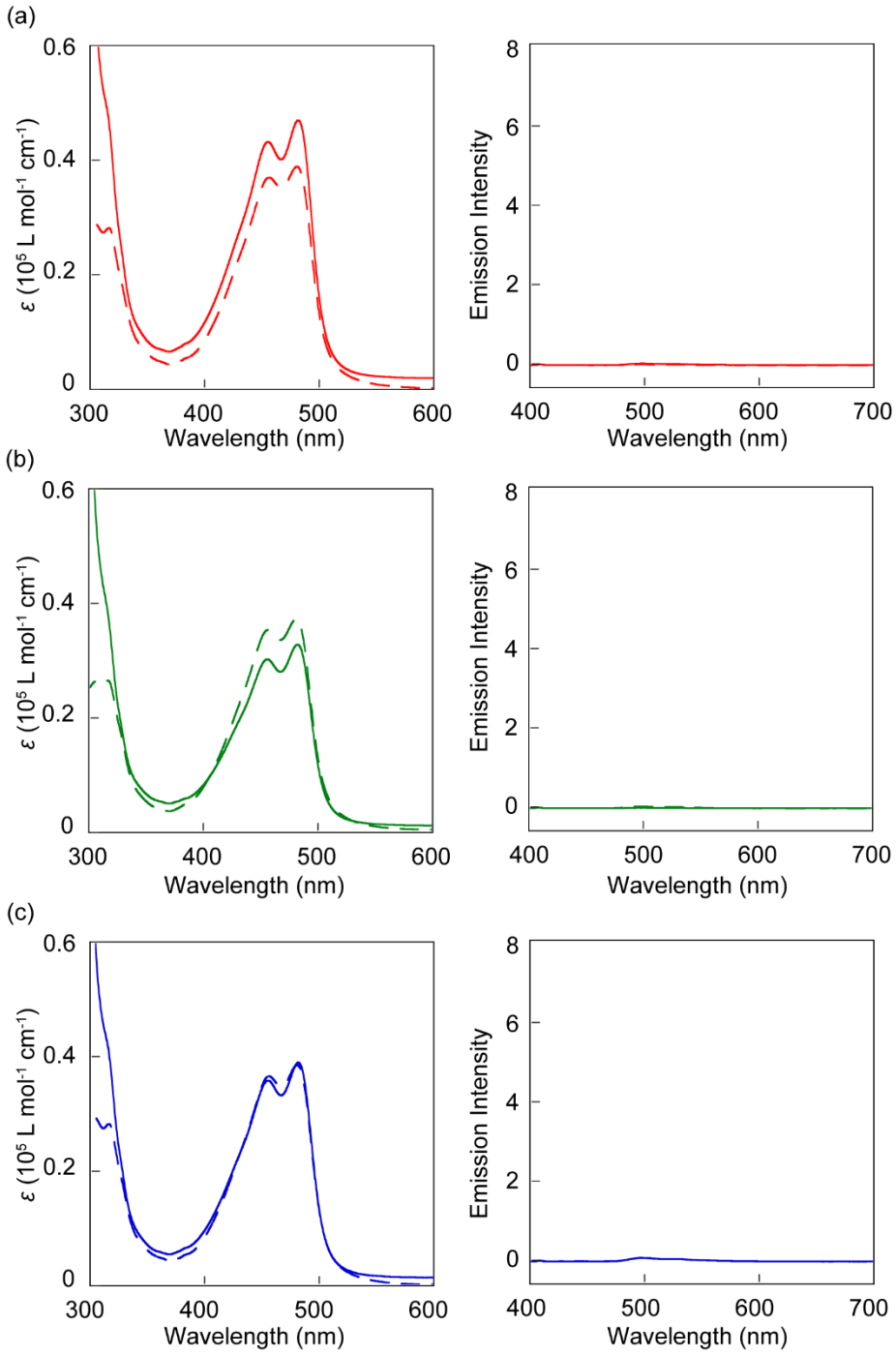

Figure 3-10. Comparison of the absorption (left) and fluorescence (right) spectra of the individual rotaxanes (dashed lines) and the corresponding polyurethanes (solid lines). (a) **Rot1** and **Rot1PU**, (b) **Rot2** and **Rot2PU**, and (c) **Rot3** and **Rot3PU**. The spectra of the rotaxanes were recorded at a concentration of 1.0×10^{-5} M in chloroform. The concentration of the different PUs in THF were adjusted so that the concentration of rotaxane was ca. 1.0×10^{-5} M. All fluorescence spectra were recorded under the same conditions as for the spectra of solutions of **An** (see Figure 3-4).

Thin films of **Rot1PU**, **Rot2PU**, and **Rot3PU** with a thickness of 60−90 μm were prepared by solvent casting from THF. The thermal and mechanical properties of the polymers were characterized by thermogravimetric analysis (TGA, Figure 3-11), differential scanning calorimetry (DSC, Figure 3-12), dynamic mechanical analysis (DMA, Figure 3-13), and tensile testing (Figure 3-14 and Table 1). The mechanical properties of the three PUs are essentially identical and mirror those of previously reported PU elastomers,[37−39,42,62,63] allowing me to compare the behavior of the present polymers to that of other rotaxane-based mechanochromic PUs.

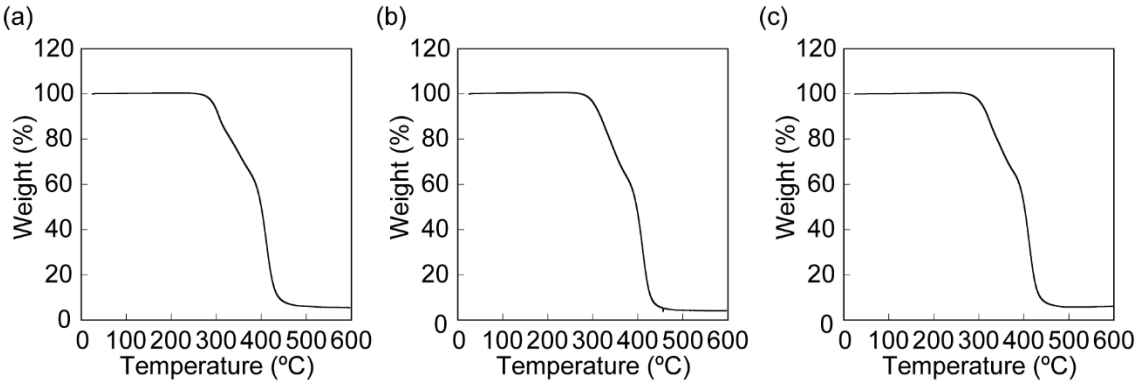

Figure 3-11. TGA traces of (a) **Rot1PU**, (b) **Rot2PU**, and (c) **Rot3PU** films. A heating rate of 10 °C/min was used for all measurements

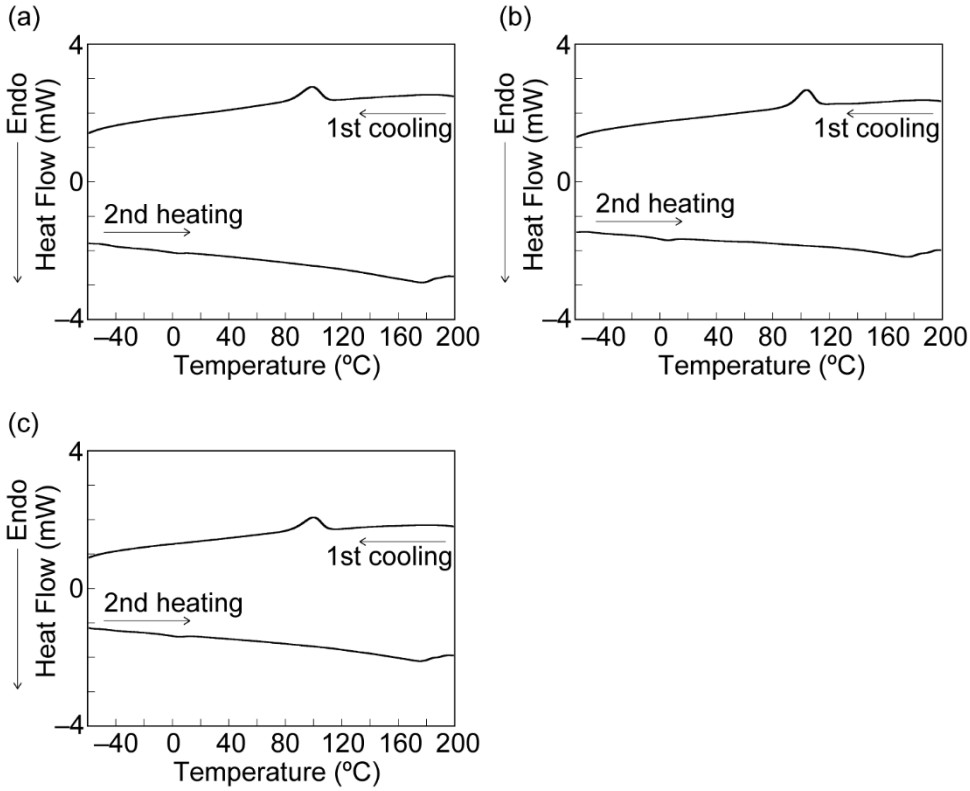

Figure 3-12. DSC traces of (a) **Rot1PU**, (b) **Rot2PU**, and (c) **Rot3PU** films. A heating and cooling rate of 10 °C/min was employed for all measurements.

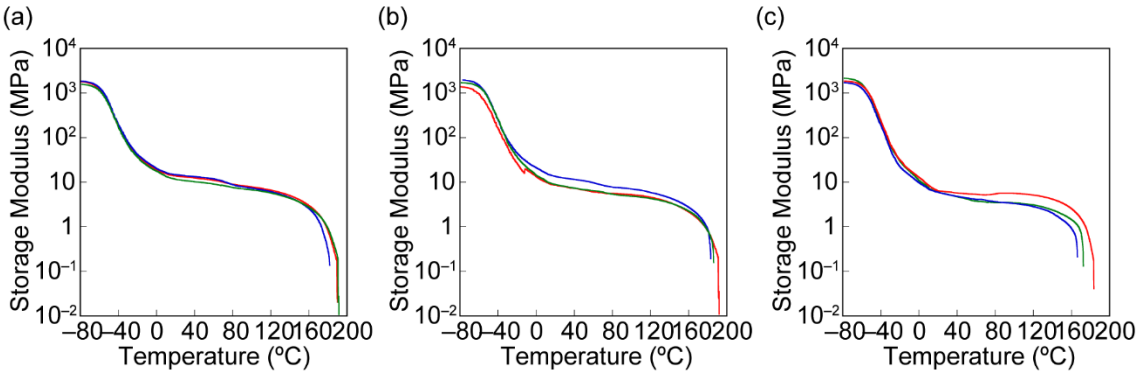

Figure 3-13. DMA traces of (a) **Rot1PU**, (b) **Rot2PU**, and (c) **Rot3PU** films. Each graph shows data obtained from three individual specimen. The tests were conducted under a N_2 atmosphere with a heating rate of 3 °C/min, a frequency of 1 Hz, and an amplitude of 15 μm.

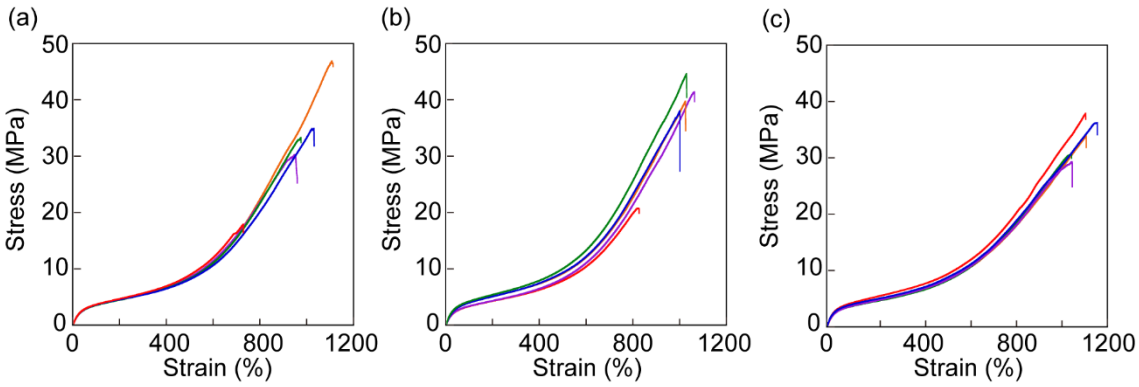

Figure 3-14. Stress-strain curves of (a) **Rot1PU**, (b) **Rot2PU**, and (c) **Rot3PU** films. The individual stress-strain curves of five different specimens are shown for each polymer. The experiments were conducted with a strain rate of 120 mm/min at r.t.

Table 1. Overview of the mechanical properties of **Rot1PU**, **Rot2PU**, and **Rot3PU** films as determined from stress-strain curves recorded during uniaxial tensile deformation (see Figure 3-14).[a)]

	Elongation at break (%)	Stress at break (MPa)	Young's modulus[b)] (MPa)
Rot1PU	962 ± 233	31.2 ± 15.2	11.9 ± 1.1
Rot2PU	981 ± 197	36.4 ± 18.2	12.8 ± 1.2
Rot3PU	1095 ± 63	33.4 ± 4.6	12.4 ± 3.6

a) All data were extracted from the stress-strain curves shown in Figure 3-14 and represent averages of 5 measurements ± standard deviation. b) The Young's moduli were derived from the slopes of the stress-strain curves in the strain regime between 0.5–1.0%.

As prepared **Rot1PU**, **Rot2PU**, and **Rot3PU** films show faint green fluorescence when excited at 365 nm (Figure 3-15), although the THF solutions hardly fluoresce (Figure 3-10). I ascribe this to the fact that a minor fraction of the rings is kinetically trapped in positions away from the quencher when the films solidify. The as-prepared **Rot1PU** films also display non-negligible photoluminescence around 580 nm, perhaps due to exciplex formation between the luminophore and PMDI, which was not observed in rotaxanes containing the same luminophore and a naphthalene diimide quencher.[38] The photoluminescence spectra of **Rot2PU** and **Rot3PU** films only show very weak monomer emission; presumably the longer axle in these rotaxanes leads to a higher fraction of rings that become trapped away from the quencher upon drying, leading to stronger monomer fluorescence and a weaker exciplex band than in **Rot1PU**.

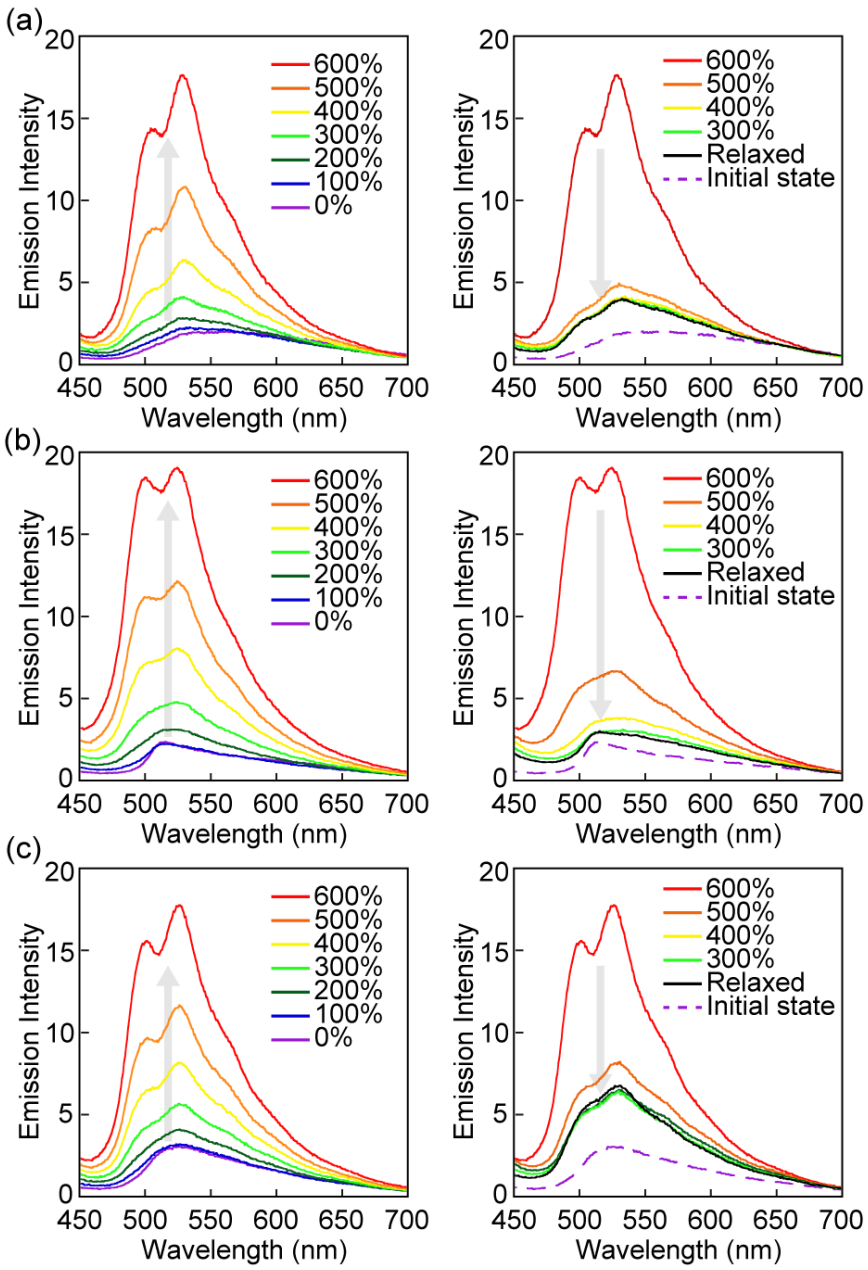

Figure 3-15. Fluorescence spectra of (a) **Rot1PU**, (b) **Rot2PU**, and (c) **Rot3PU** films recorded upon uniaxial deformation to the indicated strains (left) and subsequent relaxation from the maximum strain of 600% (right). In the right panels, the spectra before deformation (dotted lines) are reproduced for the purpose of comparison. All fluorescence spectra were recorded with excitation at 365 nm at r.t.

3.2.4. Mechanoresponsive Luminescence Behavior of Rot1–3PU

When subjecting **Rot1PU**, **Rot2PU**, and **Rot3PU** films to uniaxial tensile deformation, fluorescence turn-on is observed (Figure 3-16). In all cases, the fluorescence intensity increases with the applied strain (Figure 3-15, left). The spectral shapes differ a bit from those of **An** in chloroform (Figure 3-4), notably on the high-energy end, due to self-absorption. When the stress is removed and the samples relax, the fluorescence intensity decreases immediately (Figure 3-15, right). Thus, in spite of all modifications, all three rotaxanes function as supramolecular mechanophores and display an instant, at least partially reversible fluorescence turn-on, similar to previously reported rotaxane-based mechanophores.[37–39]

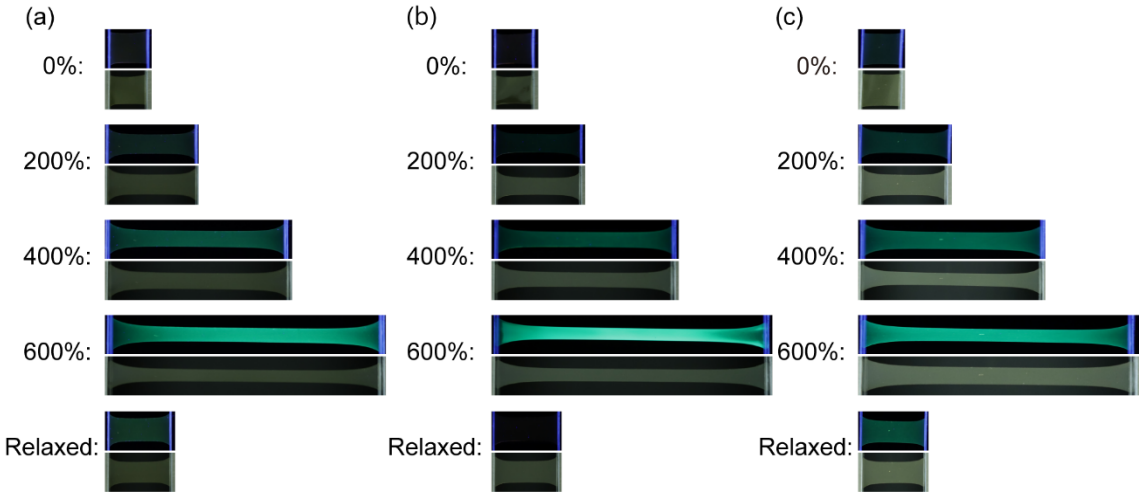

Figure 3-16. Photographs of (a) **Rot1PU**, (b) **Rot2PU**, and (c) **Rot3PU** films upon stretching. The top images were taken in the dark with illumination by UV light (365 nm), while the bottom images were taken under ambient light illumination, at the different indicated strains.

A closer inspection of the spectra shown in Figure 3-15 shows that the fluorescence intensity of **Rot1PU** and **Rot3PU** films after straining to 600% and allowing the samples to relax is slightly higher than in the pristine films (Figure 3-15a,c). By contrast, **Rot2PU** films that feature the rotaxane with bulky tris(*p*-*tert*-butylphenyl)phenylmethane stoppers

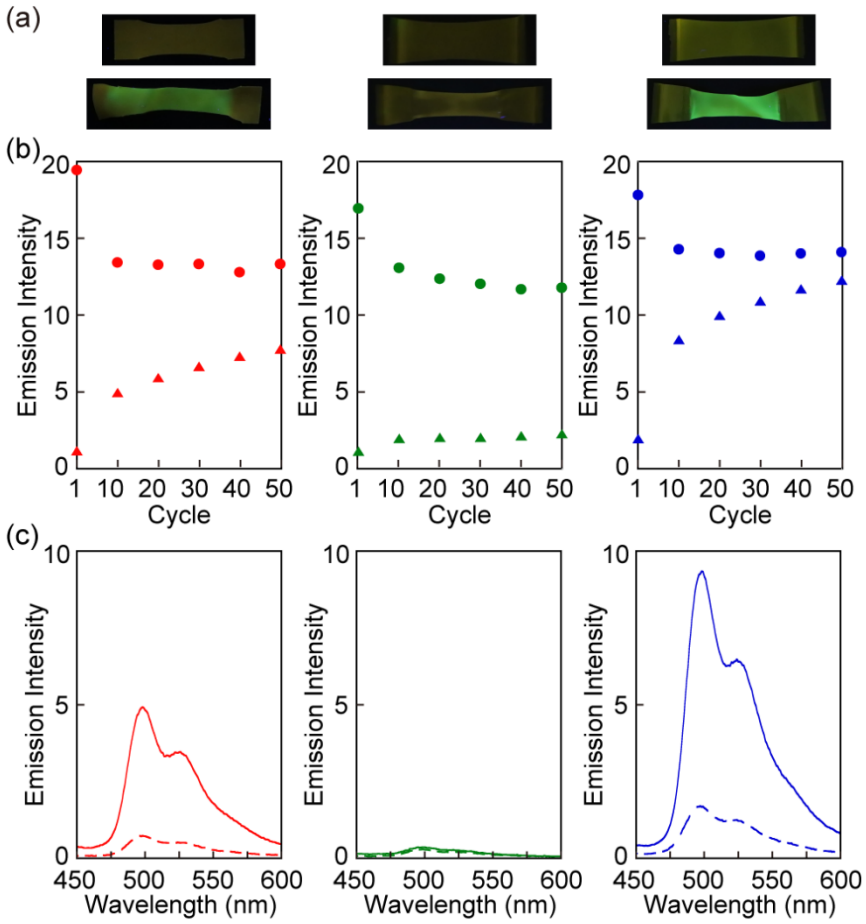

Figure 3-17. (a) Photographs of the pristine films (top) and the films in the relaxed state after 50 deformation/relaxation cycles (bottom) for **Rot1PU** (left), **Rot2PU** (middle), and **Rot3PU** (right). The images were taken under UV light illumination (λ_{ex} = 365 nm) at r.t., and the applied strain was 600%. (b) Plot of the fluorescence intensity at 500 nm of **Rot1PU** (left), **Rot2PU** (middle), and **Rot3PU** (right) films in the relaxed state (triangles) and upon deformation to a strain of 600% (circles) over the course of 50 loading−unloading cycles. (c) Fluorescence spectra of THF solutions (8.1 mg/mL) of the pristine films (dashed line) and of the stretched portions of films that were subjected to 50 loading−unloading cycles to 600% (solid line) of **Rot1PU** (left), **Rot2PU** (middle), and **Rot3PU** (right). All spectra were recorded at r.t. with λ_{ex} = 365 nm.

show almost no change in the fluorescence intensity after experiencing the same strain (Figure 3-15b). The differences become even more apparent when samples were subjected to 50 loading−unloading cycles (Figure 3-17). Photographs of relaxed **Rot1PU** and **Rot3PU** films display strong green fluorescence in the deformed sections after being deformed 50 times to a strain of 600% (Figure 3-17a, left and right), whereas hardly any emission is seen in the case of **Rot2PU** (Figure 3-17a, middle). The different behaviors are also discernible in the fluorescence intensities of **Rot1PU**, **Rot2PU**, and **Rot3PU** films in the relaxed and strained (600%) states recorded at 500 nm after up to 50 cycles of deformation and relaxation (Figure 3-17b). In all materials, the fluorescence intensity in the stretched state decreases in the first cycles, which is ascribed to the intrinsic hysteresis of the PUs, i.e., irreversible rearrangements when pristine films are first deformed.[64] In the case of **Rot1PU** and **Rot3PU**, the fluorescence intensity in the relaxed state gradually increases with the number of stress-release cycles, while the one of **Rot2PU** hardly changes, even after 50 cycles. After the cyclic testing, the stretched portions of the films were dissolved in THF, and the fluorescence spectra were recorded (Figure 3-17c). In the case of **Rot1PU** and **Rot3PU**, the fluorescence intensity is much higher than in the corresponding solutions of the pristine polymers, whereas the solution of the strained **Rot2PU** film shows the same weak emission as the pristine polymer. Thus, the data indicate that in **Rot1PU** and **Rot3PU** repeated extensive deformation causes the irreversible separation between the luminophore and the quencher. I conclude that this disassembly is related to dethreading and not chain scission, which is supported by the results of thermal treatment experiments and other experiments (see below). I note that **Rot3PU** shows a higher extent of dethreading upon deformation than **Rot1PU**, possibly due to interactions between the stopper and the triazole that affect the conformation of **Rot1** in the PU and slightly hinders dethreading when compared to **Rot3**. This is supported by the observed differences in the chemical shifts of the peaks corresponding

to the stoppers of **Rot1** and **Rot3** in the ^{1}H NMR spectra (Figure 3-3). I speculate that this interaction in solution remains after solvent casting to form solid films.

To obtain further insights into the behavior of the new mechanophores, additional experiments were performed with **Rot3PU**, which based on the data shown in Figures 3-15 and 3-17 seems to show a slightly higher extent of dethreading upon deformation than **Rot1PU**. First, the cyclic stretch and release experiment was repeated, but the strain was increased stepwise from 300% to 600% (Figure 3-18). No significant increase of the emission intensity in the relaxed state was observed over the course of 50 cycles when the maximum strain was limited to 300%, indicating that at low strain dethreading is negligible. When the maximum strain was increased to 600%, the emission intensity in the relaxed state increased gradually with the number of cycles and the applied strain, with a much larger effect at the higher strain, at which dethreading becomes significant. I also monitored the emission intensity of a film that was kept deformed to a strain of 600% for 2 min and subsequently relaxed (Figure 3-19). In the stretched state, the emission intensity gradually decreases and thereby reflects the material's dynamic stress−relaxation. After removing the stress, the sample shows almost the same emission intensity as a sample that was stretched and immediately relaxed, suggesting that dethreading occurs when the stress experienced by an individual motif exceeds a given threshold.

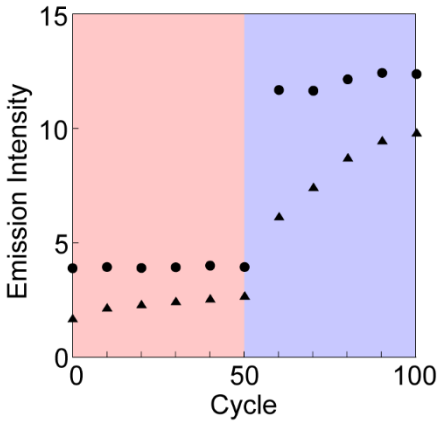

Figure 3-18. Plot of the changes in the fluorescence intensity at 500 nm for **Rot3PU** films in the relaxed state (triangles) and upon deformation (circles) to a strain of 300% (red) and 600% (blue) over the course of 50 loading-unloading cycles. All spectra were recorded at r.t. with λ_{ex} = 365 nm.

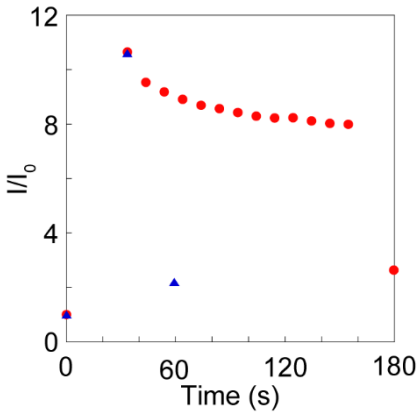

Figure 3-19. Plots of fluorescence intensities of **Rot3PU** films as a function of time upon normal deformation and relaxation (triangles) and upon deformation, keeping the strain 600% for 2 min and subsequent relaxation (circles). For each case, the deformation ended at ~33 s. The fluorescence intensities were measured at 500 nm.

3.2.5. Sonomechanochemical Experiments of Rot1–3PU

Sonomechanochemical experiments were performed to further corroborate that the mechanoresponsive behavior of **Rot1PU** and **Rot3PU** is different from that of **Rot2PU**. Upon sonication for 120 min, the fluorescence intensity of solutions of both **Rot1PU** and **Rot3PU** increases significantly and irreversibly (Figure 3-20a,c), whereas solutions of **Rot2PU** show barely any change of the fluorescence intensity (Figure 3-20b). These results indicate that force-induced dethreading indeed occurs for **Rot1** and **Rot3**. Size

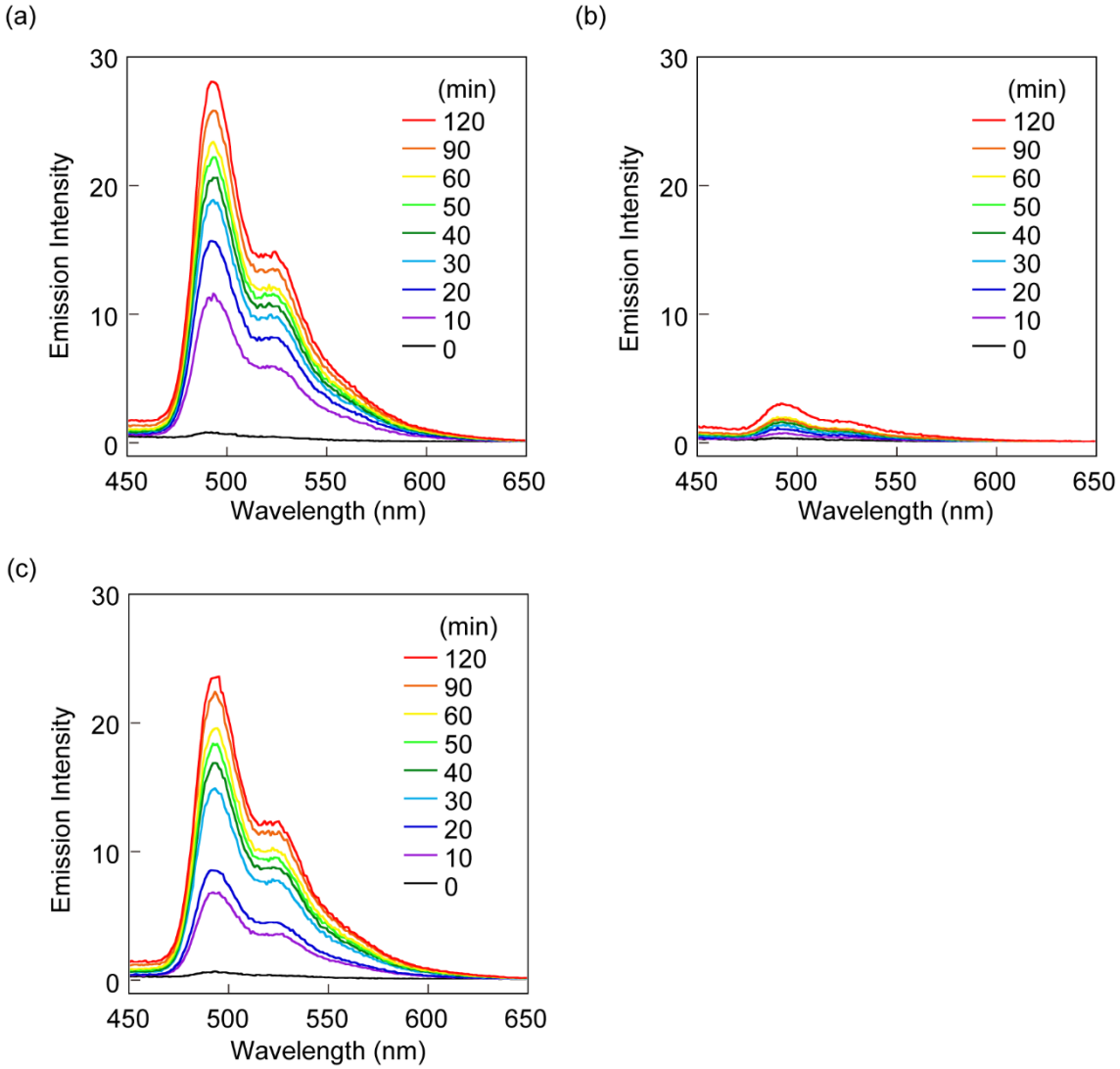

Figure 3-20. Fluorescence spectra of THF solutions of (a) **Rot1PU** (0.95 mg/mL), (b) **Rot2PU** (1.1 mg/mL), and (c) **Rot3PU** (1.1 mg/mL) after sonication for 2 h. All fluorescence spectra were recorded with excitation at 365 nm.

exclusion chromatography (SEC) measurements show that the molecular weights gradually decreased for all samples (Figure 3-21). A comparison of the rate of this decrease shows a similar behavior for **Rot1PU** and **Rot2PU**, which have similar molecular weights but different stopper sizes, suggesting that random chain scission and not dethreading of the rotaxane mechanophore is the major contributor to the decrease in molecular weight (Figure 3-22).[65,66] This is consistent with the facts that chain scission upon sonication occurs close to the center of the macromolecules, where the elongational

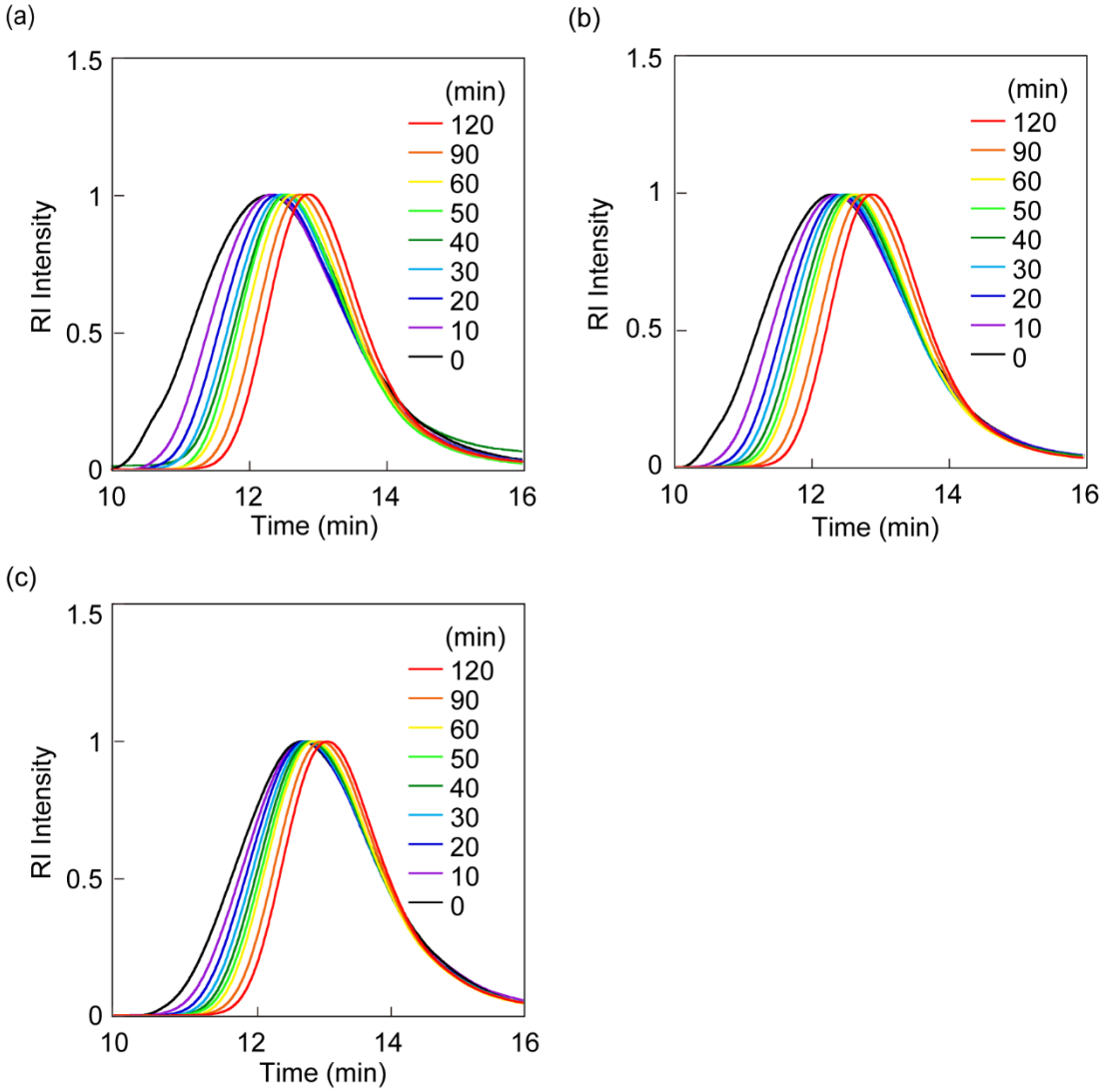

Figure 3-21. Size exclusion chromatography (SEC) traces of (a) **Rot1PU**, (b) **Rot2PU**, and (c) **Rot3PU** upon sonication for 2 h. The traces were normalized to the peak maximum of the chromatograms

forces are highest,[1,67] and that in the present PUs the rotaxanes are randomly incorporated in the polymer backbone.

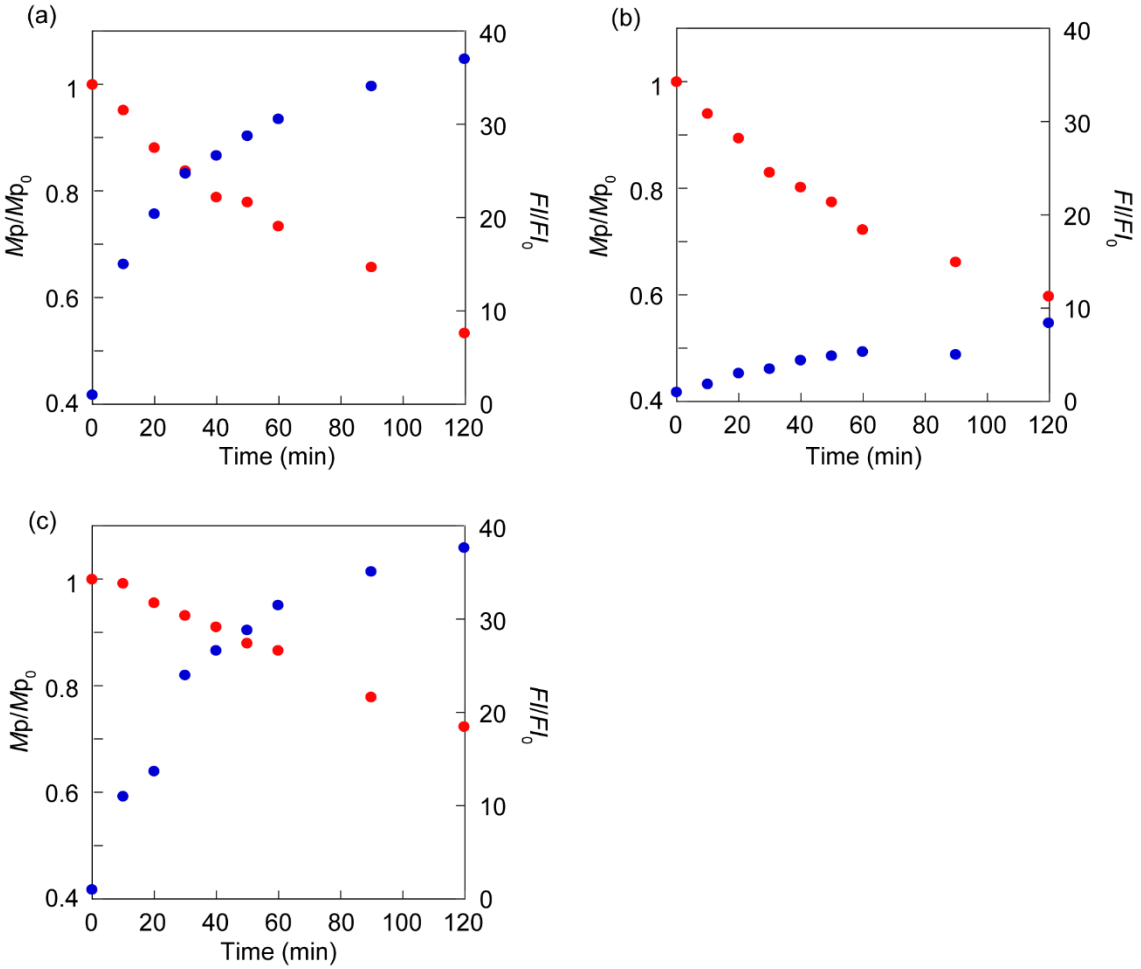

Figure 3-22. Plots of the peak molecular weight ratios Mp/Mp_0 (red) and fluorescence intensity ratio FI/FI_0 (blue) as a function of sonication time for (a) **Rot1PU**, (b) **Rot2PU**, and (c) **Rot3PU**. Mp/Mp_0 is the ratio between the polymer's molar mass determined at the peak maximum of the SEC trace after sonication for time t and the molar mass at t = 0 min. FI/FI_0 is the ratio of the fluorescence intensity at 500 nm of each polymer solution before sonication and after sonication for time *t*.

3.2.5. Verification of Force-Induced Dethreading

To unequivocally confirm that the irreversible dissociation of quencher and emitter in polymers containing **Rot1** and **Rot3** is not caused by covalent chain scission of the rotaxane's axle or ring, mechanophore **Rot4** was devised. Its design resembles that of **Rot1**, but the axle was extended beyond one of the stoppers and contains a second PMDI quencher and an additional, bulkier tris(*p-tert*-butylphenyl)phenylmethane stopper (Figure 3-23). This structure is based on the rationale that once the ring slips past the first (smaller) stopper, it becomes trapped between the two stoppers, and unless covalent chain scission events occur, no irreversible activation should be possible. **Rot4** was synthesized and characterized in the same way as the other rotaxanes (see Figure 3-24 and the Experimental Section for details). **Rot4** features a similar absorption spectrum as **Rot1**, and in solution the fluorescence is also almost completely quenched (Figure 3-25). **Rot4** was incorporated into the backbone of a PU elastomer (**Rot4PU**) by using the same synthetic framework as for the other PUs, and the polymer was processed into 60−90 μm thick films by using the same solution-casting process that was applied for the other materials. The photophysical properties of **Rot4PU** in THF are similar to the ones of **Rot4** in chloroform (Figures 3-25 and 3-26), and the ^{1}H NMR spectra and thermomechanical properties of **Rot4PU** mirror those of **Rot1PU**, **Rot2PU**, and **Rot3PU** (Figures 3-27 and 3-28, Table 2)

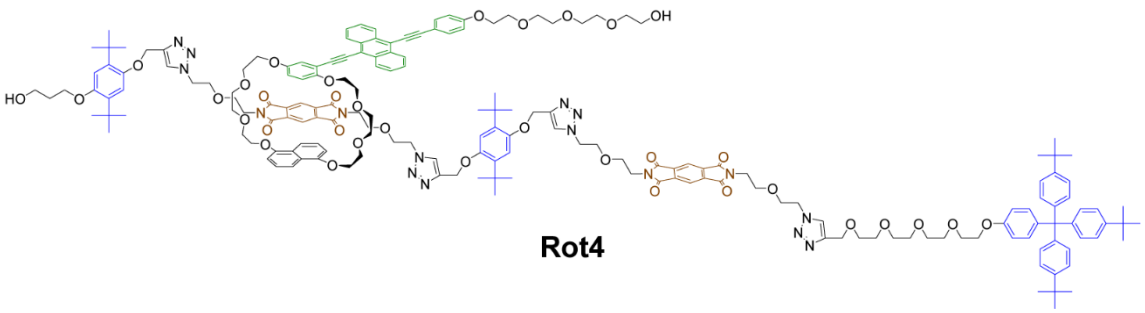

Figure 3-23. Molecular structure of the rotaxane-based supramolecular mechanophore **Rot4**.

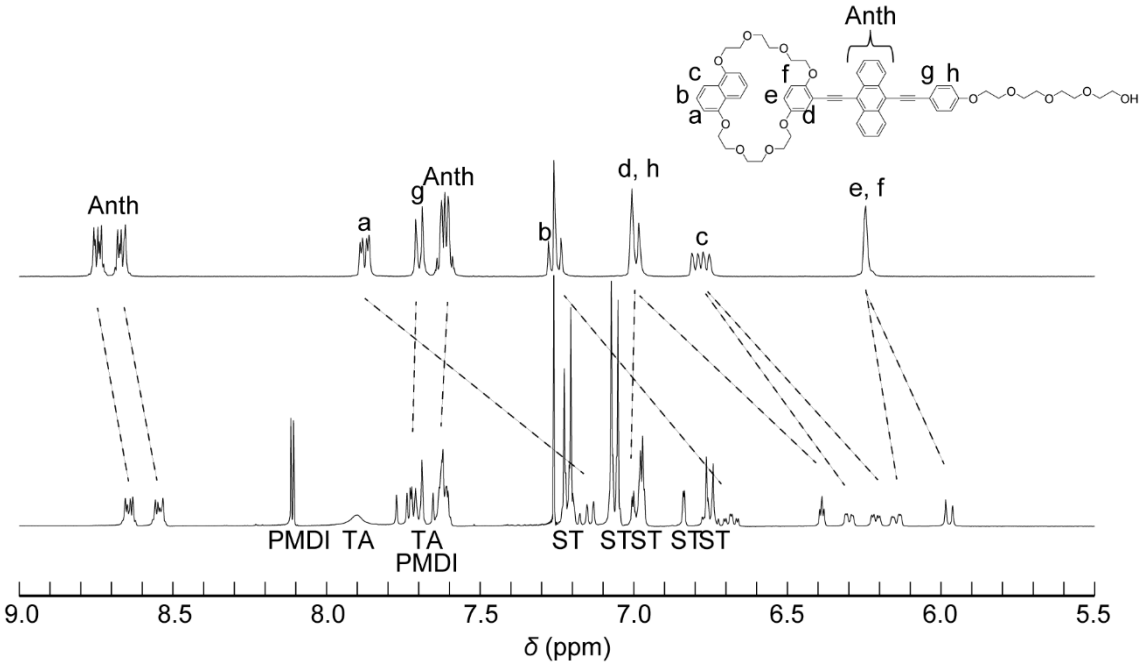

Figure 3-24. Comparison of the aromatic region of the ^{1}H NMR spectra of **An** (top) and **Rot4** (bottom). The abbreviations "ST", "TA", and "PMDI" indicate signals ascribed to the stoppers, triazole, and quencher moieties, respectively. This spectrum was recorded at 400 MHz in $CDCl_3$ at r.t.

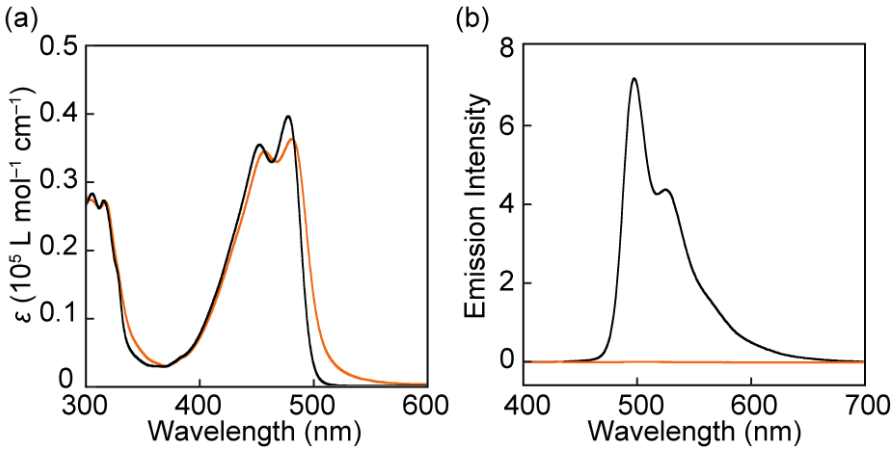

Figure 3-25. Comparison of the (a) absorption and (b) fluorescence spectra of chloroform solutions of **An** (black) and **Rot4** (orange) (c = 1.0 × 10^{-5} M; λ_{ex} = 365 nm). The absorption and fluorescence spectra were recorded at r.t.

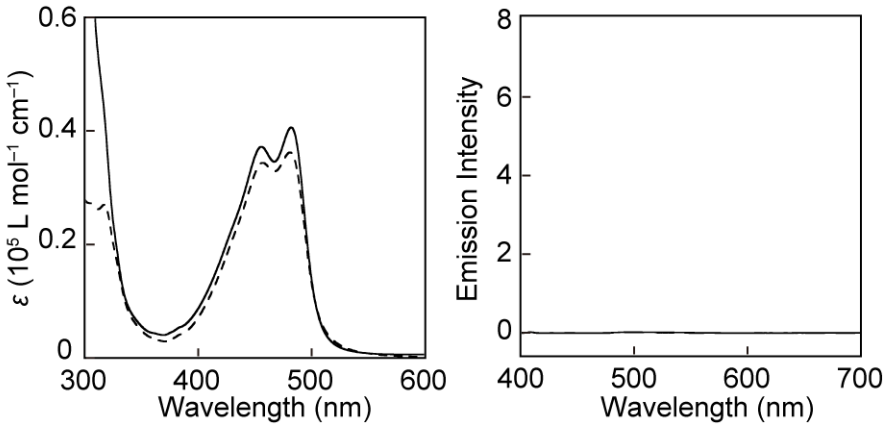

Figure 3-26. Absorption (left) and fluorescence spectra (right) of **Rot4** in chloroform (dashed line) and the corresponding PUs in THF (solid line). The concentrations of rotaxanes were 1.0×10^{-5} M. The concentration of **Rot4PU** in THF solution was adjusted so that the concentrations of corresponding rotaxanes inside the polymer were 1.0×10^{-5} M. The fluorescence spectra were recorded under the same condition as the solution of **An** shown in Figure 3-4.

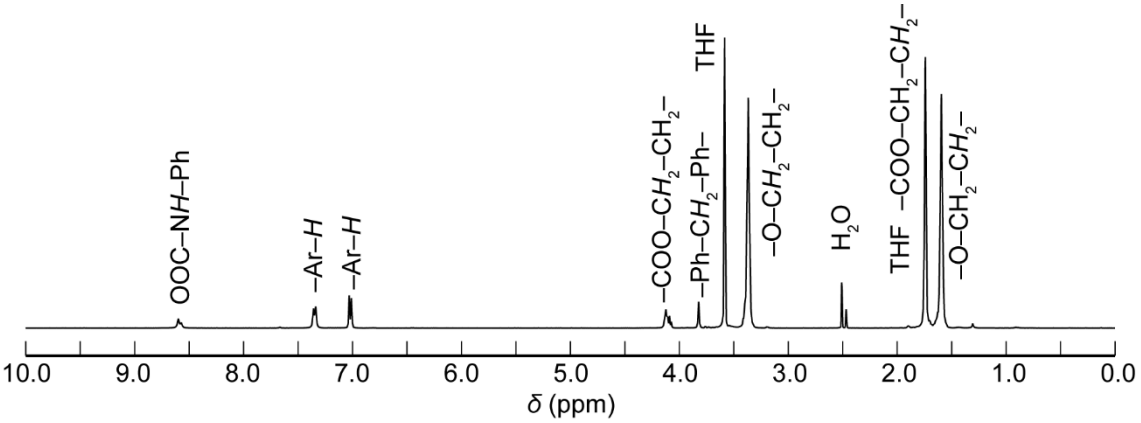

Figure 3-27. ^{1}H NMR spectrum of **Rot4PU** in THF-d_8. Signals are characterized as protons of the polyurethane chains. No signals ascribed to the rotaxane mechanophores were observed due to their very low concentration. This spectrum was measured at r.t.

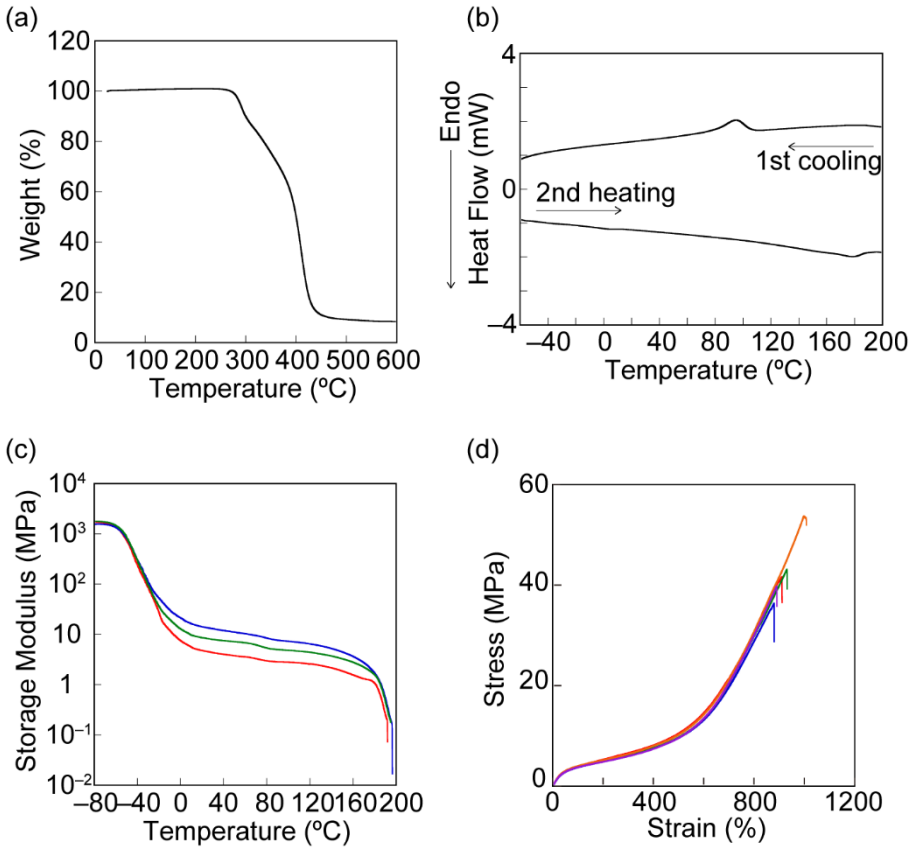

Figure 3-28. (a) TGA trace of **Rot4PU** films. The heating rate was 10 °C/min. (b) DSC traces of **Rot4PU** films. The heating and cooling rates were 10 °C/min. (c) DMA traces of **Rot4PU** films. The graph shows data obtained from three different specimen. The tests were conducted under N_2 at a heating rate of 3 °C/min, a frequency of 1 Hz, and an amplitude of 15 μm. (d) Stress-strain curves of Rot4PU films. The graph shows data obtained from five different specimen. The experiments were conducted with a strain rate of 120 mm/min at r.t.

Table 2. Overview of the mechanical properties of **Rot4PU** films as determined from stress-strain curves recorded during uniaxial tensile deformation (see Figure 3-28d)[a)]

	Elongation at break (%)	Stress at break (MPa)	Young's modulus[b)] (MPa)
Rot4PU	924 ± 84	42.8 ± 10.2	11.4 ± 0.5

a) All data were extracted from the stress-strain curves shown in Figure 3-28d and represent averages of 5 measurements ± standard deviation. b) The Young's modulus was derived from the slopes of the stress-strain curves in the strain regime between 0.5–1.0%.

Gratifyingly, the mechanochromic response of the **Rot4PU** film is indeed similar to that of **Rot2PU**. The fluorescence increases and decreases gradually and rapidly upon stretching and releasing the strain (Figure 3-29a, Figure 3-30). In the relaxed state, almost no increase of the fluorescence intensity is observed after 50 loading–unloading cycles

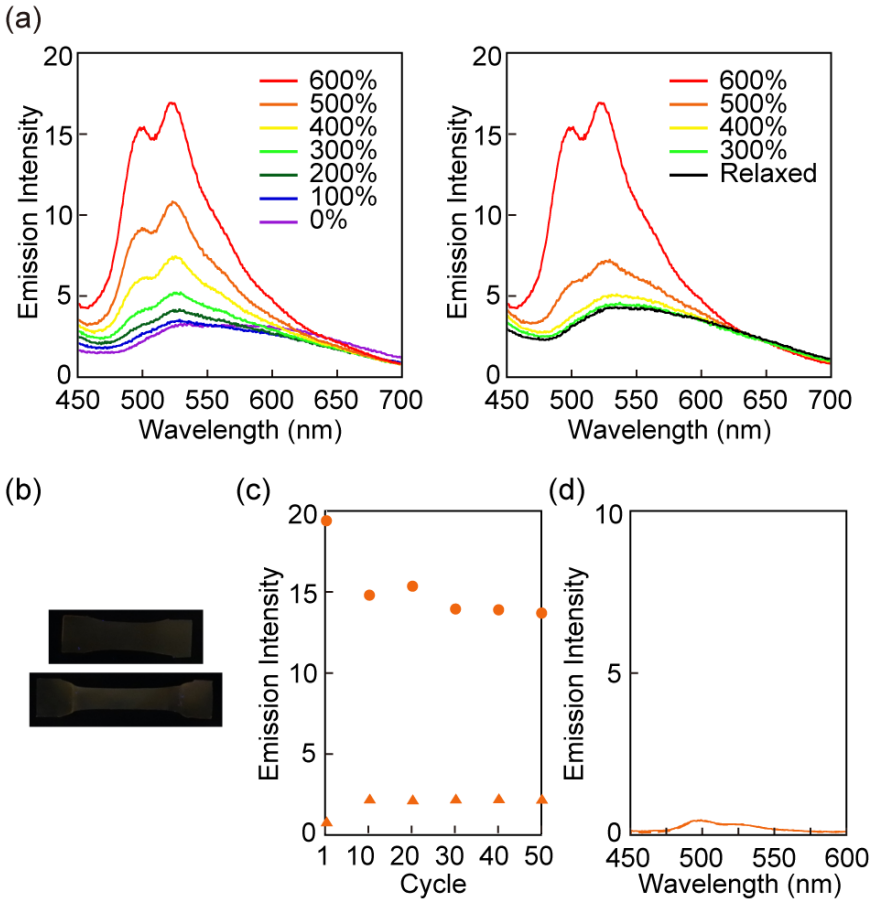

Figure 3-29. (a) Fluorescence spectra of a **Rot4PU** film recorded upon uniaxial deformation to the indicated strains (left) and subsequent relaxation from the maximum strain of 600% (right). In the right panel, the spectrum before deformation (dotted lines) is reproduced for the purpose of comparison. (b) Photographs of a **Rot4PU** film before (top) and after (bottom) 50 deformation/relaxation cycles. The images were taken under UV light illumination (λ_{ex} = 365 nm) at r.t., and the applied strain was 600%. (c) Plot of the fluorescence intensity at 500 nm of a **Rot4PU** film in the relaxed state (triangles) and upon deformation to a strain of 600% (circles) over the course of 50 loading–unloading cycles. (d) Fluorescence spectra of THF solutions (10.2 mg/mL) of a pristine **Rot4PU** (dashed line) film and of the stretched portion of a film that was subjected to 50 loading–unloading cycles to 600%. All spectra were recorded at r.t. with λ_{ex} = 365 nm.

(Figure 3-29b,c). Concomitantly, a THF solution of the stretched segment is only weakly fluorescent, and the intensity matches that of a solution of the pristine polymer (Figure 3-29d). These findings support the conclusion that the deformation of **Rot4PU**—and by extension in **Rot1PU** and **Rot3PU**—causes no covalent bond scission. I also sonicated THF solutions of **Rot4PU** (Figure 3-31), and the results mirror those of **Rot2PU**. While the molecular weight was considerably reduced upon sonication, the fluorescence intensity hardly increased. Thus, the results indicate that dethreading of the ring does not occur past the larger stopper. Moreover, high-resolution electrospray ionization mass spectrometry was performed for filtrates isolated after precipitating solutions of the segments of **Rot1PU** or **Rot4PU** samples that were subjected to 50 deformation/ relaxation cycles (see the Experimental Section for details). The MS spectra (Figures 3-32 and 3-33) show no fragments that are derived from the scission of covalent bonds, corroborating that the mechanical bond of the **Rot1** rotaxane is broken by dethreading across the stopper.

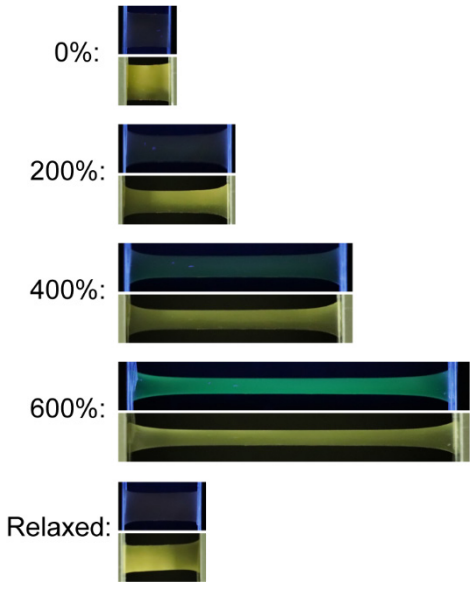

Figure 3-30. Photographs of **Rot4PU** films upon stretching. The top images were taken upon excitation at 365 nm in the dark, while the bottom images were taken under ambient illumination, for each strained state.

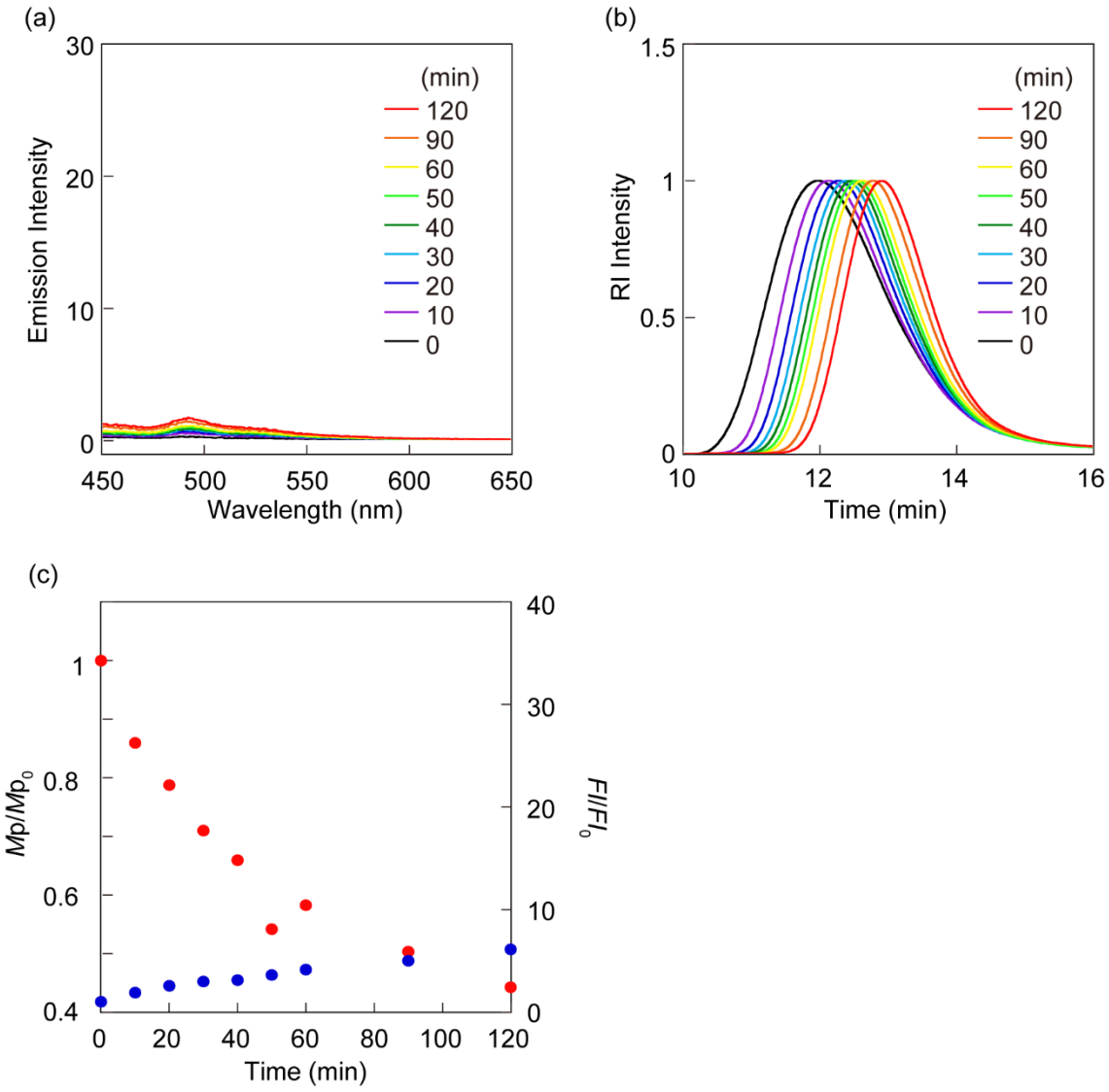

Figure 3-31. (a) Fluorescence spectra of THF solutions of **Rot4PU** (1.0 mg/mL) upon sonication for 2 h. All fluorescence spectra were recorded under the same condition as the solutions of **Rot1PU**, **Rot2PU**, and **Rot3PU** shown in Figure 3-20. (b) SEC traces of **Rot4PU** upon sonication for 2 h. The SEC traces were normalized to the peak maximum. (c) Plots of the peak molecular weight ratios Mp/Mp_0 (red) and fluorescence intensity ratio FI/FI_0 (blue) as a function of sonication time of **Rot4PU**.

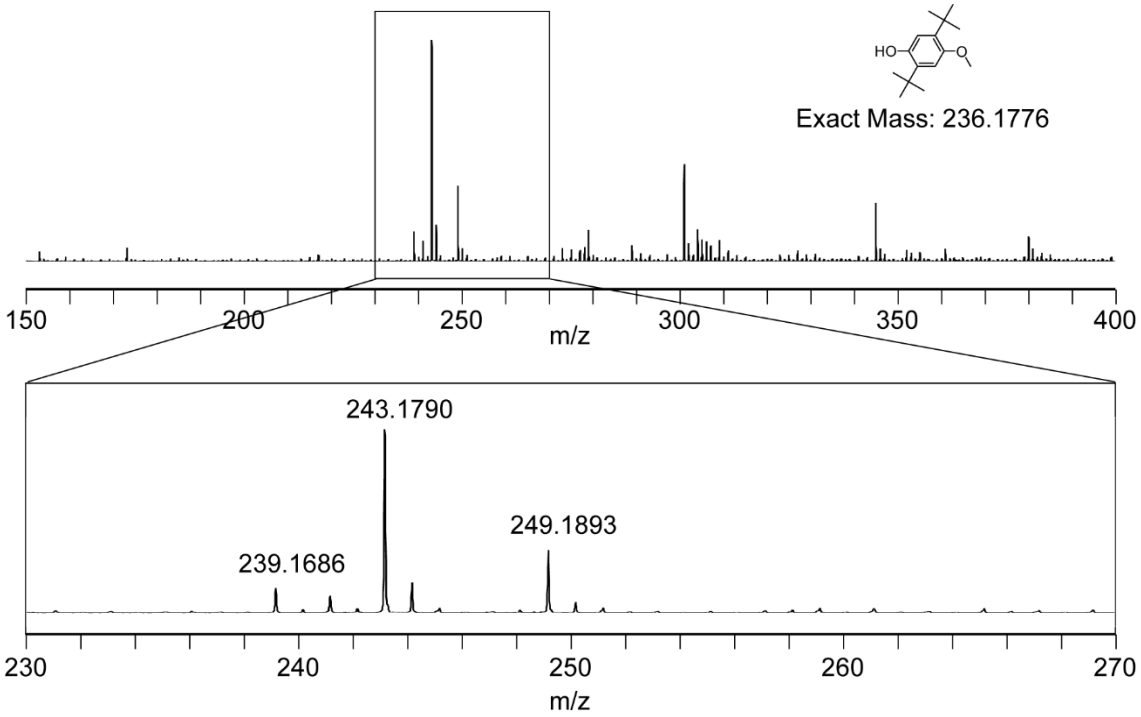

Figure 3-32. An HRMS spectrum recorded for the filtrate after reprecipitating stretched **Rot1PU** films (400 mg) from THF/methanol.

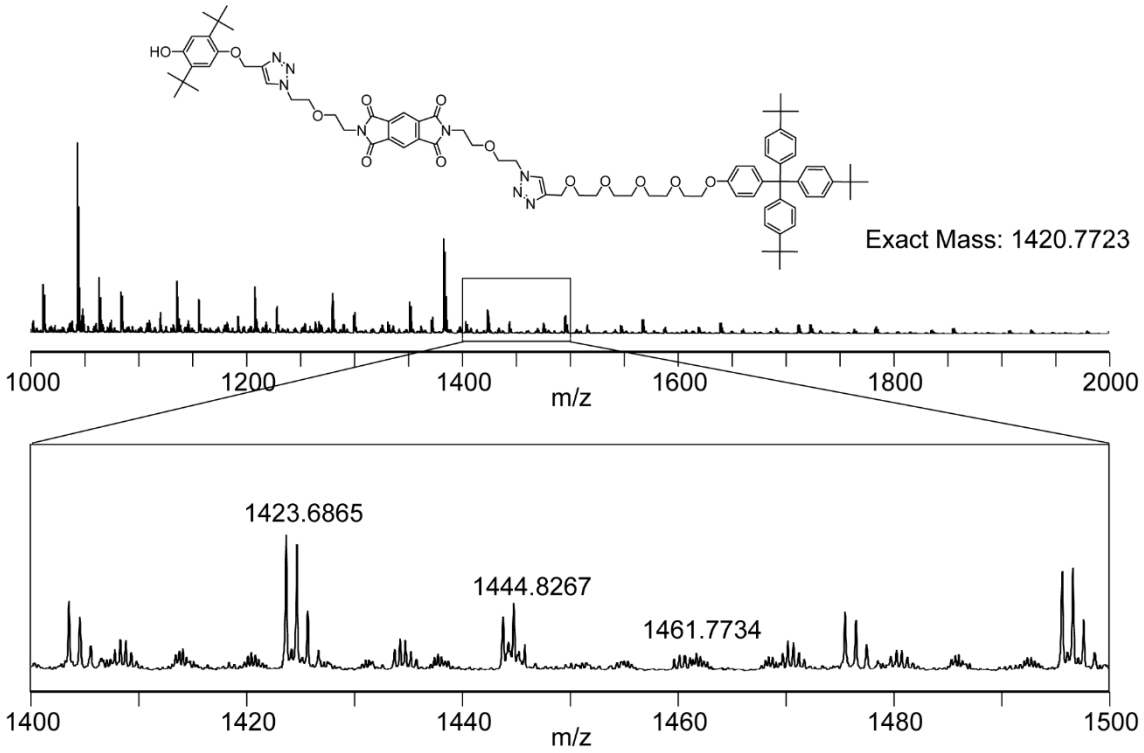

Figure 3-33. An HRMS spectrum recorded for the filtrate after reprecipitating stretched **Rot4PU** films (400 mg) from THF/methanol.

Considering all results described above, the process at play in **Rot4PU** appears to follow the steps depicted in Figure 8. In the pristine state, the ring is located between the two *p*-di-*tert*-butylbenzene stoppers and under stress-free conditions resides near the PMDI. When a sufficiently large force is applied, the ring slips past the central *p*-di-*tert*-butylbenzene stopper, but it cannot dethread entirely, as it is retained by the bulkier tris(*p*-*tert*-butylphenyl)phenylmethane stopper.

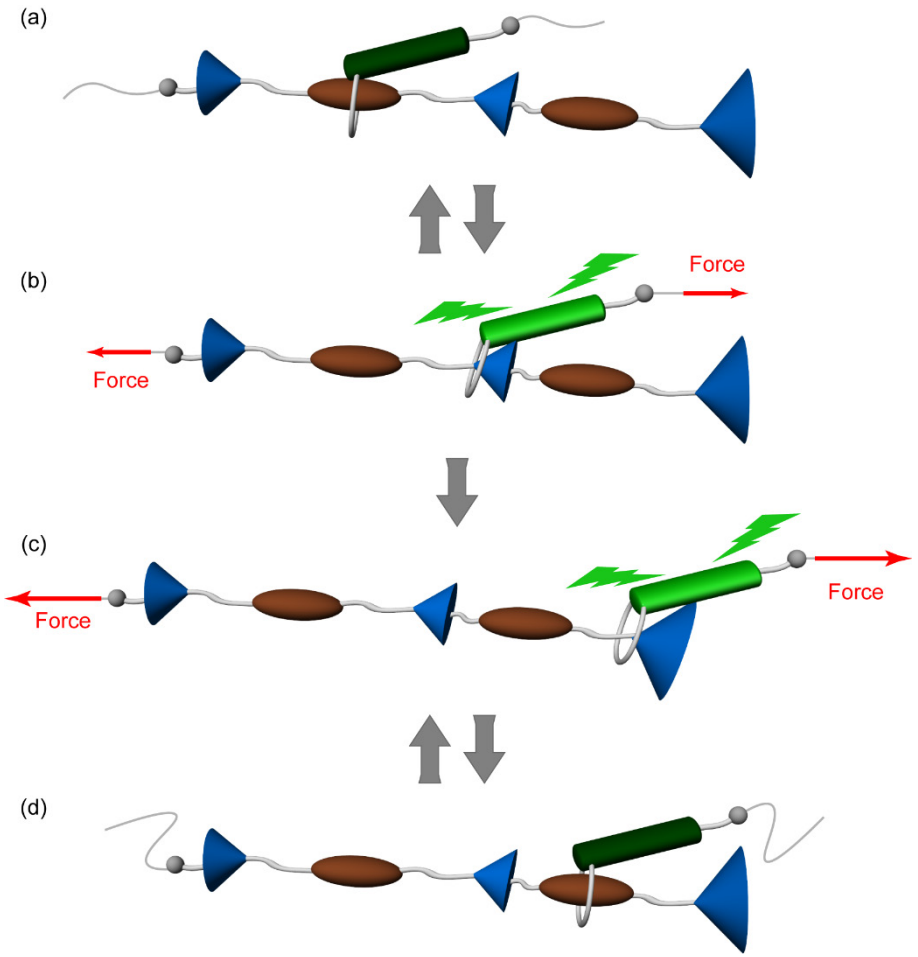

Figure 3-34. Schematic illustration of the operating principle of **Rot4**. (a) In the initial force-free state the ring carrying the luminophore is located between the two small stoppers and resides preferentially near the quencher. (b) The application of a small force displaces the ring toward the smaller stopper, and the fluorescence of the luminophore is switched on. This effect is reversible, unless the force is so high that the ring slips past the stopper. (c) The bulky stopper at the terminus of the extended axle does not allow dethreading. (d) Once the ring has passed the first stopper, the mechanochromic response is reversible and only dictated by the molecular shuttling.

3.3. Conclusion

In summary, I report new mechanophores that display reversible and irreversible fluorescence changes that are achieved by exploiting the molecular shuttling function and force-induced dethreading of rotaxanes. The combination of judiciously selected ring and stopper moieties is crucial to attain interlocked structures that display such a dual response. PU elastomers that contain such doubly responsive rotaxanes exhibit reversible fluorescence changes over multiple loading− unloading cycles due to the shuttling function, whereas permanent changes are observed upon repeated deformations to high strains due to breakage of the mechanical bond upon dethreading of the ring from the axle. The number of dethreaded rings gradually increases upon repeated stretching, resulting in an irreversible change of the photoluminescence intensity. This response allows one, at least conceptually, to monitor the actual deformation of polymer materials and also to record the mechanical history on the basis of an optical signal. The fact that in the present materials the strain regimes in which reversible and irreversible responses are triggered overlap reflects that not all mechanophores experience the same force. The results of the cyclic experiments further reveal that the force which a given mechanophore experiences upon macroscopic deformation of a sample may, at least in the presently investigated, physically cross-linked PUs, changes over the course of multiple deformation events. It will be interesting to explore to what extent this effect is related to the nature of the polymer matrix.

3.4. Experimental Section

3.4.1. General Methods

All reagents and solvents were purchased from FUJIFILM Wako Pure Chemical Corporation, Tokyo Kasei, Kanto Chemical, or Merck. All reactions were carried out under nitrogen atmosphere unless otherwise noted. Flash silica gel column chromatography was conducted with a Biotage Isolera Flash system using SHOKO-scientific Purif-Pack-EX cartridges. Silica gel from Kanto Chemicals (silica gel 60 N,spherical, 63–210 μm) was used when flash silica gel column chromatography was conducted in a conventional manner. Recycling preparative gel permeation chromatography (GPC) was performed with a Japan Analytical Industry LaboACE. Inhibitor-free anhydrous tetrahydrofuran was utilized as solvent during the synthesis of polymers. Telechelic poly(tetrahydrofuran)diol (M_n = 2,000 g/mol) was dried in vacuo at 100 °C for 2 h before use. 4,4'-Methylenebis(phenylisocyanate) and 1,4-butandiol were distilled under vacuum and stored over molecular sieves at 4 °C and at room temperature (r.t.), respectively.

^{1}H NMR spectra were measured with a JEOL JNM-ECX 400 spectrometer or a JEOL JNM-ECZ400S/L1 spectrometer and all chemical shifts are reported on the δ-scale in ppm relative to the signal of tetramethylsilane (TMS at 0.00) or residual solvent protons (THF at 1.72) as an internal standard. Coupling constants (J) are quoted in Hz and relative intensities are reported. Proton-decoupled ^{13}C NMR spectra were acquired on a JEOL JNM-ECX 400 spectrometer or a JEOL JNM-ECZ400S/L1 spectrometer and all chemical shifts are expressed in ppm using solvents as the internal standards ($CDCl_3$ at 77.16; THF-d_8 at 67.21). Matrix Assisted Laser Desorption Ionization Time-of-Flight (MALDI-TOF) mass spectroscopy was performed with an AB SCIEX TOF/TOF 5800 system or a SHIMAZHU AXIMA-Performance. High resolution electrospray ionization (ESI) mass spectra were measured with a Thermo Scientific Exactive or Bruker Daltonics micrOTOF II.

Absorption spectra were measured on a JASCO V-550. Steady-state fluorescence spectra of solutions were recorded with a JASCO FP-6500 and the spectra were corrected for the detector nonlinearity. Steady-state fluorescence spectra of polyurethane films during stretching experiments were monitored with an Ocean Optics QEPro-FL equipped with an LLS-365 LED light source and a Reflection/Backscattering Probe R400-7-UV-VIS; these spectra were not corrected.

Size-exclusion chromatography (SEC) experiments were performed on an Agilent 1200 series HPLC system equipped with an Agilent PLgel mixed guard column (particle size = 5 μm) and two Agilent PLgel mixed-D columns (ID = 7.5 mm, L = 300 mm, particle size = 5 μm). Signals were monitored on a UV detector (Agilent 1200 series), an Optilab REX interferometric refractometer, and a miniDawn TREOS light scattering detector (Wyatt Technology Corp.). Prior to SEC analysis, all samples were filtered through a 0.22 μm nylon syringe filter. Samples were injected using THF as the eluent at 30 °C and a flow rate of 1.0 mL/min. Data analyses were conducted on Astra software (Wyatt Technology Corp.) and molecular weights were calculated based on narrow-molecular-weight polystyrene calibration (from 860–303,000 g/mol).

Thermogravimetric analyses (TGA) were performed under nitrogen with a Mettler-Toledo Stare system at a rate of 10 °C/min. Differential scanning calorimetry (DSC) measurements were conducted under N_2 on a Hitachi DSC7020 at heating and cooling rates of 10 °C/min. Dynamic mechanical analyses (DMA) were carried out under N_2 with a TA Instruments DMA Q800 at a heating rate of 3 °C/min, a frequency of 1 Hz, and an amplitude of 15 μm. Stress–strain measurements were conducted under ambient conditions with a SHIMADZU AGS-100NX equipped with a 100 N load cell at a strain rate of 120 mm/min. Sonication experiments were conducted on a Branson Model 450 ultrasonic 1/2 inhorn sonicator equipped with a 13 mm sonicator tip. A MX07R-20 refrigerating/heating bath obtained from VWR S3 D containing 1/1 v/v water and ethylene glycol was used to maintain the sample temperature at 20 °C during sonication

experiments. A THF solution containing polymer with a concentration of ~1 mg/mL was prepared, and 20 mL were added to a Suslick cell equipped with a gas outlet and a septum. The solution was degassed by purging with nitrogen for 15 min, cooled to 20 °C in the cooling bath, and submitted to sonication pulses of 0.5 s with an amplitude of 15% and delayed by pauses of 1 s. Samples (450 μL) were taken after 0, 10, 20, 30, 40, 50, 60, 90, and 120 min with a syringe. Fluorescence spectroscopy was carried out with a Horiba Fluorolog 3 spectrometer with right angle illumination equipped with a 450 W Xenon light source for excitation and a FL-1030-UP photomultiplier as the detector. Spectra were recorded with a beam slit of 2 nm and an excitation wavelength of 365 nm.

High performance liquid chromatography (HPLC) analysis was carried out on a system composed of SHIMADZU HPLC system with a GL Sciences Inc. InertSustain AQ-C18 column (ID = 4.6 mm, L = 250 mm).

3.4.2. Synthesis of Rotaxanes

1,5-Bis{2-[2-(2-hydroxyethoxy)ethoxy]ethoxy}naphthalene, 2-(4-ethynylphenoxy)tetrahydro-2*H*-pyran, 2-{2-[2-(2- hydroxyethoxy)ethoxy]ethoxy}ethyl toluenesulfonate, compound **18**, compound **20**, and compound **27** were synthesized following previous reports.[68-71]

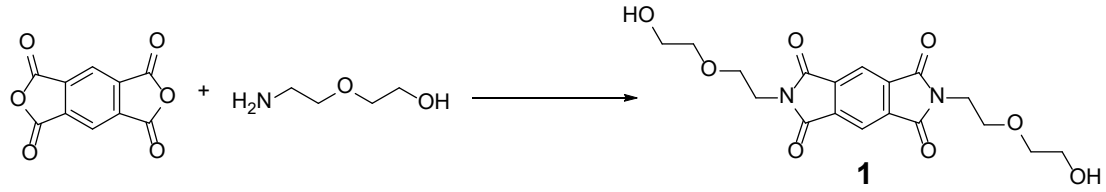

Conditions: DMF, reflux, 17 h.

Compound 1. A mixture of pyromellitic dianhydride (3.00 g, 13.8 mmol) and 2-(2-aminoethoxy)ethanol (5.78 g, 55.0 mmol) in DMF (150 mL) was stirred for 17 h under reflux. After the solvent was evaporated under reduced pressure, the crude product was purified by flash column chromatography on silica gel (eluent: dichloromethane/acetone = 2:1 v/v) and subsequently precipitated from a mixture of chloroform and hexane to afford compound **1** (4.29 g, 10.9 mmol, 80%) as a white solid.

^{1}H NMR (400 MHz, $CDCl_3$): δ = 2.16 (t, J = 6.0 Hz, 2H), 3.59–3.62 (m, 4H), 3.66–3.70 (m, 4H), 3.78 (t, J = 5.6 Hz, 4H), 3.98 (t, J = 5.6 Hz, 4H), 8.29 (s, 2H). ^{13}C NMR (100 MHz, $CDCl_3$): δ = 38.46, 61.90, 68.14, 72.45, 118.57, 137.43, 166.39. MS (MALDI-TOF): m/z: 415.17 (calcd. $[M+Na]^+$ = 415.11).

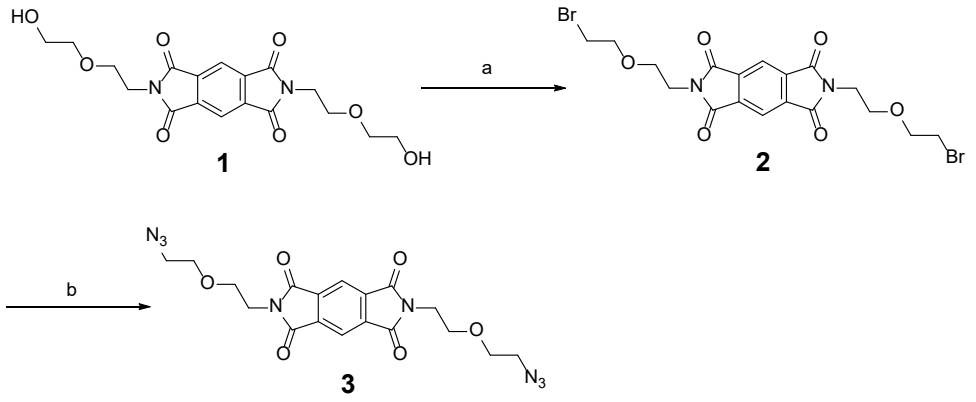

Conditions: (a) PBr_3, DMF, 70 °C, 5 h; (b) NaN_3, DMF, 60 °C, 22 h.

Compound 2. PBr_3 (7.19 g, 26.6 mmol) was added to a solution of compound **1** (4.53 g, 11.5 mmol) in DMF (200 mL), and the mixture was stirred for 5 h at 70 °C. After cooling to r.t., the reaction mixture was slowly poured into water (150 mL). The resulting precipitate was filtered off and washed with water (3 × 50 mL). The solid residue was dissolved in dichloromethane, and the solution was washed with saturated aq. NaCl (150 mL), dried over $MgSO_4$, and filtered. After the solvent was evaporated under reduced pressure, the crude product thus isolated was purified by flash column chromatography on silica gel (eluent: dichloromethane/ethyl acetate = 7:1 v/v) and subsequently precipitated from a mixture of chloroform and hexane to afford compound **2** (5.73 g, 11.1 mmol, 96%) as a white solid.

^{1}H NMR (400 MHz, $CDCl_3$): δ = 3.40 (t, J = 6.0 Hz, 4H), 3.78–3.82 (m, 8H), 3.98 (t, J = 5.6 Hz, 4H), 8.29 (s, 2H). ^{13}C NMR (100 MHz, $CDCl_3$): δ = 30.55, 37.92, 67.44, 70.46, 118.34, 137.25, 166.19. MS (MALDI-TOF): m/z: 539.00 (calcd. $[M+Na]^+$ = 538.94).

Compound 3. NaN_3 (1.80 g, 27.6 mmol) was added to a solution of compound **2** (5.73 g, 11.1 mmol) in DMF (150 mL), and the mixture was stirred for 22 h at 60 °C. After cooling to r.t., the reaction mixture was poured into water (150 mL). The resulting precipitate was filtered off and washed with water (3 × 50 mL). The solid residue was dissolved in dichloromethane, and the solution was washed with saturated aq. NaCl (150 mL), dried over $MgSO_4$, and filtered. After the solvent was evaporated under reduced pressure, the crude product was precipitated from a mixture of chloroform and hexane to afford compound **3** (4.70 g, 10.6 mmol, 96%) as a white solid.

^{1}H NMR (400 MHz, $CDCl_3$): δ = 3.31 (t, J = 4.8 Hz, 4H), 3.68 (t, J = 4.8 Hz, 4H), 3.80 (t, J = 5.6 Hz, 4H), 3.99 (t, J = 5.6 Hz, 4H), 8.28 (s, 2H). ^{13}C NMR (100 MHz, $CDCl_3$): δ = 37.98, 50.59, 67.62, 69.86, 118.30, 137.22, 166.22. MS (MALDI-TOF): m/z: 465.14 (calcd. $[M+Na]^+$ = 465.12).

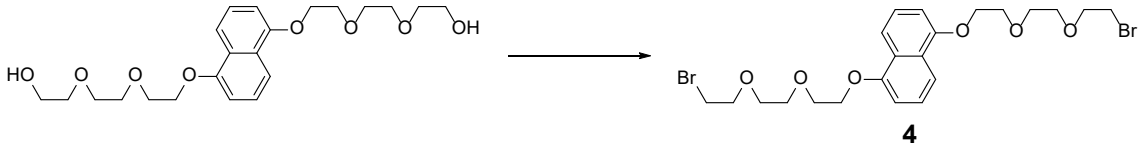

4

Conditions: CBr_4, PPh_3, CH_2Cl_2, 0 °C → r.t., 4 h.

Compound 4. A solution of tetrabromomethane (4.94 g, 14.9 mmol) in dichloromethane (20 mL) was added dropwise to a solution of 1,5-bis{2-[2-(2-hydroxyethoxy)ethoxy]ethoxy}naphthalene[68] (2.52 g, 5.94 mmol) and triphenylphosphine (3.75 g, 14.3 mmol) in dichloromethane (200 mL) at 0 °C. The reaction mixture was subsequently stirred for 4 h at r.t. before most of the dichloromethane was evaporated under reduced pressure. The crude product thus obtained was purified by flash column chromatography on silica gel (eluent: gradient from hexane/dichloromethane = 1:4 v/v to dichloromethane) to afford compound **4** (2.74 g, 4.98 mmol, 84%) as a pale yellow liquid.

^{1}H NMR (400 MHz, $CDCl_3$): δ = 3.46 (t, J = 6.4 Hz, 4H), 3.71–3.74 (m, 4H), 3.81–3.84 (m, 8H), 4.00–4.02 (m, 4H), 4.29–4.32 (m, 4H), 6.85 (d, J = 7.2 Hz, 2H), 7.33–7.37 (m, 2H), 7.87 (d, J = 8.4 Hz, 2H). ^{13}C NMR (100 MHz, $CDCl_3$): δ = 30.52, 68.04, 70.03, 70.77, 71.13, 71.39, 105.80, 114.74, 125.22, 126.89, 154.45. MS (MALDI-TOF): m/z: 548.08 (calcd. $[M]^+$ = 548.04).

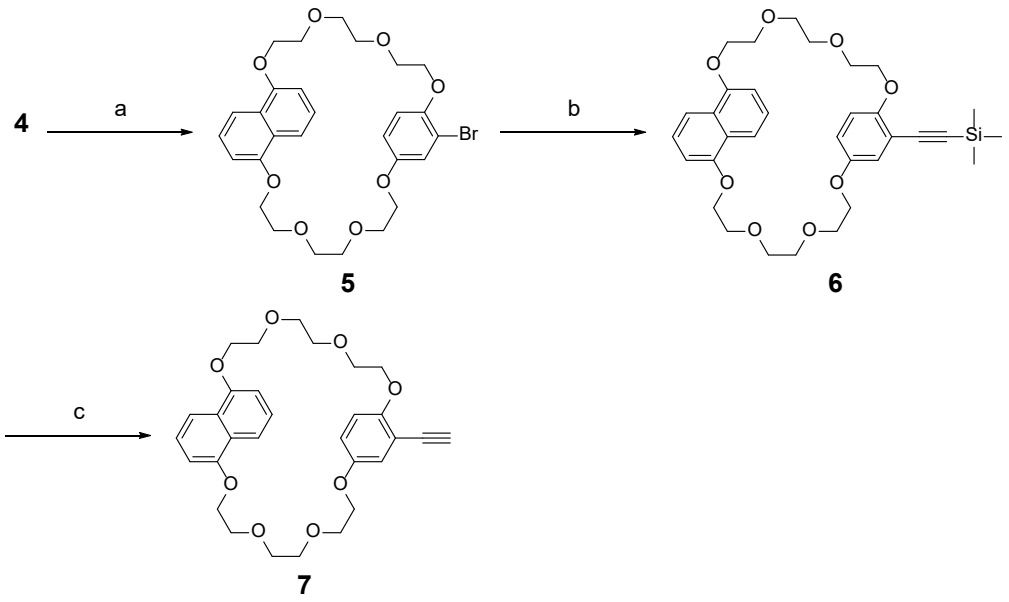

Conditions: (a) bromohydroquinone, K_2CO_3, DMF, 80 °C, 22 h; (b) trimethylsilylacetylene, $Pd(PPh_3)_4$, CuI, *i*-Pr_2NH, THF, 80 °C, 17 h; (c) TBAF, THF, r.t., 2 h.

Compound 5. A solution of bromohydroquinone (941 mg, 4.98 mmol) and compound **4** (2.74 g, 4.98 mmol) in DMF (30 mL) was added over the course of 6 h and under vigorous stirring to a suspension of K_2CO_3 (13.8 g, 99.5 mmol) in DMF (400 mL) at 80 °C. After further stirring for 16 h at 80 °C, the solvent was evaporated under reduced pressure. Chloroform (200 mL) was added, and the solution was washed with saturated aq. NH_4Cl (4 × 200 mL). The organic layer was dried over $MgSO_4$ and filtered, and the solvent was evaporated under reduced pressure. The crude product thus isolated was purified by flash column chromatography on silica gel (eluent: gradient from dichloromethane to dichloromethane/ethyl acetate = 22:3 v/v) to afford compound **5** (749 mg, 1.30 mmol, 26%) as a pale brown solid.

^{1}H NMR (400 MHz, $CDCl_3$): δ = 3.51–3.53 (m, 2H), 3.71–3.86 (m, 14H), 3.98–4.02 (m, 4H) 4.28–4.32 (m, 4H), 6.01 (dd, *J* = 9.2, 3.2 Hz, 1H), 6.36 (d, *J* = 8.8 Hz, 1H), 6.79–

6.82 (m, *2*H), 6.85 (d, J = 3.2 Hz, 1H), 7.24–7.29 (m, 2H), 7.85–7.88 (m, 2H). ^{13}C NMR (100 MHz, $CDCl_3$): δ = 67.62, 67.86, 68.25, 69.75, 69.81, 69.84, 70.18, 70.81, 71.03, 71.34, 71.42, 105.58, 105.71, 112.77, 113.72, 114.55, 114.61, 116.09, 120.19, 125.20, 125.23, 126.78, 149.65, 153.46, 154.31, 154.39. MS (MALDI-TOF): m/z: 599.14 (calcd. $[M+Na]^+$ = 599.13).

Compound 6. A mixture of compound **5** (2.27 g, 3.93 mmol), trimethylsilylacetylene (1.93 g, 19.7 mmol), $Pd(PPh_3)_4$ (228 mg, 0.197 mmol), CuI (37.5 mg, 0.197 mmol), and *i*-Pr_2NH (10 mL) in THF (30 mL) was stirred under nitrogen atmosphere for 17 h at 80 °C. After cooling to r.t., the reaction mixture was poured into ethyl acetate (150 mL). The solution was washed with 5% aq. HCl (100 mL), saturated aq. $NaHCO_3$ (100 mL), and saturated aq. NaCl (100 mL). The organic layer was dried over $MgSO_4$ and filtered, and the solvent was evaporated under reduced pressure. The crude product thus isolated was purified by flash column chromatography on silica gel (eluent: gradient from hexane/ethyl acetate = 3:1 v/v to hexane/ethyl acetate = 13:7 v/v) to afford compound **6** (532 mg, 0.894 mmol, 65%) as a yellow liquid.

^{1}H NMR (400 MHz, $CDCl_3$): δ = 0.22 (s, 9H), 3.59–3.61 (m, 2H), 3.71–3.73 (m, 4H), 3.77–3.80 (m, 8H), 3.83–3.86 (m, 2H), 3.98–4.01 (m, 4H), 4.26–4.31 (m, 4H), 6.12 (dd, J = 9.2, 3.2 Hz, 1H), 6.24 (d, J = 9.2 Hz, 1H), 6.68 (d, J = 3.2 Hz, 1H), 6.77–6.82 (m, 2H), 7.22–7.28 (m, 2H), 7.84–7.87 (m, 2H). ^{13}C NMR (100 MHz, $CDCl_3$): δ= 0.10, 67.68, 67.82, 68.19, 69.56, 69.74, 69.77, 69.78, 70.83, 71.10, 71.28, 71.37, 97.91, 101.58, 105.62, 105.74, 113.33, 114.51, 114.66, 114.93, 116.50, 119.61, 125.18, 126.78, 152.47, 154.22, 154.30, 154.36. MS (MALDI-TOF): m/z: 617.28 (calcd. $[M+Na]^+$ = 617.25).

Compound 7. A THF solution of tetrabutylammonium fluoride (ca. 1 mol/L, 0.91 mL, 0.91 mmol) was added to a solution of compound **6** (452 mg, 0.760 mmol) in THF (30 mL) at r.t. After stirring the reaction mixture at r.t. for 2 h, ethyl acetate (150 mL) and water (150 mL) were added to the reaction mixture. The organic layer was separated off, washed with saturated aq. NaCl (100 mL), dried over $MgSO_4$ and filtered, and the solvent was evaporated under reduced pressure. The crude product thus isolated was purified by flash column chromatography on silica gel (eluent: gradient from hexane/ethyl acetate = 3:2 v/v to hexane/ethyl acetate = 2:3 v/v) to afford compound **7** (342 mg, 0.654 mmol, 86%) as a pale brown solid.

^{1}H NMR (400 MHz, $CDCl_3$): δ = 3.15 (s, 1H), 3.54–3.56 (m, 2H), 3.71–3.81 (m, 12H), 3.88–3.91 (m, 2H), 3.98–4.01 (m, 4H), 4.28–4.32 (m, 4H), 6.09 (dd, J = 9.2, 3.2 Hz, 1H), 6.30 (d, J = 9.2 Hz, 1H), 6.74 (d, J = 3.2 Hz, 1H), 6.79–6.83 (m, 2H), 7.25–7.29 (m, 2H), 7.86–7.88 (m, 2H). ^{13}C NMR (100 MHz, $CDCl_3$): δ = 67.63, 67.84, 68.12, 69.49, 69.72, 69.79, 69.81, 70.78, 71.03, 71.26, 71.35, 80.15, 80.73, 105.60, 105.73, 112.25, 114.52, 114.58, 114.89, 116.32, 120.12, 125.17, 125.21, 126.76, 152.44, 154.29, 154.33, 154.35. MS (MALDI-TOF): m/z: 522.22 (calcd. $[M]^+$ = 522.23).

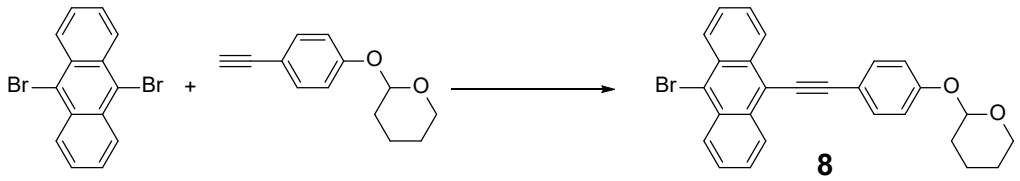

Conditions: $Pd(PPh_3)_4$, CuI, *i*-Pr_2NH, THF, 80 °C, 18 h.

Compound 8. A mixture of 9,10-dibromoanthracene (1.66 g, 4.94 mmol), 2-(4-ethynylphenoxy)tetrahydro-2*H*-pyran[69] (1.00 g, 4.94 mmol), $Pd(PPh_3)_4$ (289 mg, 0.250 mmol), CuI (47.6 mg, 0.250 mmol), and *i*-Pr_2NH (5 mL) in THF (40 mL) was stirred

under nitrogen atmosphere for 18 h at 80 °C. After cooling to r.t., the reaction mixture was poured into ethyl acetate (150 mL). The solution was washed with 5% aq. HCl (100 mL), saturated aq. $NaHCO_3$ (100 mL), and saturated aq. NaCl (100 mL). The organic layer was dried over $MgSO_4$ and filtered, and the solvent was evaporated under reduced pressure. The crude product thus isolated was purified by flash column chromatography on silica gel (eluent: hexane/chloroform = 1:1) and subsequently precipitated from a mixture of dichloromethane and hexane to afford compound **8** (867 mg, 1.90 mmol, 38%) as a yellow solid.

^{1}H NMR (400 MHz, $CDCl_3$): δ = 1.62–1.78 (m, 3H), 1.89–1.93 (m, 2H), 1.99–2.10 (m, 1H), 3.63–3.68 (m, 1H), 3.89–3.95 (m, 1H), 5.52 (t, J = 3.2 Hz, 1H), 7.14 (d, J = 8.8 Hz, 2H), 7.59–7.66 (m, 4H), 7.70 (t, J = 8.8 Hz, 2H), 8.54–8.59 (m, 2H), 8.67–8.71 (m, 2H).

^{13}C NMR (100 MHz, $CDCl_3$): δ= 18.76, 25.28, 30.37, 62.19, 84.93, 96.35, 102.17, 116.35, 116.76, 118.86, 123.78, 126.81, 127.50, 127.57, 128.33, 130.42, 133.00, 133.18, 157.64.

MS (MALDI-TOF): m/z: 456.70 (calcd. $[M]^+$ = 456.07).

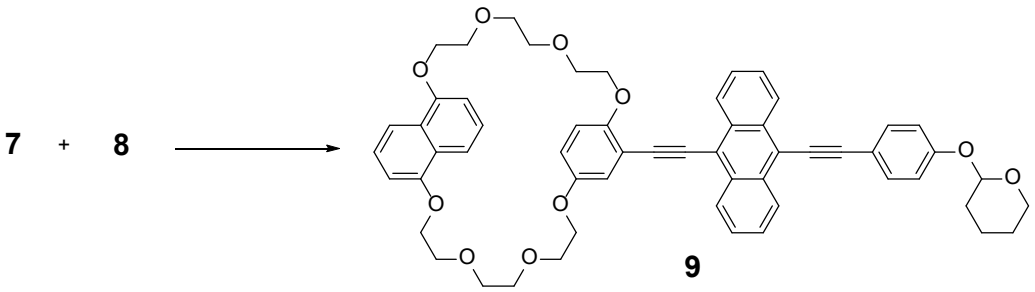

Conditions: $Pd(PPh_3)_4$, CuI, *i*-Pr_2NH, THF, 80 °C, 18 h.

Compound 9. A mixture of compound **7** (342 mg, 0.654 mmol), compound **8** (299 mg, 0.654 mmol), $Pd(PPh_3)_4$ (37.8 mg, 3.27×10^{-2} mmol), CuI (6.23 mg, 3.27×10^{-2} mmol), and *i*-Pr_2NH (5 mL) in THF (20 mL) was stirred under nitrogen atmosphere for 18 h at 80 °C. After cooling to r.t., the reaction mixture was poured into ethyl acetate (150 mL).

The solution was washed with 5% aq. HCl (100 mL), saturated aq. $NaHCO_3$ (100 mL), and saturated aq. NaCl (100 mL). The organic layer was dried over $MgSO_4$ and filtered, and the solvent was evaporated under reduced pressure. The crude product thus isolated was purified by flash column chromatography on silica gel (eluent: gradient from hexane/chloroform = 1:1 v/v to hexane/chloroform = 1:4 v/v) and subsequently precipitated from a mixture of chloroform and hexane to afford compound **9** (471 mg, 0.524 mmol, 80%) as a yellow solid.

^{1}H NMR (400 MHz, $CDCl_3$): δ = 1.59–1.77 (m, 3H), 1.88–1.92 (m, 2H), 1.98–2.09 (m, 1H), 3.62–3.67 (m, 1H), 3.74–3.83 (m, 12H), 3.89–4.02 (m, 9H), 4.21–4.23 (m, 2H), 4.29–4.31 (m, 2H), 5.51 (t, J = 3.2 Hz, 1H), 6.24–6.24 (m, 2H), 6.75–6.80 (m, 2H), 7.00–7.01 (m, 1H), 7.13 (d, J = 8.8 Hz, 2H), 7.23–7.27 (m, 2H), 7.58–7.64 (m, 4H), 7.70 (d, J = 8.8 Hz, 2H), 7.86–7.89 (m, 2H), 8.65–8.69 (m, 2H), 8.72–8.77 (m, 2H). ^{13}C NMR (100 MHz, $CDCl_3$): δ = 18.71, 25.20, 30.29, 62.11, 67.66, 67.70, 68.46, 68.74, 69.80, 69.85, 69.95, 70.95, 71.11, 71.35, 85.60, 90.53, 96.30, 99.46, 102.62, 105.58, 105.68, 113.40, 113.68, 114.51, 114.65, 116.39, 116.45, 116.69, 118.49, 118.80, 119.30, 125.23, 126.64, 126.72, 126.79, 127.22, 127.70, 132.02, 133.12, 152.53, 154.00, 154.34, 154.38, 157.53. MS (MALDI-TOF): m/z: 893.45 (calcd. $[M]^+$ = 898.37).

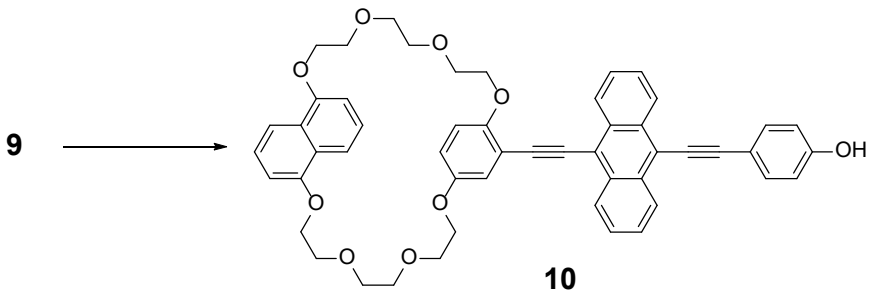

10

Conditions: 10% aq. HCl, THF, 80 °C, 1 h.

Compound 10. 10% aq. HCl (2 mL) was added to a solution of compound **9** (471 mg, 0.524 mmol) in THF (30 mL), and the reaction mixture was stirred for 1 h at 80 °C. After cooling to r.t., the reaction mixture was poured into ethyl acetate (150 mL) and water (100 mL). The organic layer was separated off, washed with saturated aq. NaCl (2 ×100 mL), dried over $MgSO_4$, and filtered. After the solvent was evaporated under reduced pressure, the crude product thus isolated was precipitated from a mixture of chloroform and hexane to afford compound **10** (397 mg, 0.487 mmol, 93%) as a yellow solid.

^{1}H NMR (400 MHz, $CDCl_3$): δ = 3.75–3.86 (m, 12H), 3.93–4.04 (m, 8H), 4.24–4.26 (m, 2H), 4.31–4.33 (m, 2H), 5.54 (s, 1H), 6.22 (dd, J = 9.2, 2.8 Hz, 1H), 6.28 (d, J = 9.2 Hz, 1H), 6.78–6.83 (m, 2H), 6.87 (d, J = 8.8 Hz, 2H), 6.96 (d, J = 3.2 Hz, 1H), 7.25–7.30 (m, 2H), 7.51–7.61 (m, 6H), 7.88–7.91 (m, 2H), 8.53–8.57 (m, 2H), 8.68–8.72 (m, 2H). ^{13}C NMR (100 MHz, THF-d_8): δ = 68.50, 68.55, 69.04, 70.37, 70.40, 70.43, 70.59, 71.79, 72.05, 72.21, 85.26, 90.75, 100.49, 103.99, 106.15, 106.19, 113.49, 113.63, 114.72, 114.98, 115.08, 116.37, 117.00, 119.24, 119.31, 119.57, 125.63, 125.65, 127.29, 127.32, 127.62, 127.64, 127.70, 128.42, 132.56, 132.67, 133.89, 153.36, 154.85, 155.26, 155.28, 159.43. MS (MALDI-TOF): m/z: 814.33 (calcd. $[M]^+$ = 814.31).

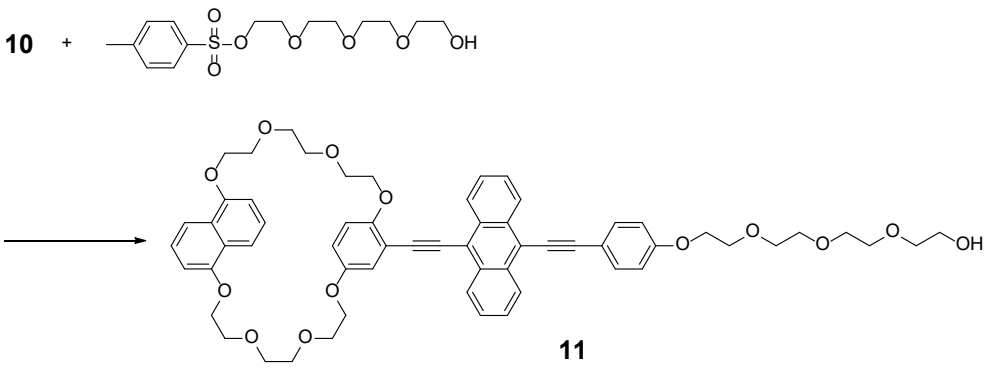

Conditions: K_2CO_3, DMF, 80 °C, 22 h.

Compound 11 (An). A mixture of compound **10** (397 mg, 0.487 mmol), 2-{2-[2-(2-hydroxyethoxy)ethoxy]ethoxy}ethyl toluenesulfonate[70] (204 mg, 0.585 mmol), and K_2CO_3 (202 mg, 1.46 mmol) in DMF (30 mL) was stirred for 22 h at 80 °C. After cooling to r.t., the reaction mixture was poured into ethyl acetate (150 mL). The solution was washed with saturated aq. NH_4Cl (3 × 100 mL). The organic layer was dried over $MgSO_4$ and filtered, and the solvent was evaporated under reduced pressure. The crude product thus isolated was purified by flash column chromatography on silica gel (eluent: gradient from dichloromethane/acetone = 4:1 to dichloromethane/acetone = 7:3 v/v) and subsequently precipitated from a mixture of chloroform and hexane to afford compound **11** (**An**, 370 mg, 0.373 mmol, 77%) as an orange solid.

^{1}H NMR (400 MHz, $CDCl_3$): δ = 2.54 (br, 1H), 3.61–3.63 (m, 2H), 3.69–3.81 (m, 22H), 3.88–4.03 (m, 10H), 4.19–4.22 (m, 4H), 4.29–4.30 (m, 2H), 6.24–6.25 (m, 2H), 6.75–6.81 (m, 2H), 6.98–7.00 (m, 3H), 7.23–7.28 (m, 2H), 7.58–7.64 (m, 4H), 7.70 (d, J = 9.2 Hz, 2H), 7.86–7.89 (m, 2H), 8.64–8.69 (m, 2H), 8.72–8.77 (m, 2H). ^{13}C NMR (100 MHz, $CDCl_3$): δ = 61.67, 67.43, 67.53, 67.57, 68.36, 68.59, 69.56, 69.68, 69.73, 69.84, 70.26, 70.49, 70.58, 70.74, 70.82, 70.99, 71.23, 72.46, 85.49, 90.43, 99.44, 102.56, 105.47, 105.57, 113.23, 113.52, 114.40, 114.54, 114.82, 115.65, 116.28, 118.38, 118.67, 119.22, 125.15, 126.59, 126.67, 127.12, 127.61, 131.88, 131.90, 133.11, 152.41, 153.89, 154.23, 154.27, 159.15. MS (MALDI-TOF): m/z: 990.47 (calcd. $[M]^+$ = 990.42).

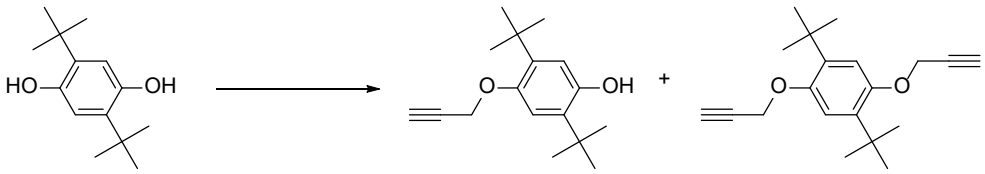

12 **13**

Conditions: propargyl bromide, NaH, DMF, 0 °C → r.t., 23 h.

Compounds 12 and **13.** NaH (60% dispersion in paraffin liquid, 1.98 g, 49.5 mmol) was added to a solution of 2,5-di-*tert*-butylhydroquinone (10.0 g, 45.0 mmol) in DMF (200 mL), and subsequently a toluene solution of propargyl bromide (ca. 9.2 mol/L, 5.38 mL, 49.5 mmol) was added to the mixture at 0 °C. After stirring the reaction mixture for 23 h at r.t., ethyl acetate (150 mL) was added to the reaction mixture. The solution was washed with saturated aq. NH_4Cl (2 × 100 mL) and saturated aq. NaCl (100 mL). The organic layer was dried over $MgSO_4$ and filtered, and the solvent was evaporated under reduced pressure. The crude product thus isolated was purified by flash column chromatography on silica gel (eluent: gradient from hexane to hexane/dichloromethane = 4:1 v/v) to afford compound **12** (2.58 g, 9.91 mmol, 22%) as a pale yellow solid and compound **13** (2.58 g, 8.65 mmol, 19%) as a white solid.

Compound 12: ^{1}H NMR (400 MHz, $CDCl_3$): δ = 1.35 (s, 9H), 1.40 (s, 9H), 2.50 (t, J = 2.4 Hz, 1H), 4.46 (s, 1H), 4.67 (d, J = 2.4 Hz, 2H), 6.59 (s, 1H), 6.95 (s, 1H). ^{13}C NMR (100 MHz, $CDCl_3$): δ = 29.69, 30.02, 34.32, 34.51, 56.91, 74.89, 79.66, 113.46, 115.70, 133.77, 137.63, 148.02, 150.50. MS (MALDI-TOF): m/z: 260.19 (calcd. $[M]^+$ = 260.18).

Compound 13: ^{1}H NMR (400 MHz, $CDCl_3$): δ = 1.38 (s, 18H), 2.50 (t, J = 2.4 Hz, 1H), 4.68 (d, J = 2.8 Hz, 2H), 6.97 (s, 1H). ^{13}C NMR (100 MHz, $CDCl_3$): δ = 30.01, 34.75, 56.69, 74.97, 79.57, 113.12, 136.86, 150.88. MS (MALDI-TOF): m/z: 298.60 (calcd. $[M]^+$ = 298.19).

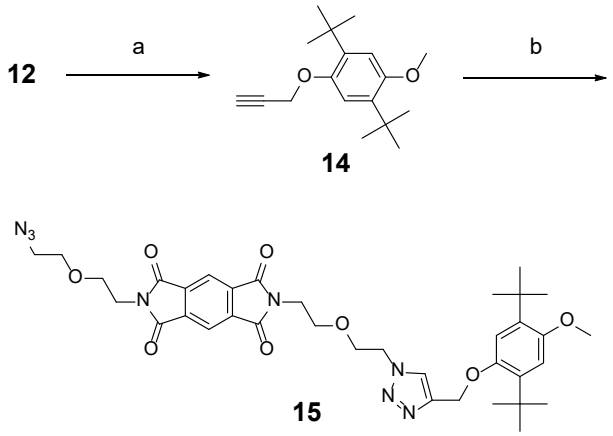

Conditions: (a) iodomethane, Cs_2CO_3, CH_3CN, reflux, 6 h; (b) compound **3**, CuI, *i*-Pr_2NEt, $CHCl_3$, 40 °C, 4 h.

Compound 14. A mixture of compound **12** (2.01 g, 7.72 mmol), iodomethane (1.21 g, 8.49 mmol), and Cs_2CO_3 (5.03 g, 15.4 mmol) in CH_3CN (100 mL) was stirred for 6 h under reflux. After cooling to r.t., the reaction mixture was poured into ethyl acetate (150 mL). The solution was washed with saturated aq. NH_4Cl (2 × 100 mL) and saturated aq. NaCl (100 mL). The organic layer was dried over $MgSO_4$ and filtered, and the solvent was evaporated under reduced pressure. The crude product thus isolated was purified by flash column chromatography on silica gel (eluent: gradient from hexane to hexane/dichloromethane = 9:1 v/v) to afford compound **14** (2.08 g, 7.58 mmol, 98%) as a colorless liquid.

^{1}H NMR (400 MHz, $CDCl_3$): δ = 1.36 (s, 9H), 1.38 (s, 9H), 2.49 (t, J = 2.4 Hz, 1H), 3.81 (s, 3H), 4.67 (d, J = 2.4 Hz, 2H), 6.83 (s, 1H), 6.97 (s, 1H). ^{13}C NMR (100 MHz, $CDCl_3$): δ = 29.87, 30.09, 34.73, 34.74, 55.87, 56.86, 74.87, 79.70, 111.58, 113.31, 136.45, 137.04, 150.29, 152.72. MS (MALDI-TOF): m/z: 274.23 (calcd. $[M]^+$ = 274.19).

Compound 15. A mixture of compound **3** (3.85 g, 8.70 mmol), compound **14** (1.59 g, 5.80 mmol), CuI (1.10 g, 5.80 mmol), and *i*-Pr_2NEt (10 mL) in $CHCl_3$ (100 mL) was stirred for 4 h at 40 °C. The reaction mixture was poured into chloroform (100 mL), and the solution was washed with 5% aq. HCl (100 mL), saturated aq. $NaHCO_3$ (100 mL), and saturated aq. NaCl (100 mL). The organic layer was dried over $MgSO_4$ and filtered, and the solvent was evaporated under reduced pressure. The crude product thus isolated was purified by flash column chromatography on silica gel (eluent: gradient from dichloromethane to dichloromethane/ethyl acetate = 17:3 v/v) to afford compound **15** (1.70 g, 2.37 mmol, 41%) as a pale yellow solid.

^{1}H NMR (400 MHz, $CDCl_3$): δ = 1.36 (s, 9H), 1.38 (s, 9H), 3.30 (t, J = 5.2 Hz, 2H), 3.66–3.69 (m, 4H), 3.78–3.81 (m, 5H), 3.86 (t, J = 5.2 Hz, 2H), 3.92 (t, J = 5.6 Hz, 2H), 3.98 (t, J = 5.6 Hz, 2H), 4.51 (t, J = 5.2 Hz, 2H), 5.19 (s, 2H), 6.84 (s, 1H), 6.97 (s, 1H), 7.74 (s, 1H), 8.28 (s, 2H). ^{13}C NMR (100 MHz, $CDCl_3$): δ = 29.74, 29.88, 34.57, 37.75, 37.94, 50.22, 50.49, 55.78, 63.02, 67.49, 67.91, 68.95, 69.80, 111.56, 112.75, 118.25, 123.66, 136.33, 136.39, 137.02, 137.26, 144.83, 150.42, 152.27, 166.02, 166.03. MS (MALDI-TOF): m/z: 739.35 (calcd. $[M+Na]^+$ = 739.32).

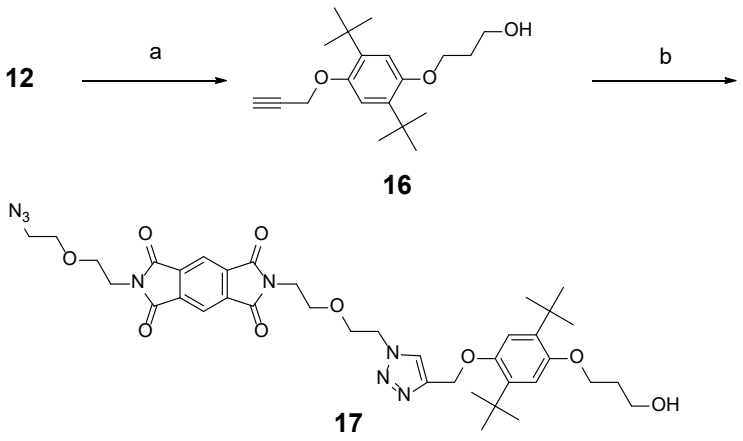

Conditions: (a) 3-bromopropanol, Cs_2CO_3, DMF, 80 °C, 18 h; (b) compound **3**, CuI, *i*-Pr_2NEt, $CHCl_3$, 40 °C, 2 h.

Compound 16. A mixture of compound **12** (4.10 g, 15.7 mmol), 3-bromopropanol (2.61 g, 18.8 mmol), and Cs_2CO_3 (15.3 g, 47.1 mmol) in DMF (100 mL) was stirred for 18 h at 80 °C. After cooling to r.t., the reaction mixture was poured into ethyl acetate (150 mL). The solution was washed with saturated aq. NH_4Cl (3 × 100 mL) and saturated aq. NaCl (100 mL). The organic layer was dried over $MgSO_4$ and filtered, and the solvent was evaporated under reduced pressure. The crude product thus isolated was purified by flash column chromatography on silica gel (eluent: gradient from hexane to hexane/ethyl acetate = 17:3 v/v) to afford compound **16** (2.82 g, 8.86 mmol, 56%) as a pale brown solid.

^{1}H NMR (400 MHz, $CDCl_3$): δ = 1.37 (s, 18H), 2.07–2.13 (m, 2H), 2.50 (t, J = 2.4 Hz, 1H), 3.92 (t, J = 6.4 Hz, 2H), 4.11 (t, J = 6.0 Hz, 2H), 4.68 (d, J = 2.4 Hz, 2H), 6.85 (s, 1H), 6.98 (s, 1H). ^{13}C NMR (100 MHz, $CDCl_3$): δ = 29.96, 30.05, 32.65, 34.69, 34.71, 56.82, 60.49, 65.72, 74.90, 79.63, 111.95, 113.39, 136.17, 137.04, 150.27, 151.79. MS (MALDI-TOF): m/z: 318.24 (calcd. $[M]^+$ = 318.22).

Compound 17. A mixture of compound **3** (400 mg, 1.26 mmol), compound **16** (836 mg, 1.89 mmol), CuI (240 mg, 1.26 mmol), and *i*-Pr_2NEt (5 mL) in $CHCl_3$ (100 mL) was stirred for 2 h at 40 °C. The reaction mixture was poured into chloroform (100 mL), and the solution was washed with 5% aq. HCl (50 mL), saturated aq. $NaHCO_3$ (100 mL), and saturated aq. NaCl (100 mL). The organic layer was dried over $MgSO_4$ and filtered, and the solvent was evaporated under reduced pressure. The crude product thus isolated was purified by flash column chromatography on silica gel (eluent: gradient from

dichloromethane/acetone = 19:1 v/v to dichloromethane/acetone = 4:1 v/v) to afford compound **17** (300 mg, 0.394 mmol, 31%) as a yellow solid.

^{1}H NMR (400 MHz, $CDCl_3$): δ = 1.37 (s, 9H), 1.37 (s, 9H), 1.64 (t, J = 5.2 Hz, 1H), 2.07–2.13 (m, 2H), 3.30 (t, J = 4.8 Hz, 2H), 3.67 (t, J = 5.2 Hz, 4H), 3.79 (t, J = 5.6 Hz, 2H), 3.86 (t, J = 5.2 Hz, 2H), 3.90–3.93 (m, 4H), 3.98 (t, J = 5.2 Hz, 2H), 4.11 (t, J = 6.0 Hz, 2H), 4.50 (t, J = 5.2 Hz, 2H), 5.19 (s, 2H), 6.86 (s, 1H), 6.97 (s, 1H), 7.74 (s, 1H), 8.27 (s, 2H). ^{13}C NMR (100 MHz, $CDCl_3$): δ = 30.03, 32.69, 34.78, 37.91, 38.12, 50.42, 50.68, 60.66, 63.18, 65.82, 67.70, 68.14, 69.14, 70.01, 112.12, 113.00, 118.50, 123.83, 136.31, 136.59, 137.18, 137.44, 145.09, 150.59, 151.54, 166.22. MS (MALDI-TOF): m/z: 761.29 (calcd. $[M+H]^+$ = 761.36).

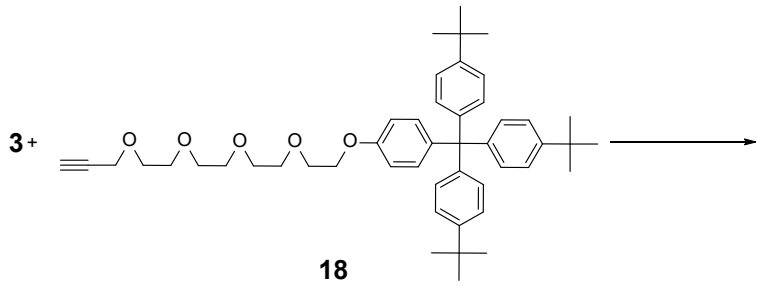

18

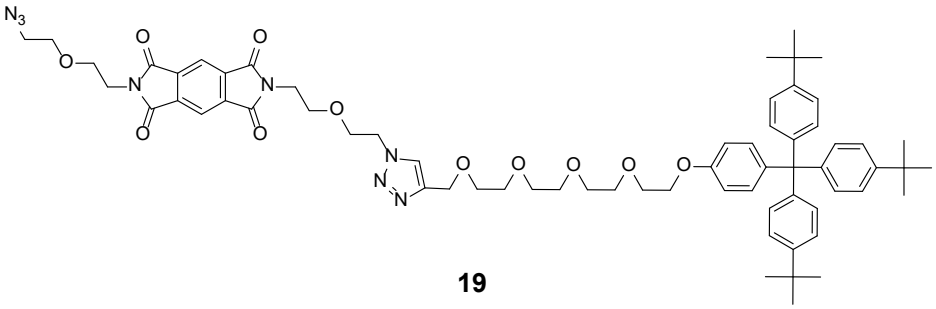

19

Conditions: compound **3**, CuI, *i*-Pr_2NEt, $CHCl_3$, 40 °C, 3 h.

Compound 19. A mixture of compound **3** (1.41 g, 3.18 mmol), compound **18** (1.57 g, 2.12 mmol), CuI (404 mg, 2.12 mmol), and *i*-Pr_2NEt (10 mL) in $CHCl_3$ (100 mL) was stirred for 3 h at 40 °C. The reaction mixture was poured into chloroform (100 mL), and

the solution was washed with 5% aq. HCl (100 mL), saturated aq. $NaHCO_3$ (100 mL), and saturated aq. NaCl (100 mL). The organic layer was dried over $MgSO_4$ and filtered, and the solvent was evaporated under reduced pressure. The crude product thus isolated was purified by flash column chromatography on silica gel (eluent: gradient from dichloromethane/acetone = 9:1 v/v to dichloromethane/acetone = 4:1 v/v) to afford compound **19** (406 mg, 0.350 mmol, 17%) as a white solid.

^{1}H NMR (400 MHz, $CDCl_3$): δ = 1.30 (s, 27H), 3.30 (t, J = 4.8 Hz, 2H), 3.66–3.73 (m, 16H), 3.78–3.85 (m, 6H), 3.93 (t, J = 5.2 Hz, 2H), 3.99 (t, J = 5.2 Hz, 2H), 4.09 (t, J = 5.2 Hz, 2H), 4.45 (t, J = 5.2 Hz, 2H), 4.61 (s, 2H), 6.76 (d, J = 9.2 Hz, 2H), 7.06–7.09 (m, 8H), 7.21–7.24 (m, 6H), 7.66 (s, 1H), 8.28 (s, 2H). ^{13}C NMR (100 MHz, $CDCl_3$): δ = 31.45, 34.34, 37.93, 38.06, 50.17, 50.60, 63.08, 64.59, 67.24, 67.62, 67.98, 68.98, 69.74, 69.80, 69.92, 70.56, 70.64, 70.66, 70.82, 113.09, 118.43, 123.97, 124.09, 130.76, 132.26, 137.10, 137.37, 139.77, 144.18, 145.01, 148.32, 156.59, 166.15, 166.17. MS (MALDI-TOF): m/z: 1183.55 (calcd. $[M+Na]^+$ = 1183.58).

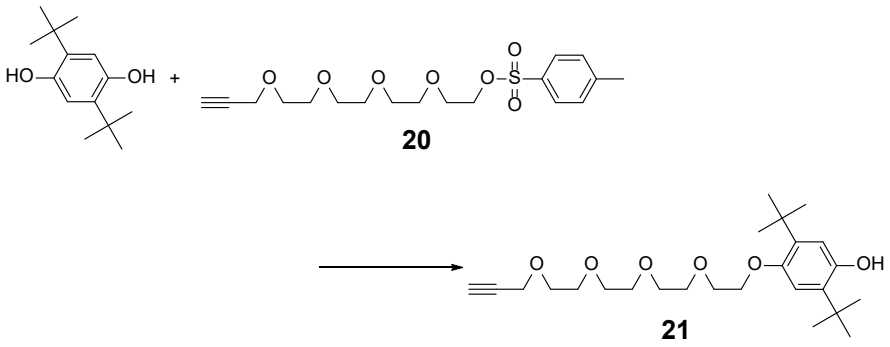

Conditions: NaH, DMF, 0 °C → r.t., 18 h.

Compound 21. NaH (60% dispersion in paraffin liquid, 546 mg, 13.6 mmol) was added to a solution of 2,5-di-*tert*-butylhydroquinone (2.78 g, 12.5 mmol) and compound **20**[71] (5.80 g, 15.0 mmol) in DMF (150 mL) at 0 °C, and the reaction mixture was stirred for

18 h at r.t. The reaction mixture was poured into ethyl acetate (150 mL), and the solution was washed with saturated aq. NH_4Cl (2 × 100 mL) and saturated aq. NaCl (100 mL). The organic layer was dried over $MgSO_4$ and filtered, and the solvent was evaporated under reduced pressure. The crude product thus isolated was purified by flash column chromatography on silica gel (eluent: gradient from hexane to hexane/ethyl acetate = 1:1 v/v) to afford compound **21** (2.23 g, 5.11 mmol, 41%) as a pale yellow solid.

^{1}H NMR (400 MHz, $CDCl_3$): δ = 1.34 (s, 9H), 1.38 (s, 9H), 2.42 (t, J = 2.4 Hz, 1H), 3.65–3.74 (m, 12H), 3.87 (t, J = 5.2 Hz, 2H), 4.11 (t, J = 5.2 Hz, 2H), 4.20 (d, J = 2.4 Hz, 2H), 4.55 (s, 1H), 6.58 (s, 1H), 6.79 (s, 1H). ^{13}C NMR (100 MHz, $CDCl_3$): δ = 29.65, 29.94, 34.31, 34.44, 58.47, 67.97, 69.16, 70.28, 70.48, 70.69, 70.70, 70.77, 70.77, 74.69, 79.69, 112.35, 115.59, 133.57, 136.75, 147.66, 151.01. MS (MALDI-TOF): m/z: 436.29 (calcd. $[M]^+$ = 436.28).

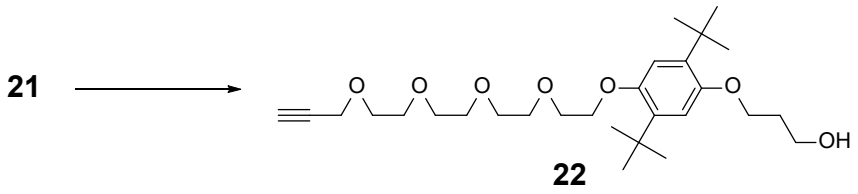

22

Conditions: 3-bromopropanol, Cs_2CO_3, DMF, 80 °C, 18 h.

Compound 22. A mixture of compound **21** (800 mg, 1.83 mmol), 3-bromopropanol (306 mg, 2.20 mmol), and Cs_2CO_3 (1.79 g, 5.49 mmol) in DMF (50 mL) was stirred for 18 h at 80 °C. After cooling to r.t., the reaction mixture was poured into ethyl acetate (150 mL). The solution was washed with saturated aq. NH_4Cl (3 × 100 mL) and saturated aq. NaCl (100 mL). The organic layer was dried over $MgSO_4$ and filtered, and the solvent was evaporated under reduced pressure. The crude product thus isolated was purified by flash column chromatography on silica gel (eluent: gradient from hexane/ethyl acetate = 17:3

v/v to hexane/ethyl acetate = 13:7 v/v) to afford compound **22** (444 mg, 0.898 mmol, 49%) as a brown liquid.

^{1}H NMR (400 MHz, $CDCl_3$): δ = 1.36 (s, 9H), 1.37 (s, 9H), 2.06–2.12 (m, 2H), 2.42 (t, J = 2.4 Hz, 1H), 3.65–3.74 (m, 12H), 3.88 (t, J = 5.2 Hz, 2H), 3.92 (t, J = 6.0 Hz, 2H), 4.09–4.13 (m, 4H), 4.20 (d, J = 2.4 Hz, 2H), 6.83 (s, 1H), 6.84 (s, 1H). ^{13}C NMR (100 MHz, $CDCl_3$): δ = 29.93, 29.98, 32.67, 34.64, 34.70, 58.45, 60.48, 65.84, 67.96, 69.15, 70.24, 70.46, 70.67, 70.74, 70.77, 74.63, 79.70, 112.08, 112.37, 136.08, 136.34, 151.08, 151.17. MS (MALDI-TOF): m/z: 494.36 (calcd. $[M]^+$ = 494.32).

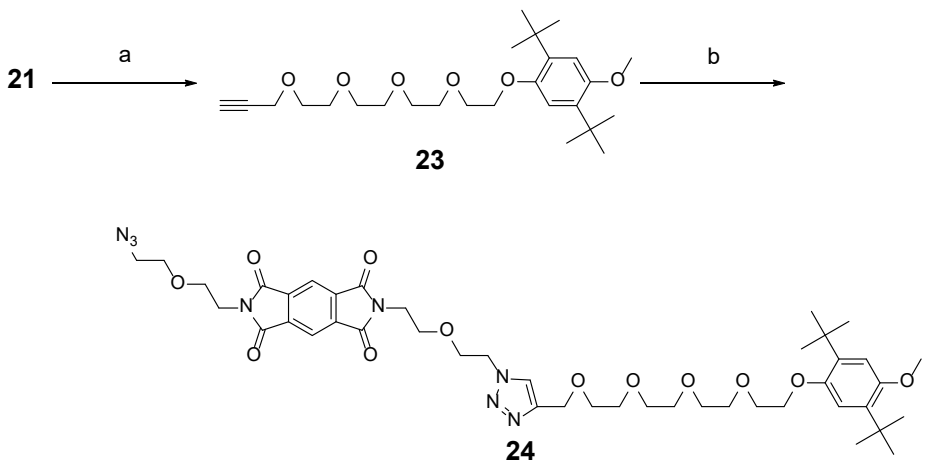

Conditions: (a) iodomethane, Cs_2CO_3, CH_3CN, reflux, 23 h; (b) compound 3, CuI, *i*-Pr_2NEt, $CHCl_3$, 40 °C, 2 h.

Compound 23. A mixture of compound **21** (770 mg, 1.76 mmol), iodomethane (275 mg, 1.94 mmol), and Cs_2CO_3 (1.15 g, 3.52 mmol) in CH_3CN (50 mL) was stirred for 23 h under reflux. After cooling to r.t., the reaction mixture was poured into ethyl acetate (150 mL). The solution was washed with saturated aq. NH_4Cl (2 × 100 mL) and saturated aq. NaCl (100 mL). The organic layer was dried over $MgSO_4$ and filtered, and the solvent was evaporated under reduced pressure. The crude product thus isolated was purified by

flash column chromatography on silica gel (eluent: gradient from hexane to hexane/ethyl acetate = 4:1 v/v) to afford compound **23** (642 mg, 1.42 mmol, 81%) as a pale yellow liquid.

^{1}H NMR (400 MHz, $CDCl_3$): δ = 1.35 (s, 9H), 1.38 (s, 9H), 2.42 (t, J = 2.4 Hz, 1H), 3.65–3.74 (m, 12H), 3.80 (s, 3H), 3.88 (t, J = 5.2 Hz, 2H), 4.12 (t, J = 5.2 Hz, 2H), 4.20 (d, J = 2.4 Hz, 2H), 6.82 (s, 1H), 6.82 (s, 1H). ^{13}C NMR (100 MHz, $CDCl_3$): δ = 29.84, 29.92, 34.61, 34.69, 55.90, 58.43, 67.95, 69.14, 70.24, 70.46, 70.67, 70.68, 70.74, 70.77, 74.61, 79.70, 111.68, 112.25, 136.28, 136.30, 151.05, 152.05. MS (MALDI-TOF): m/z: 450.30 (calcd. $[M]^+$ = 450.30).

Compound 24. A mixture of compound **3** (922 mg, 2.08 mmol), compound **23** (626 mg, 1.39 mmol), CuI (265 mg, 1.39 mmol), and *i*-Pr_2NEt (5 mL) in $CHCl_3$ (30 mL) was stirred for 2 h at 40 °C. The reaction mixture was poured into chloroform (150 mL), and the solution was washed with 5% aq. HCl (100 mL), saturated aq. $NaHCO_3$ (100 mL), and saturated aq. NaCl (100 mL). The organic layer was dried over $MgSO_4$ and filtered, and the solvent was evaporated under reduced pressure. The crude product thus isolated was purified by flash column chromatography on silica gel (eluent: gradient from dichloromethane/acetone = 17:3 v/v to dichloromethane/acetone = 4:1 v/v) to afford compound **24** (437 mg, 0.489 mmol, 35%) as a pale brown liquid.

^{1}H NMR (400 MHz, $CDCl_3$): δ = 1.34 (s, 9H), 1.37 (s, 9H), 3.30 (t, J = 4.8 Hz, 2H), 3.65–3.74 (m, 16H), 3.78–3.84 (m, 7H), 3.88 (t, J = 5.2 Hz, 2H), 3.93 (t, J = 5.2 Hz, 2H), 3.99 (t, J = 5.2 Hz, 2H), 4.12 (t, J = 5.2 Hz, 2H), 4.47 (t, J = 5.2 Hz, 2H), 4.62 (s, 2H), 6.82 (s, 1H), 6.82 (s, 1H), 7.66 (s, 1H), 8.29 (s, 2H). ^{13}C NMR (100 MHz, $CDCl_3$): δ = 29.83, 29.92, 34.61, 34.69, 37.92, 38.06, 50.18, 50.60, 55.94, 64.58, 67.62, 67.94, 67.98, 68.98,

69.73, 69.92, 70.23, 70.56, 70.63, 70.67, 70.70, 70.75, 111.72, 112.26, 118.42, 123.97, 136.30, 137.09, 137.36, 145.00, 151.05, 152.06, 166.15, 166.16. MS (MALDI-TOF): m/z: 915.46 (calcd. $[M+Na]^+ = 915.42$)

13 + **19** ⟶

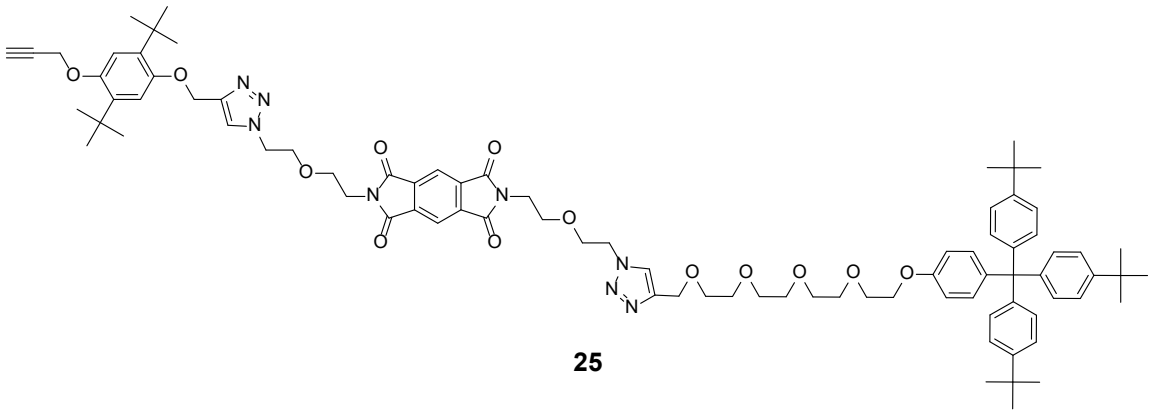

25

Conditions: CuI, *i*-Pr_2NEt, $CHCl_3$, 40 °C, 2 h.

Compound 25. A mixture of compound **13** (677 mg, 2.27 mmol), compound **19** (264 mg, 0.227 mmol), CuI (43.2 mg, 0.227 mmol), and *i*-Pr_2NEt (5 mL) in $CHCl_3$ (100 mL) was stirred for 2 h at 40 °C. The reaction mixture was poured into chloroform (100 mL), and the solution was washed with 5% aq. HCl (100 mL), saturated aq. $NaHCO_3$ (100 mL), and saturated aq. NaCl (100 mL). The organic layer was dried over $MgSO_4$ and filtered, and the solvent was evaporated under reduced pressure. The crude product thus isolated was purified by flash column chromatography on silica gel (eluent: gradient from dichloromethane to dichloromethane/acetone = 7:3 v/v) to afford compound **25** (226 mg, 0.155 mmol, 68%) as a yellow solid.

^1H NMR (400 MHz, $CDCl_3$): δ = 1.30 (s, 27H), 1.37 (s, 9H), 1.38 (s, 9H), 2.51 (s, 1H), 3.66–3.71 (m, 16H), 3.80–3.87 (m, 6H), 3.92 (t, J = 5.2 Hz, 4H), 4.09 (t, J = 4.8 Hz, 2H),

4.44 (t, J = 5.2 Hz, 2H), 4.50 (t, J = 4.8 Hz, 2H), 4.61 (s, 2H), 4.68 (s, 2H), 5.19 (s, 2H), 6.76 (d, J = 8.8 Hz, 2H), 6.98 (s, 1H), 6.99 (s, 1H), 7.07 (d, J = 8.4 Hz, 8H), 7.23 (d, J = 8.4 Hz, 6H), 7.65 (s, 1H), 7.75 (s, 1H). ^{13}C NMR (100 MHz, $CDCl_3$): δ = 29.98, 30.06, 31.51, 34.42, 34.78, 37.95, 38.01, 50.23, 50.41, 56.75, 63.06, 63.15, 64.66, 67.28, 68.01, 68.09, 69.03, 69.14, 69.80, 69.88, 70.63, 70.72, 70.89, 74.98, 79.60, 112.74, 113.14, 113.25, 118.58, 123.81, 124.03, 124.17, 130.83, 132.34, 136.56, 137.15, 137.28, 139.85, 144.24, 144.98, 145.06, 148.41, 150.63, 151.21, 156.64, 166.13. MS (MALDI-TOF): m/z: 1460.21 (calcd. $[M]^+$ = 1459.80).

11 + **15** + **16** ⟶

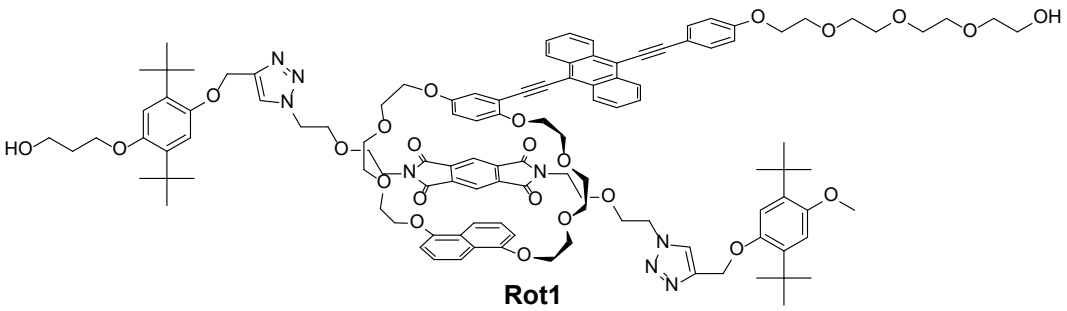

Rot1

+

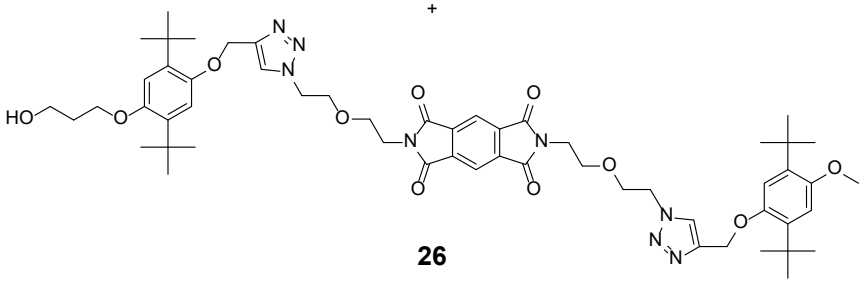

26

Conditions: $CuSO_4$, sodium ascorbate, $CHCl_3$, H_2O, 5 °C, 20 h.

Rot1 and **compound 26.** A mixture of sodium ascorbate (120 mg, 0.606 mmol) and copper(II) sulfate (48.4 mg, 0.303 mmol) in water (1 mL) was added to a solution of

compound **11** (200 mg, 0.202 mmol), compound **15** (145 mg, 0.202 mmol), and compound **16** (64.3 mg, 0.202 mmol) in chloroform (0.7 mL) and the mixture was vigorously stirred for 20 h at 5 °C. The suspension was poured into the mixture of water (100 mL) and chloroform (150 mL). The organic layer was separated off, washed with saturated aq. NaCl (100 mL), dried over $MgSO_4$, and filtered. After the solvent was evaporated under reduced pressure, the crude product thus isolated was purified by flash column chromatography on silica gel (eluent: gradient from dichloromethane/acetone = 4:1 v/v to dichloromethane/acetone = 1:1 v/v) and recycling GPC (eluent: chloroform) to afford **Rot1** (75.1 mg, 3.71×10^{-2} mmol, 18%) as a reddish brown solid and **26** (67.0 mg, 6.47×10^{-2} mmol, 32%) as a pale brown solid.

Rot1: ^{1}H NMR (400 MHz, $CDCl_3$): δ = 1.36–1.37 (m, 36H), 1.94 (s, 1H), 2.05–2.11 (m, 2H), 2.68 (s, 1H), 3.24–4.50 (m, 63H), 5.20 (s, 2H), 5.21 (s, 2H), 5.98 (d, J = 9.2 Hz, 1H), 6.15 (dd, J = 9.2, 2.8 Hz, 1H), 6.22–6.32 (m, 2H), 6.40 (d, J = 2.8 Hz, 1H), 6.68–6.79 (m, 2H), 6.83–6.85 (m, 2H), 6.97–7.01 (m, 4H), 7.17–7.24 (m, 2H), 7.61–7.76 (m, 8H), 7.93 (br, 2H), 8.56–8.60 (m, 2H), 8.64–8.68 (m, 2H). ^{13}C NMR (100 MHz, $CDCl_3$): δ = 29.87, 30.02, 32.68, 34.72, 34.74, 36.49, 36.57, 50.31, 50.41, 55.90, 60.45, 61.85, 63.16, 63.21, 65.77, 67.63, 67.66, 67.74, 67.81, 67.87, 67.92, 68.10, 68.36, 68.59, 69.44, 69.75, 69.83, 69.92, 70.43, 70.70, 70.78, 70.95, 71.00, 72.61, 85.36, 91.12, 98.34, 103.12, 105.23, 105.35, 110.69, 111.68, 112.05, 112.21, 112.84, 112.93, 114.04, 114.23, 115.03, 115.58, 117.10, 117.13, 118.04, 118.22, 118.95, 123.51, 123.56, 124.02, 124.17, 125.59, 125.74, 126.94, 127.01, 127.22, 127.81, 131.91, 132.02, 133.31, 134.27, 134.38, 136.28, 136.51, 145.01, 145.06, 145.10, 145.15, 150.60, 151.55, 151.89, 152.43, 152.97, 153.92, 153.86, 159.42, 166.61, 166.69. HRMS (ESI): m/z: 2047.9559 (calcd. $[M+Na]^+$ = 2047.9565).

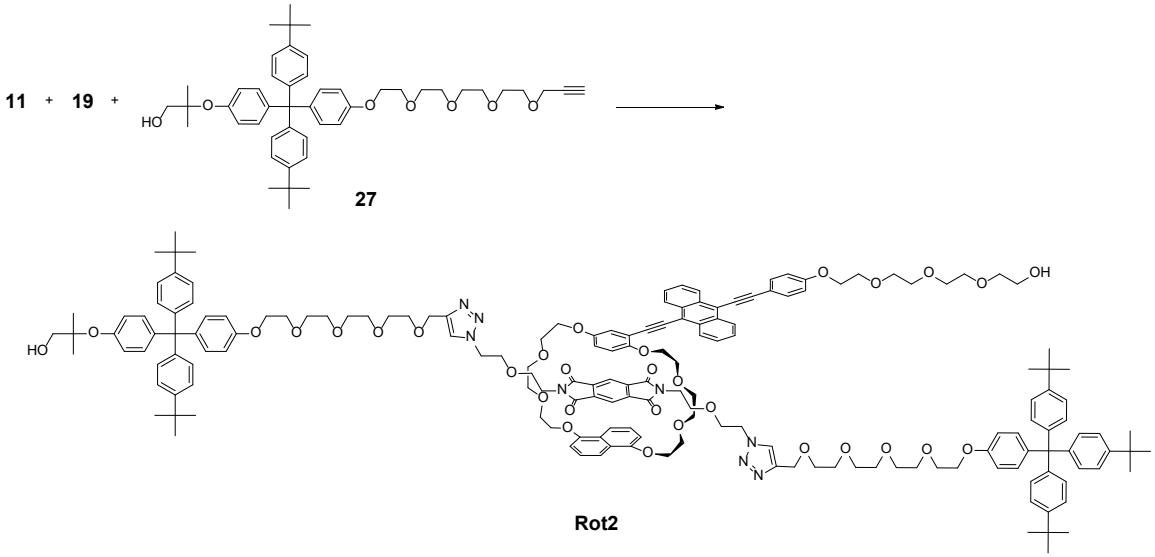

Conditions: $CuSO_4$, sodium ascorbate, $CHCl_3$, H_2O, 5 °C, 19 h.

Rot2. A mixture of sodium ascorbate (95.1 mg, 0.480 mmol) and copper(II) sulfate (38.3 mg, 0.240 mmol) in water (1 mL) was added to a solution of compound **11** (159 mg, 0.160 mmol), compound **19** (186 mg, 0.160 mmol), and compound **27**[S4] (120 mg, 0.160 mmol) in chloroform (0.7 mL) and the mixture was vigorously stirred for 19 h at 5 °C. The suspension was poured into the mixture of water (100 mL) and chloroform (150 mL). The organic layer was separated off, washed with saturated aq. NaCl (100 mL), dried over $MgSO_4$, and filtered. After the solvent was evaporated under reduced pressure, the crude product thus isolated was purified by flash column chromatography on silica gel (eluent: gradient from dichloromethane/acetone = 3:1 v/v to dichloromethane/acetone = 1:1 v/v) and recycling GPC (eluent: chloroform) to afford **Rot2** (16.5 mg, 5.68×10^{-3} mmol, 4%) as a reddish brown solid.

^{1}H NMR (400 MHz, $CDCl_3$): δ = 1.28–1.29 (m, 51H), 2.24 (t, J = 6.4 Hz, 1H), 2.57 (s, 1H), 3.29–4.46 (m, 92H), 4.66 –4.67 (m, 2H), 6.00 (d, J = 9.2 Hz, 1H), 6.16 (dd, J = 9.2, 3.2 Hz, 1H), 6.24–6.34 (m, 2H), 6.43 (d, J = 3.2 Hz, 1H), 6.70–6.85 (m, 8H), 7.00–7.08 (m, 18H), 7.18–7.25 (m, 12H), 7.61–7.73 (m, 8H), 7.94 (br, 2H), 8.57–8.61 (m, 2H),

8.65–8.70 (m, 2H). ^{13}C NMR (100 MHz, $CDCl_3$): δ = 23.29, 31.50, 34.41, 36.60, 36.70, 50.23, 50.31, 61.90, 63.06, 63.15, 64.65, 64.67, 67.27, 67.30, 67.68, 67.81, 67.91, 67.97, 68.13, 68.40, 68.62, 69.50, 69.80, 69.86, 69.97, 70.49, 70.62, 70.70, 70.75, 70.82, 70.86, 70.97, 71.01, 71.05, 72.63, 80.54, 85.41, 91.19, 98.39, 103.15, 105.29, 105.40, 110.78, 112.26, 113.15, 113.23, 114.09, 114.28, 115.08, 115.64, 117.17, 118.07, 118.27, 119.00, 122.31, 123.80, 123.85, 124.15, 124.23, 125.63, 125.78, 127.00, 127.08, 127.28, 127.84, 130.77, 130.83, 131.96, 131.99, 132.06, 132.24, 132.32, 133.37, 134.30, 134.42, 139.68, 139.83, 142.77, 144.12, 144.24, 145.11, 145.21, 148.40, 148.56, 151.94, 152.46, 153.03, 153.91, 153.97, 156.65, 156.74, 159.46, 166.68, 166.76. HRMS (ESI): m/z: 2924.4543 (calcd. $[M+Na]^+$ = 2924.4530).

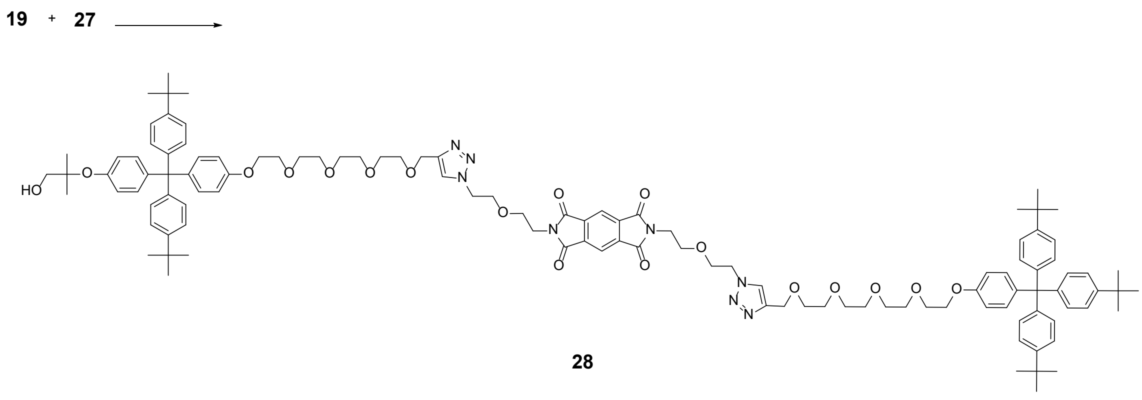

Conditions: CuI, *i*-Pr_2EtN, $CHCl_3$, 40 °C, 3 h.

Compound 28. A mixture of compound **19** (100 mg, 8.61×10^{-2} mmol), compound **27** (64.7 mg, 8.61×10^{-2} mmol), CuI (16.8 mg, 8.61×10^{-2} mmol), and *i*-Pr_2EtN (10 mL) in $CHCl_3$ (100 mL) was stirred for 3 h at 40 °C. The reaction mixture was poured into chloroform (100 mL), and the solution was washed with 5% aq. HCl (100 mL), saturated aq. $NaHCO_3$ (100 mL), and saturated aq. NaCl (100 mL). The organic layer was dried over $MgSO_4$ and filtered, and the solvent was evaporated under reduced pressure. The

crude product thus isolated was purified by flash column chromatography on silica gel (eluent: gradient from dichloromethane/acetone = 9:1 v/v to dichloromethane/acetone = 4:1 v/v) to afford compound **28** (47.0 mg, 2.46×10^{-2} mmol, 29%) as a pale yellow solid. ^{1}H NMR (400 MHz, $CDCl_3$): δ = 1.28 (s, 6H), 1.30 (s, 45H), 2.3 (t, J = 6.4 Hz, 1H), 3.57 (d, J = 6.4 Hz, 2H), 3.66–3.73 (m, 28H), 3.80–3.85 (m, 8H), 3.93 (t, J = 5.2 Hz, 4H), 4.09 (t, J = 4.8 Hz, 4H), 4.45 (t, J = 4.8 Hz, 4H), 4.62 (s, 4H), 6.77 (d, J = 8.4 Hz, 4H), 6.84 (d, J = 8.4 Hz, 2H), 7.04–7.08 (m, 16H), 7.20–7.24 (m, 10H), 7.67 (s, 2H), 8.29 (s, 2H). ^{13}C NMR (100 MHz, $CDCl_3$): δ = 23.26, 31.48, 31.62, 34.39, 37.98, 50.20, 63.02, 63.10, 64.60, 67.25, 67.98, 69.00, 69.75, 69.83, 70.42, 70.59, 70.68, 70.85, 113.10, 113.18, 118.58, 122.31, 124.01, 124.13, 124.22, 130.73. 130.79, 131.96, 132.22, 132.30, 137.23, 139.66, 139.80, 142.74, 144.07, 144.20, 145.00, 148.36, 148.53, 152.40, 156.59, 156.68, 166.14. MS (MALDI-TOF): m/z: 1934.03 (calcd. $[M+Na]^+$ = 1934.03).

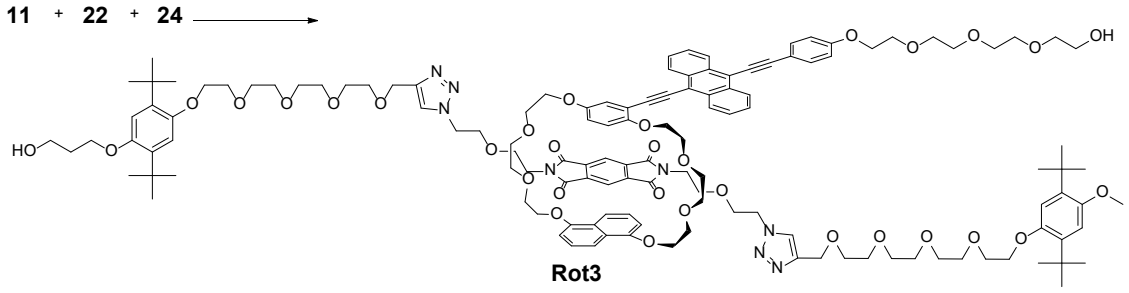

Conditions: $CuSO_4$, sodium ascorbate, $CHCl_3$, H_2O, 5 °C, 17 h.

Rot3. A mixture of sodium ascorbate (119 mg, 0.601 mmol) and copper(II) sulfate (47.9 mg, 0.300 mmol) in water (1 mL) was added to a solution of compound **11** (139 mg, 0.140 mmol), compound **22** (98.9 mg, 0.200 mmol), and compound **24** (179 mg, 0.200 mmol) in chloroform (0.6 mL) and the mixture was vigorously stirred for 17 h at 5 °C. The suspension was poured into the mixture of water (100 mL) and chloroform (150 mL). The

organic layer was separated off, washed with saturated aq. NaCl (100 mL), dried over $MgSO_4$, and filtered. After the solvent was evaporated under reduced pressure, the crude product thus isolated was purified by flash column chromatography on silica gel (eluent: gradient from dichloromethane/acetone = 7:3 v/v to dichloromethane/acetone = 2:3 v/v) and recycling GPC (eluent: chloroform) to afford **Rot3** (14.7 mg, 6.18×10^{-3} mmol, 4%) as a reddish brown solid.

^{1}H NMR (400 MHz, $CDCl_3$): δ = 1.34–1.36 (m, 36H), 2.05–2.11 (m, 2H), 3.28–4.45 (m, 95H), 4.66–4.68 (m, 4H), 5.99 (d, J = 9.2 Hz, 1H), 6.15 (dd, J = 9.2, 3.2 Hz, 1H), 6.23–3.64 (m, 2H), 6.42 (d, J = 3.2 Hz, 1H), 6.69–6.83 (m, 6H), 7.02 (d, J = 8.8 Hz, 2H), 7.17–7.24 (m, 2H), 7.60–7.74 (m, 8H), 7.94 (br, 2H), 8.57–8.61 (m, 2H), 8.65–8.69 (m, 2H).

^{13}C NMR (100 MHz, $CDCl_3$): δ = 29.87, 29.95, 30.01, 32.70, 34.64, 34.67, 34.72, 36.55, 36.65, 50.20, 50.28, 55.97, 60.51, 61.85, 64.61, 64.63, 65.87, 67.64, 67.77, 67.86, 67.95, 68.10, 68.36, 68.57, 69.45, 69.76, 69.79, 69.84, 69.92, 70.25, 70.45, 70.58, 70.65, 70.68, 70.70, 70.73, 70.76, 70.78, 70.93, 70.96, 71.01, 72.59, 85.38, 91.14, 98.36, 103.11, 105.26, 105.36, 110.73, 111.74, 112.10, 112.21, 112.28, 112.38, 114.04, 114.23, 115.04, 115.55, 115.60, 117.14, 118.04, 118.22, 118.95, 123.75, 123.80, 124.04, 124.19, 125.59, 125.74, 126.96, 127.04, 127.23, 127.80, 131.09, 131.91, 132.02, 133.32, 134.27, 134.38, 136.09, 136.34, 145.07, 145.16, 151.07, 151.10, 151.20, 151.89, 152.09, 152.98, 153.87, 153.93, 159.43, 166.63, 166.71. HRMS (ESI): m/z: 2400.1649 (calcd. $[M+Na]^+$ = 2400.1662).

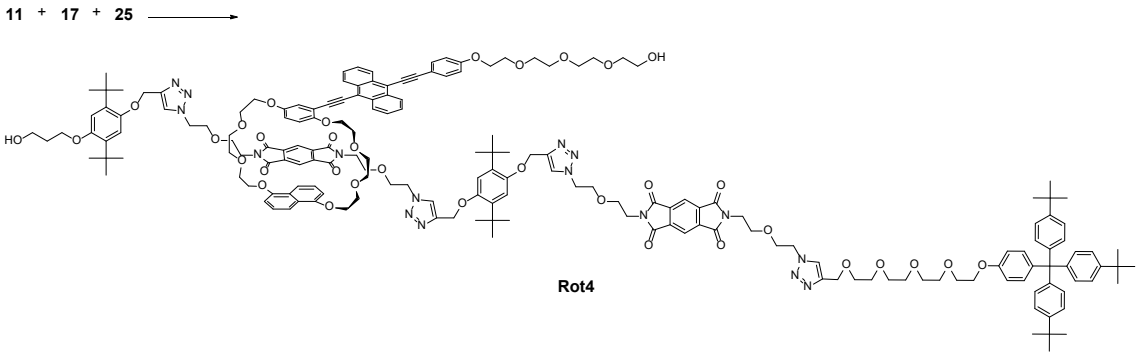

Conditions: $CuSO_4$, sodium ascorbate, $CHCl_3$, H_2O, 5 °C, 19 h.

Rot4. A mixture of sodium ascorbate (92.1 mg, 0.465 mmol) and copper(II) sulfate (37.2 mg, 0.233 mmol) in water (1 mL) was added to a solution of compound **11** (154 mg, 0.155 mmol), compound **17** (118 mg, 0.155 mmol), and compound **25** (226 mg, 0.155 mmol) in chloroform (0.7 mL) and the mixture was vigorously stirred for 19 h at 5 °C. The suspension was poured into the mixture of water (100 mL) and chloroform (150 mL). The organic layer was separated off, washed with saturated aq. NaCl (100 mL), dried over $MgSO_4$, and filtered. After the solvent was evaporated under reduced pressure, the crude product thus isolated was purified by flash column chromatography on silica gel (eluent: gradient from dichloromethane/acetone = 4:1 v/v to dichloromethane/acetone = 2:3 v/v) and recycling GPC (eluent: chloroform) to afford **Rot4** (63.0 mg, 1.96×10^{-2} mmol, 13%) as a reddish brown solid.

^{1}H NMR (400 MHz, $CDCl_3$): δ = 1.29 (s, 27H), 1.35–1.38 (m, 36H), 1.96–2.01 (m, 1H), 2.05–2.12 (m, 2H), 2.84 (s, 1H), 3.24–4.52 (m, 92H), 4.60 (s, 2H), 5.20–5.26 (m, 6H), 5.98 (d, J = 9.2 Hz, 1H), 6.15 (dd, J = 8.8, 2.0 Hz, 1H), 6.22 (d, J = 7.6 Hz, 1H), 6.31 (d, J = 7.6 Hz, 1H), 6.40 (t, J = 2.4 Hz, 1H), 6.67–6.79 (m, 4H), 6.85 (s, 1H), 6.98–7.01 (m, 5H), 7.05–7.08 (m, 8H), 7.14–7.24 (m, 8H), 7.61–7.78 (m, 10H), 7.91 (br, 2H), 8.12 (s, 1H), 8.13 (s, 1H), 8.54–8.57 (m, 2H), 8.63–8.66 (m, 2H). ^{13}C NMR (100 MHz, $CDCl_3$): δ = 30.01, 31.47, 32.67, 34.37, 34.76, 36.49, 36.59, 37.80, 37.87, 50.16, 50.35, 50.40,

60.42, 61.82, 63.09, 63.13, 64.57, 65.74, 67.23, 67.60, 67.71, 67.91, 68.01, 68.09, 68.34, 68.61, 68.95, 69.07, 69.44, 69.72, 69.82, 70.38, 70.56, 70.66, 70.75, 70.82, 70.93, 72.66, 85.31, 91.08, 98.33, 103.18, 105.23, 105.33, 110.71, 112.02, 112.14, 112.77, 112.85, 112.90, 113.10, 114.00, 114.20, 115.01, 115.55, 116.96, 117.01, 117.96, 118.26, 118.96, 123.51, 123.57, 123.65, 123.80, 123.99, 124.12, 125.50, 125.67, 126.98, 127.05, 127.21, 127.75, 130.78, 131.85, 131.96, 132.29, 133.33, 134.21, 134.34, 136.25, 136.48, 136.60, 136.66, 136.98,139.80, 144.19, 144.95, 144.99, 145.03, 145.09, 148.35, 150.54, 150.92, 151.53, 151.87, 152.96, 153.82, 153.88, 156.58, 159.39, 165.99, 166.60, 166.71. HRMS (ESI): m/z: 1627.7703 (calcd. $[M+2Na]^{2+}$ = 1627.7705).

3.4.3. Polymer Synthesis and Preparation of Polyurethane Films

Synthesis of polyurethane Rot1PU

Dibutyltin dilaurate (4 drops) was added to a stirred mixture of **Rot1** (10.0 mg, 4.93 μmol), telechelic poly(tetrahydrofuran)diol (M_n = 2,000 g/mol, 3.00 g, 1.50 mmol), and 4,4′-methylenebis(phenylisocyanate) (1.26 g, 5.04 mmol) in THF (20 mL) and the mixture was stirred at r.t. for 3 h. A solution of 1,4-butanediol (297 mg, 3.30 mmol) in THF (10 mL) was then added and the reaction mixture was stirred at r.t. for an additional 24 h. MeOH (2 mL) was added to the reaction mixture and the reaction mixture was poured into MeOH (1000 mL) after stirring for another 30 min. The pale yellow precipitate was collected by filtration and re-dissolved in THF (100 mL). The THF solution was filtrated through a cotton filter and poured into hexane (1500 mL). The precipitate was filtered off and dried in vacuo for 24 h at r.t. to afford **Rot1PU** as a yellow rubbery solid (3.92 g, 86%, M_n = 67690 g/mol).

Synthesis of polyurethanes Rot2PU, Rot3PU, and Rot4PU

Following the synthetic procedure used for **Rot1PU**, polyurethanes **Rot2PU**, **Rot3PU**, and **Rot4PU** were prepared with **Rot2** (11.7 mg, 4.93 μmol), **Rot3** (14.3 mg, 4.93 μmol), and **Rot4** (10.0 mg, 3.11 μmol), respectively. All polymers were obtained as yellow rubbery solids (**Rot2PU**: 4.12 g, 90%, M_n = 57580 g/mol; **Rot3PU**: 4.17 g, 91%, M_n = 47060 g/mol; **Rot4PU**: 3.83 g, 84%, M_n = 92340 g/mol).

Preparation of Rot1PU, Rot2PU, Rot3PU, and Rot4PU films

300 mg of the polyurethanes (**Rot1PU**, **Rot2PU**, **Rot3PU**, and **Rot4PU**) were dissolved in THF (8 mL) and the solutions were divided between two square poly(tetrafluoroethylene) molds (51 × 5.0 mm). The molds were placed under an inverted funnel so that the evaporation rate was controlled. The solvent was evaporated for 3 h under ambient conditions and the resulting films were further dried in vacuo at r.t. for 6 h. The films thus obtained were smooth and transparent or opaque. The thicknesses of the films were 60–90 μm, which were measured by a digital caliper.

3.4.4. Thermal Treatment for Rot1 or Rot2 Solutions

Toluene solutions of **Rot1** and **Rot2** were kept under reflux over the course of 3 h and monitored by fluorescence spectroscopy, and analyzed by high performance liquid chromatography (HPLC). The identity of the additional fraction in **Rot1** solution after thermal treatment was additionally confirmed by MALDI-TOF mass spectroscopy.

3.4.5. Mass Spectroscopic Studies for Rot1PU or Rot4PU Films After Stretching

After several **Rot1PU** and **Rot4PU** films were stretched 50 times, the stretched parts of the films were cut off. The collected parts were redissolved in THF (10 mL), and then the THF solutions were mixed with methanol (500 mL) while stirring. After filtration to remove precipitates, the obtained filtrates were evaporated under reduced pressure and the residues were used for HRMS analysis.

3.5. References

(1) Caruso, M. M.; Davis, D. A.; Shen, Q.; Odom, S. A.; Sottos, N. R.; White, S. R.; Moore, J. S. Mechanically-Induced Chemical Changes in Polymeric Materials. *Chem. Rev.* **2009**, *109*, 5755–5798.

(2) Li, J.; Nagamani, C.; Moore, J. S. Polymer Mechanochemistry: From Destructive to Productive. *Acc. Chem. Res.* **2015**, *48*, 2181–2190.

(3) De Bo, G. Polymer Mechanochemistry and the Emergence of the Mechanophore Concept. *Macromolecules* **2020**, *53*, 7615–7617.

(4) Traeger, H.; Kiebala, D. J.; Weder, C.; Schrettl, S. From Molecules to Polymers—Harnessing Inter- and Intramolecular Interactions to Create Mechanochromic Materials. *Macromol. Rapid Commun.* **2021**, *42*, 2000573.

(5) Davis, D. A.; Hamilton, A.; Yang, J.; Cremar, L. D.; Van Gough, D.; Potisek, S. L.; Ong, M. T.; Braun, P. V.; Martínez, T. J.; White, S. R.; Moore, J. S.; Sottos, N. R. Force-Induced Activation of Covalent Bonds in Mechanoresponsive Polymeric Materials. *Nature* **2009**, *459*, 68–72.

(6) Chen, Y.; Zhang, H.; Fang, X.; Lin, Y.; Xu, Y.; Weng, W. Mechanical Activation of Mechanophore Enhanced by Strong Hydrogen Bonding Interactions. *ACS Macro Lett.* **2014**, *3*, 141–145.

(7) Kim, T. A.; Robb, M. J.; Moore, J. S.; White, S. R.; Sottos, N. R. Mechanical Reactivity of Two Different Spiropyran Mechanophores in Polydimethylsiloxane. *Macromolecules* **2018**, *51*, 9177–9183.

(8) Lin, Y.; Barbee, M. H.; Chang, C.-C.; Craig, S. L. Regiochemical Effects on Mechanophore Activation in Bulk Materials. *J. Am. Chem. Soc.* **2018**, *140*, 15969–15975.

(9) Robb, M. J.; Kim, T. A.; Halmes, A. J.; White, S. R.; Sottos, N. R.; Moore, J. S. Regioisomer-Specific Mechanochromism of Naphthopyran in Polymeric Materials. *J. Am. Chem. Soc.* **2016**, *138*, 12328–12331.

(10) McFadden, M. E.; Robb, M. J. Force-Dependent Multicolor Mechanochromism from a Single Mechanophore. *J. Am. Chem. Soc.* **2019**, *141*, 11388–11392.

(11) Versaw, B. A.; McFadden, M. E.; Husic, C. C.; Robb, M. J. Designing Naphthopyran Mechanophores with Tunable Mechanochromic Behavior. *Chem. Sci.* **2020**, *11*, 4525–4530.

(12) Chen, Y.; Spiering, A. J. H.; Karthikeyan, S.; Peters, G. W. M.; Meijer, E. W.; Sijbesma, R. P. Mechanically Induced Chemiluminescence from Polymers Incorporating a 1,2-Dioxetane Unit in the Main Chain. *Nat. Chem.* **2012**, *4*, 559–562.

(13) Ducrot, E.; Chen, Y.; Bulters, M.; Sijbesma, R. P.; Creton, C. Toughening Elastomers with Sacrificial Bonds and Watching Them Break. *Science* **2014**, *344*, 186–189.

(14) Göstl, R.; Sijbesma, R. P. π-Extended Anthracenes as Sensitive Probes for Mechanical Stress. *Chem. Sci.* **2016**, *7*, 370–375.
(15) Sulkanen, A. R.; Sung, J.; Robb, M. J.; Moore, J. S.; Sottos, N. R.; Liu, G.-Y. Spatially Selective and Density-Controlled Activation of Interfacial Mechanophores. *J. Am. Chem. Soc.* **2019**, *141*, 4080–4085.
(16) Imato, K.; Kanehara, T.; Ohishi, T.; Nishihara, M.; Yajima, H.; Ito, M.; Takahara, A.; Otsuka, H. Mechanochromic Dynamic Covalent Elastomers: Quantitative Stress Evaluation and Autonomous Recovery. *ACS Macro Lett.* **2015**, *4*, 1307–1311.
(17) Sumi, T.; Goseki, R.; Otsuka, H. Tetraarylsuccinonitriles as Mechanochromophores to Generate Highly Stable Luminescent Carbon-centered Radicals. *Chem. Commun.* **2017**, *53*, 11885–11888.
(18) Kato, S.; Furukawa, S.; Aoki, D.; Goseki, R.; Oikawa, K.; Tsuchiya, K.; Shimada, N.; Maruyama, A.; Numata, K.; Otsuka, H. Crystallization-Induced Mechanofluorescence for Visualization of Polymer Crystallization. *Nat. Commun.* **2021**, *12*, 126.
(19) Karman, M.; Verde-Sesto, E.; Weder, C. Mechanochemical Activation of Polymer-Embedded Photoluminescent Benzoxazole Moieties. *ACS Macro Lett.* **2018**, *7*, 1028–1033.
(20) Song, Y.-K.; Lee, K.-H.; Hong, W.-S.; Cho, S.-Y.; Yu, H.-C.; Chung, C.-M. Fluorescence Sensing of Microcracks Based on Cycloreversion of a Dimeric Anthracene Moiety. *J. Mater. Chem* **2012**, *22*, 1380–1386.
(21) Kean, Z. S.; Gossweiler, G. R.; Kouznetsova, T. B.; Hewage, G. B.; Craig, S. L. A Coumarin Dimer Probe of Mechanochemical Scission Efficiency in the Sonochemical Activation of Chain-centered Mechanophore Polymers. *Chem. Commun.* **2015**, *51*, 9157–9160.
(22) Wang, Z.; Ma, Z.: Wang, Y.; Xu, Z.; Luo, Y.; Wei, Y.; Jia, X. A Novel Mechanochromic and Photochromic Polymer Film: When Rhodamine Joins Polyurethane. *Adv. Mater.* **2015**, *27*, 6469–6474.
(23) Wang, T.; Zhang, N.; Dai, J.; Li, Z.; Bai, W.; Bai, R. Novel Reversible Mechanochromic Elastomer with High Sensitivity: Bond Scission and Bending-Induced Multicolor Switching. *ACS Appl. Mater. Interfaces* **2017**, *9*, 11874–11881.
(24) Karman, M.; Verde-Sesto, E.; Weder, C.; Simon, Y. C. Mechanochemical Fluorescence Switching in Polymers Containing Dithiomaleimide Moieties. *ACS Macro Lett.* **2018**, *7*, 1099–1104.
(25) Qian, H.; Purwanto, N. S.; Ivanoff, D. G.; Halmes, A. J.; Sottos, N. R.; Moore, J. S. Fast, Reversible Mechanochromism of Regioisomeric Oxazine Mechanophore:

Developing in situ Responsive Force Probes for Polymeric Materials. *Chem* **2021**, *7*, 1–12.
(26) Klukovich, H. M.; Kouznetsova, T. B.; Kean, Z. S.; Lenhardt, J. M.; Craig, S. L. A Backbone Lever-Arm Effect Enhances Polymer Mechanochemistry. *Nat. Chem.* **2013**, *5*, 110–114.
(27) Gossweiler, G. R.; Kouznetsova, T. B.; Craig, S. L. Force-Rate Characterization of Two Spiropyran-Based Molecular Force Probes. *J. Am. Chem. Soc.* **2015**, *137*, 6148–6151.
(28) Wang, J.; Kouznetsova, T. B.; Niu, Z.; Ong, M. T.; Klukovich, H. M.; Rheingold, A. L.; Martinez, T. J.; Craig, S. L. Inducing and Quantifying Forbidden Reactivity with Single-Molecule Polymer Mechanochemistry. *Nat. Chem.* **2015**, *7*, 323–327.
(29) Barbee, M. H.; Kouznetsova, T.; Barrett, S. L.; Gossweiler, G. R.; Lin, Y.; Rastogi, S. K.; Brittain, W. J.; Craig, S. L. Substituent Effects and Mechanism in a Mechanochemical Reaction. *J. Am. Chem. Soc.* **2018**, *140*, 12746–12750.
(30) Martínez-Tong, D. E.; Pomposo, J. A.; Verde-Sesto, E. Triggering Forces at the Nanoscale: Technologies for Single-Chain Mechanical Activation and Manipulation. *Macromol. Rapid Commun.* **2021**, *42*, 2000654.
(31) Ogi, S.; Sugiyasu, K.; Takeuchi, M. Synthesis of a Doubly Strapped Light-Harvesting Porphyrin Bearing Energy Donor Molecules Hanging on to the Straps: An Attempt toward Macroscopic Control over Molecular Conformation that Affects the Efficiency of Fluorescence Resonance Energy Transfer. *Bull. Chem. Soc. Jpn.* **2011**, *84*, 40–48.
(32) Balkenende, D. W. R.; Coulibaly, S.; Balog, S.; Simon, Y. C.; Fiore, G. L.; Weder, C. Mechanochemistry with Metallosupramolecular Polymers. *J. Am. Chem. Soc.* **2014**, *136*, 10493–10498.
(33) Calvino, C.; Neumann, L.; Weder, C.; Schrettl, S. Approaches to Polymeric Mechanochromic Materials. J. *Polym. Sci., Part A: Polym. Chem.* **2017**, *55*, 640–652.
(34) Filonenko, G. A.; Khusnutdinova, J. R. Dynamic Phosphorescent Probe for Facile and Reversible Stress Sensing. *Adv. Mater.* **2017**, *29*, 1700563.
(35) Früh, A. E.; Artoni, F.; Brighenti, R.; Dalcanale, E. Strain Field Self-Diagnostic Poly(dimethylsiloxane) Elastomers. *Chem. Mater.* **2017**, *29*, 7450–7457.
(36) Filonenko, G. A.; Lugger, J. A. M.; Liu, C.; van Heeswijk, E. P. A.; Hendrix, M. M. R. M.; Weber, M.; Müeller, C.; Hensen, E. J. M.; Sijbesma, R. P.; Pidko, E. A. Tracking Local Mechanical Impact in Heterogeneous Polymers with Direct Optical Imaging. *Angew. Chem. Int. Ed.* **2018**, *57*, 16385–16390.

(37) Sagara, Y.; Karman, M.; Verde-Sesto, E.; Matsuo, K.; Kim, Y.; Tamaoki, N.; Weder, C. Rotaxanes as Mechanochromic Fluorescent Force Transducers in Polymers. *J. Am. Chem. Soc.* **2018**, *140*, 1584–1587.
(38) Sagara, Y.; Karman, M.; Seki, A.; Pannipara, M.; Tamaoki, N.; Weder, C. Rotaxane-Based Mechanophores Enable Polymers with Mechanically Switchable White Photoluminescence. *ACS Cent. Sci.* **2019**, *5*, 874–881.
(39) Muramatsu, T.; Sagara, Y.; Traeger, H.; Tamaoki, N.; Weder, C. Mechanoresponsive Behavior of a Polymer-Embedded Red-Light Emitting Rotaxane Mechanophore. *ACS Appl. Mater. Interfaces* **2019**, *11*, 24571–24576.
(40) Imato, K.; Yamanaka, R.; Nakajima, H.; Takeda, N. Fluorescent Supramolecular Mechanophores Based on Charge-Transfer Interactions. *Chem. Commun.* **2020**, *56*, 7937–7940.
(41) Kotani, R.; Yokoyama, S.; Nobusue, S.; Yamaguchi, S.; Osuka, A.; Yabu, H.; Saito, S. Bridging pico-to-nanoNewton: Ratiometric Force Probe for Nanoscale Polymer Physics Before Damage. *Nat Commun* **2022**, *13*, 303.
(42) Sagara, Y.; Traeger, H.; Li, J.; Okado, Y.; Schrettl, S.; Tamaoki, N.; Weder, C. Mechanically Responsive Luminescent Polymers Based on Supramolecular Cyclophane Mechanophores. *J. Am. Chem. Soc.* **2021**, *143*, 5519–5525.
(43) Lussis, P.; Svaldo-Lanero, T.; Bertocco, A.; Fustin, C.-A.; Leigh, D. A.; Duwez, A.-S. A Single Synthetic Small Molecule that Generates Force Against a Load. *Nat. Nanotech.* **2011**, *6*, 553–557.
(44) Zhang, M.; De Bo, G. Impact of a Mechanical Bond on the Activation of a Mechanophore. *J. Am. Chem. Soc.* **2018**, *140*, 12724–12727.
(45) Sluysmans, D.; Zhang, L.; Li, X.; Garci, A.; Stoddart, J. F.; Duwez, A. S. Viologen Tweezers to Probe the Force of Individual Donor-Acceptor π-Interactions. *J. Am. Chem. Soc.* **2020**, *142*, 21153–21159.
(46) Zhang, M.; De Bo, G. Mechanical Susceptibility of a Rotaxane. *J. Am. Chem. Soc.* **2019**, *141*, 15879–15883.
(47) Chatterjee, M. N.; Kay, E. R.; Leigh, D. A. Beyond Switches: Ratcheting a Particle Energetically Uphill with a Compartmentalized Molecular Machine. *J. Am. Chem. Soc.* **2006**, *128*, 4058–4073.
(48) Brough, B.; Northrop, B. H.; Schmidt, J. J.; Tseng, H.-R.; Houk, K. N.; Stoddart, J. F.; Ho, C.-M. Evaluation of Synthetic Linear Motor-Molecule Actuation Energetics. *Proc. Natl. Acad. Sci. U. S. A.* **2006**, *103*, 8583–8588.

(49) Dunlop, A.; Wattoom, J.; Hasan, E. A.; Cosgrove, T.; Round, A. N. Mapping the Positions of Beads on a String: Dethreading Rotaxanes by Molecular Force Spectroscopy. *Nanotechnology* **2008**, *19*, 345706.
(50) Baroncini, M.; Silvi, S.; Venturi, M.; Credi, A. Photoactivated Directionally Controlled Transit of a Non-Symmetric Molecular Axle Through a Macrocycle. *Angew. Chem. Int. Ed.* **2012**, *51*, 4223–4226.
(51) Cheng, C.; McGonigal, P. R.; Schneebeli, S. T.; Li, H.; Vermeulen, N. A.; Ke, C.; Stoddart, J. F. An Artificial Molecular Pump. *Nat. Nanotech.* **2015**, *10*, 547–553.
(52) Martinez-Cuezva, A.; Rodrigues, L. V.; Navarro, C.; Carro-Guillen, F.; Buriol, L.; Frizzo, C. P.; Martins, M. A. P.; Alajarin, M.; Berna, J. Dethreading of Tetraalkylsuccinamide-Based [2] Rotaxanes for Preparing Benzylic Amide Macrocycles. *J. Org. Chem.* **2015**, *80*, 10049–10059.
(53) Pezzato, C.; Cheng, C.; Stoddart, J. F.; Astumian, R. D. Mastering the Non-Equilibrium Assembly and Operation of Molecular Machines. *Chem. Soc. Rev.* **2017**, *46*, 5491–5507.
(54) De Bo, G. Mechanochemistry of the Mechanical Bond. *Chem. Sci.* **2018**, *9*, 15–21.
(55) Pezzato, C.; Nguyen, M. T.; Kim, D. J.; Anamimoghadam, O.; Mosca, L.; Stoddart, J. F. Controlling Dual Molecular Pumps Electrochemically. *Angew. Chem. Int. Ed.* **2018**, *57*, 9325–9329.
(56) Balan, B.; Gopidas, K. R. An Anthracene-Appended β-Cyclodextrin-Based Dyad: Study of Self-Assembly and Photoinduced Electron-Transfer Processes. *Chem. Eur. J.* **2007**, *13*, 5173–5185.
(57) Levitus, M.; Garcia-Garibay, M. A. Polarized Electronic Spectroscopy and Photophysical Properties of 9,10-Bis(phenylethynyl)anthracene. *J. Phys. Chem. A* **2000**, *104*, 8632–8637.
(58) Demeter, A. First Steps in Photophysics. I. Fluorescence Yield and Radiative Rate Coefficient of 9,10-Bis(phenylethynyl)anthracene in Paraffins. *J. Phys. Chem. A* **2014**, *118*, 9985–9993.
(59) Sagara, Y.; Weder, C.; Tamaoki, N. Tuning the Thermo- and Mechanoresponsive Behavior of Luminescent Cyclophanes. *RSC Adv.* **2016**, *6*, 80408–80414.
(60) Lübtow, M.; Helmers, I.; Stepanenko, V.; Albuquerque, R. Q.; Marder, T. B.; Fernández, G. Self-Assembly of 9,10-Bis(phenylethynyl) Anthracene (BPEA) Derivatives: Influence of π-π and Hydrogen-Bonding Interactions on Aggregate Morphology and Self-Assembly Mechanism. *Chem. Eur. J.* **2017**, *23*, 6198–6205.

(61) Rostovtsev, V. V.; Green, L. G.; Fokin, V. V.; Sharpless, K. B. A Stepwise Huisgen Cycloaddition Process: Copper(I)-Catalyzed Regioselective "Ligation" of Azides and Terminal Alkynes. *Angew. Chem. Int. Ed.* **2002**, *41*, 2596–2599.
(62) Crenshaw, B. R.; Weder, C. Self-Assessing Photoluminescent Polyurethanes. *Macromolecules* **2006**, *39*, 9581–9589.
(63) Ayer, M. A.; Simon, Y. C.; Weder, C. Azo-Containing Polymers with Degradation On-Demand Feature. *Macromolecules* **2016**, *49*, 2917–2927.
(64) Petrović, Z. S; Ferguson, J. Polyurethane Elastomers. *Prog. Polym. Sci.* **1991**, *16*, 695–836.
(65) Schaefer, M.; Icli, B.; Weder, C.; Lattuada, M.; Kilbinger, A. F. M.; Simon, Y. C. *Macromolecules* **2016**, *49*, 1630–1636.
(66) May, P. A.; Munaretto, N. F.; Hamoy, M. B.; Robb, M. J.; Moore, J. S. Is Molecular Weight or Degree of Polymerization a Better Descriptor of Ultrasound-Induced Mechanochemical Transduction *ACS Macro Lett.* **2016**, *5*, 177–180.
(67) Berkowski, K. L.; Potisek, S. L.; Hickenboth, C. R.; Moore, J. S. Ultrasound-Induced Site-Specific Cleavage of Azo-Functionalized Poly(ethylene glycol). *Macromolecules* **2005**, *38*, 8975–8978.
(68) Han, Y.; Guo, J.-B.; Cao, J.; Chen, C.-F. *Tetrahedron* **2013**, *69*, 4541.
(69) Yelamaggad, C. V.; Shanker, G. *Tetrahedron* **2008**, *64*, 3760.
(70) Gibson, H. W.; Lee, S. H.; Engen, P. T.; Lecavalier, P.; Sze, J.; Shen, Y. X.; Bheda, M. *J. Org. Chem.* **1993**, *58*, 3748.
(71) Zhu, S.; Zhang, J.; Vegesna, G.; Luo, F.-T.; Green, S. A.; Liu, H. *Org. Lett.* **2011**, *13*, 438.

Chapter 4

Force-induced Shuttling of Rotaxanes Controls Fluorescence Resonance Energy Transfer in Polymer Hydrogels

This chapter is reprinted with permission from ACS Appl. Mater. Interfaces **2023**, *15*, 8502–8509.

Abstract

Here, I synthesized rotaxane-based mechanophores in which the fluorescence resonance energy transfer (FRET) between a donor-acceptor pair is mechanically controlled. A cyclic molecule containing a green-light emitting FRET donor connected to a red-light emitting FRET acceptor was threaded onto an axle equipped with a quencher at its center and two stoppers in the peripheral positions. In the force-free state, the green emitter is located near the quencher so that charge transfer interactions or photo-induced electron transfer between the two moieties suppress green emission and prevent the FRET from the green to the red emitter. The mechanophore was covalently incorporated into a linear polyurethane-urea (PUU) and stretchable hydrogels were prepared by swelling this polymer with water. Upon deformation of the PUU hydrogels and under an excitation light which selectively excites the donor, the intensity of the red fluorescence increases, as a result of a force-induced separation of the green emitter from the quencher, which enables the FRET. The switching contrast is much more pronounced in the gels than in dry films, which is due to increased molecular mobility and hydrophobic effects in the hydrogel, which both promote the formation of inclusion complexes between the ring containing the green emitter and the quencher.

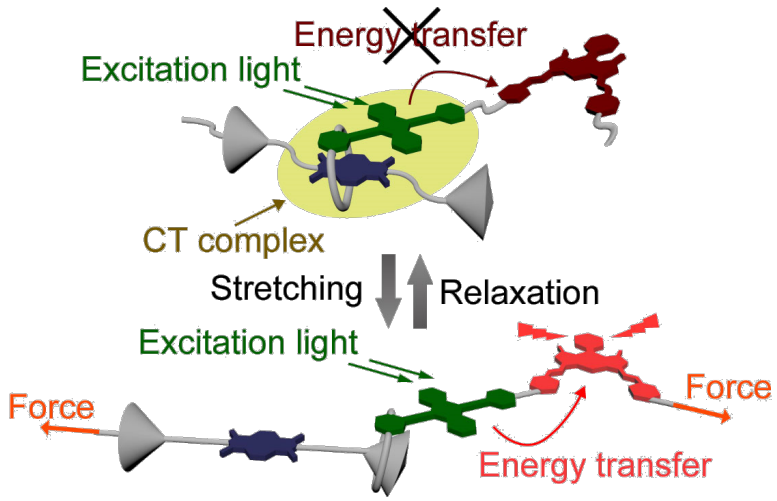

4.1. Introduction

Mechanochromic responses that are achieved by translating mechanical forces applied to polymeric objects into optical signals allow studying failure and stress-transfer mechanisms and are useful for applications such as pressure sensing, defect monitoring, electronic skins, data encryption, anti-counterfeiting features, or tamper-proof packaging materials.[1] The incorporation of so-called mechanophores – mechanoresponsive motifs – into these materials is one widely employed design approach to achieve such behavior.[2–6] The usefulness of the rotaxane structure[7–11] for the design of mechanochromic mechanophores was first recognized by Stoddart and co-workers, who reported that an intramolecular charge-transfer complex (CT) was irreversibly dissociated when a tetrahydrofuran solution of a rotaxane-containing poly(methyl acrylate) was sonicated, leading to the disappearance of the CT absorption.[12] I showed more recently that the force-induced shuttling function of rotaxanes can be utilized to prepare mechanophores that show instantly reversible changes in photoluminescence intensity.[13–16] The rotaxane-based supramolecular mechanophores Sagara group reported are composed of a cyclic molecule equipped with a fluorophore and an axle molecule containing an electronically matched quencher. When no force is applied, the cycle resides near the quencher and the fluorescence is quenched due to intramolecular CT interactions or photo-induced electron transfer (PeT). The two optically active moieties can be pulled apart by applying a force via two handles attached to the axle and the cycle, respectively, and this is accompanied by a turn-on of the fluorescence. Unless the rotaxane's stoppers are designed to allow for mechanically induced de-threading,[16] the process is fully reversible. Thus, rubbery polyurethane elastomers into which the rotaxanes were covalently incorporated display instantly reversible changes of the fluorescence intensity upon being deformed. De Bo and co-workers also reported several rotaxane mechanophores,[17,18] including a mechanochromic motif in which cycle and axle molecules interact through hydrogen bonds.[19] The motif was designed to display green fluorescence in the absence of force,

due to hydrogen bonding between a fluorophore in the cycle and an aminochloromaleimide (ACM) moiety in the axle molecule. The mechanically induced separation of the cycle and the ACM leads to a significant decrease in the fluorescence intensity.

Collectively, the above results suggest that mechanochromic responses should also be attainable in rotaxanes featuring other photofunctional groups, whose assembly and separation promote different photophysical effects. Indeed, here I report a rotaxane-based mechanophore in which a fluorescence resonance energy transfer (FRET) is mechanically switched. FRET effects have been widely used to develop photofunctional materials, including supramolecular polymers,[20–22] organogels,[23,24] fluorescent proteins,[25] and fluorescent probes.[26] Since the FRET efficiency depends on the distance between donor and acceptor fluorophores and the directions of their transition dipole moments, and because these factors can be controlled by applying mechanical forces, adequately coupled FRET pairs can display mechanochromic behavior.[27–30] Besides, combination of mechanophore and FRET has been reported to obtain mechanochromic polymer.[31,32] For our rotaxane mechanophores, bulky fluorophores are not suitable for the emitters directly incorporated into cycle structure because the association constant between the quencher and cycle becomes low, resulting in poor contrast upon stretching the films in which the mechanophores are covalently introduced. Indeed, I previously reported a red-light emitting supramolecular rotaxane mechanophore with a bulky red fluorophore in the cyclic structure, and the polyurethane film containing the mechanophore exhibited a less pronounced fluorescence contrast.[15] Introduction of FRET mechanism would make it possible for such non-planar fluorophores to be involved in rotaxane mechanophores as FRET acceptors without reducing the emission contrast upon stretching because the bulky acceptors don't need to form π-stacked structure.

Although external stimuli such as pH changes,[33,34] light irradiation,[35] and changes of solvent polarity[36] have been used to modulate the efficiency of FRET pairs in rotaxanes,

mechanical control over this process has, to our best knowledge, not been demonstrated. The rotaxane mechanophore reported here features a green-light emitting fluorophore in the cyclic molecule and this donor is connected via a short spacer to a red acceptor fluorophore (Figure 4-1). The cycle is threaded onto an axle equipped with a quencher at its center and two stoppers in the peripheral positions. In the force-free state, the emitter is located near the quencher, so that the CT interactions or PeT between the two moieties suppress green emission and prevent FRET from the green to red emitter. The mechanophore was covalently incorporated into a linear polyurethane-urea (PUU) and stretchable hydrogels were prepared by swelling with water.[37,38] Upon deformation of the PUU hydrogels, the intensity of the red fluorescence increases, as a result of the force-induced separation of the emitter from the quencher, which enables the FRET process. Importantly, the ability to tune the emission color of rotaxane-mechanophores by simply modifying an existing motif with a FRET acceptor allows one to tune the emission color, which, as I demonstrate, is critical for applications in colored materials.

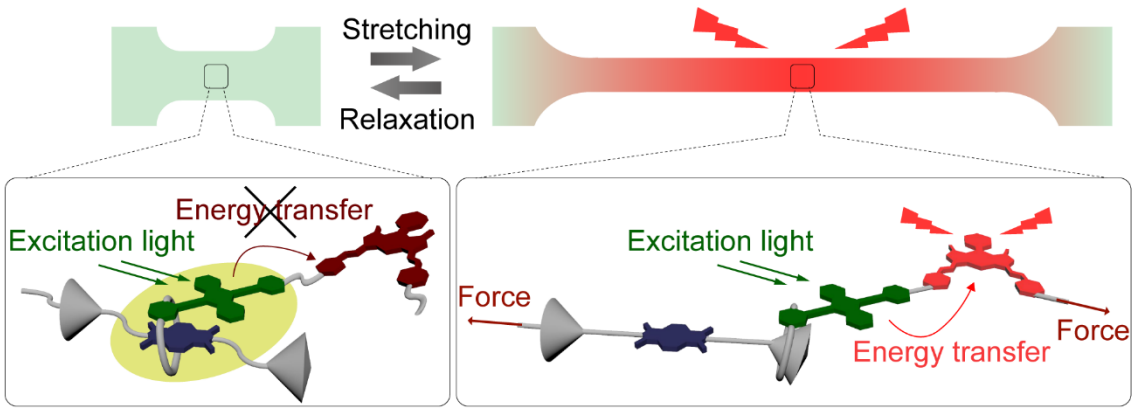

Figure 4-1. Schematic illustration of FRET control by forces on the rotaxane-based supramolecular mechanophore in stretchable hydrogels. In the force-free state (left), the green emission is quenched because of CT complex formation or PeT.

4.2. Results and Discussion

4.2.1. Molecular Designs

9,10-Bis(phenylethynyl)anthracene was selected as the green fluorophore because of its high fluorescence quantum yield and electron-donating propensity,[14,39–42] which is pivotal for CT interactions between this fluorophore and 1,4,5,8-naphthalenetetracarboxylic diimide (NpI),[43–45] which was selected as the quencher and electron-deficient. A π-extended 4,4-difluoro-4-bora-3a,4a-diaza-*s*-indacene (BODIPY) dye, which also displays a high fluorescence quantum efficiency,[46–48] was chosen as the red fluorophore. The rotaxane **RotAnBP** (Figure 4-2, left bottom) was designed based on our previously reported rotaxane mechanophores.[13–15] The cyclic molecule **AnBP** (Figure 4-2, left top) contains the green emitter and a naphthalene group, which are connected via two tetraethylene glycol chains. The red fluorophore is attached to the green fluorophore through a propyl linker so that efficient energy transfer is possible. The axle features an NpI at its center and two tetraphenylmethane units[49–51] as stoppers at both ends. **RotAnBP** was prepared through a 1,3-dipolar cycloaddition click-type reaction[52] between alkyne and azide groups of two precursors of the axle molecule in the presence of a high concentration of **AnBP**. The rotaxane mechanophore was characterized by ^{1}H NMR and ^{13}C NMR spectroscopy and high-resolution electrospray ionization mass spectroscopy. A comparison of the ^{1}H NMR spectra of cycle **AnBP** and rotaxane **RotAnBP** shows that diagnostic signals associated with aromatic protons of the cyclic structure and the 9,10-bis(phenylethynyl)anthracene residue are shifted up-field (Figure 4-3), indicating the formation of an inclusion complex between the cycle and NpI. By contrast, signals ascribed to protons of the π-extended BODIPY hardly change. The rotaxane formation is also evidenced by a decrease in the red fluorescence intensity after rotaxane formation, due to the suppression of FRET (see below). The anthracene derivative **An** (Figure 4-2, right top) and BODIPY derivative **BP** (Figure 4-2, right bottom) were also prepared as the reference compounds.

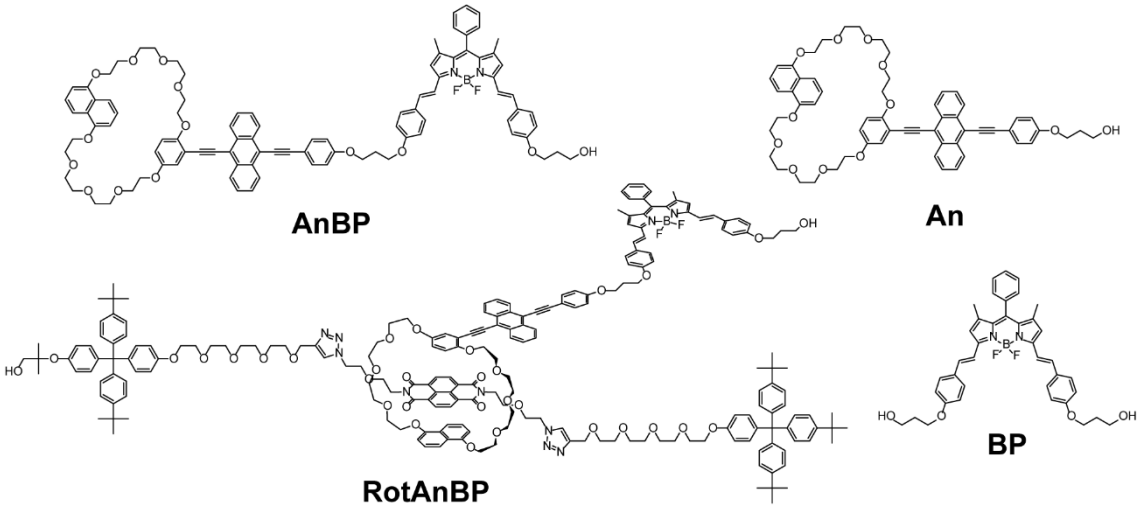

Figure 4-2. Molecular structures of cyclic compound **AnBP**, rotaxane-based supramolecular mechanophore **RotAnBP**, and reference compounds containing the green (**An**) or red (**BP**) emitter.

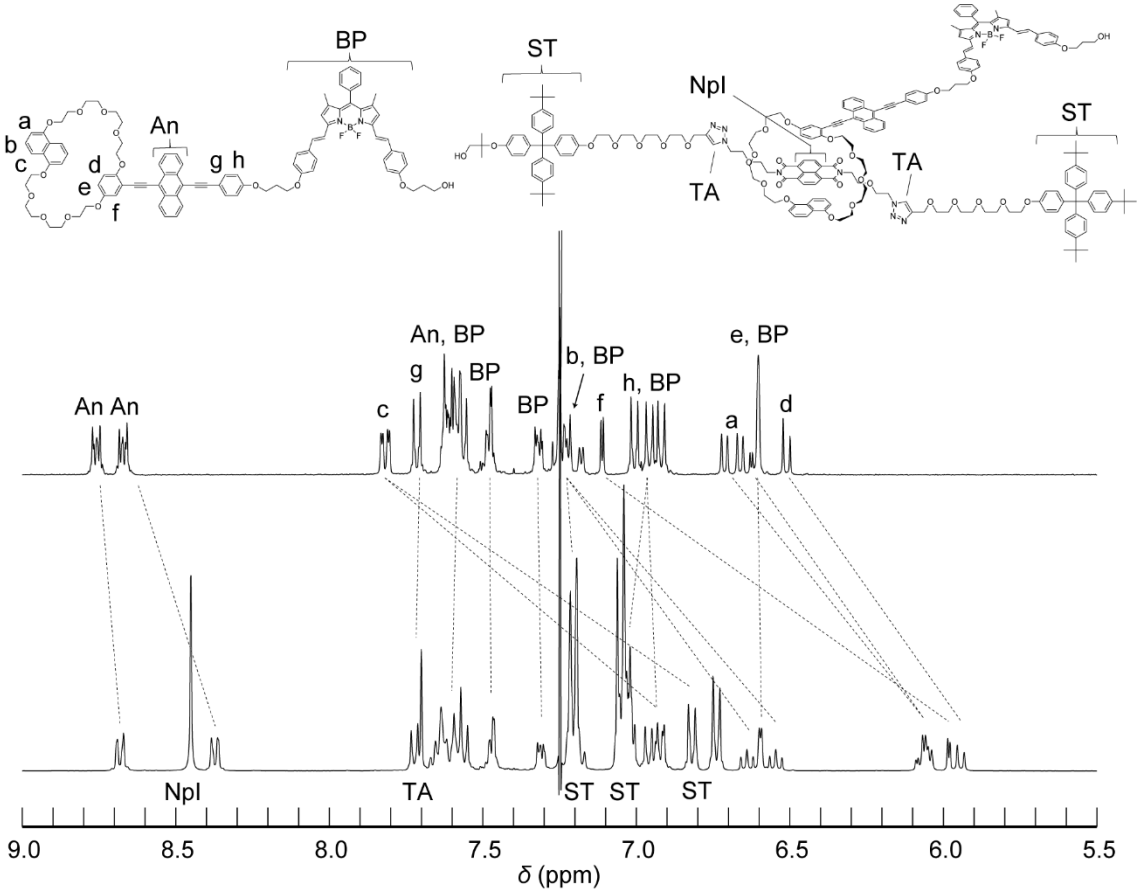

Figure 4-3. Partial ^{1}H NMR spectra of **AnBP** (top) and **RotAnBP** (bottom). The spectra were measured in $CDCl_3$ at r.t.

4.2.2. Fundamental Photophysical Properties of An, BP, AnBP, and RotAnBP in Solutions

The optical characteristics of **An**, **BP**, **AnBP**, and **RotAnBP** were first measured in THF/methanol (1:4, v/v) solutions ($c = 1 \times 10^{-5}$ M). The absorption spectrum of **An** shows a band with maxima at 450 and 476 nm (Figure 4-4a, green line). **BP** has one absorption band in the UV region with a maximum at 369 nm and a second band with well-resolved

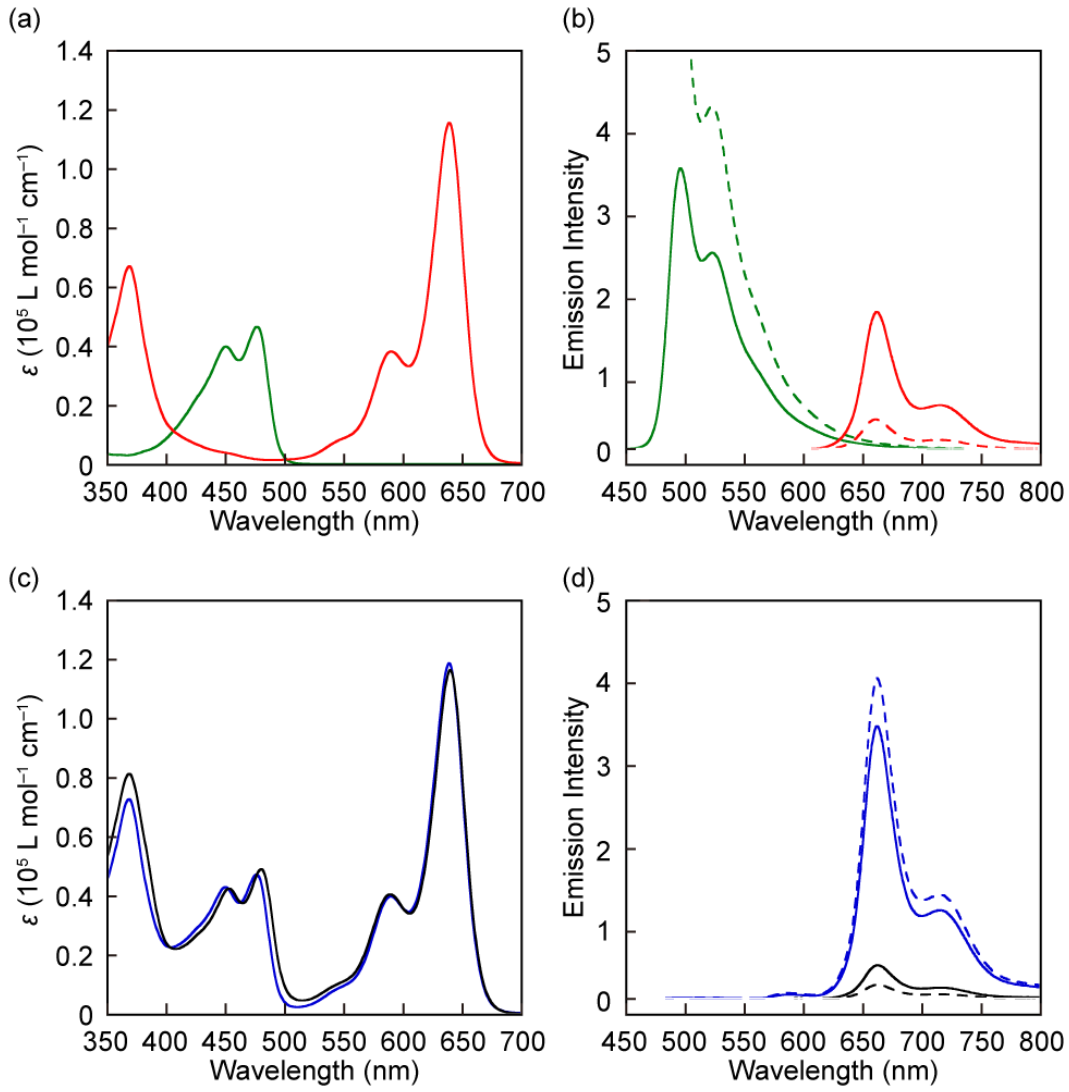

Figure 4-4. Absorption (a, c) and photoluminescence spectra (b, d) of **An** (green), **BP** (red), **AnBP** (blue), and **RotAnBP** (black) in THF/methanol (1:4, v/v) solutions ($c = 1 \times 10^{-5}$ M). The photoluminescence spectra were recorded with excitation at 410 nm (solid lines) or 490 nm (dashed lines) at r.t.

structures and maxima at 590 and 639 nm (Figure 4-4a, red line). The data show that it is possible to preferentially excite **An** at 490 nm, whereas **BP** can be selectively excited above 500 nm. Under excitation at 410 nm, where the two motifs show a similar extinction (Figure 4-4a), **An** and **BP** solutions exhibit strong green and red fluorescence, respectively. Both fluorescence spectra show well-resolved peaks with maxima at 495 and 522 nm (**An**, quantum efficiency Φ = 0.84) and 661 and 715 nm (**BP**, Φ = 0.54), respectively (Figure 4-4b, green and red solid lines). When excited at 490 nm, **BP** shows a much weaker fluorescence than **An** (Figure 4-4b, green and red dashed lines) because of the lower absorption. By contrast, **An** doesn't show any fluorescence and **BP** displays strong red fluorescence upon excitation at 590 nm (Figure 4-5a, green and red lines).

The absorption spectrum of **AnBP** shows a superposition of the absorbances of **An** and **BP** (Figure 4-4c, blue line). However, its fluorescence spectrum displays only the red fluorescence band associated with the BODYPY residue, for both, excitation at 410 and 490 nm (Figure 4-4d, blue solid and dashed lines), indicating efficient energy transfer from the 9,10-bis(phenylethynyl)anthracene donor to the π-extended BODIPY acceptor.

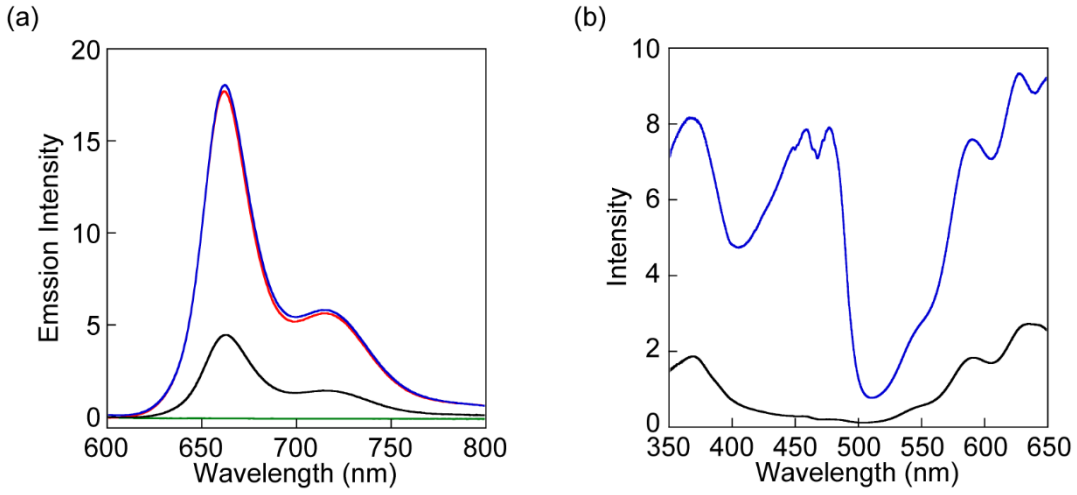

Figure 4-5. (a) Fluorescence spectra of **An** (green), **BP** (red), **AnBP** (blue), and **RotAnBP** (black) in THF/methanol (1:4, v/v) solutions (c = 1 × 10^{-5} M) with excitation at 590 nm at r.t. (b) Excitation spectra of **AnBP** (blue) and **RotAnBP** (black) in THF/methanol (1:4, v/v) solutions (c = 1 × 10^{-5} M) recorded at an emission wavelength of 660 nm at r.t.

The energy transfer efficiency exceeds 99%, as determined by comparing the intensities of the green fluorescence of solutions of **An** and **AnBP**. The spectral overlap integral of the donor fluorescence and the acceptor absorption and the Förster distance were calculated to be 5.58×10^{15} M^{-1} cm^{-1} nm^4 and 67.1 Å, respectively (see Experimental Section for details). Based on these values, the energy transfer efficiency is greater than 99% when the distance between the donor and acceptor is within 31.2 Å, supporting that efficient energy transfer occurs in **AnBP**. In a comparison of the red fluorescence intensities of **BP** and **AnBP**, the proportions of the red fluorescence attributed to the direct excitation of the red emitter in **AnBP** are calculated to be ca. 50% and 9% under the excitation lights of 410 and 490 nm, respectively. The FRET process is further supported by the fact that the excitation spectrum of **AnBP** recorded at an emission wavelength of 660 nm (Figure 4-5b, blue line) shows a broad band between 400 and 500 nm that corresponds to the absorption band of **AnBP** in the same wavelength region. The overall emission quantum yield Φ_{total} of **AnBP** is 0.54 for excitation at 410 nm, with a yield of below 0.01 for the green emitter (Φ_{An}) and 0.54 for the red emitter (Φ_{BP}). Moreover, the quantum yield of **AnBP** is hardly affected by the excitation wavelength (Φ_{total} = 0.54, excitation at 490 nm). These results also indicated highly efficient FRET.

The rotaxane **RotAnBP** displays a slightly red-shifted absorption band of the green emitter, due to the CT interaction between the 9,10-bis(phenylethynyl)anthracene and NpI (Figure 4-4c, black line).[14] By contrast, the absorption band of the π-extended BODIPY group hardly changes, suggesting that ground-state electronic interactions between the BODIPY moiety and other π-conjugated portions of the rotaxane are absent in solution. As expected, **RotAnBP** exhibits no green fluorescence and only faint red fluorescence in solution when excited at 490 nm (Φ = 0.01, Figure 4-4d, black dashed line). The excitation spectrum of **RotAnBP** (Figure 4-5b, black line) reveals that the FRET contribution to the red emission is negligible and the faint red emission is caused by direct excitation of the π-extended BODIPY dye, although the absorption of the red emitter at 490 nm is weak.

These results reflect that the energy transfer from the green-light emitting donor to the red-light emitting acceptor is suppressed, due to the CT interaction or PeT between the donor and the quencher. It is noteworthy that even upon excitation at 410 (Figure 4-4d, black solid line) and 590 (Figure 4-5a, black line) nm, the fluorescence intensity of **RotAnBP** is still weaker than that of **BP** and **AnBP** although the BODIPY residue is directly and exclusively excited. The emission quantum yield of the red fluorescence originating from **RotAnBP** is 0.14 when excited at 590 nm, which is much smaller than that of **BP** (Φ = 0.54). Besides, the emission decay of **RotAnBP** monitored at 660 nm in THF/methanol is accelerated relative to that of **BP** and **AnBP** (Figure 4-6). These results suggest that the BODIPY residue in the rotaxane in the excited state interacts with other π-conjugated groups, leading to dynamic quenching in solution, presumably due to PeT. In contrast to **AnBP**, the quantum yield of **RotAnBP** depends on the excitation wavelength (Φ_{BP} = 0.06, excitation at 410 nm), which supports our conclusion that the FRET is suppressed and red fluorescence is observed only when the BODIPY derivative is directly excited.

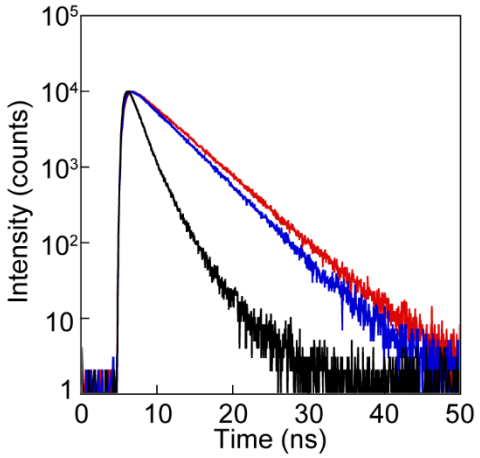

Figure 4-6. Emission decay profiles of **BP** (red), **AnBP** (blue), and **RotAnBP** (black) in THF/methanol (1:4, v/v) solutions (c = 1 × 10^{-5} M). The decay profiles were monitored at 660 nm with excitation at 470 nm.

4.2.3. Incorporation of RotAnBP into Polyurethane-urea

Recently, linear PUUs carrying carboxyl groups on the main chain were reported to form hydrogels after swelling with water.[37,38] The hydrophobic urea segments aggregate to form strong physical cross-links, which bestow the PUU hydrogels with high extensibility and toughness. Speculating that hydrophobic interactions would increase the association constant between the cycle and the quencher, I elected to investigate the mechanoresponsive behavior of **RotAnBP** in hydrogels by integrating the new mechanophore into a hydrophilic PUU. This was achieved by the polyaddition reaction between poly(ethylene glycol) (PEG) (M_n = ca. 2000 g/mol), isophorone diisocyanate, isophorone diamine, and 2,2-bis(hydroxymethyl)propionic acid in the presence of 0.004 mol% of **RotAnBP**. The reaction was modified from the reported procedures[37,38] because **RotAnBP** was unstable when heated (see Experimental Section for details). The resulting polymer **RotAnBP-PUU** is soluble in polar organic solvents, such as MeOH, DMF, and DMSO and displays a number-average molecular weight of M_n = 48 kg/mol. The successful incorporation of **RotAnBP** into the polymer was confirmed by the absorption spectrum of **RotAnBP-PUU** in methanol, which shows the diagnostic signals of the chromophores (Figure 4-7, left). However, no peaks corresponding to **RotAnBP** can be observed in the ^{1}H NMR spectrum of the polymer, on account of its low concentration (Figure 4-8). The photoluminescence spectrum of a methanol solution of **RotAnBP-PUU** (Figure 4-7, right) shows that the FRET process remains suppressed after incorporation into the polymer.

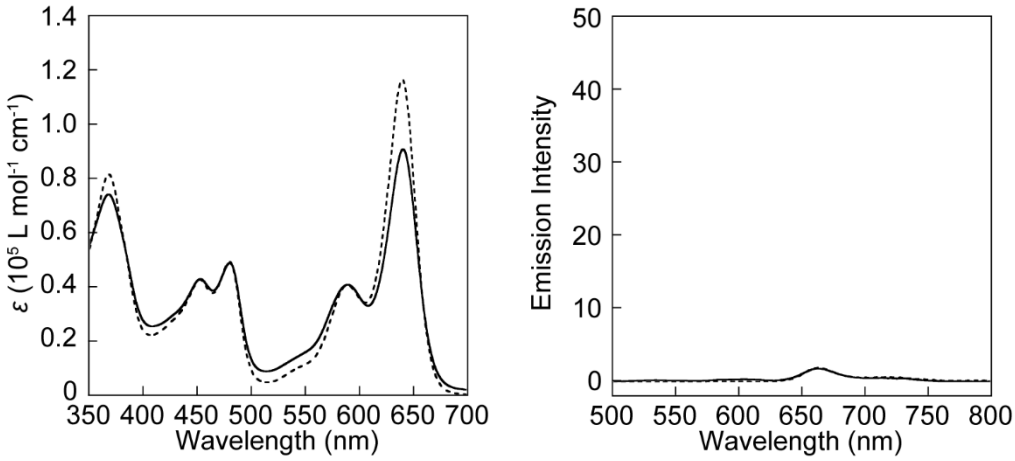

Figure 4-7. Absorption (left) and fluorescence (right) spectra of **RotAnBP** in THF/methanol (1:4, v/v) (dotted lines) and of **RotAnBP-PUU** in methanol (solid lines). The concentration of the **RotAnBP-PUU** solution was adjusted so that the absorbance at 490 nm matched the one of **RotAnBP**. The fluorescence spectra were recorded under the same conditions as the solution of **RotAnBP** shown in Figure 4-4.

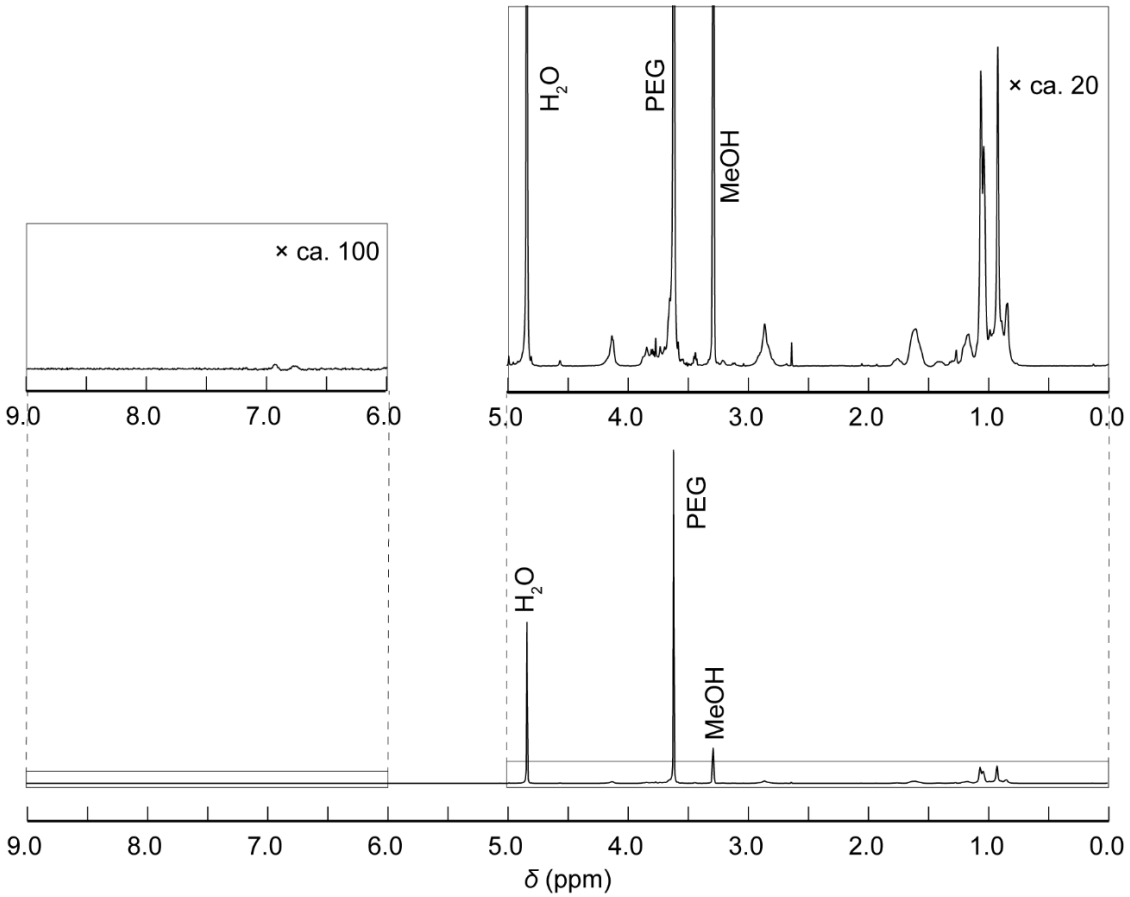

Figure 4-8. ^{1}H NMR spectrum of **RotAnBP-PUU** in methanol-d_4. No signals ascribed to the rotaxane mechanophore were observed due to the very low concentration. The spectrum was measured at r.t.

The thermal properties of **RotAnBP-PUU** were investigated by thermogravimetric analysis (TGA) (Figure 4-9a) and differential scanning calorimetric (DSC) measurement (Figure 4-9b). The TGA scan shows that decomposition sets in at ca. 220°C, and the DSC trace reveals a weak melting transition at around 15°C upon heating, which is associated with crystalline PEG domains. These data reflect that the thermal properties of **RotAnBP-PUU** are similar to a similar PUU that was reported previously.[37,38] **RotAnBP-PUU** was processed into thin films with a thickness of 70–100 μm by solvent casting (see Experimental Section for details). The mechanical properties of the material in the dry state were characterized by dynamic mechanical analysis (DMA) (Figure 4-10) and uniaxial tensile tests (Figure 4-11a, Table 1). The DMA traces reveal a glass transition temperature (T_g) of ca. –40°C, a rubbery plateau that extends to ca. 80°C, and a regime in which the storage modulus decreases with increasing temperature, before the samples fail at ca. 180°C. The tensile tests, which were carried out at r.t., reveal a Young's modulus of 29.5 ± 7.8 MPa, a tensile strength of 14.5 MPa, and an extensibility of more than 1000%.

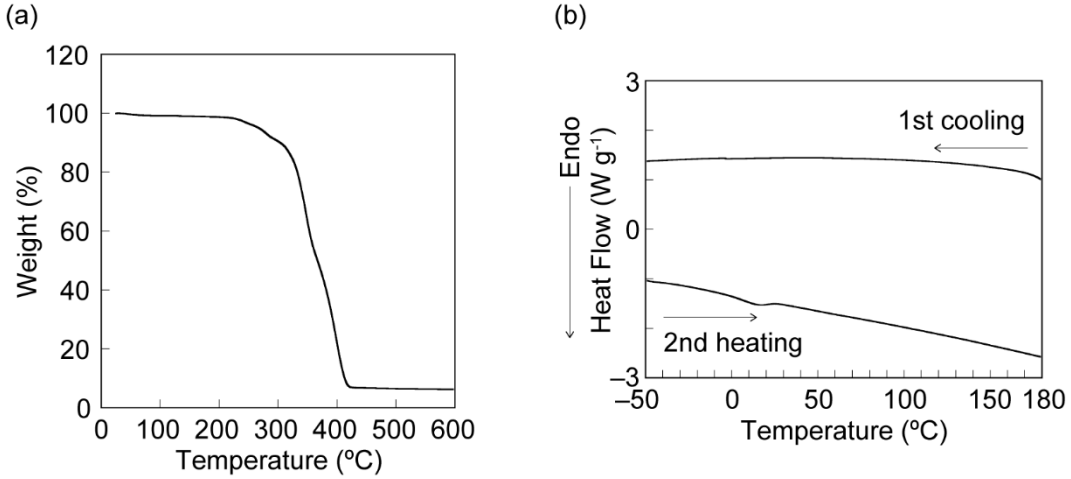

Figure 4-9. (a) TGA trace and (b) DSC traces of **RotAnBP-PUU**. The heating and cooling rates were 10 °C/min.

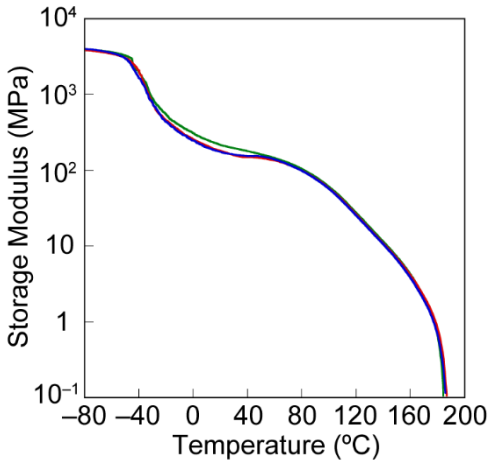

Figure 4-10. DMA traces of dried **RotAnBP-PUU** films. The graph shows data obtained from three different specimens. The tests were conducted under N_2 at a heating rate of 3 °C/min, a frequency of 1 Hz, and an amplitude of 15 μm.

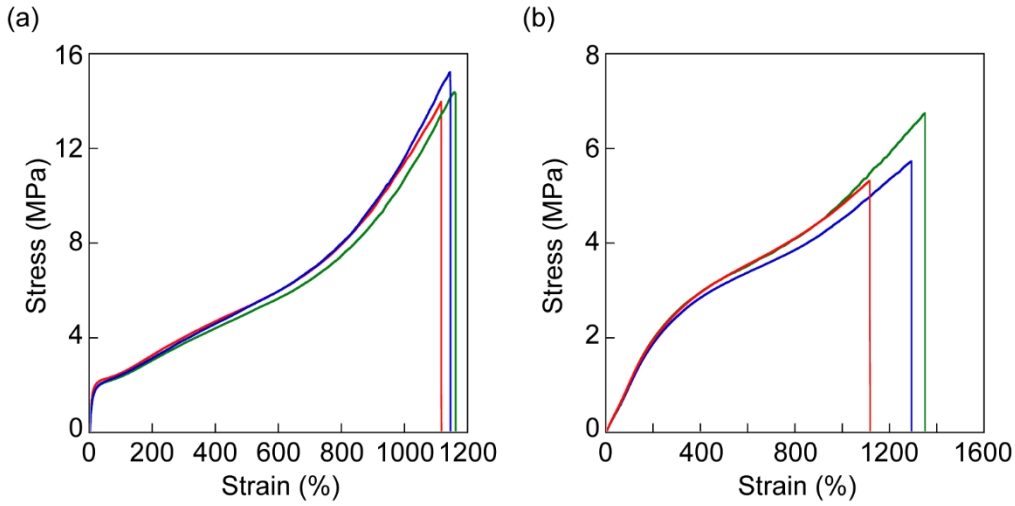

Figure 4-11. Strain-stress curves of (a) **dried RotAnBP-PUU** films and (b) **RotAnBP-PUU** hydrogels. Each graph shows data obtained from three different specimens. The experiments were conducted with a strain rate of 60 mm/min at r.t.

Table 1. Mechanical data of dried **RotAnBP-PUU** films and **RotAnBP-PUU** hydrogels extracted from tensile tests.[a)]

	Elongation at break	Stress at break	Young's modulus[b)]
Dried **RotAnBP-PUU** film	1142 ± 24 %	14.5 ± 0.8 MPa	29.5 ± 7.8 MPa
RotAnBP-PUU hydrogel	1254 ± 137 %	5.93 ± 0.82 MPa	1.19 ± 0.04 MPa

a) All data were extracted from the strain-stress curves shown in Figure 4-11 and represent averages of 3 measurements ± standard derivation. b) The Young's moduli were derived from the slopes of the strain-stress curves in the strain regime between 1.5–2%.

RotAnBP-PUU hydrogels were prepared by immersing the dried films in deionized water for two hours; after this time, an equilibrium state with a water take-up of 70% had been reached (Figure 4-12a). Under ambient conditions, the gels slowly dry and water is released with an initial rate of ca. 0.5% min^{-1} (Figure 4-12b). Tensile tests (Figure 4-11b, Table S1) reveal a Young's modulus of 1.19 ± 0.04 MPa, which is more than an order of magnitude lower than that of the dry films. The hydrogels display an elongation of ca. 1200% and a nominal tensile strength of 5.93 MPa.

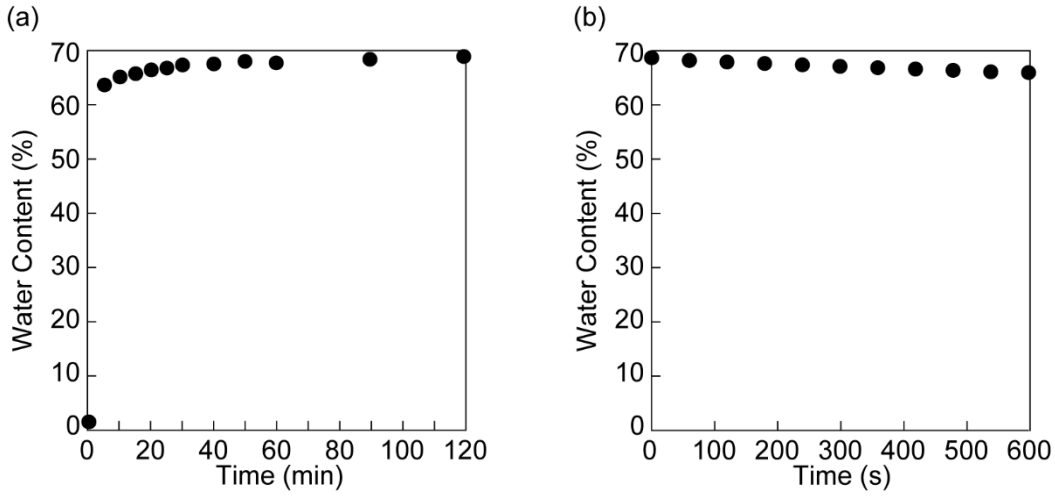

Figure 4-12. Change of (a) water content of a **RotAnBP-PUU** film as a function of immersion time in an excess amount of deionized water at r.t. and (b) water content in the **RotAnBP-PUU** hydrogel as a function of the time under ambient conditions. The water content was calculated by: Water content (%) = 100 × (M – M_0)/M, where M is the weight of the film after swelling, and M_0 is the initial weight of the dried film.

4.2.4. Investigation of Mechanoresponsive Behavior of RotAnBP-PUU Hydrogels and Dry RotAnBP-PUU Films

The dry **RotAnBP-PUU** films exhibit moderately weak red fluorescence (Φ = 0.05, excited at 490 nm), although the methanol solution of **RotAnBP-PUU** hardly fluoresces under the same excitation conditions. Residual emission in the force-free state was also observed for previously reported polyurethanes containing other rotaxane-based mechanophores,[15] and appears to be related to residual stresses in the material that cause separation of the green emitter and the quencher in a fraction of the rotaxanes. This enables energy transfer from the excited 9,10-bis(phenylethynyl)anthracene to the π-extended BODIPY. In contrast, the red fluorescence intensity of the **RotAnBP-PUU** hydrogel becomes much weaker (Φ = 0.02, excited at 490 nm) than that of the dried material, likely on account of an increased cycle-quencher association constant due to hydrophobic interactions and the increased molecular mobility, which both should reduce the fraction of activated mechanophores.

The force-induced shuttling function controls the on/off switching of FRET, as depicted in Figure 4-1. Upon uniaxial tensile deformation, the **RotAnBP-PUU** hydrogel initially shows a slight decrease in the red fluorescence intensity due to a decrease in the thickness of the hydrogel, and then, exhibits subsequently a considerable increase in the red fluorescence intensity when excited at 490 nm (Figure 4-13a, Figure 4-14a). Upon subsequent removal of the force, the fluorescence intensity gradually decreases (Figure 4-15a). This indicates that the increase in the red fluorescence intensity of the hydrogel with excitation at 490 nm is mainly due to activation of the FRET process. To the best of our knowledge, this is the first report on the on/off switching of the FRET by force on rotaxanes at single molecular level. Even upon excitation at 590 nm, the red fluorescence intensity of the hydrogels increases, however, the attainable contrast or relative increase is smaller than the one achieved when exciting the sample at 490 nm (Figure 4-15b). The fluorescence contrast between unstretched and stretched states is improved compared to

our previously reported red-emitting rotaxane, in which a BODIPY-based red-emitter was directly introduced into cyclic moiety.[15]

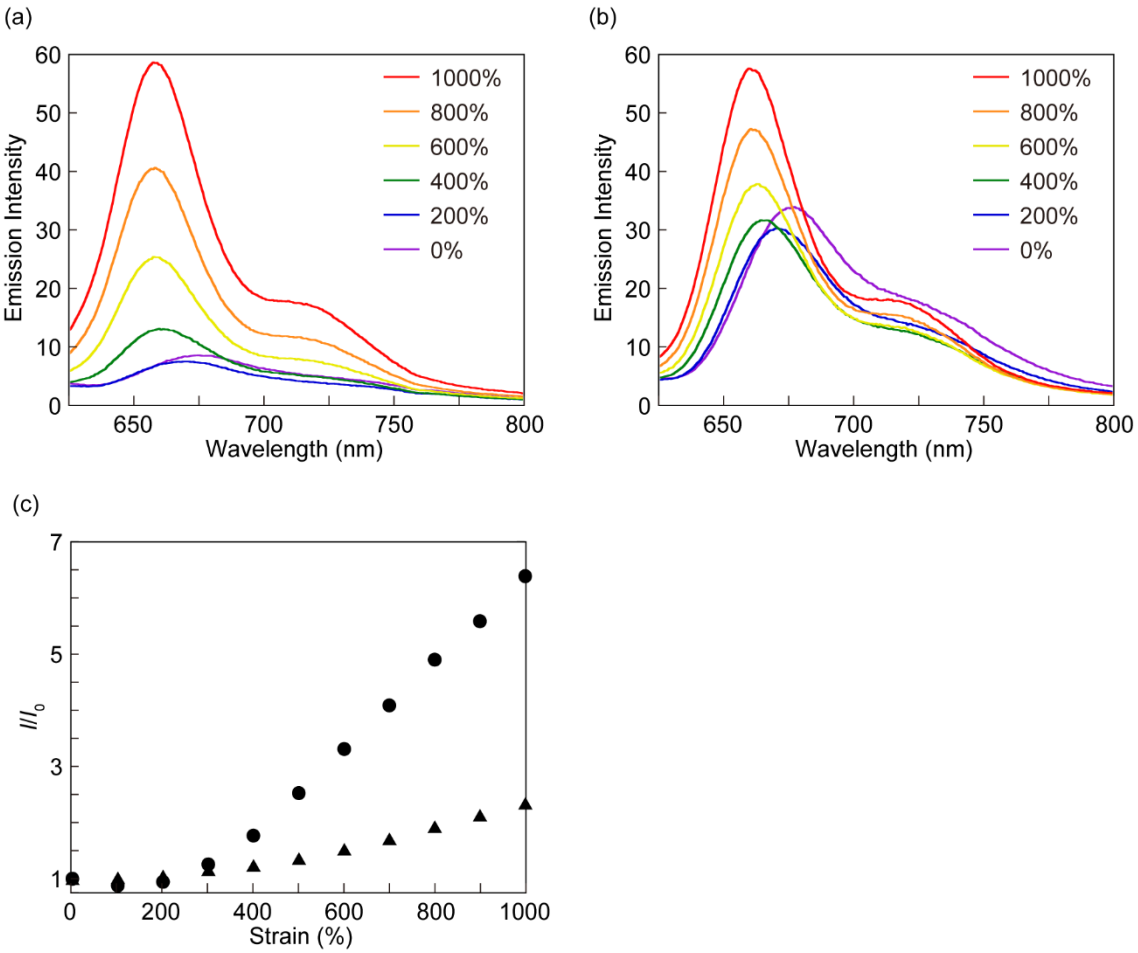

Figure 4-13. (a,b) Fluorescence spectra of a **RotAnBP-PUU** hydrogel (a) and a dried **RotAnBP-PUU** film (b) recorded upon stretching the samples to the strains indicated. (c) Plots of the relative fluorescence intensity I/I_0 of the **RotAnBP-PUU** hydrogel (circles) and the dried **RotAnBP-PUU** film (triangles) as a function of strain. All fluorescence spectra were recorded at r.t. with λ_{ex} = 490 nm. The fluorescence intensities in panel (c) were recorded at 660 nm.

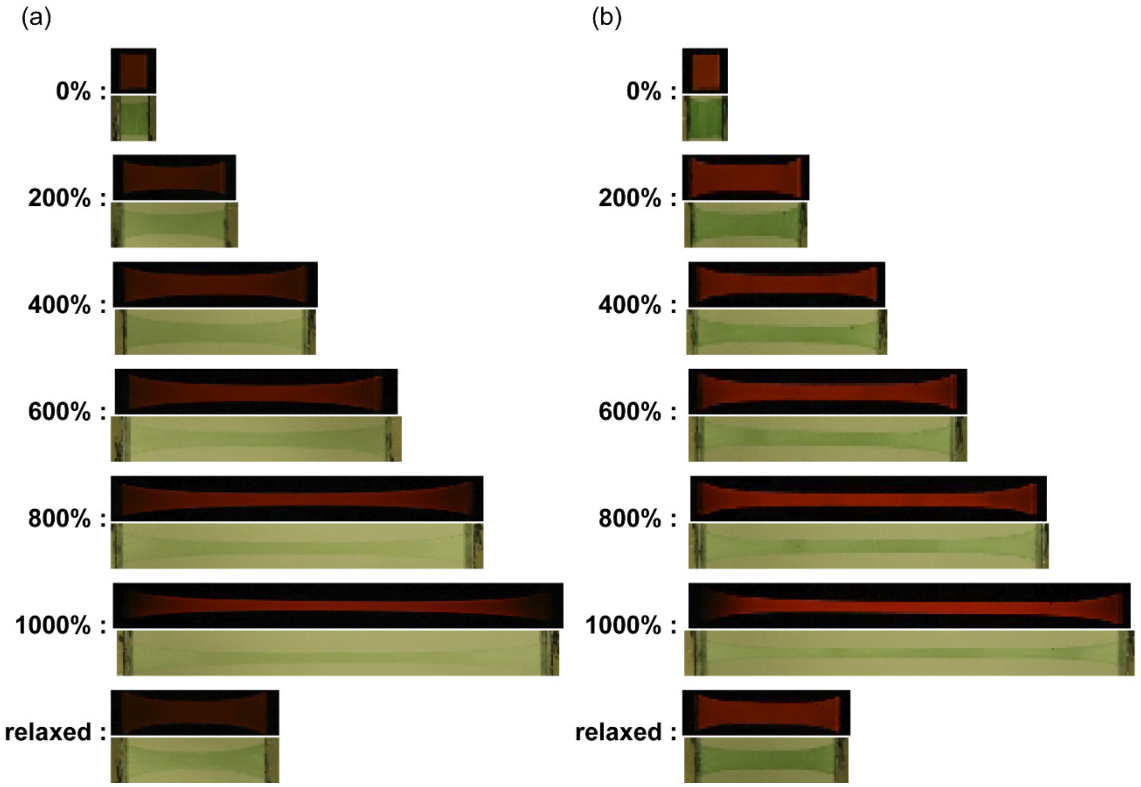

Figure 4-14. Pictures of (a) **RotAnBP-PUU** hydrogel and (b) dried **RotAnBP-PUU** films during uniaxial deformation test. In each strained state, the top picture displays the fluorescence of the hydrogel; these images were taken in the dark upon excitation at 490 nm, and a long pass filter cutting below 550 nm was placed in front of the camera. The bottom picture shown for each strain was taken under ambient illumination. All images were taken under the same ambient conditions.

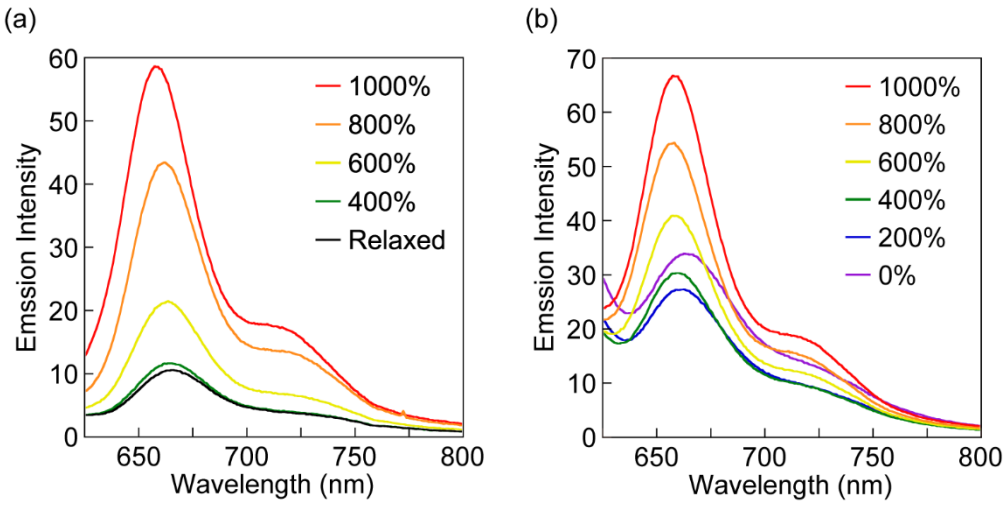

Figure 4-15. (a) Fluorescence spectra of **RotAnBP-PUU** hydrogel upon relaxation from the maximum strain of 1000% in the first cycle. The fluorescence spectra were recorded at r.t. with λ_{ex} = 490 nm. (b) Fluorescence spectra of **RotAnBP-PUU** hydrogel upon stretching the samples to the strains indicated in the first cycle. The fluorescence spectra were recorded at r.t. with λ_{ex} = 590 nm.

From a practical viewpoint, the rotaxane **RotAnBP** functions as a red-emissive supramolecular mechanophore in hydrogels. Red luminescence is useful for multicolor-imaging and for developing white-emissive materials. Besides red emission can penetrate into the living tissues deeply, making it favorable for bioimaging. Thus, the development of the red-light emitting mechanophores are desirable to expand the application of mechanophores. The possibility to readily vary the emission color of a given mechanophore is further useful for applications in colored materials. To demonstrate this, I carried out experiments in which I covered the **RotAnBP-PUU** hydrogel with a polyurethane film containing a red dye (see Figure 4-16–21 and Experimental Section for details). Gratifyingly, a clear increase in the red fluorescence intensity was observed upon stretching the **RotAnBP-PUU** hydrogel whether or not the red film cutting light of the wavelength ranging below 600 nm was applied (Figure 4-20). By contrast, when a reference polyurethane film containing the "parent", green-light emitting rotaxane mechanophore without the FRET acceptor[16] was stretched, virtually all of the green fluorescence was absorbed by the red dye (Figure 4-21).

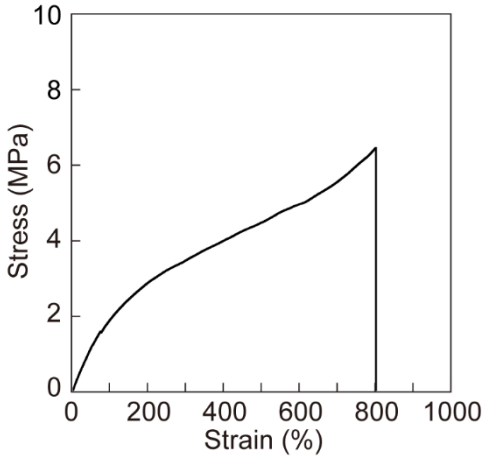

Figure 4-16. Stress-strain curve of a **RotAnBP-PUU** hydrogel based on a second batch of **RotAnBP-PUU**. The experiment was conducted with a strain rate of 60 mm/min at r.t.

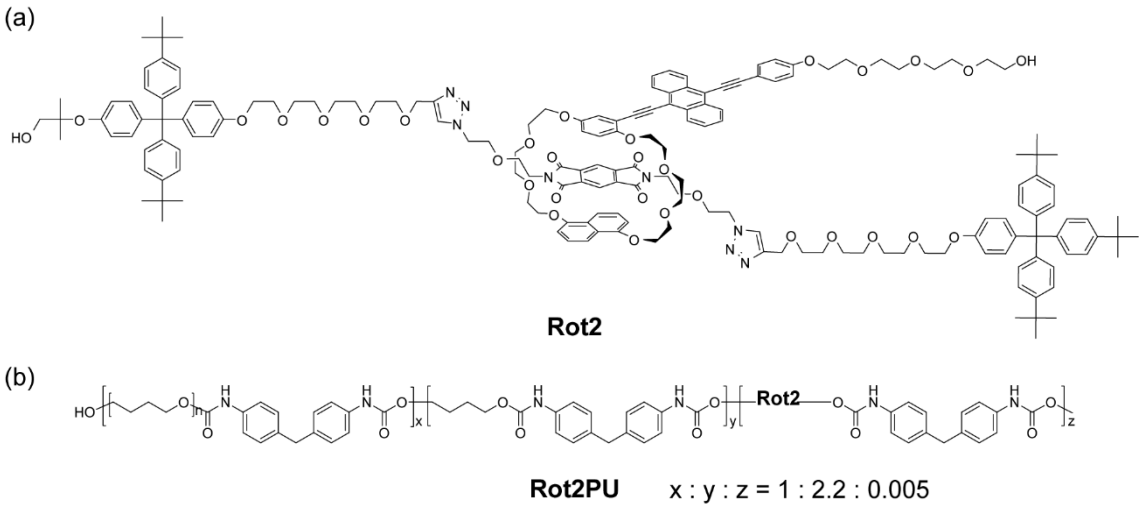

Figure 4-17. Molecular structures of (a) **Rot2** and (b) **Rot2PU**.

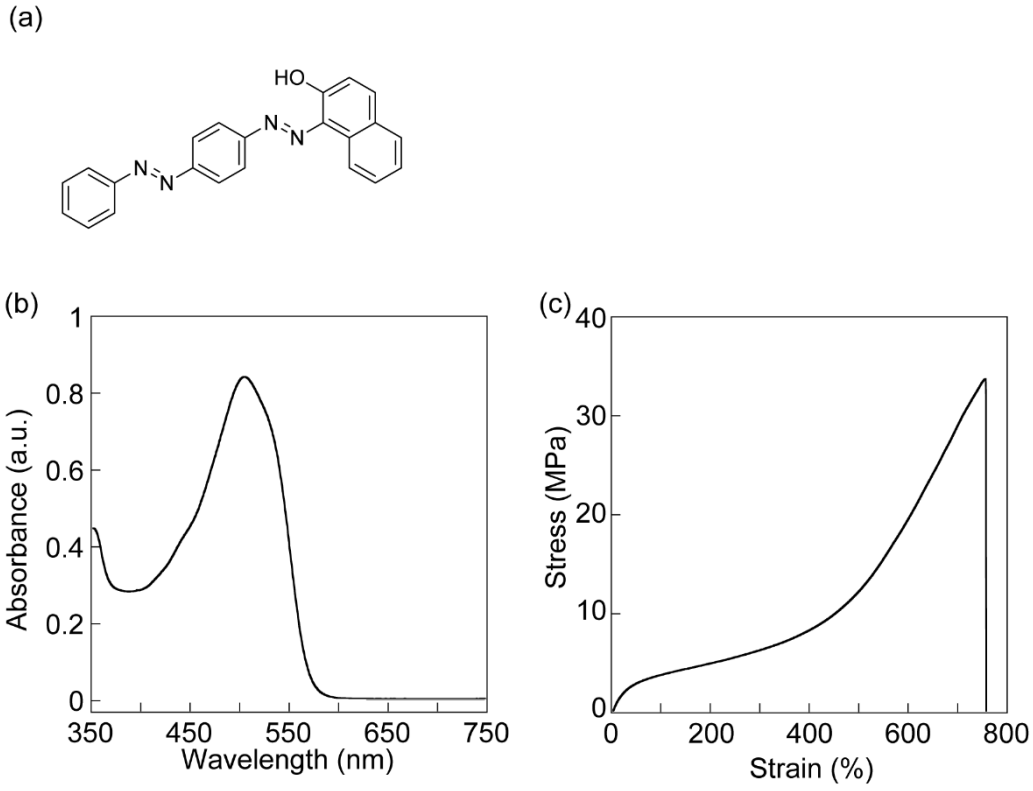

Figure 4-18. (a) Molecular structure of sudan III. (b) Absorption spectrum of sudan III in THF solution. (c) Stress-strain curve of a PU film containing sudan III. The experiment was conducted with a strain rate of 120 mm/min at r.t.

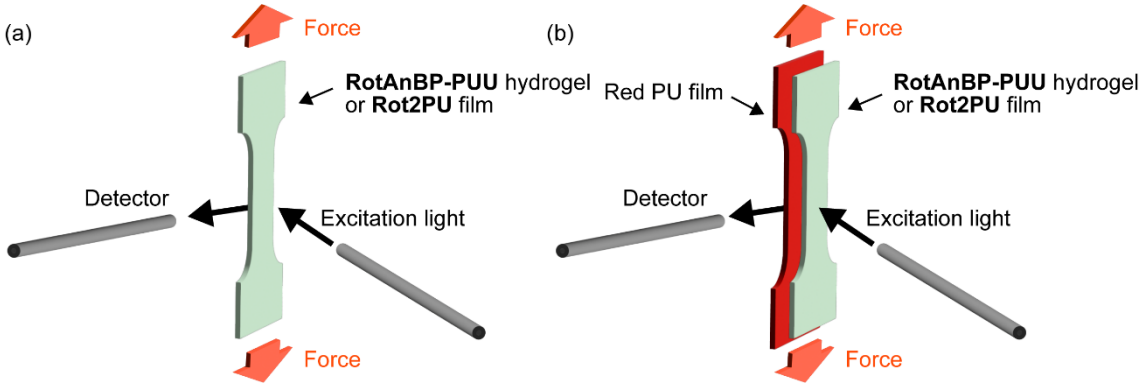

Figure 4-19. Schematic illustration of the setup used to examine the permeability of red fluorescence exhibited by **RotAnBP-PUU** hydrogels and green fluorescence of **Rot2PU** film overlaid (a) without and (b) with the red films.

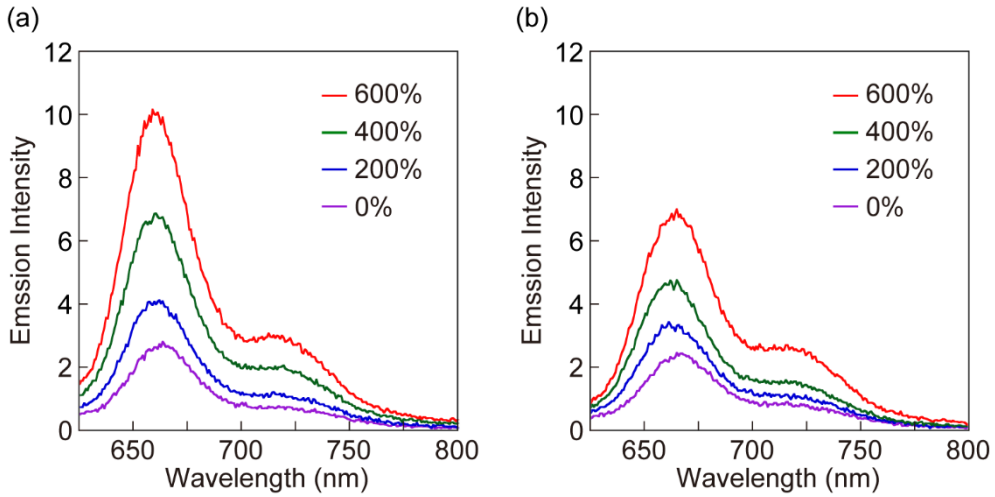

Figure 4-20. Fluorescence spectra of (a) **RotAnBP-PUU** hydrogel and (b) **RotAnBP-PUU** hydrogel overlaid with the red film upon stretching the samples to the strains indicated in the first cycle. The fluorescence spectra were recorded at r.t. with λ_{ex} = 490 nm.

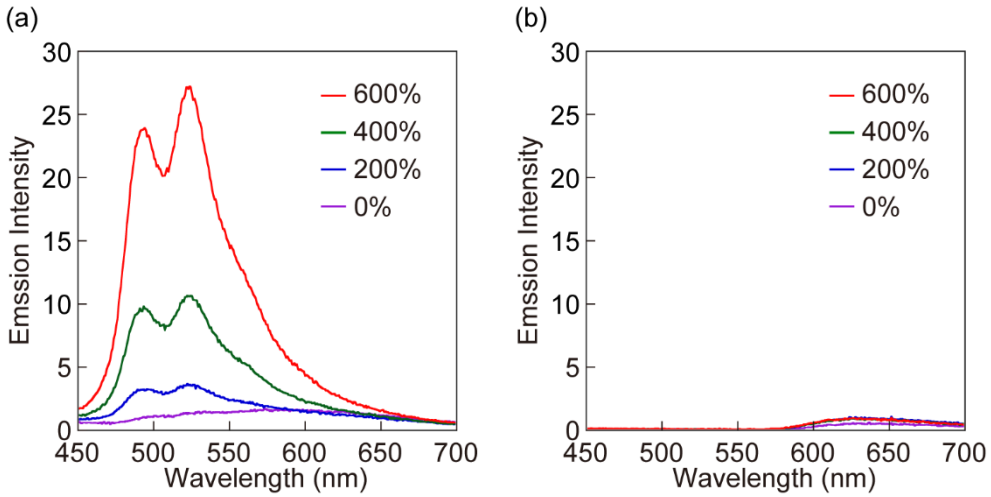

Figure 4-21. Fluorescence spectra of (a) **Rot2PU** and (b) **Rot2PU** overlaid with the red film upon stretching the samples to the strains indicated in the first cycle. The fluorescence spectra were recorded at r.t. with λ_{ex} = 365 nm.

The dry **RotAnBP-PUU** films also show a mechanoresponse upon stretching (Figure 4-13b, Figure 4-14b). However, plots of the relative fluorescence intensities, i.e., the ratio of the fluorescence intensities of the stretched (I) and unstretched (I_0) samples recorded at 660 nm (Figure 4-13c) show that the contrast observed for the **RotAnBP-PUU** hydrogels is much larger than that in the dry **RotAnBP-PUU** films, although significantly higher stresses are required to deform the dry films (Figure 4-11). The difference is caused by the weak fluorescence intensity of the hydrogel in the force-free state and perhaps also a lower fraction of activated mechanophores in the material because of the bulky structure of the ring featuring the FRET pair.

4.3. Conclusion

In conclusion, I successfully demonstrated that the mechanically induced molecular shuttling function of rotaxanes can be used to control the on/off switching of a FRET process between a donor-acceptor pair in the reporter molecule. The FRET pair, a green-emissive energy donor and a red-emissive energy acceptor, were connected via a short spacer and attached to the cyclic part of the rotaxane. The photophysical properties of the fluorophores allow the preferred (although not exclusive) excitation of the donor at 490 nm. An efficient FRET process causes the cyclic molecule to emit almost exclusively red light, even if the donor is preferentially excited. Upon rotaxane formation, CT interactions or PeT between the green emitter and NpI residue placed in the axle prevent the FRET, so that the red fluorescence becomes weak if the donor is excited. The new rotaxane mechanophore was covalently incorporated into a PUU, which was swelled with water to produce a PUU hydrogel. The hydrogel displays an up to seven-fold increase of the red emission intensity upon mechanical deformation. The contrast between the idle and the mechanically activated state is considerably higher than that observed for the dry polymer, on account of the increased association constant between the cycle and NpI as well as the higher molecular mobility.

The results of the present study suggest that rotaxane mechanophores can be used to control photophysical processes that go beyond FRET, for example circularly polarized emission, phosphorescence, and so on, allowing access fascinating and sophisticated supramolecular mechanophores. Furthermore, the data suggest that supramolecular mechanophores may function better in hydrophilic environments and that increasing the molecular mobility improve the supramolecular mechanophore property.

4.4. Experimental Section

4.4.1. General Methods

All reagents and solvents were purchased from Merck, Kanto Chemical, Tokyo Kasei, or FUJIFILM Wako Pure Chemical Corporation. Anhydrous dimethylacetamide (DMAc) and methanol were used as solvents for the synthesis of polymers and solvent casting, respectively. Telechelic poly(ethylene glycol) (M_n = 2000 g/mol) and 2,2-bis(hydroxymethyl)propionic acid were dried in vacuo at 100 °C for 1 h before use. Isophorone diisocyanate was distilled under a vacuum and stored over molecular sieves at 4 °C. Isophorone diamine was dried over molecular sieves at r.t. for 1 day before use. Deionized water for hydrogel preparation was obtained using a Merck Direct-Q UV5. All reactions were performed under nitrogen atmosphere, unless otherwise noted. Flash silica gel column chromatography was carried out with a Biotage Isolela Flash system using SHOKO-scientific Purif-Pack-EX cartridges. Silica gel from Kanto Chemicals (silica gel 60 N, spherical, 40–50 μm) was used for conventional silica gel column chromatography. Recycling preparative gel permeation chromatography (GPC) was conducted with a Japan Analytical Industry LaboACE.

^{1}H NMR spectra were acquired on a JEOL JNM-ECX 400 spectrometer or a JEOL JNM-ECZ400S/L1 spectrometer and all chemical shifts are reported on the δ-scale in ppm relative to the signal of tetramethylsilane (at 0.00 ppm) as an internal standard. Coupling constants (*J*) are quoted in Hz and relative intensities are also shown. Proton-decoupled ^{13}C NMR spectra were conducted with a JEOL JNM-ECX 400 spectrometer or a JEOL JNM-ECZ400S/L1 spectrometer and all chemical shifts are expressed in ppm using the solvent as an internal standard ($CDCl_3$ at 77.16 ppm or DMSO-d_6 at 39.52 ppm).

Matrix-assisted laser desorption ionization time-of-flight (MALDI-TOF) mass spectra were measured on an AB SCIEX TOF/TOF 5800 system or a SHIMAZHU AXIMA-performance. High-resolution electrospray ionization (ESI) mass spectroscopy was performed with a Bruker Daltonics micrOTOF II.

Size-exclusion chromatography experiments were performed on an Agilent 1260 Infinity II HPLC system equipped with one Agilent PolarGel M guard column (particle size = 8 μm) and two Agilent PolarGel M columns (ID = 7.5 mm, L = 300 mm, particle size = 8 μm). Signals were recorded by a UV detector (Agilent 1260 series) and an interferometric refractometer (Agilent 1260 series). Samples were run using DMF + 0.05 M LiBr as the eluent at 60 °C and a flow rate of 1.0 mL/min. Molecular weights were determined based on narrow molecular weight poly(ethylene oxide) calibration standards.

Thermogravimetric analysis (TGA) was performed under nitrogen with a Mettler-Toledo Stare system at a rate of 10 °C/min. Differential scanning calorimetry (DSC) measurements were conducted under N_2 on a Mettler Toledo DSC 2 STAR system at heating and cooling rates of 10 °C/min. Dynamic mechanical analyses (DMA) were carried out under N_2 with a TA Instruments DMA Q800 at a heating rate of 3 °C/min, a frequency of 1 Hz, and an amplitude of 15 μm. Stress-strain measurements were conducted under ambient conditions with a SHIMADZU AGS-100NX equipped with a 100 N load cell at a strain rate of 60 mm/min.

Absorption spectra of solutions were measured on a JASCO V-750. Steady-state fluorescence spectra of solutions were recorded with a JASCO FP-6500 and the spectra were corrected for the detector nonlinearity. The slit width at all excitation wavelengths was 3 nm. Excitation spectra were also recorded with the same fluorescence spectrometer. Steady-state fluorescence spectra of polyurethane-urea films and hydrogels during stretching experiments using a SHIMADZU AGS-100NX equipped with a 100 N load cell were monitored with an Ocean Insight QEPro-FL equipped with a Reflection/Backscattering Prove R400-7-UV-Vis; these spectra were not corrected. The excitation lights at 490 and 590 nm were obtained by passing the light of an Asahi Spectra CL-1501 equipped with an Asahi Spectra CL-H1-505-9-1 or CL-H1-590-9-1 through a respective bandpass filter (Asahi Spectra HMX490 or HMX590). The excitation light at

365 nm was obtained using an Ocean Insight LLS-365 LED light source. Photographs and movies were taken with a Canon EOS 9000D stabilized with a tripod.

4.4.2. Synthesis Procedure

4,4-Difluoro-1,3,5,7-tetramethyl-8-phenyl-4-bora-3a,4a-diaza-*s*-indacene and compounds **An**, **4**, and **5** were synthesized following previous reports.[13,14,53]

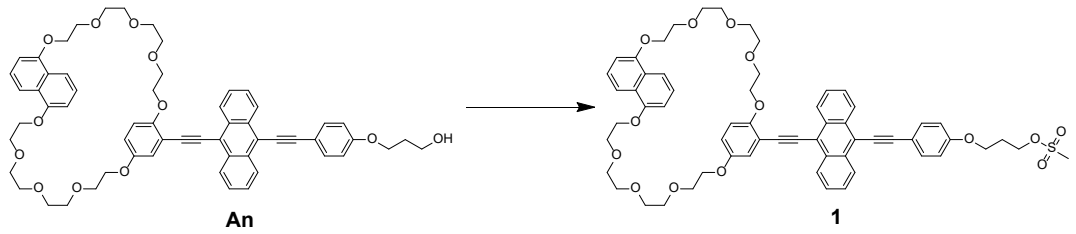

Conditions: methanesulfonyl chloride, Et_3N, CH_2Cl_2, r.t., 4 h.

Compound **1**. Methanesulfonyl chloride (32 mg, 0.28 mmol) was added to a mixture of compound **An**[14] (180 mg, 0.187 mmol) and Et_3N (189 mg, 1.87 mmol) in dichloromethane (50 mL) and the mixture was stirred for 4 h at r.t. The reaction mixture was poured into dichloromethane (50 mL), and the solution was washed with 5% aq. HCl (50 mL), saturated aq. $NaHCO_3$ (100 mL), and saturated aq. NaCl (100 mL). The organic layer was dried over $MgSO_4$ and filtered, and the solvent was evaporated. The crude product thus isolated was purified by flash column chromatography on silica gel (eluent: gradient from dichloromethane/acetone = 19:1 v/v to dichloromethane/acetone = 4:1 v/v) to afford compound 1 (180 mg, 0.173 mmol, 93%) as a yellow solid.

^{1}H NMR (400 MHz, $CDCl_3$): δ = 2.20–2.26 (m, 2H), 2.99 (s, 3H), 3.61–3.65 (m, 6H), 3.72–3.75 (m, 8H), 3.78–3.81 (m, 4H), 3.83–3.88 (m, 4H), 3.98–4.00 (m, 6H), 4.08–4.12 (m, 4H), 4.18–4.21 (m, 2H), 4.42–4.45 (m, 2H), 6.49 (d, J = 8.8 Hz, 1H), 6.60 (dd, J = 8.8, 2.8 Hz, 1H), 6.65–6.71 (m, 2H), 6,94 (d, J = 8.8 Hz, 2H), 7.12 (d, J = 2.8 Hz, 1H),

7.22–7.27 (m, 2H), 7.61–7.65 (m, 4H), 7.69 (d, J = 8.4 Hz, 2H), 7.81–7.84 (m, 2H), 8.65–8.69 (m, 4H), 8.75–8.79 (m, 2H).

^{13}C NMR (100 MHz, $CDCl_3$): δ = 29.10, 37.30, 63.37, 66.70, 67.89, 68.04, 68.51, 69.68, 69.75, 69.82, 70.81, 70.95, 71.00, 71.02, 85.67, 90.79, 99.39, 102.44, 105.58, 113.09, 113.35, 114.50, 114.67, 114.72, 116.04, 116.58, 118.46, 118.73, 125.18, 125.22, 126.68, 126.78, 127.21, 127.70, 131.98, 132.04, 133.31, 152.51, 154.02, 154.33, 154.34, 158.89.

MS (MALDI-TOF): m/z: 1060.78 (calcd. $[M+H]_+$ = 1061.38).

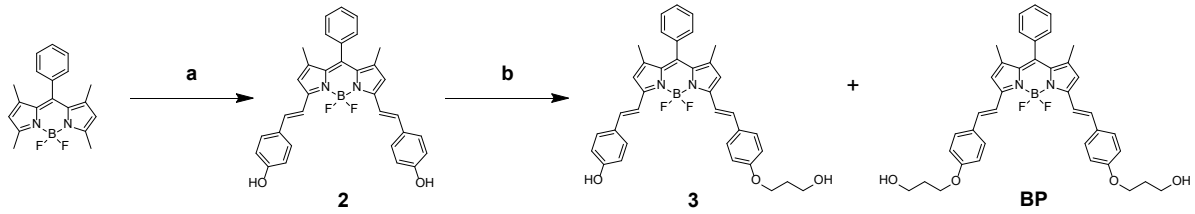

Conditions: (a) 4-hydroxybenzaldehyde, piperidine, acetic acid, toluene, reflux, 6 h; (b) 3-bromopropanol, K_2CO_3, NaI, acetone, reflux, 24 h.

Compound **2**. A mixture of 4,4-difluoro-1,3,5,7-tetramethyl-8-phenyl-4-bora-3a,4a-diaza-*s*-indacene[53] (600 mg, 1.85 mmol), 4-hydroxybenzaldehyde (422 mg, 3.70 mmol), piperidine (1.2 mL), and acetic acid (1.0 mL) in toluene (50 mL) was stirred for 6 h under reflux using a Dean-Stark trap. After cooling to r.t., the reaction mixture was poured into ethyl acetate (150 mL). The solution was washed with 5% aq. HCl (50 mL), saturated aq. $NaHCO_3$ (100 mL), and saturated aq. NaCl (100 mL). The organic layer was dried over $MgSO_4$ and filtered, and the solvent was evaporated. The crude product thus isolated was purified by flash column chromatography on silica gel (eluent: gradient from hexane/ethyl acetate = 4:1 v/v to hexane/ethyl acetate = 1:3 v/v) and subsequently precipitated from a mixture of acetone and hexane to afford compound **2** (607 mg, 1.14 mmol, 62 %) as a dark red solid.

^{1}H NMR (400 MHz, DMSO-d_6): δ = 1.40 (s, 6H), 6.85–6.92 (m, 6H), 7.34 (d, J = 16.0 Hz, 2H), 7.42–7.50 (m, 8H), 7.56–7.61 (m, 3H).

^{13}C NMR (100 MHz, DMSO-d_6): δ = 14.22, 114.98, 116.12, 117.96, 127.32, 128.41, 129.06, 129.18, 132.33, 134.36, 137.06, 137.64, 141.23, 152.26, 159.06.

MS (MALDI-TOF): m/z: 555.66 (calcd. $[M]^+$ = 555.20).

Compounds **3** and **BP**. A mixture of compound **2** (500 mg, 0.939 mmol), 3-bromopropanol (109 mg, 0.783 mmol), and K_2CO_3 (325 mg, 2.35 mmol) in acetone (100 mL) was stirred for 24 h under reflux. After cooling to r.t., the reaction mixture was poured into ethyl acetate (150 mL). The solution was washed with saturated aq. NaCl (2 × 100 mL). The organic layer was dried over $MgSO_4$ and filtered, and the solvent was evaporated. The crude product thus isolated was purified by flash column chromatography on silica gel (eluent: gradient from dichloromethane/acetone = 19:1 v/v to dichloromethane/acetone = 4:1 v/v) and subsequently precipitated from a mixture of acetone and hexane to afford compound **3** (53 mg, 0.090 mmol, 11%) as a dark blue solid and compound **BP** (20 mg, 0.031 mmol, 4%) as a dark blue solid.

Compound **3**: ^{1}H NMR (400 MHz, $CDCl_3$): δ = 1.44 (s, 6H), 1.71 (t, J = 5.2 Hz, 1H), 2.06–2.12 (m, 2H), 3.88–3.92 (m, 2H), 4.18 (t, J = 6.0 Hz, 2H), 5.01 (s, 1H), 6.62 (s, 2H), 6.87 (d, J = 8.4 Hz, 2H), 6.94 (d, J = 8.8 Hz, 2H), 7.18–7.23 (m, 2H), 7.32–7.34 (m, 2H), 7.48–7.63 (m, 9H).

^{13}C NMR (100 MHz, DMSO-d_6): δ = 14.20, 14.24, 32.08, 57.24, 64.79, 114.96, 115.12, 115.90, 116.13, 117.92, 118.12, 127.31, 128.37, 128.75, 128.82, 129.14, 129.18, 132.31, 132.51, 134.33, 136.33, 137.38, 137.85, 141.09, 141.61, 151.77, 152.69, 159.12, 159.81.

MS (MALDI-TOF): m/z: 590.29 (calcd. $[M]^+$ = 590.26).

Compound **BP**: ^{1}H NMR (400 MHz, $CDCl_3$): δ = 1.43 (s, 6H), 1.74 (t, J = 5.2 Hz, 2H), 2.05–2.11 (m, 4H), 3.88–3.92 (m, 4H), 4.18 (t, J = 6.0 Hz, 4H), 6.62 (s, 2H), 9.94 (d, J =

8.4 Hz, 4H), 7.21 (d, J = 16.0 Hz, 2H), 7.32–7.34 (m, 2H), 7.49–7.52 (m, 3H), 7.57–7.63 (m, 6H).

^{13}C NMR (100 MHz, $CDCl_3$): δ =14.76, 32.06, 60.51, 65.85, 114.88, 117.37, 117.63, 128.63, 129.02, 129.19, 129.79, 133.29, 135.38, 135.83, 138.26, 141.95, 152.77, 159.69.

MS (MALDI-TOF): m/z: 649.09 (calcd. $[M]^+$ = 649.30).

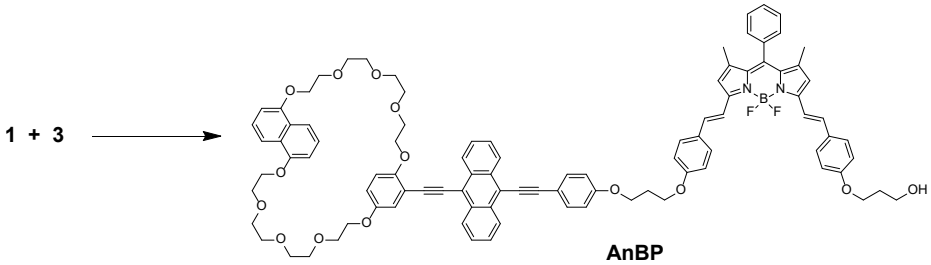

Conditions: K_2CO_3, acetone, reflux, 32 h.

Compound AnBP. A mixture of compound **1** (520 mg, 0.948 mmol), compound **3** (131 mg, 0.942 mmol), and K_2CO_3 (400 mg, 2.89 mmol) in acetone (50 mL) was stirred for 32 h under reflux. After cooling to r.t., the reaction mixture was poured into ethyl acetate (150 mL). The solution was washed with saturated aq. NaCl (2 × 100 mL). The organic layer was dried over $MgSO_4$ and filtered, and the solvent was evaporated. The crude product thus isolated was purified by flash column chromatography on silica gel (eluent: gradient from dichloromethane/acetone = 9:1 v/v to dichloromethane/acetone = 3:1 v/v) and recycling GPC (eluent: chloroform) to afford compound **AnBP** (167 mg, 0.283 mmol, 29%) as a dark green solid.

^{1}H NMR (400 MHz, $CDCl_3$): δ = 1.42 (s, 6H), 2.02–2.08 (m, 2H), 2.30–2.36 (m, 2H), 3.62–3.66 (m, 6H), 3.73–3.90 (m, 18H), 3.97–4.02 (m, 6H), 4.10–4.16 (m, 4H), 4.20–4.26 (m, 6H), 6.52 (d, J = 9.2 Hz, 1H), 6.61–6.64 (m, 3H), 6.66–6.73 (m, 2H), 6.92 (d, J = 8.8 Hz, 2H), 6.96 (d, J = 8.8 Hz, 2H), 7.01 (d, J = 9.2 Hz, 2H), 7.12 (d, J = 2.8 Hz, 1H),

7.18–7.27 (m, 4H), 7.31–7.34 (m, 2H), 7.47–7.50 (m, 3H), 7.55–7.65 (m, 10H), 7.72 (d, J = 8.8 Hz, 2H), 7.82–7.84 (m, 2H), 8.67–8.69 (m, 2H), 8.76–8.79 (m, 2H).

^{13}C NMR (100 MHz, $CDCl_3$): δ = 14.74, 29.31, 32.03, 60.38, 64.54, 64.66, 65.76, 67.94, 68.10, 68.60, 69.74, 69.81, 69.88, 70.88, 71.00, 71.07, 85.58, 90.88, 99.33, 102.70, 105.63, 113.18, 113.47, 114.55, 114.73, 114.88, 115.74, 116.64, 117.32, 117.62, 118.49, 118.67, 125.22, 125.26, 126.74, 126.80, 127.31, 127.72, 128.60, 129.15, 129.72, 132.02, 132.10, 132.26, 133.33, 135.33, 135.84, 138.21, 141.90, 152.57, 152.75, 154.07, 154.38, 159.37, 159.68, 159.72.

HRMS (ESI): m/z: 1555.6429 (calcd. $[M+Na]^+$ = 1555.6441).

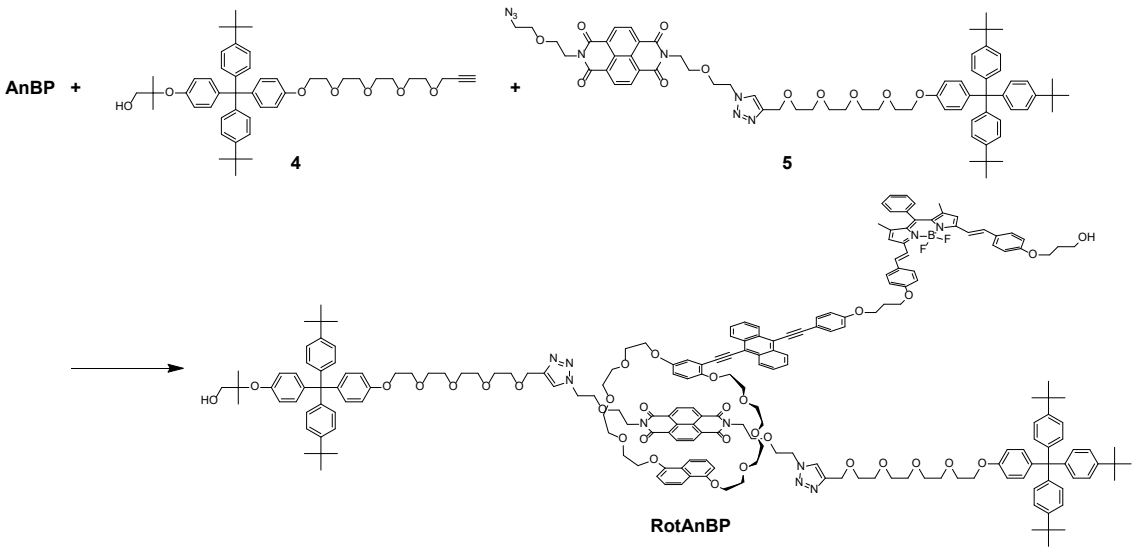

Conditions: $CuSO_4$, sodium ascorbate, $CHCl_3$, H_2O, 5 °C, 15 h.

Compound **RotAnBP**. A mixture of sodium ascorbate (59.4 mg, 0.300 mmol) and copper (II) sulfate (23.9 mg, 0.150 mmol) in water (1 mL) was added to a solution of compound **AnBP** (153 mg, 0.100 mmol), compound **4**[13] (73.5 mg, 0.100 mmol), and compound **5**[13] (121 mg, 0.100 mmol) in chloroform (0.5 mL) and the mixture was vigorously stirred for

15 h at 5 °C. The suspension was poured into a mixture of water (100 mL) and chloroform (150 mL). The organic layer was separated off, washed with saturated aq. NaCl (100 mL), dried over $MgSO_4$, and filtered. After the solvent was evaporated, the crude product thus isolated was purified by flash column chromatography on silica gel (eluent: gradient from dichloromethane/acetone = 4:1 v/v to dichloromethane/acetone = 2:3 v/v) and recycling GPC (eluent: chloroform) to afford **RotAnBP** (30.3 mg, 8.66×10^{-3} mmol, 9%) as a dark green solid.

^{1}H NMR (400 MHz, $CDCl_3$): δ = 1.27 (s, 6H), 1.29 (s, 45H), 1.43 (s, 6H), 2.00 (br, 1H), 2.04–2.08 (m, 2H), 2.26 (t, J = 6.4 Hz, 1H), 2.35 (quin, J = 6.0 Hz, 2H), 3.46–4.08 (m, 80H), 4.17 (t, J = 6.0 Hz, 2H), 4.24–4.29 (m, 4H), 4.45–4.47 (m, 4H), 4.68 (s, 4H), 5.96 (d, J = 9.2 Hz, 1H), 6.00 (d, J = 3.2 Hz, 1H), 6.05–6.19 (m, 3H), 6.56–6.67 (m, 4H), 6.75 (d, J = 8.8 Hz, 4H), 6.82–6.84 (m, 3H), 6.92–7.08 (m, 23H), 7.31–7.34 (m, 2H), 7.48–7.50 (m, 3H), 7.56–7.75 (m, 14 H), 8.38–8.40 (m, 2H), 8.47 (s, 4H), 8.68–8.70 (m, 2H).

^{13}C NMR (100 MHz, $CDCl_3$): δ = 14.74, 23.27, 29.33, 31.50, 32.09, 34.41, 38.50, 50.43, 60.29, 63.04, 63.12, 64.57, 64.65, 65.76, 67.25, 67.45, 67.59, 67.70, 68.66, 69.55, 69.77, 69.84, 69.99, 70.07, 70.47, 70.60, 70.67, 70.84, 71.09, 71.18, 71.29, 71.40, 71.45, 80.54, 85.53, 90.44, 98.26, 103.08, 103.57, 103.61, 110.12, 111.69, 113.12, 113.20, 113.88, 114.25, 114.38, 114.89, 114.93, 114.99, 115.55, 117.28, 117.36, 117.62, 117.99, 118.85, 122.32, 123.75, 123.96, 124.15, 124.23, 124.40, 124.95, 125.25, 126.97, 127.01, 127.31, 127.48, 128.62, 129.00, 129.16, 129.75, 130.75, 130.81, 131.26, 131.93, 131.98, 132.23, 132.31, 133.27, 133.39, 135.37, 135.83, 138.23, 139.65, 139.80, 141.91, 142.77, 144.10, 144.15, 144.23, 145.04, 148.38, 148.55, 151.19, 152.42, 152.76, 153.18, 156.62, 156.71, 159.52, 159.73, 163.07.

HRMS (ESI): m/z: 1769.8463 (calcd. $[M+2Na]^{2+}$ = 1769.8470).

4.4.3. Polymer Synthesis and Preparation of Dried RotAnBP-PUU Films and RotAnBP-PUU Hydrogels

Polymer Synthesis

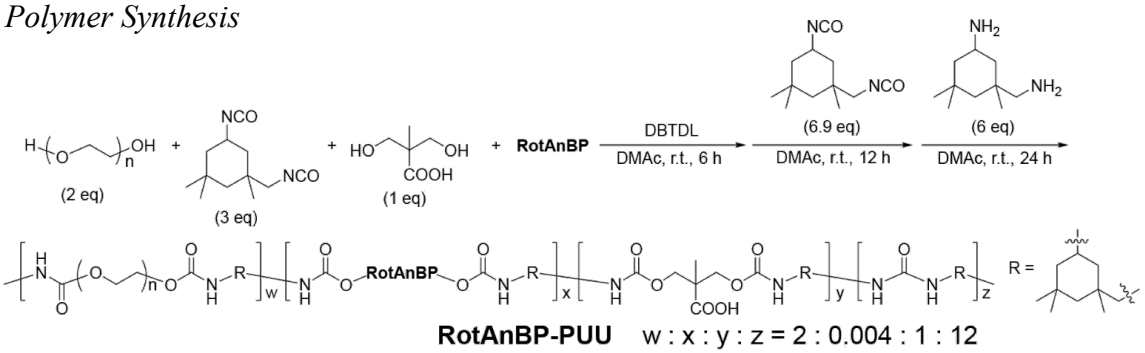

Dibutyltin dilaurate (2 drops) was added to a stirred mixture of **RotAnBP** (6.0 mg, 1.7 μmol), telechelic hydroxy-terminated poly(ethylene glycol) (M_n= 2000 g/mol, 1.0 g, 0.50 mmol), isophorone diisocyanate (167 mg, 0.750 mmol), and 2,2-bis(hydroxymethyl)propionic acid (33.5 mg, 0.250 mmol) in DMAc (4 mL) and the mixture was stirred at r.t. for 6 h. A solution of isophorone diisocyanate (383 mg, 1.72 mmol) in DMAc (2 mL) was then added. After the reaction mixture was stirred at r.t. for an additional 12 h, a solution of isophorone diamine (255 mg, 1.50 mmol) in DMAc (4 mL) was added dropwise over the course of 2 h and the reaction mixture was stirred at r.t. for another 24 h. Methanol (10 mL) was added, and the reaction mixture was stirred for 30 min. Then, the reaction mixture was poured into a mixture of hexane (400 mL) and ethyl acetate (800 mL). The green precipitate was collected by filtration and dried in vacuo for 12 h at 40 °C to afford **RotAnBP-PUU** as a green rubbery solid (1.70 g, 92%, M_n = 48 kg/mol, PDI = 2.04).

Preparation of Dry PUU Films and PUU Hydrogel

RotAnBP-PUU (400 mg) was dissolved in methanol (8 mL), and the solution was divided between two square poly-(tetrafluoroethylene) molds (51 × 51 × 5.0 mm^3). The molds were placed under an inverted funnel to control the evaporation rate. The solvent

was evaporated over the course of 12 h under ambient conditions, and the resulting films were further dried in vacuo at 40 °C for 6 h. The green films thus obtained were smooth and transparent with a thickness of 70−100 μm. After fully swelling the films in a large amount of deionized water for 2 h, transparent hydrogels were obtained with a thickness of 110−150 μm.

4.4.4. Calculation of Spectral Overlap Integral and Förster Distance

Using equations (1) and (2), the spectral overlap integral ($J(\lambda)$) between the donor fluorescence and the acceptor absorption, and the Förster distance (R_0) of the donor/acceptor pair were determined:[54]

$$J(\lambda) = \int_0^\infty f(\lambda)\varepsilon(\lambda)\lambda^4 \mathrm{d}\lambda \quad (1)$$

$$R_0{}^6 = \frac{9}{4(2\pi)^5} * \frac{2303}{N} * \kappa^2 \varphi_D n^{-4} J(\lambda) \quad (2)$$

Here, $f(\lambda)$ is the normalized fluorescence intensity of the 9,10-bis(phenylethynyl)anthracene donor, $\varepsilon(\lambda)$ is the extinction coefficient of the π-extended BODIPY acceptor, N is Avogadro's number, κ^2 is the orientation factor of 2/3, φ_D is the fluorescence quantum yield of the donor (0.91),[14] n is the refractive index of the 1:4, v:v THF/methanol solution (estimated to be 1.345), and the constants preceding κ have an aggregate value of 8.79×10^{-11} M cm nm^2. Using these values, $J(\lambda)$ and R_0 were calculated to be 5.581 × 1015 M^{-1} cm^{-1} nm^4 and 67.1 Å, respectively.

The energy transfer efficiency (E) is described by equation (3), where r is the distance between the donor and acceptor molecules. Using the value of the Förster distance reported above, the energy transfer efficiency should be higher than 99% when r is below 31.2 Å.

$$E = \frac{R_0^6}{R_0^6 + r^6} \quad (3)$$

4.4.5. Examination of the Penetration of the Red Fluorescence Emitted by RotAnBP-PUU Hydrogels

Preparation of RotAnBP-PUU Hydrogels Based on a Second Batch of RotAnBP-PUU.

In this experiment, **RotAnBP-PUU** hydrogels were prepared using a second batch of **RotAnBP-PUU** that was synthesized according to the procedure and reaction scheme described above. The mechanical response of the newly prepared hydrogel (Figure 4-16) is similar to that of the hydrogels used in other experiments (Figure 4-11).

Reference Polyurethane Films in which a Rotaxane Mechanophore Showing On/Off Switching of Green Emission Was Incorporated.

For reference purposes, a polyurethane that I reported as **Rot2PU** in a previous paper[15] and which contained the green-light emitting rotaxane **Rot2** was employed. The molecular structures of **Rot2** and **Rot2PU** are shown in Figure 4-17.

Preparation of Red PU Films without Any Mechanophores.

The red-colored PU films were prepared by physically doping sudan III (Figure 4-18a, b) into the reference polyurethane without any mechanophores. Thus, PU (300 mg, M_n = 121 kg/mol, PDI = 2.04) synthesized according to the method that me research group previously reported[14] and 10 mg of sudan III were dissolved in THF (5 mL) and the solution was divided between two square poly(tetrafluoroethylene) molds (51 × 51 × 5.0 mm). The molds were placed under an inverted funnel to control the evaporation of the solvent. The solvent was evaporated over the course of 4 h under ambient conditions and the resulting films were further dried in vacuo at r.t. for 12 h. The red films thus obtained were smooth and opaque with a thickness of 60–80 μm. A characteristic stress-strain curve of the films thus obtained is shown in Figure 4-18c.

Changes in Fluorescence Spectra of Hydrogels and Films Overlaid with the Red Films upon Stretching.

Tensile tests were performed for samples of **RotAnBP-PUU** hydrogel or **Rot2PU** film overlaid without and with the red films (Figure 4-19). While stretching tests, the excitation light was irradiated to the center of **RotAnBP-PUU** hydrogel or **Rot2PU** film from one optical fiber connected to the light source, and the fluorescence of the **RotAnBP-PUU** hydrogel or **Rot2PU** film passing through the red PU film was monitored by the other optical fiber connected to the detector.

4.5. References

(1) Guo, Q.; Zhang, X. A Review of Mechanochromic Polymers and Composites: From Material Design Strategy to Advanced Electronics Application. *Compos. B Eng.* **2021**, *227*, 109434.

(2) Caruso, M. M.; Davis, D. A.; Shen, Q.; Odom, S. A.; Sottos, N. R.; White, S. R.; Moore, J. S. Mechanically-Induced Chemical Changes in Polymeric Materials. *Chem. Rev.* **2009**, *109*, 5755–5798.

(3) Li, J.; Nagamani, C.; Moore, J. S. Polymer Mechanochemistry: From Destructive to Productive. *Acc. Chem. Res.* **2015**, *48*, 2181–2190.

(4) De Bo, G. Polymer Mechanochemistry and the Emergence of the Mechanophore Concept. *Macromolecules* **2020**, *53*, 7615–7617.

(5) Traeger, H.; Kiebala, D. J.; Weder, C.; Schrettl, S. From Molecules to Polymers—Harnessing Inter- and Intramolecular Interactions to Create Mechanochromic Materials. *Macromol. Rapid Commun.* **2021**, *42*, 2000573.

(6) He, S.; Stratigaki, M.; Centeno, S. P.; Dreuw, A.; Göstl, R. Tailoring the Properties of Optical Force Probes for Polymer Mechanochemistry. *Chem. Eur. J.* **2021**, *27*, 15889–15897.

(7) Balzani, V.; Gómez-López, M.; Stoddart, J. F. Molecular Machines. *Acc. Chem. Res.* **1998**, *31*, 405–414.

(8) Okumura, Y.; Ito, K. The Polyrotaxane Gel: A Topological Gel by Figure-of-Eight Cross-links. *Adv. Mater.* 2**001**, *13*, 485‑487.

(9) Arai, T.; Jang, K.; Koyama, Y.; Asai, S.; Takata, T. Versatile Supramolecular Cross-linker: A Rotaxane Cross-linker That Directly Endows Vinyl Polymers with Movable Cross-links. *Chem. Eur. J.* **2013**, *19*, 5917–5923.

(10) Stoddart, J. F. Putting Mechanically Interlocked Molecules (MIMs) to Work in Tomorrow's World. *Angew. Chem. Int. Ed.* **2014**, *53*, 11102–11104.

(11) Erbas-Cakmak, S.; Leigh, D. A.; McTernan, C. T.; Nussbaumer, A. L. Artificial Molecular Machines. *Chem. Rev.* **2015**, *115*, 10081–10206.

(12) Stoll, R. S.; Friedman, D. C.; Stoddart, J. F. Mechanically Interlocked Mechanophores by Living-Radical Polymerization from Rotaxane Initiators. *Org. Lett.* **2011**, *13*, 2706–2709.

(13) Sagara, Y.; Karman, M.; Verde-Sesto, E.; Matsuo, K.; Kim, Y.; Tamaoki, N.; Weder, C. Rotaxanes as Mechanochromic Fluorescent Force Transducers in Polymers. *J. Am. Chem. Soc.* **2018**, *140*, 1584–1587.

(14) Sagara, Y.; Karman, M.; Seki, A.; Pannipara, M.; Tamaoki, N.; Weder, C. Rotaxane-Based Mechanophores Enable Polymers with Mechanically Switchable White Photoluminescence. *ACS Cent. Sci.* **2019**, *5*, 874–881.
(15) Muramatsu, T.; Sagara, Y.; Traeger, H.; Tamaoki, N.; Weder, C. Mechanoresponsive Behavior of a Polymer-Embedded Red-Light Emitting Rotaxane Mechanophore. *ACS Appl. Mater. Interfaces* **2019**, *11*, 24571–24576.
(16) Muramatsu, T.; Okado, Y.; Traeger, H.; Schrettl, S.; Tamaoki, N.; Weder, C.; Sagara, Y. Rotaxane-Based Dual Function Mechanophores Exhibiting Reversible and Irreversible Responses. *J. Am. Chem. Soc.* **2021**, *143*, 9884–9892.
(17) Zhang, M.; De Bo, G. Impact of a Mechanical Bond on the Activation of a Mechanophore. *J. Am. Chem. Soc.* **2018**, *140*, 12724–12727.
(18) Zhang, M.; De Bo, G. Mechanical Susceptibility of a Rotaxane. *J. Am. Chem. Soc.* **2019**, *141*, 15879–15883.
(19) Sandoval-Torrientes, R.; Carr, T. R.; De Bo, G. A Mechanochromic Hydrogen-Bonded Rotaxane. *Macromol. Rapid Commun.* **2021**, *42*, 2000447.
(20) Praveen, V. K.; George, S. J.; Varghese, R.; Vijayakumar, C.; Ajayaghosh, A. Self-Assembled π-Nanotapes as Donor Scaffolds for Selective and Thermally Gated Fluorescence Resonance Energy Transfer (FRET). *J. Am. Chem. Soc.* **2006**, *128*, 7542–7550.
(21) Kim, S.; Yoon, S.-J.; Park, S. Y. Highly Fluorescent Chameleon Nano-particles and Polymer Films: Multicomponent Organic Systems that Com-bine FRET and Photochromic Switching. *J. Am. Chem. Soc.* **2012**, *134*, 12091–12097.
(22) Rajdev, P.; Ghosh, S. Fluorescence Resonance Energy Transfer (FRET): A Powerful Tool for Probing Amphiphilic Polymer Aggregates and Supramolecular Polymers. *J. Phys. Chem. B* **2019**, *123*, 327–342.
(23) Vijayakumar, C.; Praveen, V. K.; Kartha, K. K.; Ajayaghosh, A. Excitation Energy Migration in Oligo(p-phenylenevinylene) Based Organogels: Structure-property Relationship and FRET Efficiency. *Phys. Chem. Chem. Phys.* **2011**, *13*, 4942–4949.
(24) Vijayakumar, C.; Praveen, V. K.; Ajayaghosh, A. RGB Emission through Controlled Donor Self-Assembly and Modulation of Excitation Energy Transfer: A Novel Strategy to White-Light-Emitting Organogels. *Adv. Mater.* **2009**, *21*, 2059–2063.
(25) Piston, D. W.; Kremers, G.-J. Fluorescent Protein FRET: the Good, the Bad and the Ugly. *Trends Biochem. Sci.* **2007**, *32*, 407–414.
(26) Yuan, L.; Lin, W.; Zheng, K.; Zhu, S. FRET-Based Small-Molecule Fluorescent Probes: Rational Design and Bioimaging Applications. *Acc. Chem. Res.* **2013**, *46*, 1462–1473.

(27) Grashoff, C.; Hoffman, B. D.; Brenner, M. D.; Zhou, R.; Parsons, M.; Yang, M. T.; McLean, M. A.; Sligar, S. G.; Chen, C. S.; Ha, T.; Schwartz, M. A. Measuring mechanical tension across vinculin reveals regulation of focal adhesion dynamics. *Nature* **2010**, *466*, 263–266.
(28) Merindol, R.; Delechiave, G.; Heinen, L.; Catalani, L. H.; Walther, A. Modular Design of Programmable Mechanofluorescent DNA Hydrogels. *Nat. Commun.* **2019**, *10*, 528.
(29) Bruns, N.; Pustelny, K.; Bergeron, L. M.; Whitehead, T. A.; Clark, D. S. Mechanical Nanosensor Based on FRET within a Thermosome: Damage-Reporting Polymeric Materials. *Angew. Chem. Int. Ed.* **2009**, *48*, 5666–5669.
(30) Ogi, S.; Sugiyasu, K.; Takeuchi, M. Synthesis of a Doubly Strapped Light-Harvesting Porphyrin Bearing Energy Donor Molecules Hanging on to the Straps: An Attempt toward Macroscopic Control over Molecular Con-formation that Affects the Efficiency of Fluorescence Resonance Energy Transfer. *Bull. Chem. Soc. Jpn.* **2011**, *84*, 40–48.
(31) Jia, Y.; Wang, S.; Wang, W.-J.; Li, B.-G.; Zhu, S. Design and Synthesis of a Well-Controlled Mechanoluminescent Polymer System Based on Fluorescence Resonance Energy Transfer with Spiropyran as a Force-Activated Acceptor and Nitrobenzoxadiazole as a Fluorescent Donor. *Macromolecule* **2019**, *52*, 7920–7928.
(32) Khang, T. M.; Huang, R.; Khan, A.; Chuang, W.-T.; Nhien, P. Q.; Cuc, T. T. K.; Hue, B. T. B.; Wei, K.-H.; Li, Y.-K.; Lin, H.-C. Reversible Ratiometric Mechanochromic Fluorescence Switching in Highly Stretchable Polyurethane Elastomers with Ultratoughness Enhanced by Polyrotaxane. *ACS Materials Lett.* **2022**, *4*, 2537–2546.
(33) Nhien, P. Q.; Cuc, T. T. K.; Khang, T. M.; Wu, C.-H.; Hue, B. T. B.; Wu, J. I.; Mansel, B. W.; Chen, H.-L.; Lin, H.-C. Highly Efficient Förster Resonance Energy Transfer Modulations of Dual-AIEgens between a Tetraphenylethylene Donor and a Merocyanine Acceptor in Photo-Switchable [2]Rotaxanes and Reversible Photo-Patterning Applications. *ACS Appl. Mater. Interfaces* **2020**, *12*, 47921–47938.
(34) Ma, X.; Zhang, J.; Cao, J.; Yao, X.; Cao, T.; Gong, Y.; Zhao, C.; Tian, H. A Room Temperature Phosphorescence Encoding [2]Rotaxane Molecular Shuttle. *Chem. Sci.* **2016**, *7*, 4582–4588.
(35) Li, Y.; Li, H.; Li, Y.; Liu, H.; Wang, S.; He, X.; Wang, N.; Zhu, D. Energy Transfer Switching in a Bistable Molecular Machine. *Org. Lett.* **2005**, *7*, 4835–4838.
(36) Onagi, H.; Rebek, J. Fluorescence Resonance Energy Transfer Across a Mechanical Bond of a Rotaxane. *Chem. Commun.* **2005**, *36*, 4604–4606.

(37) Yang, N.; Yang, H.; Shao, Z.; Guo, M. Ultrastrong and Tough Supramo-lecular Hydrogels from Multiurea Linkage Segmented Copolymers with Tractable Processablity and Recyclability. *Macromol. Rapid Commun.* **2017**, *38*, 1700275.
(38) Cao, B.-H.; Chen, W.; Wei, W.-Y.; Chen, Y.; Yuan, Y. Carbon Dots Intensified Mechanochemiluminescence from Waterborne Polyurethanes as Tunable Force Sensing Materials. Chinese *J. Polym. Sci.* **2021**, *39*, 1403–1411.
(39) Sagara, Y.; Weder, C.; Tamaoki, N. Tuning the Thermo- and Mecha-noresponsive Behavior of Luminescent Cyclophanes. *RSC Adv.* **2016**, *6*, 80408–80414.
(40) Levitus, M.; Garcia-Garibay, M. A. Polarized Electronic Spectroscopy and Photophysical Properties of 9,10-Bis(phenylethynyl)anthracene. *J. Phys. Chem. A* **2000**, *104*, 8632–8637.
(41) Demeter, A. First Steps in Photophysics. I. Fluorescence Yield and Radiative Rate Coefficient of 9,10-Bis(phenylethynyl)anthracene in Paraffins. *J. Phys. Chem. A* **2014**, *118*, 9985–9993.
(42) Lübtow, M.; Helmers, I.; Stepanenko, V.; Albuquerque, R. Q.; Marder, T. B.; Fernández, G. Self-Assembly of 9,10-Bis(phenylethynyl) Anthracene (BPEA) Derivatives: Influence of pi-pi and Hydrogen-Bonding Interactions on Aggregate Morphology and Self-Assembly Mechanism. *Chem. Eur. J.* **2017**, *23*, 6198–6205.
(43) Jacquot de Rouville, H.-P.; Iehl, J.; Bruns, C. J.; McGrier, P. L.; Frasconi, M.; Sarjeant, A. A.; Stoddart, J. F. A Neutral Naphthalene Diimide [2]Rotaxane. *Org. Lett.* **2012**, *14*, 5188–5191.
(44) Choudhary, U.; Northrop, B. H. Rotaxanes and Biofunctionalized Pseudorotaxanes via Thiol-Maleimide Click Chemistry. *Org. Lett.* **2012**, *14*, 2082–2085.
(45) Hamilton, D. G.; Davies, J. E.; Prodi, L.; Sanders, J. K. M. Synthesis, Structure and Photophysics of Neutral p-Associated [2]Catenanes. *Chem. Eur. J.* **1998**, *4*, 608–620.
(46) Loudet, A.; Burgess, K. BODIPY Dyes and Their Derivatives: Syn-theses and Spectroscopic Properties. *Chem. Rev.* **2007**, *107*, 4891–4932.
(47) Wang, C.; Xia, X.; Luo, J.; Qian, Y. A Novel Near-infrared Styryl-BODIPY Fluorescent Probe for Discrimination of GSH and Its Application in Living Cells. *Dyes Pigments* **2018**, *152*, 85–92.
(48) Ansteatt, S.; Meares, A.; Ptaszek, M. Amphiphilic Near-IR-Emitting 3,5-Bis(2-Pyrrolylethenyl)BODIPY Derivatives: Synthesis, Characterization, and Comparison with Other (Hetero)Arylethenyl-Substituted BODIPYs. *J. Org. Chem.* **2021**, *86*, 8755–8765.
(49) Gibson, H. W.; Lee, S.-H.; Engen, P. T.; Lecavalier, P.; Sze, J.; Shen, Y. X.; Bheda, M. New Triarylmethyl Derivatives: "Blocking Groups" for Rotaxanes and Polyrotaxanes. *J. Org. Chem.* **1993**, *58*, 3748–3756.

(50) Dichtel, W. R.; Miljanić O. S.; Spruell, J. M.; Heath, J. R.; Stoddart, J. F. Efficient Templated Synthesis of Donor-Acceptor Rotaxanes Using Click Chemistry. *J. Am. Chem. Soc.* **2006**, *128*, 10388–10390.
(51) Gong, C.; Gibson, H. W. Synthesis and Characterization of a Polyester/Crown Ether Rotaxane Derived from a Difunctional Blocking Group. *Macromolecules* **1996**, *29*, 7029–7033.
(52) Rostovtsev, V. V.; Green, L. G.; Fokin, V. V.; Sharpless, K. B. A Step-wise Huisgen Cycloaddition Process: Copper(I)-Catalyzed Regioselective "Ligation" of Azides and Terminal Alkynes. *Angew. Chem. Int. Ed.* **2002**, *41*, 2596–2599.
(53) Zhang C.; Zhao J.; Wu S.; Wang Z.; Wu W.; Ma J.; Guo S.; Huang L. Intramolecular RET Enhanced Visible Light-Absorbing Bodipy Organic Triplet Photosensitizers and Application in Photooxidation and Triplet–Triplet Annihilation Upconversion. *J. Am. Chem. Soc.* **2013**, *135*, 10566–10578.
(54) Patterson, G. H.; Piston D. W.; Barisas B. G. Förster Distances between Green Fluorescent Protein Pairs. *Anal. Biochem.* **2000**, *284*, 438–440.

Chapter 5

Conclusions and Perspectives

Conclusions and Perspectives

In this thesis, I described the development of a highly functionalized supramolecular mechanophore based on rotaxane.

In Chapter 2, a rotaxane-based supramolecular mechanophore that can reversibly control the change in red fluorescence intensity was developed by introducing a π-extended BODIPY derivative exhibiting red fluorescence into the cyclic molecule. The rotaxane shows almost no red fluorescence in solution, but when the rotaxane is incorporated into polyurethane, the polyurethane film shows relatively strong fluorescence even in the stress-free state. This is because the steric hindrance between the bulky BODIPY derivative and the quencher, which lowers the association constant between the cyclic molecule and the quencher. The low association constant causes the increase in the proportion of cyclic molecules that are fixed at a position away from the quencher as the solvent evaporates during the film formation. The intensity of the initial red fluorescence can be reduced by swelling the film with organic solvents. This is because the mobility of the cyclic molecules recovers upon swelling and the cycles move to near the quencher. Both the dry and the swollen films showed an instantaneous and reversible changes in the red fluorescence intensities upon deformation, similar to conventional rotaxane-based mechanophores.

In Chapter 3, I introduced rotaxane-based mechanophores that exhibit both reversible and irreversible changes in luminescence properties depending on the magnitude of force. The dual response is ascribed to the force-induced molecular shuttling function and dethreading of the cycle. To achieve the dual response, the combination of judiciously selected ring and stopper moieties is essential. The rotaxane-incorporated polyurethane films initially show reversible changes in the fluorescence intensities, which is ascribed to the force-induced molecular shuttling. After repeated stretching with high strain, the cyclic molecules are induced to pass through the stopper, resulting in irreversible changes

in fluorescence intensities. As the amount of cyclic molecules that slip past the stopper increases upon repeated stretching, the fluorescence intensity of the relaxed film gradually increases.

In Chapter 4, I succeeded in controlling FRET at the single molecule level by mechanical force using rotaxane. In the rotaxane, the green-emissive energy donor is introduced near the cyclic structure, and the red-emissive energy acceptor is introduced next to the green fluorophore through the short spacer. The isolated cyclic molecule displays red fluorescence due to efficient FRET from the donor to the acceptor. In contrast, upon rotaxane formation, the FRET is restricted by the CT interaction between the green fluorophore and quencher or the PeT process from the green fluorophore to the quencher, resulting in weakened red fluorescence under the preferential excitation of the donor. The PUU hydrogels in which the rotaxane is covalently introduced exhibit increases in the red emission intensity upon deformation because the CT interactions and PeT process are suppressed and the efficient FRET occurs in the activated rotaxanes. The fluorescence contrast between the initial and stretched states is considerably higher than that observed for the dry PUU. This is attributed to the fact that the association constant between the cycle and quencher increases, as well as the molecular mobility recovers.

Throughout the all chapters, I can claim to have shown that supramolecular mechanophores that exhibit responses for a variety of purposes can be developed by utilizing the interlocking structure of rotaxane. For example, as a force sensor to visualize piconewton forces generated by cells, a “non-sacrificial” mechanophore that shows on/off switching of red fluorescence was required. To address this issue, I developed the rotaxane-based supramolecular mechanophore by introducing the red fluorophore into the cyclic molecule. The obtained rotaxane showed the changes in the red fluorescence intensities reversibly upon applying force. Although on/off switching of red fluorescence cannot not be achieved in the polymer due to low association constant between the cycle and the quencher, based on the findings in Chapter 4, the association constant would

increase in the hydrophilic environment due to hydrophobic interactions, and the fluorescence is expected to be sufficiently quenched in the force-free state. Therefore, cell migration would be visualized by using the red-emissive rotaxane mechanophore. In this thesis, I only examined the mechanoresponsive luminescence behavior of the rotaxane mechanophore in the polymer. Thus, future work would examine whether rotaxane mechanophores are useful as force sensors that can visualize cell migration.

As another example, the use of the force-induced dethreading mechanism would be useful as a new method for designing mechanophores that record force histories in several tens of piconewtons, which have rarely been developed so far. However, in present rotaxanes showing both reversible and irreversible changes in the fluorescence properties, the fluorescence is observed from both rotaxane activated by molecular shuttling and rotaxane activated by dethreading, complicating the distinction between whether the fluorescence expresses a force history or not. This problem would be solved by designing a molecular structure in which molecular shuttling is suppressed by shortening the axle molecule, and fluorescence is turned on only by force-induced dethreading, which is currently ongoing. In addition, the force-induced dethreading could be useful for development of polymer networks with good mechanical strength. Polymer networks that have many rotaxanes as crosslinkers have been reported to show excellent mechanical strength due to their molecular shuttling function. In polymer networks in which force-induced dethreading mechanism is introduced, the dethreading mechanism could dissipate vast amounts of energy, which would contribute to the development of materials with improved mechanical strength.

The success of mechanical control of FRET with rotaxanes in Chapter 4 should motivate research on the use of rotaxanes to control other photo-functions. In fact, the development of rotaxane mechanophores that control circularly polarized emission or phosphorescence is ongoing in Sagara lab. Besides, the introduction of FRET mechanism would enable on/off switching of fluorescence of more diverse fluorophores on rotaxane

mechanophores. In the conventional molecular designs of rotaxane-based supramolecular mechanophores, the on/off switching of the fluorescence was achieved only when the planar fluorophores are introduced into the cyclic structure. As shown in Chapter 2, bulky fluorophores are not suitable for the emitters directly incorporated into the cycle structure because the association constant between the quencher and cycle becomes low, resulting in poor contrast upon stretching the films in which the mechanophores are covalently introduced. If FRET is incorporated into rotaxane mechanophores, nonplanar fluorophores could be involved in rotaxane mechanophores as FRET acceptors without reducing the emission contrast because the bulky acceptors don't need to form a π-stacked structure with the quencher. In addition, even in case of fluorophores that do not form CT complexes with the quencher or that do not undergo PeT with the quencher, conventional rotaxane-based supramolecular mechanophores cannot exhibit on/off switching of fluorescence of such fluorophores. However, using FRET would solve this problem, similar to non-planar fluorophores. Development of rotaxanes that exhibit on/off switching of various fluorescence colors by utilizing FRET is desirable in future.

Although the development of various rotaxane-based mechanophores has been encouraged, the magnitude of force required to activate each rotaxane-based mechanophore has not been evaluated at the single molecule level. Quantitative evaluation of the magnitude of this force will certainly be necessary for further development of rotaxane mechanophores and their application to force sensors in mechanobiology. A method is currently being developed to evaluate the magnitude of the force required to activate the rotaxane using atomic force microscopy.

Furthermore, other interlocked structures such as catenanes and molecular knots can also be applied as supramolecular mechanophores, and supramolecular mechanophores with different features from rotaxane mechanophore could be developed. The field of supramolecular mechanophores is expected to develop further in the future.

Lists of Publications

Original Papers

1. “Mechanoresponsive Behavior of a Polymer Embedded Red Light Emitting Rotaxane Mechanophore” T. Muramatsu, Y. Sagara, H. Traeger, N. Tamaoki, C. Weder *ACS Appl. Mater. Interfaces* **2019**, *11*, 24571–24576.

2. “Rotaxane-Based Dual Function Mechanophores Exhibiting Reversible and Irreversible Responses” T. Muramatsu, Y. Okado, H. Traeger, S. Schrettl, N. Tamaoki, C. Weder, Y. Sagara *J. Am. Chem. Soc.* **2021**, *143*, 9884–9892.

3. “Force-induced Shuttling of Rotaxanes Controls Fluorescence Resonance Energy Transfer in Polymer Hydrogels” T. Muramatsu, S. Shimizu, J. M. Clough, C. Weder, Y. Sagara *ACS Appl. Mater. Interfaces* **2023**, *15*, 8502–8509.

References

1. “Development of Imidazo[1,2a]pyridine Derivatives with an Intramolecular Hydrogen Bonded Seven Membered Ring Exhibiting Bright ESIPT Luminescence in the Solid State” T. Mutai, T. Muramatsu, I. Yoshikawa, H. Houjou, M. Ogura *Org. Lett.* **2019**, *21*, 2143–2146.

2. “A 1,6-Diphenylpyrene-Based, Photoluminescent Cyclophane Showing a Nematic Liquid-Crystalline Phase at Room Temperature” Y. Sagara, T. Muramatsu, N. Tamaoki *Crystals*, **2019**, *9*, 92.

3. “Two-step mechanoresponsive luminescence and mechanical stimuli-induced release of small molecules exhibited by a luminescent cyclophane” Y. Sagara, K. Takahashi, A. Seki, T. Muramatsu, T. Nakamura, N. Tamaoki *J. Mater. Chem. C* **2021**, *9*, 1671–1677.

4. “Excited State Charge-Transfer Complexes Enable Fluorescence Color Changes in a Supramolecular Cyclophane Mechanophore” S. Thazhathethil, T. Muramatsu, N. Tamaoki, C. Weder, Y. Sagara *Angew. Chem. Int. Ed.* **2022**, *61*, e202209225.

5. “Tuning the mechanoresponsive luminescence of rotaxane mechanophores by varying the stopper size” K. Hiratsuka, T. Muramatsu, T. Seki, C. Weder, G. Watanabe, Y. Sagara *J. Mater. Chem. C* **2023**, *11*, 3949–3955.

Acknowledgements

The research work presented in this thesis was carried out under the supervision of Associate Professor Yoshimitsu Sagara at the Hokkaido University from 2018 to 2020 and Tokyo Institute of Technology from 2020 to 2023.

The author would like to dedicate his deep gratitude to Associate Professor Yoshimitsu Sagara for his extensive guidance for research, fruitful discussion, continual support, useful suggestions, and hearty encouragements throughout this research work. Not only the creative and pioneering researches under his supervision, but also his guidance in writing of papers and applications helped the author to grow as a researcher. The author is also grateful for the various experimental instruments and environments that allowed him to conduct his researches.

The author expresses his gratitude to Professor Christoph Weder at University of Fribourg for his valuable advises and discussion. The author also would like to thank to Professor Stephen Schrettl, Assistant Professor Jessica M. Clough, Dr. Hanna Traegar and every member in Weder laboratory who assisted his fellowship from January 2022 to April 2022 and his research.

The author is grateful to Professor Teruaki Hayakawa, Professor Tsuyoshi Michinobu, Professor Martin Vacha, and Associate Professor Yuta Nabae for the helpful comments and intensive suggestions for improving this thesis.

The author also would like to thank Professor Nobuyuki Tamaoki, Assistant Professor Kazuya Matsuo, and Assistant Professor Yuna Kim at Hokkaido University from 2018 to 2020 for helpful suggestion and discussion during his master course.

The author expresses my gratitude to all members of Tamaoki Laboratory and Sagara Laboratory. The author deeply thanks to Dr. Thazhathethil Shakkeeb, Mr. Yuji Okado, Mr. Kaito Ueda, Mr. Shinya Yutani, Mr. Thuluvanchery Salim Fazil, Mr. Silu Liu, Mr. Takumi Kuroda, Mr. Qiming Liu, Mr. Shohei Shimizu, Ms. Keiko Hiratsuka, Mr. Keigo Nonaka, Mr. Riku Yamamoto, Mr. Ryusei Mori, Ms. Tianyue Zhang, Mr. Shunsuke Imaoka, and Mr. Yuto Yoshida for his enjoyable research life.

The author thanks to the Research Fellowships of the JSPS for Young Scientists for financially support.

Finally, the author sincerely thanks to his parents for their constant support and encouragement.